IMPROVED DELIVERY OF POLYMER THERAPEUTICS TO PROSTATE TUMORS USING PLASMONIC PHOTOTHERMAL THERAPY

by

Adam Joseph Gormley

A dissertation submitted to the faculty of
The University of Utah
in partial fulfillment of the requirements for the degree of

Doctor of Philosophy

Department of Bioengineering

The University of Utah

December 2012

The University of Utah Graduate School

STATEMENT OF DISSERTATION APPROVAL

The dissertation of **Adam Joseph Gormley**

has been approved by the following supervisory committee members:

Hamidreza Ghandehari	, Chair	**September 26, 2012**
		Date Approved
Vladimir Hlady	, Member	**September 19, 2012**
		Date Approved
David Grainger	, Member	**September 19, 2012**
		Date Approved
Marc Porter	, Member	**September 21, 2012**
		Date Approved
Jindrich Kopecek	, Member	**September 19, 2012**
		Date Approved

and by **Patrick Tresco**, Chair of the Department of **Bioengineering**

and by Charles A. Wight, Dean of The Graduate School.

ABSTRACT

When a patient is presented with locally advanced prostate cancer, it is possible to provide treatment with curative intent. However, once the disease has formed distant metastases, the chances of survival drops precipitously. For this reason, proper management of the disease while it remains localized is of critical importance. Treating these malignant cells with cytotoxic agents is effective at cell killing; however, the nonspecific toxicity profiles of these drugs often limit their use until the disease has progressed and symptom palliation is required. Incorporation of these drugs in nanocarriers such as polymers help target them to tumors with a degree of specificity, though major vascular barriers limit their effective delivery. In this dissertation, it is shown that plasmonic photothermal therapy (PPTT) can be used to help overcome some of these barriers and improve delivery to prostate tumors. First, the concept of using PPTT to improve the delivery of macromolecules to solid tumors was validated. This was done by measuring the tumor uptake of albumin. Next, the concept of targeting gold nanorods (GNRs) directly to the tumor's vasculature to better modulate vascular response to heating was tested. Surface conjugation of cyclic RGD (Arg-Gly-Asp) to GNRs improved their binding and uptake to endothelial cells *in vitro*, but not *in vivo*. Nontargeted GNRs and PPTT were then utilized to guide the location of polymer therapeutic delivery to prostate tumors. *N*-(2-hydroxypropyl)methacrylamide (HPMA) copolymers, which were designed to be targeted to cells previously exposed to heat

shock, were used in this study. Treatment of tumors with PPTT facilitated a burst accumulation of the copolymers over 4 hours, and heat shock targeting to cells allowed them to be retained for an extended period of time. Finally, the tumor localization of the HPMA copolymers following PPTT was evaluated by magnetic resonance imaging (MRI). These results show that PPTT may be a useful tool to enhance delivery of polymeric drug carriers to locally advanced prostate tumors.

To Mom and Dad.

For providing me the drive to excel, passion to create, and humility to help.

Send forth your light and your truth, let them guide me;

let them bring me to your holy mountain, to the place where you dwell.

- Psalm 43:3

CONTENTS

LIST OF FIGURES

Figure

LIST OF TABLES

Table

ABBREVIATIONS

ADME	Absorption, distribution, metabolism and excretion
AHGDM	Aminohexylgeldanamycin
AIBN	Azobisisobutyronitrile
ANOVA	One-way analysis of variance
APMA-benzyl-DOTA	aminopropylmethacrylamide-benzyl-1,4,7,10 tetraazacyclododecane-1,4,7,10-tetraacetic acid
APMA-FITC	5-[3-(methacryloylaminopropyl)thioureidyl] fluorescein
AR	Aspect ratio
ATF	Amino-terminal fragment
AuNPs	Gold nanoparticles
BCA	Bicinchoninic assay
CID	Chemical interference damping
CMC	Critical micelle concentration
CTAB	Cetyltrimethylammonium bromide
DHT	Dihydrotestosterone
DI	Deionized
DIPEA	Diisopropylethylamine
DMSO	Dimethyl sulfoxide

DMXAA	5,6-dimethylxanthenone-4-acetic acid
DTT	Dithiothreitol
EBD	Evans blue dye
ECM	Extracellular matrix
EDTA	Ethylenediaminetetraacetic acid
EGFR	Epidermal growth factor receptor
EPR	Enhanced permeability and retention
ER	Endoplasmic reticulum
FDA	Food and Drug Administration
GFLG	Gly-Phe-Leu-Gly
GNRs	Gold nanorods
GRG	Generalized reduced gradient
GRP78	Glucose-regulated protein-78
HES	Hydroxyethyl starch
HIFU	High-intensity focused ultrasound
HPMA	*N*-(2-hydroxypropyl)methacrylamide
HSP	Heat shock protein
HUVEC	Human umbilical vein endothelial cells
IACUC	Institutional Animal Care and Use Committee
ICP-MS	Inductively coupled plasma mass spectrometry

ID	Injected dose
IFP	Interstitial fluid pressure
IHC	Immunohistochemical
IR	Infrared
LHRG	Luteinizing hormone (LH)-releasing hormone
LUMO	Lowest unoccupied molecular orbital
MA-GG-TT	3-[(*N*-methacryloylglycyl)glycyl]thiazolidine-2-thione
MA-GFLG-OH	*N*-methacryloyl-glycylphenylalanylleucylglycine
MA-Tyr-$CONH_2$	*N*-methacryloyl-tyrosinamide
MRI	Magnetic resonance imaging
MTD	Maximum tolerated dose
NHS	Succinimidyl ester
NIR	Near-infrared
NO	Nitric oxide
OD	Optical density
OPSS	Ortho-pyridyl-disulfide
PAMAM	Poly(amido amine)
PBS	Phosphate buffered saline
PDE	Partial differential equation
PEG	Poly(ethylene glycol)
PEI	Poly(ethyleneimine)

PGA	Poly(glutamic acid)
PLGA	Poly(lactic-co-glycolic acid)
PNIPAAm	Poly(*N*-isopropylacrylamide)
PPO	Poly(propylene oxide)
PPTT	Plasmonic photothermal therapy
PSA	Prostate specific antigen
PVP	Poly(*N*-vinyl-2-pyrolidone)
RAFT	Reversible addition-fragmentation chain-transfer
RGD	Arg-Gly-Asp
ROI	Regions of interest
SEC	Size exclusion chromatography
SMANCS	Styrene maleic anhydride-neocarzinostatin
SPR	Surface plasmon resonance
TE	Echo time
TEM	Transmission electron microscopy
TER	Thermal enhancement ratio
TNF-α	Tumor necrosis factor-alpha
TR	Repetition time
URI	Ultra resolution imaging
VDA	Vascular disrupting agent

VEGF	Vascular endothelial growth factor
WIFPWIQL	Trp-Ile-Phe-Pro-Try-Ile-Gln-Leu

ACKNOWLEDGEMENTS

The work described in this dissertation is the culmination of efforts by many individuals besides myself. Each person's contributions played a unique role in the development of this project and me as a scientist and engineer. It would be an impossible task to thank each person as I have so many great friends, colleagues and role models. However, below I would like to acknowledge a few select individuals whose contributions stand out and I would like to thank individually.

Dr. David Grainger, a member of my PhD supervisory committee, played an incredibly important role on my committee. During my proposal, at committee meetings and through personal interactions, he was relentless not to accept anything from me but the very best. His demand for perfection in not only my science, but also my understanding of the most fundamental concepts pushed me to attain the highest level of competency that I could manage. It was apparent through these interactions that his high expectations were meant to make me better, not bring me down. Through his mentorship, there is no doubt that I am better for it.

Dr. Vladimir Hlady, also a member of my PhD supervisory committee, had a similar role on my committee as Dr. Grainger. His in depth understanding of the physical sciences and many more of the fundamentals surrounding my work pushed me to learn these concepts in great detail. He was able to recognize my areas of weakness and spend time with me to ensure that my education was complete and of the highest quality.

Dr. Jindrich Kopeček, another member of my PhD supervisory committee, is a particular role model and source of inspiration for me and this work. Many of the basic principles, techniques and concepts were adapted from him, particularly his development of HPMA copolymers for drug delivery. The evolution of his career as a world renowned polymer chemist and the impact he has made on the field of drug delivery and biomaterials is inspiring. On multiple occasions he was willing to meet with me to discuss my ideas and provide me feedback about these ideas and overall career direction. The expertise he provided me throughout my graduate studies was truly invaluable and appreciated.

Dr. Marc Porter, the fourth member of my PhD supervisory committee, provided a unique perspective due to his expertise in gold nanoparticles and cancer diagnostics. Our conversations during committee meetings helped guide my understanding of gold colloid properties. Additionally, our casual conversations on a daily to weekly basis discussing general features of the graduate experience and more casual subjects were something I looked forward to and enjoyed.

Dr. Abhijit Ray, a great friend and mentor, brought me from a student with no chemistry experience to one whose dissertation project was spent almost entirely in the chemistry lab. I have him to thank for almost the entirety of my experience with and knowledge of chemistry. Additionally, his positive attitude towards research, patience and desire to teach played a significant role in my development. Finally, his kindness and friendship helped me throughout as a student and developing individual.

Dr. Khaled Greish was another individual with whom for two years I worked closely in the lab. I learned a great deal from him. His experience with *in vivo* animal

tumor models helped propel my research. Additionally, our discussions about tumor biology introduced me to tumor permeability which laid the foundation for this work.

Dr. Alexander Malugin taught me cell biology and all related methods. He is a true scientist whose attention to detail and methodology is admirable. In cases where many would overlook details, he taught me to pay closest attention. His approach to the scientific method is a feature which I learned from.

Nate Larson is a graduate student in the Department of Pharmaceutics and Pharmaceutical Chemistry. Throughout this project, he and I worked closely together as a team. His input on all project ideas and methods were essential to the project's success. I am fortunate to have worked so closely with such a great pharmaceutical scientist and friend. I look forward to many years of continued friendship and collaboration.

Ryan Robinson is an undergraduate bioengineering student who worked with me for over three years. Each week Ryan went above and beyond what was required of him and was hugely supportive of this work. In some respects, he helped me with most of the experiments in this dissertation and therefore armed himself with invaluable skills before entering graduate school. His loyalty to the project is greatly appreciated.

Drs. Josh Gustafson, Shawn Reese and Mr. Monir Parikh were graduate students with me in the program and are my three closest friends to this effect. The support they provided as well as their friendship made each week worth the effort. Feedback on ideas and results provided me the independent opinion of my research that is essential to success. The importance of their support could not be over emphasized.

Dr. Glenn Gormley, my father and life mentor, provided me the foundation for my interests and aspirations. His dedication to science and treating the sick in a

responsible fashion taught me to do the same. When times were tough, he would tell me to work harder. And when time permitted, he also taught me the value of balancing hard work with recreational fun. His passion for developing healthcare to meet the needs of those who need help has kept my work in perspective. The passion for my work is truly a product of his mentorship.

Dr. Hamid Ghandehari, my research advisor, provided me the mentorship and resources for this dissertation and my development as a scientist. When I entered his lab and requested that I work on my own project idea, he provided trust and allowed me to continue. For this in particular, I am very thankful. Additionally, his constant attention to my development by providing me all available opportunities shaped my career. His attention to detail, particularly in regards to conjugate characterization, taught me to do the same. As a lab PI, he was able to provide ambition, enthusiasm, care and maturity. As a leader in the field, he was forward thinking whose ultimate intentions were for science, and not necessarily for personal gain. These characteristics and values are something that I learned from him in particular. I joined his lab one and one-half years into my PhD, and there is no doubt that joining his lab was the single greatest decision of my education and career. There is no way that I can acknowledge or thank Dr. Ghandehari enough for his contributions to this dissertation and my professional development.

CHAPTER 1

INTRODUCTION

1.1: Introduction

Prostate cancer is a disease that afflicts a large percentage of men in the United States. The American Cancer Society's "Cancer Facts and Figures" report estimates that in 2012 there will be 241,740 new cases and 28,170 deaths related to this disease.[1] Indeed, prostate cancer is one of the most prevalent forms of cancer, but also has one of the lowest mortality rates relative to its large number of cases. This somewhat encouraging statistic is due to the number of cases whose disease remains localized to the prostate gland (Stage I-II). When such cases are presented, removal of the prostate can generally provide cure. Once the disease has progressed beyond the prostatic capsule and invaded nearby tissue (Stage III), termed advanced localized prostate cancer, complete removal of the cancerous tissue becomes difficult. In these cases, radiotherapy often in combination with hormone therapy can provide curative treatment, though not with the same confidence. Unfortunately, once the disease has progressed and formed distant metastases often to the lymph and bone (Stage IV), patient survival reduces dramatically (29% 5-year survival rate). In these cases, treatment with hormone and/or chemotherapy only provides extension of life with symptom palliation.

The large difference in patient survival when presented with Stage III vs. IV highlights the need to focus on therapies which target advanced localized disease and reduces the chances of disease progression. Radio- and hormone therapy offer many opportunities in this regard, though these therapies often suffer with adverse effects. Hyperthermia, particularly in combination with radiotherapy, is another effective form of localized therapy for prostate cancer.[2-5] Though difficulties in delivering therapeutic doses of heat in a diseased tissue specific manner limits its utility. Cytotoxic chemotherapy is effective at cancer cell killing, but systemic administration and distribution to healthy organs causes significant toxicity and is therefore not used to treat these patients. Methods to increase the localization of these agents and limit their accumulation in other organs therefore represent a rich area of investigational research.

A developing means of delivering therapies in a more localized and diseased tissue specific manner focus on using drug carriers or nanoparticles. Gold nanoparticles (AuNPs), for example, are able to strongly absorb light and transduce its energy in the form of heat.[6] When localized in prostate cancer tissue, AuNP activated heating represents an effective way of producing hyperthermia with high control of thermal dose and tissue specificity. Termed plasmonic photothermal therapy (PPTT), such heating has been used to thermally ablate a wide variety of tumor models in mice including prostate cancer.[7-11] Similarly, polymeric drug carriers are able to preferentially accumulate in cancerous tissue and deliver therapeutic warheads at the site of disease.[12] These polymer therapeutics can be tailor-made to solubilize poorly soluble drugs, retain them in circulation for extended periods of time, extravasate from the vasculature in tumors and be uptaken for controlled, intracellular chemical delivery.[13] In this way, the nonspecific

toxicity of these drugs can be dramatically reduced which may enable their use to treat localized disease.

The rational combination of therapies can improve treatment outcome through synergism. For example, hyperthermia is known to potentiate radiotherapy as well as chemotherapy and is therefore used in adjuvant therapy.[3, 14-17] This is due to increased tumor blood perfusion and vascular permeability during heating.[18-19] More recently, hyperthermia has been used to improve the delivery of nanocarriers such as liposomes due to these improvements in vascular dynamics with heating.[20-23] Indeed, treatment of tumors with hyperthermia is able to facilitate the accumulation of liposomes in a size, temperature and heating time dependent manner. Unfortunately, the limited ability to selectively deliver the appropriate dose of heat to promote liposome extravasation remains a significant barrier to success.

1.2: Aims and scope of this dissertation

The major focus of this dissertation is to utilize a targeted approach towards the combined treatment of advanced localized prostate cancer. As mentioned previously, PPTT can initiate hyperthermia in a tissue selective, localized and controllable manner. The use of a laser as the source of energy enables one to easily choose the location of heating and therefore the area of greater blood perfusion and permeability. Because of these reasons, PPTT is used in this dissertation to heat cancerous tissue and facilitate nanomedicine delivery.

In this work, polymer therapeutics are used to test the utility of PPTT to enhance delivery. Polymer therapeutics, and more specifically HPMA copolymers, are useful in

this regard due to their multifunctional potential.[24] In these systems, it is easy to conjugate drugs or therapeutic radionuclides, targeting moieties and imaging agents to the polymeric side chains. Also, their size and degradability can be tailor made to allow for clearance through the kidneys as well as greater tumor mass penetration. Such conjugates can have stealth-like characteristics which reduce nonspecific organ accumulation. These properties make HPMA copolymer-drug conjugates useful for directed delivery to localized prostate tumors.

The central hypothesis in this work is that PPTT can be used to direct the delivery of HPMA copolymers to prostate tumors (Figure 1.1). GNRs, which have a surface plasmon resonance (SPR) peak in the near-infrared (NIR) spectra, are first delivered to prostate tumors by intravenous administration and passive accumulation. Subsequent administration of HPMA copolymers provides blood availability of these conjugates. Laser light heating of a prostate tumor then enhances blood perfusion and vascular permeability. These changes in vascular dynamics then facilitate their accumulation and tumor mass penetration. In this way, one might be able to enhance site specific delivery. This overall hypothesis was tested through the completion of four Specific Aims:

Specific Aim 1: To provide proof-of-concept by enhancing the delivery of albumin to mouse sarcoma tumors using PPTT.

To begin testing the central hypothesis, it was essential to first provide proof-of-concept. This was done by using PPTT to enhance the delivery of albumin, a model macromolecule, to mouse sarcoma tumors. To begin, GNRs were synthesized to have an SPR peak at 800 nm, then grafted with a surface coating of poly(ethylene glycol) (PEG).

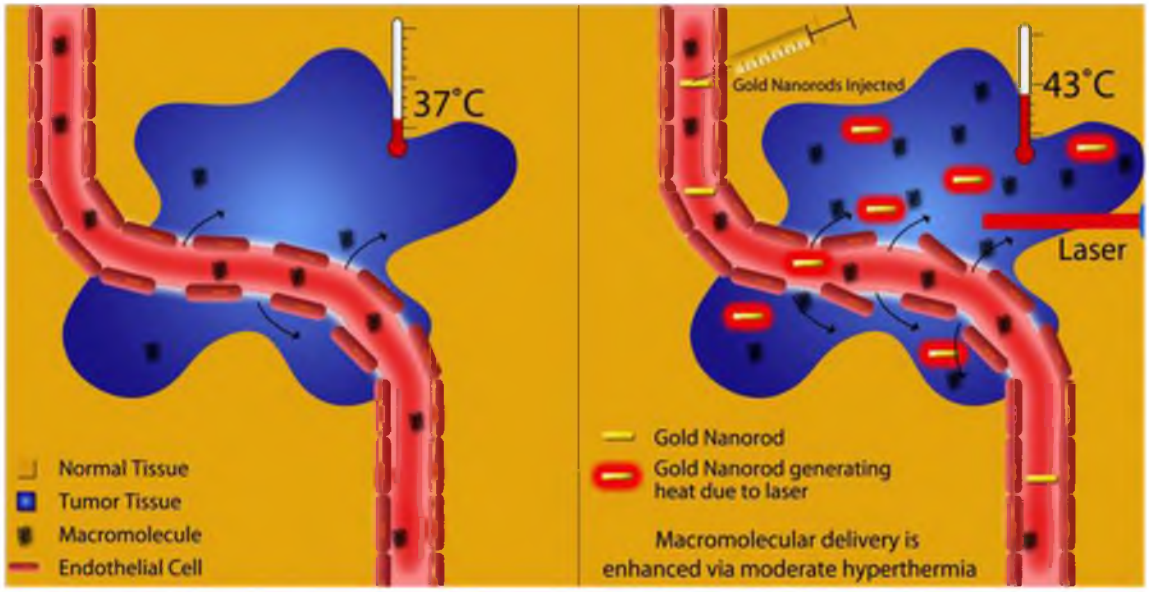

Figure 1.1: Scheme of concept showing that PPTT can be used to treat tumors with hyperthermia and therefore increase tumor blood flow and vascular permeability. This may then facilitate the delivery of macromolecules such as polymer therapeutics from the vasculature.

Characterization of these GNRs in terms of size, shape, charge, SPR peak and stability confirmed their properties and utility as photothermal antennas. To develop mouse sarcomas, CD1 mice were inoculated with S180 cells on each flank. Once appropriately sized tumors were obtained, GNRs were administered. Twenty-four hours later, Evans blue dye was administered to serve as a tracer of albumin due to their known affinity. Laser treatment of tumors then induced tissue heating which was maintained for 10 minutes to enhance albumin delivery. Five hours after PPTT, the tumors were harvested and the Evans blue dye content was measured and compared to controls. Results from this study[25] confirmed the main hypothesis by showing that PPTT could enhance the tumor delivery of albumin by 1.8-fold. This effect was seen when tumors were heated at either 43°C or 46°C, though greater tissue damage was observed at the higher temperature. Such results provided the necessary proof-of-concept information to continue with the project.

Specific Aim 2: To evaluate the potential of enhancing PPTT by targeting GNRs directly to the tumor's vasculature

As the main goal of this dissertation was to use PPTT to modulate tumor vascular dynamics, it was hypothesized that targeting of GNRs directly to endothelial cells could provide greater control. Also, targeting to the vasculature may increase the concentration of GNRs in the tumor which may reduce the laser power needed to initiate PPTT. The RGDfK peptide was chosen here due to its known affinity to $\alpha_v\beta_3$ cell adhesion integrins as well as its proven track record of targeting angiogenesis in prostate tumors.[26] GNRs were synthesized as before, though for the targeted conjugates prior attachment of

RGDfK to PEG was done before PEGylation. Amino acid analysis of the resulting nanoparticles confirmed and quantified the presence of the peptide. The endothelial cell targeting potential of the resulting GNRs was then evaluated by imaging and quantifying binding and uptake with DU145 and human umbilical vein endothelial cells (HUVEC). These experiments showed that attachment of RGDfK to PEGylated GNRs facilitated binding and uptake with both cell lines, though this effect was most apparent with endothelial cells (20-fold increase). Competitive inhibition of binding with echistatin confirmed specificity to integrins. The system was then tested *in vivo* using a prostate tumor xenograft model. Unfortunately, rapid blood clearance of the targeted GNRs by the liver and spleen dramatically reduced the availability of these nanoparticles to target tumors relative to the untargeted GNRs. This study[27] provided indication that vascular targeting GNRs, at least under the conditions tested, may not be a viable approach to improve the overall hypothesis, and therefore all subsequent studies used GNRs which were not targeted.

Specific Aim 3: To evaluate PPTT as a tool to enhance delivery of HPMA copolymers to prostate tumors.

Next, the overall hypothesis of the dissertation was tested by confirming PPTT could be used to enhance the delivery of HPMA copolymers to prostate tumors. In this study, an additional component was also tested. Previously, Pasqualini and coworkers had shown that the WIFPWIQL peptide could be used to target prostate tumors via binding to glucose-regulated protein-78 (GRP78).[28] Because this protein is a member of the heat shock protein-70 (HSP70) family, it was hypothesized that incorporation of this

peptide could enable these polymers to target cells which were previously treated with hyperthermia. To test this, cells were treated with hyperthermia followed by heat shock targeted HPMA copolymers to determine if this could increase conjugate binding and uptake. Indeed, prior treatment of cells with heat enabled significantly enhanced uptake of the targeted conjugates. Next this system was tested *in vivo*. Mice bearing prostate tumors were treated with PPTT and GRP78 receptor expression was confirmed by immunohistochemical (IHC) staining. Then, mice were administered radiolabeled untargeted or heat shock targeted HPMA copolymers and the animal's right tumor was treated with PPTT. The left tumor was used in this case as an internal control. Evaluation of conjugate tumor delivery showed that treatment with PPTT resulted in a burst accumulation over 4 hours. After 4 hours, while the untargeted conjugates diffused back out of the tumor, the heat shock targeted HPMA copolymers were retained for an extended period of time. This observation is most likely due to GRP78 receptor expression after heating. Results from this study[29] thus confirm the overall hypothesis of the dissertation that PPTT can be used to guide the location of HPMA copolymer delivery to prostate tumors.

Specific Aim 4: To visualize HPMA copolymer delivery enhancement by magnetic resonance and fluorescence imaging.

Effective drug delivery to tumors requires both transport through the vasculature as well as interstitium. Therefore, in this aim it is hypothesized that PPTT is also capable of increasing the distribution of these conjugates in tumors. To study this, gadolinium labeled HPMA copolymers were administered to mice bearing prostate tumors

immediately before treatment of the right tumor with PPTT. The left tumor served as internal, untreated control. MRI and fluorescence microscopy of both tumors showed that PPTT was capable of improving the tumor mass penetration of HPMA copolymers. Thermal enhancement of delivery, roughly 1.5-fold, to both the tumor center and periphery was observed. Results from this study[30] further suggests that PPTT may be a useful tool to improve the delivery of polymer-drug conjugates.

1.3: Clinical relevance

The long term goal of the work described in this dissertation is to design a new treatment strategy for patients with advanced localized prostate cancer. In this context, the following is a description of the potential utility of the aforementioned approach.

When a patient is presented with advanced localized prostate cancer, an alternative to radiotherapy or hormone therapy could be directed drug delivery using PPTT. In this case, patients would be administered AuNPs some time before drug treatment such that the nanoparticles would passively accumulate in the cancerous tissue. The oncologist would then access the prostate gland and surrounding areas via the urethra or rectum with a fiber optic. The polymer-drug conjugate would then be administered and the prostate gland and surrounding tissue would be radiated with laser light whose wavelength induces AuNP SPR and therefore tissue heating. PPTT is beneficial in this case as the physician can heat all suspected tissue without significant concern of damage to healthy tissue which does not contain the AuNPs. Tumor heating then increases vascular blood flow and permeability which facilitates polymer-drug conjugate delivery in these regions. Finally, once the therapeutic has cleared through the kidneys

(approximately 30-60 minutes) and is no longer available in the blood, laser treatment can be terminated leaving only the prostate cancer tissue with drug. In this way, the location of drug delivery can be dictated by the physician without significant concern of treatment side effects due to either the drug or hyperthermia.

In the following chapters of this dissertation, efforts towards the overall goal of the project will be discussed. In Chapter 2, a review of the literature relevant to this work will be provided. In Chapters 3-6, the scientific work used to complete Specific Aims 1-4 respectively will be described in detail. Finally, in Chapter 7, the project's conclusions and future directions will be discussed.

All of the experimental work described in Chapters 3-6 was performed and collected by Adam Gormley. However, the published paper[29] from Chapter 5 was first co-authored by Adam Gormley and Nate Larson. Data collected by Larson and published in this paper are not included in this dissertation. As his thesis focuses on heat shock targeting of HPMA copolymers, the data he collected in this area will be included in his dissertation. These data include: a) synthesis and characterization of heat shock targeted HPMA copolymers with drug (aminohexylgeldanamycin) attached to its side chains, b) *in vitro* GRP78 receptor expression after heat shock, c) quantification of binding and uptake of heat shock targeted conjugates to prostate cancer cells, d) *in vitro* anticancer activity of these conjugates with and without hyperthermia, and e) pharmacokinetic modeling of the tumor and blood concentration data. The remaining data in that paper were collected by either me alone or in collaboration with Larson.

1.4: References

1. ACS, *Cancer Facts and Figures 2012*. American Cancer Society: Atlanta, GA, 2012.

2. Baronzio, G.; Gramaglia, A.; Fiorentini, G. Current role and future perspectives of hyperthermia for prostate cancer treatment. *In vivo* **2009,** 23, 143-146.

3. Algan, O.; Fosmire, H.; Hynynen, K.; Dalkin, B.; Cui, H.; Drach, G.; Stea, B.; Cassady, J. External beam radiotherapy and hyperthermia in the treatment of patients with locally advanced prostate carcinoma. *Cancer* **2000,** 89, 399-403.

4. Servadio, C.; Leib, Z. Hyperthermia in the treatment of prostate cancer. *Prostate* **1984,** 5, 205-211.

5. Van Vulpen, M.; De Leeuw, A.; Raaymakers, B.; Van Moorselaar, R.; Hofman, P.; Lagendijk, J.; Battermann, J. Radiotherapy and hyperthermia in the treatment of patients with locally advanced prostate cancer: preliminary results. *BJU Int.* **2004,** 93, 36-41.

6. Link, S.; El-Sayed, M. A. Shape and size dependence of radiative, non-radiative and photothermal properties of gold nanocrystals. *Int. Rev. Phys. Chem.* **2000,** 19, 409-453.

7. Hirsch, L. R.; Stafford, R. J.; Bankson, J. A.; Sershen, S. R.; Rivera, B.; Price, R. E.; Hazle, J. D.; Halas, N. J.; West, J. L. Nanoshell-mediated near-infrared thermal therapy of tumors under magnetic resonance guidance. *Proc. Natl. Acad. Sci. USA.* **2003,** 100, 13549-13554.

8. O'Neal, D. P.; Hirsch, L. R.; Halas, N. J.; Payne, J. D.; West, J. L. Photo-thermal tumor ablation in mice using near infrared-absorbing nanoparticles. *Cancer Lett.* **2004,** 209, 171-176.

9. Stern, J. M.; Stanfield, J.; Kabbani, W.; Hsieh, J. T.; Cadeddu, J. A. Selective prostate cancer thermal ablation with laser activated gold nanoshells. *J. Urol.* **2008,** 179, 748-753.

10. Dickerson, E. B.; Dreaden, E. C.; Huang, X.; El-Sayed, I. H.; Chu, H.; Pushpanketh, S.; McDonald, J. F.; El-Sayed, M. A. Gold nanorod assisted near-infrared plasmonic photothermal therapy (PPTT) of squamous cell carcinoma in mice. *Cancer Lett.* **2008,** 269, 57-66.

11. Huang, X.; Jain, P. K.; El-Sayed, I. H.; El-Sayed, M. A. Plasmonic photothermal therapy (PPTT) using gold nanoparticles. *Lasers Med. Sci.* **2008,** 23, 217-228.

12. Duncan, R. Polymer conjugates as anticancer nanomedicines. *Nat. Rev. Cancer* **2006,** 6, 688-701.

13. Kopecek, J.; Kopecková, P.; Minko, T.; Lu, Z. R. HPMA copolymer–anticancer drug conjugates: design, activity, and mechanism of action. *Eur. J. Pharm. Biopharm.* **2000,** 50, 61-81.

14. Overgaard, J. Combined adriamycin and hyperthermia treatment of a murine mammary carcinoma in vivo. *Cancer Res.* **1976,** 36, 3077-3081.

15. Anscher, M. S.; Samulski, T. V.; Dodge, R.; Prosnitz, L. R.; Dewhirst, M. W. Combined external beam irradiation and external regional hyperthermia for locally advanced adenocarcinoma of the prostate. *Int. J. Radiat. Oncol. Biol. Phys.* **1997,** 37, 1059-1065.

16. Issels, R. Hyperthermia combined with chemotherapy–biological rationale, clinical application, and treatment results. *Onkologie* **2000,** 22, 374-381.

17. Horsman, M.; Overgaard, J. Hyperthermia: a potent enhancer of radiotherapy. *Clin . Oncol.* **2007,** 19, 418-426.

18. Song, C. W.; Kang, M. S.; Rhee, J. G.; Levitt, S. H. Effect of hyperthermia on vascular function in normal and neoplastic tissues. *Ann. NY Acad. Sci.* **1980,** 335, 35-47.

19. Song, C. W. Effect of local hyperthermia on blood flow and microenvironment: a review. *Cancer Res.* **1984,** 44, 4721s-4730s.

20. Kong, G.; Braun, R. D.; Dewhirst, M. W. Characterization of the effect of hyperthermia on nanoparticle extravasation from tumor vasculature. *Cancer Res.* **2001,** 61, 3027-3032.

21. Kong, G.; Braun, R. D.; Dewhirst, M. W. Hyperthermia enables tumor-specific nanoparticle delivery: effect of particle size. *Cancer Res.* **2000,** 60, 4440-4445.

22. Matteucci, M. L.; Anyarambhatla, G.; Rosner, G.; Azuma, C.; Fisher, P. E.; Dewhirst, M. W.; Needham, D.; Thrall, D. E. Hyperthermia increases accumulation of technetium-99m-labeled liposomes in feline sarcomas. *Clin. Cancer Res.* **2000,** 6, 3748-3755.

23. Ponce, A. M.; Vujaskovic, Z.; Yuan, F.; Needham, D.; Dewhirst, M. W. Hyperthermia mediated liposomal drug delivery. *Int. J. Hyperthermia* **2006,** 22, 205-213.

24. Kopecek, J.; Kopecková, P. HPMA copolymers: origins, early developments, present, and future. *Adv. Drug Deliv. Rev.* **2010,** 62, 122-149.

25. Gormley, A. J.; Greish, K.; Ray, A.; Robinson, R.; Gustafson, J. A.; Ghandehari, H. Gold nanorod mediated plasmonic photothermal therapy: A tool to enhance macromolecular delivery. *Int. J. Pharm.* **2011,** 415, 315-318.

26. Pike, D. B.; Ghandehari, H. HPMA copolymer-cyclic RGD conjugates for tumor targeting. *Adv. Drug Deliv. Rev.* **2009,** 62, 167-183.

27. Gormley, A. J.; Malugin, A.; Ray, A.; Robinson, R.; Ghandehari, H. Biological evaluation of RGDfK-gold nanorod conjugates for prostate cancer treatment. *J. Drug Target.* **2011,** 19, 915-924.

28. Arap, M. A.; Lahdenranta, J.; Mintz, P. J.; Hajitou, A.; Sarkis, A.; Arap, W.; Pasqualini, R. Cell surface expression of the stress response chaperone GRP78 enables tumor targeting by circulating ligands. *Cancer Cell* **2004,** 6, 275-284.

29. Gormley, A. J.; Larson, N.; Sadekar, S.; Robinson, R.; Ray, A.; Ghandehari, H. Guided delivery of polymer therapeutics using plasmonic photothermal therapy. *Nano Today* **2012,** 7, 158-167.

30. Gormley, A. J.; Larson, N.; Banisadr, A.; Robinson, R.; Frazier, N.; Ray, A.; Ghandehari, H. Plasmonic photothermal therapy increases the tumor mass penetration of HPMA copolymers. *J. Control. Release* **Submitted**.

CHAPTER 2

LITERATURE BACKGROUND

2.1 Introduction

The prevalence of cancer in the United States is substantial. In 2008, it was estimated that nearly 12 million Americans were alive who have had a history of cancer.[1] Such figures and statistics project that about 1,638,910 new diagnoses and 577,190 deaths (or 1,500 people per day) will occur in 2012 alone.[2] These numbers make malignant neoplasms the second leading cause of death in the United States by only a small margin.[3]

The costs associated with this disease from a health and economical standpoint are enormous. From the patient's perspective, the implications of being diagnosed with cancer can be life threatening and quality-of-life reducing. In best-case scenarios where the prognosis is good, watchful waiting can add significant anxiety to the patient's life.[4] In worst-case scenarios, severe side effects to both the disease and therapy are expected in addition to dramatically reduced life expectancy. As a result, there is a very high prevalence (0-58%) of major depression in cancer patients which can impact both mood, lifestyle and overall outcome.[5]

The financial costs associated with this disease are similarly harmful to both the individual and economy as a whole. In 2007, it is estimated that the combined direct and

indirect costs of cancer were $226.8 billion.[2] In terms of direct medical expenditures (i.e. not including loss of productivity), the costs of cancer have doubled in the last 20 years.[6] This trend, however, is directly proportional to the number of new cases over the same period of time indicating that the cost per treatment is not likely the dominant contributor to this increase. In fact, there has been a slight decrease in the average medical expenditures per patient over time due to improved treatment technologies and a trend towards increased outpatient procedures.[7] While these figures are partially positive, as the prevalence of cancer continues to increase at the current rate, so will the financial burden on the United States' healthcare system.

To best mitigate some of these personal and financial costs, clearly the best approach is prevention. This is often difficult, however, as genetic and environmental factors are the primary causes of cancer. Lifestyle choices such as maintaining a healthy diet, participating in daily exercise and abstaining from smoking and drinking are positively correlated with decreased risk.[2] Given this and considering that the incidence of cancer continues to increase, an epidemiological survey of cancer types provides information where efforts may have the greatest impact. In 2012, it is estimated that cancer of the prostate, breast and lung will have the three highest numbers of new cases; 241,740, 229,060 and 226,160 respectively.[2] For this reason, significant attention and resources are provided to these three cancer types.

In this chapter, the topic of prostate cancer treatment will be discussed. An overview of prostate cancer such as disease development and progression will be followed by current treatment strategies including surgery, radiation, hormone and chemotherapy. In the context of improving drug delivery to prostate tumors, the field of

polymer therapeutics will be introduced including advantages, limitations and methods for improving delivery. Finally, PPTT will be described and how this technique might be able to improve the delivery of polymer therapeutics to prostate tumors.

2.2 Prostate Cancer

The human prostate, a walnut sized gland surrounding the urethra just below the urinary bladder, functions to secrete seminal fluid during male ejaculation. The pH of this secretion is regulated to be slightly alkaline to prolong sperm survival in the acidic environment within the vaginal tract. As men age, the risk of developing prostate cancer increases. Very few (<0.1%) men under the age of 50 develop neoplasms in the prostate.[8] However, after about 60-65 years of life, the risk of developing abnormal tissue growth in the prostate rises exponentially. In fact, some autopsy studies suggest that most men over 85 years of age are likely to have some histological evidence of prostate cancer.[9]

2.2.1 Disease development and progression

The causes of prostate cancer are mostly unknown. There appears to be a genetic basis behind this disease as mutations in several genes such as ribonuclease L (2',5'-oligoisoadenylate synthetase-dependent) (RNASEL) have been linked with familial prostate cancer.[10] Additionally, there is also a large difference in the incidence of prostate cancer between men of different races and cultures. While Asian men in China have the lowest incidence in the world (1.9 per 100,000 per year), African-American men in the United States are at the greatest risk for developing prostate cancer (137 per

100,000 per year).[8] The etiology of this disparity is likely to be a combination of genetic predisposition and differences in lifestyle associated with each culture.[11] For example, variants on chromosome 8q24 are strongly associated with increasing prostate cancer risk, a variant which is found more often in African-American men than those with European ancestry.[12] Also, the high-fat diet of men from Western societies is described as a potential risk factor which is in contrast to Asian men who typically consume less fat and more soy.[11]

Given the high incidence of prostate cancer in men over 60, regular screening has become commonplace. By far the most common screening method has been by detection of prostate-specific antigen (PSA) levels in blood. PSA is a serine protease found mostly in seminal fluid. During conditions of abnormal tissue growth in the prostate, PSA may be released into the blood. Such characteristic increase in blood level concentration can therefore be used as an indicator of prostate tumor development.[13] Men with PSA levels less than 4 ng/ml are generally considered at low risk with no further action required. As the PSA level reaches or rises above this threshold level, prostate biopsies may be recommended to confirm the presence or absence of neoplastic tissue.[13] While this screening tool is highly regarded, controversy surrounding its overuse and resulting high rates of unnecessary biopsies and treatments has led many to question its role in regular medical exams.

A positive prostate cancer diagnosis after biopsy is typically graded based on the pervasiveness of the disease and staged accordingly. Patients whose tumors are locally confined to the prostate, have a Gleason score less than 6 and maintain a PSA level of 10 ng/ml or less are generally considered low risk and have a 5-year survival rate of nearly

100%.[2, 11] Detection of cells in regional lymph nodes increases the overall risk, however the 5-year survival rate remains near 100%. Unfortunately, when cells have metastasized to distant organs such as the bone, have a Gleason score of 8 or more and a PSA level greater than 20 ng/ml, the prognosis drops dramatically. Patients in this category face a 5-year survival rate of 29% and make up the large majority of those who ultimately die of this disease.[2, 11]

2.2.2 Treatment

The treatment strategy for prostate cancer depends on the stage of the disease and the patient's life expectancy. In many cases where the PSA level is <10 ng/ml and the disease is locally confined, watchful waiting may be sufficient.[14-15] In such cases, the physician takes into account the patient's age as well as the risks associated with treatment. For example, if an 85-year old patient is presented with low grade prostate cancer where the 15-year survival rate is high, it may not be necessary to receive treatment as it is unlikely that this patient will ultimately die of this disease. On the other hand, if the patient is 50 years of age and has a 20-year life expectancy, more aggressive action may outweigh the risks of therapy.[16]

2.2.2.1 Radical prostatectomy

When the tumors are confined to the prostate gland itself, the most common treatment option is to remove the entire prostate. First performed in 1904 at John Hopkins Hospital,[17] a radical prostatectomy can be performed through either open surgery or laparoscopically. In both cases, three major concerns exist besides the usual

risks of surgery. First, the bundle of nerves which are responsible for erections are located on either side of the prostate. This proximity may then result in erectile dysfunction (~14% of patients[18]) if the nerves are damaged during surgery. Second, because the prostate gland is located just below the bladder and completely encircles the urethra, urinary incontinence is also possible (~7% of patients[18]). Finally, in locally advanced cases where some of the tumor mass is extracapsular, the boundaries of tumor mass invasion can complicate surgery as total resection may be difficult. Despite these complications, in general such procedures for local disease are considered curative with a strong history of success independent of procedure type.[19]

2.2.2.2 Radiotherapy

When the site of disease extends beyond the gland itself but remains localized to the surrounding tissue, the benefits of surgery may be limited. In such cases of locally advanced prostate cancer, the principle method for treatment is radiotherapy. The delivery of therapeutic radiation to the prostate can be by external beam radiotherapy or brachytherapy.[20] Both of these are considered to be curative treatments with equal efficacy and are often used in combination with hormonal therapy.[21] In the case of external beam radiotherapy, a typical treatment includes an initial dose of 45-50 Gy of the whole pelvis followed by dose escalation to about 78 Gy in a focused area around the prostate gland.[20] Above this 78 Gy dose, undesirable side effects of therapy such as incontinence or rectal bleeding are likely.[22] When brachytherapy is preferred, 60-120 metal seeds which contain Iodine-125 or Palladium-103 are strategically inserted within

the prostate.[20] In this way, a continuous low-dose of radiation is emitted near the cancerous tissue.

Following treatment with surgery or radiotherapy, the PSA level of the patient is monitored to evaluate treatment efficacy and detect tumor recurrence. If treatment was successful, then the PSA level should recede to a normal level with minimal rise over time. However, if a rise in PSA concentration is detected after therapy, then it is likely that the disease remains intact. In cases where it is believed that the disease remains local, second-line therapy using either of the approaches described above is possible. On the other hand, if the PSA concentration rises rapidly after treatment, a sign of metastases, then more aggressive action is required with palliative intentions.[23]

2.2.2.3 Androgen-ablation therapy

In 1941, Charles Huggins found that either castration or oestrogen therapy resulted in atrophy of the prostate gland as well as prostate cancer remission.[24] Since this initial discovery, it is now understood that conversion of testosterone to dihydrotestosterone (DHT) and subsequent binding to the androgen receptor regulates cell growth and survival of prostate and prostate cancer cells.[25-26] Such cell cycle dependence on circulatory androgens is therefore leveraged in the treatment of metastatic prostate cancer.

To deprive the prostate of androgens, several treatments can be employed either separately or in combination. These include surgical resection of the testes, administration of oestrogens, as well as inhibition of the pituitary gland using luteinizing hormone (LH)-releasing hormone (LHRH) receptor agonists. Each of these therapies

ultimately depletes the blood concentration of androgens and curtails the growth of prostate tumors.[27]

Androgen-ablation therapy in patients with bone metastases works very well to alleviate painful symptoms for an average of 14-20 months.[28] During this time, however, adverse effects due to endocrine manipulation are expected. These include hot flashes, bone loss and fractures, loss of sexual function, and weight gain.[28] After this period of time, an insensitivity to androgen depletion typically develops as androgen-independent prostate cancer cells are selected for survival.[27] For this reason, hormonal therapy is not considered a curative line of therapy.

2.2.2.4 Chemotherapy

The most dangerous and deadly form of prostate cancer is hormone refractory, metastatic prostate cancer.[11] In these cases, the last line of defense to relieve pain and extend life is cytotoxic chemotherapy. In general, the response of prostate cancer to most chemotherapeutic agents is disappointing.[29] In the 1980s, a number of drugs were tested in Phase II studies where a partial or complete response to therapy was observed in only 5% of patients.[30] This dampened enthusiasm, however, was reversed when new studies indicated that prostate cancer cells are particularly sensitive to mitotic spindle inhibitors such as paclitaxel and docetaxel.[31-32] These findings led to two major clinical trials investigating their utility against hormone-refractory prostate cancer.[33-34] Results from these studies indicate that treatment with Docetaxel can increase median survival by 18.9 months with significantly reduced pain in 35% of patients. Since then, palliative

treatment of hormone refractory, metastatic prostate cancer with chemotherapy has become the standard-of-care.[35-37]

2.2.2.5 Hyperthermia

A less common form of prostate cancer therapy, but one which is relevant to the present review, is treating tumors with hyperthermia. The treatment of neoplastic tissue with heat alone is tumoricidal for which there are several known reasons. The treatment of cells with heat results in cytotoxicity as a function of thermal dose (i.e. temperature and time).[38] While there are several reasons for this, the main belief is that heat induces protein denaturation and irreversible aggregation. Under conditions of mild hyperthermia (<41°C), cells are thermotolerant due to HSP expression which prevents or refolds denatured proteins.[39] As temperature and time is increased, the cells are not able to respond to the heat stress effectively and the cells undergo programmed cell death.[40] Such effects are more cytotoxic when the cell is undergoing mitosis thus making cancer cells more thermosensitive.[38, 41]

The other and more significant reason why tumors are sensitive to hyperthermia relates to its poorly formed vasculature and blood flow. Relative to healthy tissue, tumor vasculature is heterogeneous in architecture, largely devoid of smooth muscle and highly fenestrated.[42] This has several consequences on the tumor microenvironment. First, because the microvascular density is highly variable, blood perfusion is sluggish and not uniformly distributed resulting in regions with high interstitial hypertension, hypoxia and acidosis.[43] Second, tumor vasculature is hyperpermeable and therefore the transport of fluid as well as large and small molecules is unregulated.[44] Lastly, the lack of a

significant basement membrane and smooth muscle layer in much of the tumor microvasculature limits the capacity of this tissue to respond to stress.

The natural response of healthy tissues to heat stress is to vasodilate, increase blood flow and ultimately dissipate the heat through greater tissue perfusion.[45] Such activity is viable over a broad spectrum of temperatures (typically up to 50°C) and is therefore resistant to heat induced stress. In tumors, however, the above differences in the tumor microenvironment become problematic at elevated temperatures. Insufficient blood flow and perfusion, particularly in the hypoxic regions of the tumor, do not allow residual heat to be dissipated efficiently.[46-47] As temperatures within the tumor rise above 43°C, the weak microvasculature is unable to withstand the added stress and damage results followed by blood flow stasis.[48] The added heat and lack of tissue oxygenation then causes a dramatic decrease in intratumor pH resulting in ischemia and cell death.[49-50]

Despite these apparent advantages of treating tumors with hyperthermia, practice in the clinic particularly in patients with prostate cancer has been slow. The primary reason for this has been due to difficulties in delivering therapeutic doses of heat only to the cancerous tissue.[51] Current strategies such as interstitial or regional hyperthermia using micro- or radiowave emitters as well as whole body hyperthermia have been met with some degree of success,[52] though direct control of tissue heating is limiting. For this reason, most have used clinical hyperthermia as an adjuvant therapy with either chemo- or radiotherapy.

2.2.2.6 Adjuvant hyperthermia and chemo- or radiotherapy

In the 1970s and 80s, it became apparent to the clinical community that hyperthermia alone was unlikely to be a standalone form of therapy for reasons mentioned above. Also around this time, however, it was discovered that hyperthermia significantly sensitizes cells and tissue to both chemo and radiotherapy.[51] These findings reenergized enthusiasm for hyperthermia and a number of studies and clinical trials sought to determine the mechanism of synergism and its overall utility in the clinical setting.

Exposure of cancer cells to elevated temperatures was found in some cases to sensitize them to chemotherapeutic drugs.[53-54] This effect was drug and temperature dependent. While hyperthermia is able to potentiate the activity of platinum-containing anticancer drugs at low temperatures[55] as well as doxorubicin at higher temperatures,[56-59] other drugs such as docetaxel have only an additive or independent effect.[60-61] Experiments which attempt to elucidate the underlying mechanism for this thermal enhancement, typically expressed as a thermal enhancement ratio (TER), suggest that heat facilitates membrane transport resulting in higher cytoplasmic drug loading.[56, 58]

In clinical trials, adjuvant hyperthermia with chemotherapy has had mixed results but are mostly encouraging. For example, in cases where the patient has peritoneal surface malignancies such as with ovarian or cervical cancer, the use of hyperthermic intraperitoneal chemotherapy with cisplatin is shown to improve overall outcome.[62-64] In the case for prostate cancer, there are very few reports suggesting that this technique is valuable most likely due to the insensitivity of drugs like docetaxel to hyperthermia.[65]

Combining hyperthermia with radiotherapy is also synergistic and has been shown to provide greater benefit in patients than hyperthermia plus chemotherapy.[51] The underlying mechanisms which provide this synergism are somewhat controversial, though several hypotheses are supported by experimental findings. At the cellular level, it is believed that heat inhibits the cells' ability to repair radiation-induced DNA damage.[66] This process is heavily dependent on treatment sequence and timing as well as temperature such that maximum efficacy is achieved when heat ($\geq$43°C) and radiation exposure are applied concurrently.[67] At the whole tissue level, changes in blood perfusion during heating are believed to be responsible for radiosensitization. In general, cancer cells are less sensitive to radiation in hypoxic environments. During mild hyperthermia (<43°C), increased blood perfusion and therefore reoxygenation of the hypoxic tumor environment decreases the survival rate of cells during exposure.[67]

Clinical trials which study the potential of adjuvant hyperthermia and radiotherapy to treat locally advanced prostate tumors are also mixed.[68-71] Each of these trials show some benefit of combining heat with radiation, however patient survival and overall outcome were typically no different than those treated with radiation alone.

2.2.3 Treatment limitations and the need for targeted therapies

It was mentioned earlier that when prostate cancer is localized, it is probable that the disease can be treated with curative intentions. In many of these cases, however, watchful waiting is chosen because the risks may outweigh the benefits of therapy despite the high cure rate. When the disease has metastasized beyond the prostate and invaded other organs such as the bone, more aggressive therapy is required. These therapies are

however quite harmful and are thus limited by non-specific toxicities. This highlights a significant need for improvement.

The concept of developing therapies which are targeted to specific cells while leaving the healthy ones intact is credited to Paul Ehrlich who postulated "we have to learn how to aim chemically."[72] Indeed, when the goal is to impose a pharmacologic or physical effect on diseased tissue, any collateral damage to healthy tissue can have devastating consequences. Ehrlich's concept of the magic bullet ultimately led to the development of today's chemotherapeutic strategies which have some pharmacologic bias towards cancerous cells, though uptake in non-intended cells remains still the greatest challenge.

With advances in polymer chemistry and antibody based therapies in the 1970s, macromolecular based targeted therapies were born. In systems like those conceptualized by Helmut Ringsdorf,[73] large carriers can be used to target sites of disease and deliver therapeutic payloads. Such targeted therapies are an important component of a field now coined "nanomedicine," and represent a significant improvement in cancer therapies which limit side effects while maximizing treatment efficacy.[74] Indeed, such targeted therapies have attracted widespread attention in oncology and are likely to provide substantial benefits in future prostate cancer therapies.[75]

2.3 Polymer Therapeutics

The use of polymers in medicine has been evolving since their introduction during World War II. Polymers can be tailor made with numerous properties depending on the monomers used, their stoichiometic ratios, the molecular weight, as well as the degree of

crosslinking among many other design parameters. Also, recent advances in synthetic techniques such as with living free radical polymerization allow these polymers to be synthesized with a high degree of control. In this way, polymers can be designed to be biocompatible, biodegradable, stimuli responsive, functionalizable and bioactive.[76]

One of the greatest uses of polymers as biomaterials lies in their capability to be designed for controlled delivery of bioactive agents. In most cases where drugs or proteins are used to impose therapeutic action, it is advantageous to control its local or systemic concentration within the therapeutic index as a function of time. For example, a bolus dose of free drug may only temporarily bring the drug's concentration within a therapeutic range prior to rapid redistribution and elimination. As most drugs are more effective when this concentration is maintained over longer periods of time, many biomedical devices and therapeutics leverage the tailorability of polymers to control chemical delivery. Examples of such systems include drug-eluting stents, hydrogels and transdermal patches.

In the context of developing controlled delivery systems for systemic disease, water-soluble polymers have proven very useful.[77] The incorporation of drugs or therapeutic macromolecules within polymeric drug carriers provides several distinct advantages. First, for drugs which are poorly miscible in blood plasma, the highly water-soluble backbone of the polymers provide enough hydrophilicity to dissolve the drugs without the need of other excipients.[78-79] This characteristic is of particular importance considering the large number of new drugs which exhibit poor absorption, distribution, metabolism, and excretion (ADME) due to poor aqueous solubility.[80] Second, by incorporating drugs within carriers, it is possible to substantially alter their

pharmacokinetics to provide longer plasma retention.[81] Third, the macromolecular size of these conjugates allow them to preferentially accumulate in neoplastic tissue due to the leaky nature of its vascular.[82] Fourth, the wide diversity of available linker chemistries enables one to control both the drug release mechanism and rate.[83] Fifth, as many drugs and therapeutic proteins are easily degraded by plasma components such as enzymes, the polymers are able to provide some protection. Finally, the multifunctional nature of many of the polymeric systems allow for the incorporation of other moieties such as targeting groups or imaging agents for targeting and theranostic applications.[84-85]

2.3.1 Polymer therapeutic types

The wide diversity of available polymer chemistries, architectures and linkers provide a rich environment for investigational research in the development of new polymer therapeutics. Some of these designs are currently being used in the clinic, and many more are in clinical trials.[86] While these parameters offer a large number of possible polymer therapeutic designs, the majority fall into four basic categories: polymer-protein conjugates, polymer-DNA complexes, polymeric micelles and polymer-drug conjugates.[87]

2.3.1.1 Polymer-protein conjugates

Since the early 1980's, the biotechnology industry has grown substantially.[88] Starting with the development of recombinant insulin, many large pharmaceutical and small biotech companies have been developing a wide range of therapeutic proteins and peptides with striking clinical impact. While many hurdles such as cost of production are

prohibitive, more often it is their poor plasma solubility, stability, immunogenicity and half-life which compromise their therapeutic potential.[89] One approach many companies and drug delivery scientists have taken to improve their biocompatibility is to link them to water-soluble polymers such as PEG.[90] Conjugation of PEG in this way can help mask the protein's surface to reduce immune detection and degradation.[91] Addition of PEG can also increase the solubility of the protein, provide charge shielding as well as increase its molecular weight which ultimately improves its pharmacokinetics and biodistribution.[92]

Because of these apparent benefits, the process of protein PEGylation has become an industry standard. PEG is most often the polymer of choice here due to high water-solubility and flexibility, low immunogenicity and toxicity, and the number of available conjugation chemistries.[90] It is also a Food and Drug Administration (FDA) approved material which helps companies obtain fast approval for their therapeutics relative to similar polymers which are not yet found in the clinic. This has led to a wide variety of PEGylated proteins which are currently being used in the clinic such as PEG-L-asparaginase (Oncaspar®), PEG-interferon-α (PEG-Intron®) and PEG-granulocyte colony-stimulating factor (Neulasta®).[87] While such PEGylation is most commonly used, other polymers such as styrene maleic anhydride (SMA),[93] hydroxyethyl starch (HES),[94] and dextrin,[95] are also used.

2.3.1.2 Polymer-DNA complexes

The field of gene delivery has likewise been met with many opportunities as well as challenges. Many diseases such as muscular dystrophy and cystic fibrosis are caused

by defective genes which may be effectively treated by gene replacement. Unfortunately, gene replacement or supplementation is difficult due to biological barriers for gene delivery.[96] Currently, the two main methods for delivering genes are by using either recombinant viruses or synthetic vectors such as polymer-DNA complexes.[97] Both mechanisms of delivery have weaknesses, however significant concerns over the immunogenicity of viral vectors have caused many to focus on polymeric systems called polyplexes.

Polyplexes are typically formed by complexing negatively charged DNA with cationic polymers. When such systems form, large DNA coils which are typically several hundred nanometers in hydrodynamic diameter are condensed into toroidal or spherical particles which are significantly smaller in size (tens of nanometers).[98] Of particular importance in the formation of these polyplexes is the ratio of +/- charges as this determines the final size and shape of the particle as well as the residual charge. For example, while complete neutralization of charges is advantageous in terms of particle pharmacokinetics, colloidal instability often necessitates some residual charge.[99] Control over these features mostly arrives from the choice of cationic polymers and from their size, architecture and composition. Linear copolymers of PEG-poly(L-lysine)[100] and PEG-poly(ethyleneimine) (PEI)[101] with amino terminated pendant groups as well as branched polymers of PEI and poly(amidoamine) (PAMAM) dendrimers[102] are among the most commonly used polymers in this regard. Use of these polymers also serves a similar function as was described for polymer-protein conjugates. They are able to protect the DNA from nuclease degradation and immune detection as well as improve overall pharmacokinetics and diseased tissue specificity through targeting. Despite

significant progress in gene delivery using nonviral vectors, the barriers for gene delivery have limited this class of polymer therapeutics and none have obtained clinical success to date.[103]

2.3.1.3 Polymeric micelles

Another class of polymer therapeutics takes advantage of the poor aqueous solubility of most drugs by incorporating them within the hydrophobic domains of polymeric micelles. Polymeric micelles form by the self-assembly of amphiphilic polymers into colloidal dispersion.[104] Therefore, by sequestering hydrophobic drugs within the core of micelles which are protected by a highly hydrated corona, these drugs can be easily transported in the blood and specifically delivered to the site of interest upon micelle disassembly. The formation of micelles from amphiphilic compounds are a common occurrence due to the minimization of free energy when the monomeric amphiphiles reach a certain concentration.[105] This critical micelle concentration (CMC) varies greatly depending on the nature of the surfactant and the temperature of the solution. The process of micelle self-assembly can result in a wide variety of shapes and sizes, though most micelles used for drug delivery are spherical and 10-80 nm in size.

The composition of the polymers which form into micelles for drug delivery varies. Polymers can be polymerized to form homopolymers, or copolymerized as random, block or graft copolymers. While homopolymers are unable to form into micelles, copolymerization with hydrophilic and hydrophobic monomeric units can result in the formation of micelles, particularly as di- or tri-block copolymers. The choice of hydrophilic and hydrophobic monomers is also important. Given the biocompatibility

and hydrophilicity of PEG, most micelles have PEG based coronas.[106-107] Though other hydrophilic polymers such as poly(*N*-isopropylacrylamide) (PNIPAAm)[108-109] and poly(*N*-vinyl-2-pyrrolidone) (PVP)[110] are also used. The choice in the composition of the hydrophobic cores is more variable. Many use poly(lactic-co-glycolic acid) (PLGA) due to its known biodegradability.[106, 111] Others incorporate poly(styrene),[112] poly(propylene oxide) (PPO),[113] and poly(caprolactone)[114] blocks due to their hydrophobic character. Taken together, the combination of these hydrophilic and hydrophobic blocks allow for the formation of highly stable and tailorable micelles for drug delivery. A common example of such systems is Pluronic® micelles made from PEG-PPO-PEG tri-block copolymers.[115]

Using these miceller drug delivery carriers, it is possible to achieve drug loading efficiencies between 5 and 25% wt.[116] Because these otherwise poorly soluble drugs are able to be retained in the plasma for extended periods of time, many of these micelle systems are being evaluated in clinical studies.[117] Examples include NK105, a PEG-poly(aspartate) micelle loaded with paclitaxel,[118] NC-6004 which is a PEG-poly(glutamic acid) micelle with cisplatin,[119] NK012 which is a PEG-poly(glutamate) micelle with a SN-38 payload,[120] and SP1049C Pluronic®-doxorubicin micelle.[121] In the future, it will be exciting to see the outcome of these clinical trials and the emergence of newer formulations.

2.3.1.4 Polymer-drug conjugates

While polymeric micelles carry drugs by noncovalently sequestering them within their hydrophobic cores, polymer-drug conjugates act by covalently linking the drugs to

the polymer backbone.[87, 122-123] Conjugation of drugs to polymers offer the same advantages as the other polymer therapeutics, i.e.: increased drug solubility, prolonged plasma retention, improved biodistribution, protection from immune detection and degradation, macromolecular size and added multifunctionality. Unlike the other systems, however, by tailoring the linker chemistry it is possible to provide a high degree of control over drug release mechanism and rate with improved overall stability. The linking of drugs to the polymer via a pH sensitive or hydrolysable bond is one such example, though these methods for drug release often lack the necessary sensitivity towards release in the tumor compartment, or suffer from poor stability and premature drug release.[124-126] Kopeček and coworkers have investigated a number of linker chemistries which are susceptible to enzymatic degradation in the lysosome.[127-134] The end result was the identification of the oligopeptide sequence Gly-Phe-Leu-Gly (GFLG) which degrades in the presence of cathepsin B in the lysosome, a tetrapeptide now used in most HPMA copolymer-drug conjugates.[83, 133] Much work remains, however, to optimize linker chemistries for sufficient drug release in tumors.

In the scope of polymer-drug conjugates, many designs exist. The most fundamental of these, like in other polymer therapeutics, relates to the choice in polymer backbone. Most are water-soluble and offer a range of conjugation chemistries. Below is a brief description of the most commonly used polymers.

Similar to PEG-protein conjugates, PEG-drug conjugates offer high water-solubility, flexibility, low immunogenicity and toxicity and can be produced with low polydispersities. PEG is also available with many different functional groups at its terminal ends, and so conjugation to drugs is straightforward using click chemistry.[135]

Unfortunately, because only two drug molecules can be attached per linear polymer chain, low drug loading (1.7 wt%) reduces the efficacy of these systems as exemplified by the fact that only one PEG-drug conjugate has been evaluated in clinical trials (PEG-camptothecin).[136]

PGA potentially represents one of the most clinically relevant polymers for use as a polymer therapeutic, mainly due to its biodegradability.[137] Formed by the polymerization of glutamic acid monomers, enzymatic degradation of its amide bonds results in the formation of degradation products which are non-toxic. Drugs can be conjugated to its backbone by taking advantage of the γ-carboxylic acid side chains and released by enzymatic degradation. A major advantage of these systems relative to the non-degradable synthetic polymers such as PEG is that their molecular weight can be kept high so that they are not excreted through the kidneys.[138] This significantly lengthens their plasma pharmacokinetics and thus the opportunity for accumulation in cancerous tissue. A major disadvantage though is the high density of negative charges on these polymers as each pendant group contains a carboxylic acid which can initiate rapid reticuloendothelial system (RES) uptake. Several PGA-drug conjugates are currently being evaluated in clinical trials,[139-141] though the most promising of these (PGA-paclitaxel or CT-2103) has recently shown disappointing results in phase III clinical trials.[142-143]

Dextrin and HES are two other biodegradable polymers for use as polymer-drug conjugates. Both are naturally derived, generate nontoxic degradation products and are approved for use in humans. Dextrin is derived from corn starch and can be fractionated to obtain large or small molecular weight linear polymers. Subsequent succinylation

provides sites for drug conjugation and therefore can be used as a long circulating drug carrier.[144] HES is derived from waxy maize starch and has a highly branched like structure and is currently used as a plasma expander due to its high molecular weight and hydrophilicity.[94] Drug or protein conjugation can be obtained by modification with hexamethylene diamine or *N*-carbobenzyloxy glutaminyl glycine.[145] Though native dextrin and HES are degradable, attachment of drugs or proteins may reduce their rate of degradation and therefore concerns over long-term toxicity with repeated infusions raise similar issues as with synthetic, nondegradable polymers.[146]

While most of the synthetic polymers used in drug delivery have a linear structure, PAMAM dendrimers are unique due to their highly branched architecture. Starting with an ethylenediamine core, stepwise addition of methyl acrylate, then ethylenediamine increases the size and generation with each step.[147-148] For example, Michael addition of methyl acrylate to ethylenediamine results in a 0.5 generation or G0.5 PAMAM dendrimer which has four branches with methyl ester terminating functional groups.[149] Subsequent amidation of the esters creates the first full generation dendrimer, G1.0. With this method, full and half generation PAMAM dendrimers can be created up to G10.0 after which point charge shielding and steric hindrance prevent further generations from being easily synthesized. The resulting dendrimers typically have very low polydisersities (1.0005-1.10), and have very high charge densities on their surface.[148]

The large number of available functional groups provides many sites for drug attachment. Early examples of this concept by Duncan and colleagues showed the conjugation of cisplatin where high drug loading (20-25 wt%) and tumor accumulation

was observed.[150] Since then, many more combinations of dendrimers and anticancer drugs have been applied including G4.0-doxorubicin,[151] G4.0-camptothecin,[152] G3.5-SN38,[153-154] and G5.0-methotrexate.[155] One of the advantages of these conjugates relates to the dendrimer's ability to cross biological barriers such as the intestinal epithelia.[154, 156-163] Though studies which show significant dendrimer toxicity due to their high surface charge, particularly full generation amino terminated dendrimers, provide some cautionary examples of their use.[164-166]

Of all the polymers which have been investigated for use as polymer-drug conjugates, HPMA copolymers are probably the most studied in detail.[167] Led by the pioneering work of Kopeček and colleagues,[168] followed by collaboration with Duncan, HPMA copolymers have proven to be a versatile platform for the development of anticancer polymer therapeutics. The reason for this relates to their known biocompatibility, ease of synthesis and available multifunctionality.[169] The HPMA monomer provides these copolymers with high water-solubility, and copolymerization with side chains containing drugs, targeting moieties and imaging agents makes these conjugates multifunctional.

Given their utility as drug carriers, many HPMA copolymer-drug conjugates have been tested in clinical trials.[170] The first of these polymer-drug conjugate was PK1, a HPMA copolymer-doxorubicin conjugate.[171] This landmark study provided initial excitement with these conjugates as polymer conjugation enabled patients to be dosed with four- to five-fold more doxorubicin compared to free drug. Unfortunately, poor phase II outcomes where only six of 62 patients showed signs of partial response dampened this enthusiasm.[172] Similarly, when a new conjugate (PK2) which contained

galactosamine for active tumor targeting was tested, few patients benefited from this therapeutic.[173-174] Since these initial results using HPMA copolymers in the clinical setting, more conjugates have entered clinical trials such as HPMA copolymer-paclitaxel,[126] -camptothecin,[175-177] and –platinates.[178-179] Excluding HPMA-camptothecin which had problems with nonspecific drug release, each of these conjugates have also shown only partial response in patients.

2.3.2 Limitations of polymer therapeutics

As discussed above, polymer therapeutics provide clear advantageous to treat disease over small molecular weight drugs. They are water-soluble, have prolonged plasma half-life, can distribute to diseased tissue with higher specificity, may overcome multidrug resistance, and reduce overall toxicity such that higher maximum tolerated doses (MTDs) can be achieved. Despite these indications for improved treatment performance, the number of available polymer therapeutics in the market remains limited. The reasons for this have to do with problems with the therapeutics' overall design as well as the biological barriers that prevent them from reaching the target. Such challenges include carrier toxicity, insufficient release rate, instability, uptake by RES, limited therapeutic scalability and characterization, as well as suboptimal delivery and tissue mass penetration. Detailed discussion of each of these is beyond the scope of this Chapter, though for more information the reader is encouraged to read a comprehensive review elsewhere.[86]

Of the limitations which were just listed, possibly the most influential barrier to success is limited tumor delivery and penetration. A common method for displaying

tumor accumulation data is by calculating the percent injected dose per gram of tissue (%ID/g). Using these units, a nanomedicine is considered to have high tumor localization when above 10 %ID/g. If you consider, however, that most tumors used in preclinical studies are on average 50 mg by weight, then the total dose delivered to the tumor is only 0.5 %ID. Translating this idealized scenario in mice bearing subcutaneous tumors to humans, where the average cost of treatment using an approved polymer therapeutic is about $30,000 not including hospital costs,[180-181] then only about $150 worth of therapeutic is actually imposing any therapeutic effect. The remaining $29,850 is either urinated out or accumulates in organs of the RES where toxicity occurs. This major imbalance coupled with severe side effects that patients have to endure highlights the need for improved methods for drug delivery.

2.4 Methods and Tools for Improved Delivery to Solid Tumors

For a particular drug or therapeutic protein within a nanocarrier to go from the injection to the subcellular target (protein, nucleic acid, etc), it must successfully navigate multiple barriers.[182] Upon injection, the therapeutic must become soluble in the blood plasma and be resistant to protein opsonization.[183] If significant opsonization occurs and forms a protein corona, phagocytic detection and RES clearance is probable. As most drug delivery systems require prolonged blood circulation to be efficacious, the therapeutic must then avoid both RES and renal clearance for an extended period of time (several hours to days). As the nanomedicine enters the tumor's vasculature, it must then permeate through the vascular endothelium and enter the tumor interstitial space. In order to have maximal effect, it must then be transported through the dense interstitial

space and reach cells which are distant from the tumor's viable vasculature.[184-185] As macromolecules are unable to diffusively cross the cell's plasma membrane, they must then bind to the cell's surface and initiate endo- or phagocytic uptake. If bound via degradable linker, the drugs must then be cleaved from the polymeric carrier and escape the endosome. Finally, binding to the target protein, or transport through the nuclear envelope and subsequent binding to nucleic acids represents the last step before therapy can initiate. Given this daunting journey, it is perhaps not surprising then that much less than 1% of the injected dose actually has any effect.

Given this grand challenge, many strategies are employed by drug delivery scientists to improve outcome. In the following sections, some of these strategies are reviewed in the context of improving the delivery of nanomedicines to solid tumors.

2.4.1 Passive targeting and the EPR effect

It has been known for a long time that the blood vessels which supply solid tumors are disorganized and have higher than average permeability to macromolecules.[186-187] In the 1970s, this increased permeability was leveraged to screen for tumors by scintigraphy using gallium-67 which has known affinity for transferrin.[188-189] Then, in 1986 when Maeda and colleagues were studying the tumor delivery of SMANCS (SMA-neocarzinostatin), they observed that this hyperpermeability in combination with poor lymphatic drainage caused the micelles to accumulate and be retained in tumors.[93] Recognizing the contributions of hyperpermeability and poor drainage, they described their observation by coining the phrase 'Enhanced Permeability and Retention' (EPR) effect.[190] Since this landmark paper,[93] the EPR effect has been

applied ubiquitously to describe the passive delivery of macromolecules and nanomedicines to solid tumors.

The underlying principles and translatability of EPR remain somewhat controversial, particularly considering that most studies are performed in rodents bearing fast growing, subcutaneous tumors. However, studies with these tumor models provide some insight. When one initially compares the vasculature of tumors versus healthy tissue, it is apparent that tumor vessels form with an abnormal and disorganized architecture.[43, 191-192] The spatial distribution of blood vessels lacks order and continuity which ultimately generates a heterogeneous distribution of tissue which is poorly perfused.[193] The structure of individual blood vessels is also poorly formed and lacks smooth muscle. The endothelial cells have overlapping and branched morphologies with large intercellular and transcellular openings up to 4.7 μm in size.[82] These large fenestrae then explain tumor blood vessel leakiness which allows macromolecules such as albumin to permeate.

The disorganized and tortuous nature of tumor vasculature coupled with macromolecular hyperpermeability and limited lymphatic drainage has a consequential impact on the tumor microenvironment.[194] Poor plasma drainage and increased red blood cell accumulation causes a significant increase in the viscosity of the blood in tumors.[195] This increased viscosity provides resistance to flow and may be responsible for overall decreased blood flow in tumors.[42] The higher concentration of albumin and other proteins in this tissue also causes hypertension which increases the tumor's interstitial pressure.[196-197] This too limits the degree of convective transport of small and large molecules into the tumor interstitial space. Finally, high cell and extracellular matrix

(ECM) density provides more resistance to convective and diffusive transport of macromolecules.[198] Taken together, these transport barriers reduce the availability of oxygen and other essential nutrients in tumors thereby creating large regions which are hypoxic and necrotic.[199]

In the context of delivering nanomedicines to solid tumors, these transport barriers become exaggerated due to their large size. The population of intercellular openings in the tumor's vasculature is highly heterogeneous in size, location and density. While some may exist as large as several microns in size, the majority are 1-2 μm.[82] This size cutoff thereby excludes particles which are greater than roughly 1.5 μm from taking advantage of the EPR effect.[200] Also, as much of the transport of molecules out of the tumor's vasculature and through the interstitial space depends on diffusion, the size of the particle will dictate how far it can travel. As described by the Stokes-Einstein equation, larger particles will have less diffusive transport than smaller particles and therefore may not access cancerous cells which are distant from the vasculature. Also, given that the density of the ECM in tumors is prohibitively high for effective diffusive transport over long distances,[201] larger particles such as liposomes and inorganic colloids may lack overall effectiveness even though they are within the size range of EPR.[202-203]

Despite these barriers, the passive delivery of nanomedicines such as polymer therapeutics by EPR remains a viable approach. Many drug delivery systems from polymer therapeutics, to monoclonal antibodies to AuNPs rely on EPR to selectively accumulate in cancerous tissue.[204] And while issues such as human translatability and pervasive distribution throughout the whole tumor mass raise significant concerns over

the effectiveness of this approach, it is partially responsible for the 20 plus biologicals and nanomedicines available in the clinic.

2.4.2 Receptor-mediated active targeting

Monoclonal antibody therapies have received significant attention in the last two decades and many are currently used in the clinic. When properly humanized and protected from the immune system, they are able to circulate for extended periods of time and bind with high specificity and affinity to their target receptors on cancer cells.[205] In this way, antibodies can directly initiate cancer cell apoptosis upon binding, tag cancer cells for immune detection and elimination, or be used as carriers for drugs and radionuclides.[206] Such systems therefore represent a series of emerging nanomedicine based technologies which utilize receptor-mediated active targeting to deliver therapeutics with high cellular specificity.

Inspired by Paul Ehrlich's concept of targeted therapies, many drug delivery scientists aim to improve the delivery of their 'magic bullets' by conjugating a wide variety of biomolecules which have known specificity to cancer cell receptors. Popular examples of targeting approaches include antibodies against epidermal growth factor receptor (EGFR) such as anti-HER2,[207-209] folate receptor targeting with folic acid,[210-212] transferrin receptor targeting,[213-216] and angiogenesis targeting with RGD.[217-221] Each of these examples have proven selectivity towards cancerous tissue due to overexpression of the targeted receptors.

Many liposomal based systems have been functionalized with antibody or antibody fragments for this purpose.[208, 222-224] In some cases, this approach has resulted

in increased delivery of the targeted liposomes relative to control liposomes.[225] In most examples, however, equal or less tumor accumulation is achieved.[208, 226] Such results do not necessarily preclude these systems from being more valuable than the untargeted systems. Unless the targeting ligand is used to target the tumor's vasculature, passive delivery by EPR is the necessary first and often delivery-limiting step.[227] Then, as the nanocarriers diffuse through the tumor interstitium, receptor-mediated targeting may facilitate cellular binding and uptake and therefore drug delivery.[228]

Due to the known advantages of this approach, clinical translation of an actively targeted HPMA copolymer-doxorubicin conjugate was attempted.[173] Galactosamine, a derivative of galactose, has known affinity for asialoglycoprotein receptors which are overly expressed in liver and hepatocellular tissue.[229] When linked to an HPMA copolymer containing doxorubicin, liver targeting was achieved in both rats and mice.[230-232] These results led to pursuing this conjugate in a Phase I clinical trial.[173-174] Results from these studies showed that targeting to the liver was high (15-20 %ID), but that targeting to hepatic tumors was substantially lower (3.3 %ID). Additionally, relative to its untargeted PK1, targeting to the liver significantly lowered the MTD of this conjugate. Such accumulation in the healthy liver tissue is thus limiting and highlights the need for active targeting improvements.

Based on the number of reports which provide conflicting support for active targeting, there are clearly a large number of challenges that may reduce the viability of this approach. From a formulation or colloidal dispersion standpoint, functionalization with antibodies, antibody fragments, peptides, etc may reduce the overall stability of the nanocarriers in water or plasma. Once in the blood, these ligands which are designed to

be biorecognizable may then facilitate RES clearance and dramatically reduce blood circulation time. Then, as was the case for the HPMA copolymer-galactosamine conjugates, targeting to healthy cells which also express the targeted receptor may expose these cells to the drug and result in unwanted toxicity. Other examples of variables which may impact active targeting viability include ligand-receptor binding affinity, receptor expression heterogeneity within the same tumor or across patient populations and receptor saturation. Each of these barriers prevent the majority of active targeted nanomedicines from having real clinical benefit and a better understanding of these events is ultimately required.

2.4.3 Pharmacologic enhancement of delivery

As mentioned in Section 2.4.1, there are several tumor microenvironment characteristics that resist diffusive and convective transport of drugs and nanomedicines. These characteristics are: 1) vascular heterogeneity, 2) high blood viscosity, 3) sluggish blood flow, 4) elevated interstitial pressure, 5) poor lymphatic drainage, and 6) dense interstitial matrix due to abnormally high cellular and ECM densities.[233] Though most often discussed in the context of improving delivery, neither EPR, a natural phenomenon, nor receptor-mediated targeting act to alleviate any of these major delivery barriers. This may be because these barriers are a direct consequence of tumor physiology which cannot be easily resolved by changing the design of the therapeutic. Therefore, efforts which aim to improve delivery by decreasing the contribution of each of these barriers have focused on pharmacologic based interventions.

One method which Maeda, Jain and others have used to increase tumor blood flow and transmural pressure (ratio of arterial pressure to tumor interstitial pressure) between the vasculature and tumor interstitial space is to elevate overall blood pressure.[234-238] It was previously observed that raising the mean arterial blood pressure to 150 mmHg using angiotensin II results in a marked increase in tumor blood flow.[239] This effect was found to be selective to cancerous tissue. The mechanism behind this phenomenon is most likely related to the inability of tumor microvessels to respond to elevated blood pressure by autoregulatory contraction as well as increased transmural pressure which drives convective transport.[234] To show then that this technique can be used to improve the delivery of macromolecules, Maeda and colleagues artificially raised the blood pressure in mice using angiotensin II followed by administration of SMANCS.[235] Treatment in this way resulted in a 1.2-1.8-fold increase in overall tumor delivery while less accumulation occurred in the bone marrow and small intestine. Translating this concept into a clinical setting, patients with a variety of carcinomas were co-administered angiotensin II and SMANCS and evaluated for tumor delivery and overall outcome.[236] Similar to their previous findings, hypertension was able to improve the delivery of SMANCS as well as overall response to the drug. This pharmacologic based technique is thus an interesting and clinically relevant approach for improving the delivery of nanomedicines.

Similar approaches using other vasoactive drugs to modulate tumor blood flow and permeability have been tried.[240] Maeda and others have leveraged nitric oxide (NO) as a tool to vasodilate surrounding blood vessels to permit greater blood flow and therefore drug delivery.[234, 241] Indeed, topical application of nitroglycerin on the tumor

resulted in 2 to 3-fold enhancement of polymer-drug conjugate delivery.[241] Alternatively, when inhibitors of NO were tested, significant decreases in tumor blood flow occured.[242] Interestingly, when vasoconstrictor drugs other than angiotensin II such as phenylephrine were tested for similar purposes, no changes or slight decreases in tumor blood flow were observed.[243]

Vascular disrupting agents (VDAs), drugs or proteins which act on the already established tumor vasculature, have also been tested. For example, tumor necrosis factor-α (TNF-α), a major proinflammatory cytokine, acts strongly on vascular endothelial cells and increases vascular permeability by formation of large intercellular gaps.[244] Administration then of TNF-α is capable of enhancing EPR and the delivery of macromolecules.[245] Because systemic administration of TNF-α produces significant toxicity, delivery by adsorption to AuNPs is being evaluated in a Phase II clinical trial.[246] Using this delivery scheme, AuNP-TNF-α conjugates were also able to improve macromolecular permeability.[247]

Because of its known effect on macrophages to stimulate TNF-α production, 5,6-dimethylxanthenone-4-acetic acid (DMXAA) has also been tested for its capacity to increase tumor vascular permeability. Administration of DMXAA in mice with or without TNF receptor or gene knockdown was found to enhance EPR.[248] Because enhanced permeability occurred in mice with or without TNF receptor or gene knockdown, these authors suggest that DMXAA can improve vascular permeability in a TNF-α independent manner. Though VDAs have shown to increase vascular permeability, they are also well known to reduce tumor blood flow,[249] and an appropriate

balance of dose may therefore be required to leverage the full potential of these drugs to improve macromolecular delivery.

Unlike VDAs whose target is already established vasculature, antiangiogenic drugs aim to prevent the formation of new tumor blood vessels. In the 1970's, Judah Folkman postulated that tumor growth is dependent on continual angiogenesis and that inhibition of this process might stunt its growth.[250] Since this landmark paper, a large number of groups have investigated the utility of this line of therapy, and many antiangiogenic therapies are used clinically. More recently, Rakesh Jain has described an alternative use of antiangiogenic therapy which at first seems counter intuitive.[191] The inhibition of angiogenic stimulators such as vascular angiogenic growth factor (VEGF) initiates vascular remodeling.[251] This remodeling process effectively prunes those vessels which are characteristically leaky and immature and thus limit blood flow. The result is a "normalization" of the tumor's vasculature to a state which has improved blood flow and therefore tissue perfusion.[43] The impact of this vessel normalization was observed when antiangiogenic therapy was combined with radiation therapy. Increased vascular function and therefore tumor oxygenation due to antiangiogenic normalization has been shown to synergistically improve radiation therapy.[252] When anti-VEGF antibodies were used to decrease colon adenocarcinoma microvessel density, increased tumor perfusion and chemotherapeutic delivery was achieved.[253] While increased blood flow and decreased intratumoral pressure occur after this process, it is likely that decreased vessel leakiness and therefore EPR will also result. To study this, Jain et. al. evaluated the passive delivery of differently sized nanoparticles after vascular normalization. Indeed, antiangiogenic treatment did reduce vascular pore size suggesting

that smaller nanocarriers are required for efficient delivery after vascular normalization.[254]

Each of the previously described methods for enhancing drug delivery pharmacologically has used drugs which act on the tumor's vasculature to improve blood flow and/or vascular permeability. This is because drug delivery is primarily vascularization limited. However, improving local blood flow and permeability may not necessarily improve overall outcome because the dense tumor interstitium limits the diffusivity of small and large molecules.[185] High cellular and ECM density coupled with high interstitial fluid pressure (IFP) resists transport in a size dependent manner. One method then to improve overall delivery is to reduce interstitial density and IFP. For example, treatment of tumors with chemotherapy initiates cell death and therefore reduces cellular density.[255] This decompression then allows for greater transport of drug after repeated drug administration. Direct injection of ECM enzymes such as collagenase produces a similar result. Digestion of ECM components increases the diffusion of macromolecules in a size dependent manner.[256] For this reason, many now are developing multistage nanoparticle systems which are initially large for prolonged blood circulation, but then break apart into smaller particles or release free drug once in the tumor space.[257-259]

2.4.4 Physical enhancement of delivery

Tumor blood vessels are also subject to externally applied forces to increase blood flow and permeability. If the location of the diseased tissue is known, the physician may be able to treat the region with either ultrasound or heat for this purpose. Each of these

may be useful tools for enabling the clinician to play a more active role in choosing the location of enhanced drug delivery.

Ultrasound has been used primarily for medical imaging due in part to its low cost and safety. The absorption of ultrasound by various tissues can also be used with therapeutic intentions.[260] High-intensity and focused ultrasound (HIFU) can ablate tissue through heating and is used in some cases in the treatment of prostate cancer.[261] Another interesting application of ultrasound in the context of the current review topic is in its ability to improve the delivery of macromolecules across biological barriers.[262] Depending on the frequency and intensity of the ultrasound, acoustic cavitations can occur in tissue during ultrasound treatment. These cavitations produce mechanical deformations and cell-cell junction disruption which causes normally semi-permeable barriers to become hyperpermeable.[263] For example, Mitragotri and Langer have used ultrasound to permeabilize skin and enable transdermal adsorption of proteins.[264] The transport of drugs, macromolecules and nucleic acids through the plasma membrane can also be improved using ultrasound through sonoporation.[265-266] In regards to transvascular transport, the effect is similar. Ultrasound treatment of the blood-brain barrier, an endothelial lining with characteristically tight cell-cell junctions, temporarily disrupts this tissue and allows for drug delivery to the brain.[267-268] In tumors, such treatment can also improve transvascular delivery.[269] Increased vascular permeability from ultrasound treatment is capable of improving the tumor accumulation of drug carrying macromolecules.[270] This effect is, however, significantly less advantageous in tumor tissue relative to that observed with the BBB as this tissue is already permeable to macromolecules.[271]

In Section 2.2.2.6, the advantages of combining hyperthermia with chemotherapy were introduced. At the cellular level, hyperthermia is able to improve the intracellular delivery of small molecular weight drugs that can provide synergistic treatment.[54] When these drugs are incorporated within nanocarriers such as a polymer therapeutic, the same may also be true but by a different mechanism. Recent findings, for example, have shown that hyperthermia can increase the rate of both endo- and phagocytosis which may then potentiate macromolecular uptake and intracellular delivery.[272-273] Another level of synergism is obtained when the temperature does not significantly exceed 43°C where severe vascular damage occurs. At such elevated temperatures (41-43°C), tumor blood flow can increase roughly two-fold.[274] This change in blood flow then increases the overall availability of macromolecules to extravasate. Unfortunately, the extent of this increased blood flow is not to the same degree as healthy tissue due to the lack of a smooth muscle layer and the overall tortuous nature of intravascular circulation.[45, 48] In fact, many suggest that this observed increase is actually due to changes in surrounding blood vessels which supply the tumor and therefore force more blood inflow.

A consequence of this forced blood perfusion then is increased vascular pressure. Similar then to the tumor microvascular changes which occur with elevated blood pressure, the weak endothelial layer is not able to resist this pressure and heat adequately and increased vascular permeability results.[275-276] Such increased permeability is believed to be a result of cytoskeletal disaggregation in endothelial cells leading to further expansion of the intercellular junctions that already surround them.[38, 277-279] This increase in vascular permeability and therefore EPR has been leveraged to improve nanomedicine delivery. Initial studies in this area focused on the extravasation of

liposomes when combined with hyperthermia.[280-283] The application of heat facilitated the extravasation of PEGylated liposomes in a time and temperature dependent manner. In most cases, a low thermal dose (temperature < 42°C, time < 30 min) does not result in a substantial increase in liposomal delivery.[281] As the thermal dose is increased, so does the delivery of liposomes where a 47-fold increase has been observed using intravital microscopy.[283] Of particular interest in these studies was the use of temperature sensitive liposomes which could release their drug contents with temperature. A similar study using hyperthermia to enhance the delivery of HPMA copolymers was also completed, however in this case, no thermal enhancement of delivery was observed.[284]

These studies then led Dewhirst and colleagues to more carefully evaluate the increased permeability and its impact on nanoparticle delivery.[285-288] In one study, the thermal dose was varied and the extravasation of liposomes was imaged using intravital microscopy.[287] They observed that at temperatures below 40°C, no increased extravasation occurred. As the tumors were treated with temperatures above 40°C, liposomes began to extravasate in a temperature and time dependent manner. This increased vascular permeability continued up to 6 hours after heat treatment, after which time the tumor permeability recovered to normal levels.[287] They explain this to be because of endothelial cell repair after this time. Heating of tumors above 43°C resulted in vascular hemorrhaging. When they compared these effects as a function of nanoparticle size, major differences between small (~7 nm) and large (100-400 nm) nanoparticles were observed.[285] The smaller systems, albumin in this case, were relatively unaffected by treatment with hyperthermia. The larger nanoparticles, liposomes between 100 and 400 nm, on the other hand had low tumor accumulation

without hyperthermia but had significantly enhanced delivery with hyperthermia. This too was size dependent with the 100 nm liposomes having the greatest tumor delivery with hyperthermia, though still just as good as albumin without heat treatment. The explanation provided in this paper for this size dependency relates again to the increased pore size with heat treatment. While the smaller particles can freely extravasate due to the relative large size of the intercellular openings in the endothelial layer, larger particles may be more restricted due to their similar size. When the tissue is heated and these openings are enlargened, this resistance may play less of a dominant role allowing them to permeate to a larger extent. When tested in a feline tumor model, similar enhancement of delivery was observed.[286] Unfortunately, these nanoparticle systems continue to suffer with heterogenous tissue distribution and poor interstitial penetration after thermal therapy.[289]

2.4.5 New delivery enhancement methods

Each of the above listed techniques will not likely be sufficient as a standalone means of enhancing the delivery of polymer therapeutics. Passive delivery by EPR remains the most attractive means of enhancing delivery, and many groups tailor the physicochemical properties of these conjugates to maximize the EPR effect. Unfortunately, as seen with the large number of clinical trials which do not show significant benefits, this alone will not translate these technologies into viable therapeutics with real benefit for patients. Clearly more efforts to enhance site specific delivery are required. In this context, delivery enhancement mechanisms which are more tumor selective are preferred. Hyperthermia, for example, has a degree of selectivity

towards cancerous tissue, however the means of delivering the appropriate thermal dose without harming the surrounding healthy tissue remains a challenge. Therefore, an alternative means of delivering heat with greater tumor selectivity is preferred to enhance the accumulation of polymer therapeutics in prostate tumors.

One such method that has been applied to deliver heat in a localized fashion to treat prostate cancer is HIFU.[261, 290-291] HIFU treatment of localized prostate cancer is performed by inserting a trans-rectal ultrasound probe and positioning it such that it may provide focused ultrasound on the prostate gland. Initially, an ultrasound crystal used for imaging is utilized to determine the correct position of the probe to ensure that only the prostate tissue itself will be treated. Then, another crystal which is capable of delivering therapeutic doses of energy is turned on and the targeted tissue is heated through constructive interference of the ultrasound waves at the focal point. In this way, well defined regions of tissue are heated.

HIFU is currently approved for use in Europe and Asia for the treatment of prostate cancer, and it is likely that it will also be approved for use in the United States in the near future. Despite these apparent advantages for using HIFU to deliver heat, it has a few limitations. Mainly, its use is not selective towards cancerous tissue and therefore proper focusing of the probe on only the cancerous tissue is critical. This can be difficult considering that the margins of what is cancerous and normal are often unknown, particularly by ultrasound imaging. In cases when the disease remains localized to the gland itself (Stage I and II), this is not too problematic as complete ablation of the entire gland is acceptable. When it is locally advanced, however, the proximity of the cancerous tissue to the rectal wall makes treatment difficult. Also, slight movement of

either the patient or probe during treatment may have unintended consequences. Finally, due to the focused nature of the beam, it is difficult to uniformly heat large regions of tissue during therapy. For these reasons, though likely to provide significant treatment value in the near future, HIFU may not represent the ideal tool for treating prostate cancer tissue with heat.

2.5 Plasmonic Photothermal Therapy (PPTT)

A recent method of selectively delivering heat to tumor tissue takes advantage of the plasmonic properties of colloidal gold. Of special interest in this regard is the unique capacity of these colloids to scatter and absorb light. Under conditions of particle SPR, strong light absorption results in particle heating. When located within a tumor mass, direct tissue heating can occur with laser light excitation. Termed PPTT, this heating process can be used as a means to induce tumor hyperthermia with therapeutic intentions.[292-294]

In the following sections, AuNPs will be introduced as well as a description of their properties. Their use as antennas for PPTT will then be described as well as the potential of using this technology to enhance the delivery of other nanomedicines such as polymer therapeutics to prostate tumors.

2.5.1 AuNPs and SPR induced heating

Gold has captured human attention long before Egyptian alchemists described it as the perfect metal. As a colloid, the colors that dispersed AuNPs create led to their use in stained glass during the Roman Empire. However, the origin of this color remained

unknown until 1857. In his Bakerian lecture, Michael Faraday described colloidal gold particles (or sols) that are able to scatter and absorb light in a size dependent manner.[295] These revolutionary findings ultimately laid the foundation for the field of plasmonics and colloidal chemistry.

When an electrical potential is applied to metallic gold, the electrons which lie in the conduction band of its atoms will become mobile and move in the direction of the electrical field. As the electrical field generated from photons is also capable of remodeling the spatial charge distribution in gold, it is possible to control electron wave propagation by light excitation. When the spatial distribution of these mobile electrons is confined near their mean-free path (~40-50 nm), it is possible to coherently excite these electrons into resonance.[296] Because the surface represents the main boundary conditions for such gold structures, this coherent oscillation of free electrons produces SPR. Though SPR can be found on many roughened gold surfaces, due to the inherent nanoscale size of AuNPs, SPR represents the principal contributor to their unique optical properties.

Under conditions of SPR the free electrons are excited into the conduction band and oscillate in-phase with the electromagnetic radiation.[297] This in effect polarizes the surface of the AuNPs and creates a dipole (Figure 2.1 A).[296] Such polarization of these conductive electrons gives rise to both strong light scattering and absorption under conditions of resonance (Figure 2.1 B). This light scattering is due to the fact that the oscillating dipole also acts as an emitter of electromagnetic radiation whose frequency is equal to that of the incident light wave. Meanwhile, the intense light absorption results from the heavier ionic core of the nanoparticle which acts as a restoring force to the induced dipole. The pioneering work which first modeled these light-AuNP interactions was by Gustav Mie in 1908 where

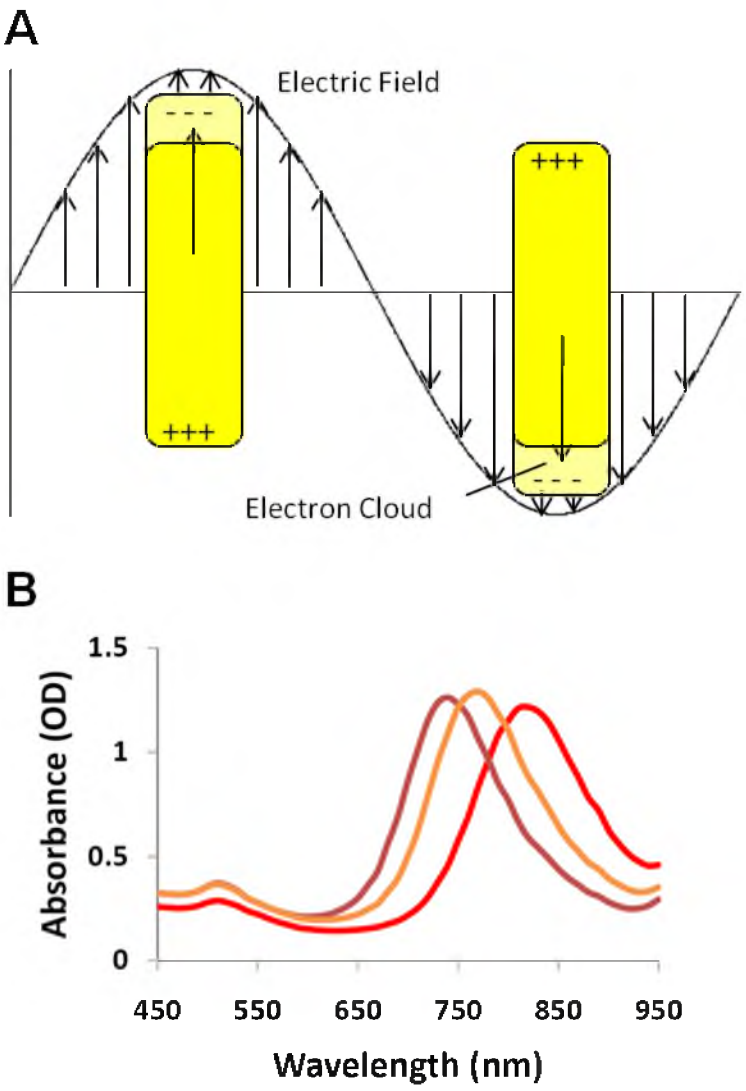

Figure 2.1: Scheme showing the interactions of light with GNRs. When photons pass near GNRs, the electrical field is capable of remodeling the spatial organization of its electrons (A). Under conditions of SPR, strong light absorption can occur over a tunable range of wavelengths (B).

he derived Maxwell's equations to describe their extinction cross-section.[298] For particles which are considered small relative to the wavelength of light (2R < 25 nm), the Mie theory is reduced to the following relationship: [299]

$$\sigma_{ext} = \frac{9\omega V \varepsilon_m^{3/2}}{c} \bullet \frac{\varepsilon_2(\omega)}{[\varepsilon_1(\omega) + 2\varepsilon_m]^2 + \varepsilon_2(\omega)^2} \qquad \text{Equation 2.1}$$

where V is the volume of the particle, ω is angular frequency of the electromagnetic radiation, c is the speed of light, and ε_m and $\varepsilon(\omega) = \varepsilon_1(\omega)+i\varepsilon_2(\omega)$ are the dielectric functions of the surrounding medium and the particle's material respectively. Here, conditions of resonance are fulfilled when $\varepsilon_1(\omega) = -2\varepsilon_m$ where the extinction cross-section is inversely proportional to the imaginary part of gold's dielectric function. In this relationship, the intrinsic size influence on light extinction originates from the dependency of gold's dielectric function on particle diameter [$\varepsilon = \varepsilon(\omega,R)$]. For particles larger than 25 nm, however, they are not able to be homogeneously polarized as equation 2.1 assumes and therefore higher-order modes of Mie's equations dictates that σ_{ext} directly depends on particle radius.[299] Such extrinsic size effects means that as particle size increases, so does the wavelength of light which induces SPR.

Besides the dependence on particle size, the shape of AuNPs significantly contributes to their light extinction cross-section. For anisotropic AuNPs, i.e., aspect ratio (AR) > 1.0 such as with GNRs, two plasmon absorption bands develop; one for the short axis (transverse) and another for the elongated axis (longitudinal) (Figure 2.1 B). Because of the anisotropic nature of these particles, unlike uniform spheres, there exists a polarization

dependency on light extinction. Therefore, Richard Gans extended Mie's theory to average light extinction over all orientations for prolate and spheroidal particles.[300-301] In this way the following relationship was developed indicating that σ_{ext} is dependent on AR instead of size:

$$\sigma_{ext} = \frac{\omega V \varepsilon_m^{3/2}}{3c} \bullet \sum_j \frac{(1/P_j^2)\varepsilon_2}{\left[\varepsilon_1 + \{(1-P_j)/P_j\}\varepsilon_m\right]^2 + \varepsilon_2^{\,2}}$$

Equation 2.2

where P_j are the depolarization factors along the three axes A, B and C with A > B = C as with GNRs and

$$P_A = \frac{1-e^2}{e^2}\left[\frac{1}{2e}\ln\left(\frac{1+e}{1-e}\right)-1\right],\ P_B = P_C = \frac{1-P_A}{2},\ \text{and}\ e = \left[1-\left(\frac{B}{A}\right)^2\right]^{1/2} = \left(1-\frac{1}{R^2}\right)^{1/2}.$$

Equation 2.3

Here the resonant condition is fulfilled when $\varepsilon_1 = -\varepsilon_m(1-P_A)/P_A$. From this model it is observed that as AR of the GNR is increased, the location of SPR is red shifted. For example, GNRs with an AR = 2.1, 3.0 and 3.7 have a λ_{max} at 610, 709 and 780 nm respectively.[301] An important point to be made about anisotropic AuNPs such as GNRs is that by increasing AR, the SPR peak is red shifted significantly such that λ_{max} can be located in the NIR or infrared (IR) spectrum. Such SPR in the NIR spectrum is advantageous for PPTT or imaging because penetration of light through tissue is greater at these wavelengths than that of visible light (though still limited to only a few centimeters).[302]

When the incident light wave is absorbed by the particle, excitation of the dense population of free electrons is enough to result in electron-electron scattering and therefore thermalization of the electron gas around the gold surface (Figure 2.2).[303-304] The heat generated in the electron gas is subsequently cooled by electron-phonon coupling where the energy is transferred to the gold lattice.[305] Finally, phonon-phonon coupling of the hot lattice to the surrounding medium results in energy transfer and Joule heating of the suspending fluid. The calculations required to compute heat generation as a function of incident light power are complex and typically require finite element models to solve the involved partial differential equations (PDEs) and are therefore beyond the scope of this Chapter. However, for such information using small ($R < 25$ nm) spheres, the following reference is provided.[306] That being said, as the light extinction cross-section is equal to the sum of the light absorbance and scattering cross-sections ($\sigma_{ext} = \sigma_{abs} + \sigma_{sca}$), one can more easily determine the efficiency of energy conversion to heat by first calculating σ_{abs} then dividing this by σ_{ext}. For AuNPs which are spherical, this calculation is relatively straightforward by applying Mie's equations. For GNRs, however, where this polarization dependency exists, the absorbance cross-section can be calculated by integrating the resistive heating over the volume of the particle and dividing by the incident power density.[307] Similarly, the scattering cross-section can be found by integrating the outgoing electromagnetic energy flux over the boundaries within which it exists:

$$\sigma_{abs} = \frac{2\int U_{av} dV}{n\sqrt{\varepsilon_0 / \mu_0}\,|\vec{E}_{inc}|^2}, \qquad \sigma_{sca} = \frac{\int |\vec{E}_{far}|^2 \, d\Omega}{|\vec{E}_{inc}|^2} \qquad \text{Equation 2.4}$$

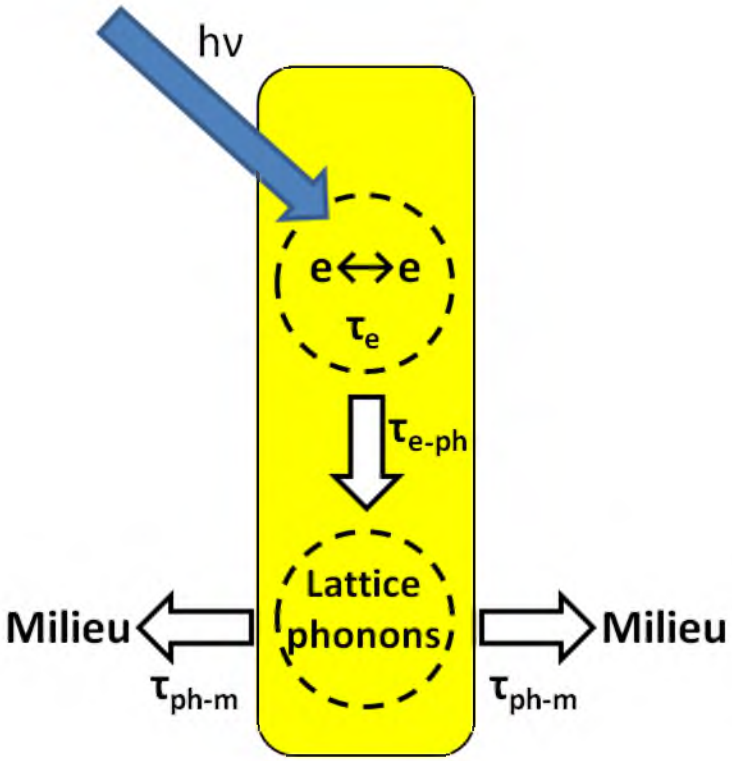

Figure 2.2: Sketch of the energy relaxation processes after excitation of nonequilibrium electrons in a GNR. τ_e, $\tau_{e\text{-}ph}$, and $\tau_{ph\text{-}m}$ are the characteristic times for internal thermalization of the electron gas, electron-lattice phonon thermalization, and particle phonon-milieu energy exchanges, respectively (adapted from [296]).

where U_{av} is the power adsorbed by the particle in the form of ohmic losses, n is the refractive index of suspending fluid and $|\vec{E}_{inc}|$ and $|\vec{E}_{far}|$ are the amplitudes of the incident and far electric field respectively. In this reference, the finite element method was also employed to solve for resistive heating as a function of volume and it was found that due to the large light absorption cross-section of GNRs relative to their scattering cross-section, an efficiency of 93% is expected.[307] Experimentally this value was found to be much less (60%), however AuNPs of this shape (rods vs. shells) were found to be the most efficient at photothermal conversion.

When describing the use of GNRs for PPTT, there are some practical issues that must be considered which may impact their light absorption and energy conversion capacity. The intensity of induced SPR under NIR excitation is heavily influenced by dephasing of the coherent plasmon oscillations. In general, such dephasing is a natural phenomenon such as when electron-surface scattering occurs. However, when exposed to the complex biological environment, a variety of changes to their physicochemical properties may amplify such dephasing and therefore reduce their energy conversion efficiencies. For example, adsorption of proteins and other biomolecules to the gold's surface is possible upon exposure to blood. In such situations, by a process known as chemical interface damping (CID), the empty lowest unoccupied molecular orbital (LUMO) of the adsorbed molecules may couple to the resonating, surface free electrons of the gold.[296] Such CID would therefore dephase this coherence and result in broadening and reduction of plasmon light adsorption. Similarly, as exposure to blood with a significant electrolyte concentration results in reduction of electrostatic repulsion of charged particles, the GNR suspension may flocculate. Under conditions of such sterically stabilized flocculation, the decreased separation distance

between GNRs may allow some resonant energy transfer between particles and therefore broadening and reduction of plasmon light adsorption. Both examples therefore highlight the need for a GNR suspension whose polymer coating is sufficiently dense that adsorption of biomolecules and flocculation is minimized so that heat conversion efficiency is maximized.

2.5.2 Delivery to tumors

The strong light absorption and heat conversion efficiency of AuNPs makes these nanoconstructs particularly apt as antennas for PPTT. However, their effectiveness is precluded by their ability to localize in tumor masses which are accessible by fiber optics. In some cases, they can be injected directly into the tumor mass immediately before laser radiation.[308] However, in situations where the boundaries of cancerous and healthy tissue are unknown, as is the case for advance localized prostate cancer, direct injection cannot be selective towards neoplastic tissue and unwanted damage can result during therapy. In this situation, systemic administration and delivery by EPR may be required to provide malignant selectivity.

In order to deliver AuNPs via EPR, they must be non-toxic and long circulating. Fortunately, as a bulk metal, gold has well known biocompatibility. However, the nanoscale size and diverse surface chemistry of AuNPs may have more impact on their overall biocompatibility than of the metal itself. For example, the size and shape of AuNPs have been shown to influence uptake and toxicity.[309-312] This design parameter though seems to be less important than surface chemistry. The surfactant cetyltrimethylammonium bromide (CTAB), which is used during GNR synthesis, is well known to be toxic to cells and therefore must be removed prior to exposure.[313]

Nanoparticle charge, which is a consequence of surface chemistry, has a significant impact on cellular toxicity. Those with strong positive surface charges or zeta potentials are known to be toxic towards cells.[314] Similarly, particle size, shape and surface charge can have a significant impact on blood retention and biodistribution where less charged and elongated AuNPs often have greater biodistribution characteristics.[315]

The importance of particle surface chemistry and zeta potential has more to do with protein opsonization and immune detection than direct interactions with the cell surface. Within seconds of exposure to blood plasma, the particle's surface quickly adsorbs proteins.[316] As the blood contains a large diversity of plasma proteins with different physicochemical properties, one would expect that adsorption would be heterogeneous with preferences for some proteins, but not others. It has been observed that while 69 different proteins can adsorb to a AuNP's surface (compared to over 3700 available proteins in plasma), there is preferential binding for albumin, apolipoprotein, immunoglobulins, complement, and fibrinogen.[317-318] This is particularly the case for fibrinogen which has the highest adsorption to gold, despite its lower concentration in plasma relative to more abundant proteins such as albumin. While gold-thiolate bond formation or Van der Waals adsorption may be the principle reason for strong protein adsorption, charge-charge interactions between the particle's surface and the protein dominate the extent to which some proteins adsorb because these forces occur over longer distances. As protein adsorption is often unwanted particularly when exposed to biological milieu, preparation of self-assembled monolayers with long, flexible organic chains such as PEG provide steric hindrance preventing such components from accessing

the gold surface and adsorbing.[319] PEGylation of the particle's surface in this way is a well proven method to extend their blood circulation.[320]

Once in circulation, they are able to extravasate into the tumor interstitium due to EPR and therefore accumulate in the diseased tissue with a degree of specificity. However, as previously discussed, this delivery is heterogeneous through the tumor volume. Microscopy studies have provided some insight into the intratumoral distribution of nanoparticles. A comparison of GNRs and gold nanoshells showed that both are primarily located in the peripheral regions of the tumor and remained within close proximity of the tumor vasculature.[321] This was most apparent for GNRs which showed greater tumor accumulations than shells. These results are not surprising given their size and therefore hindered ability to permeate through the dense tumor interstitium. Similar findings have been observed with liposomes.[203] This heterogeneous delivery then has consequences on the pattern of tissue heating which is observed to also be heterogeneous.[322]

2.5.3 PPTT and tumor ablation

The concept of PPTT was originally described by West and colleagues using gold nanoshells.[323] In this landmark paper, they developed NIR absorbing PEGylated gold nanoshells which were delivered to breast carcinoma xenografts and heated with a NIR laser. Laser radiation (4 W/cm^2) of the tumors resulted in significant tumor heating (ΔT = 37.4°C) and substantial tissue damage. When mice were treated with the same therapy and the tumors were allowed to grow, photothermal treatment resulted in cure of all tumors.[324] Since these initial reports, a large number of papers have described use of this

technique to thermally ablate tumors both *in vitro* and *in vivo*.[207, 294, 308, 325-328] In these studies, NIR absorbing GNRs or gold nanoshells were used to generate high temperatures to damage vasculature and through direct cell killing.

The mechanism by which heating causes vascular damage and cell death has been discussed in Section 2.2.2.5, and it is likely that PPTT does this primarily in the same way. The presence of heating AuNPs in the proximity of or within cells causes direct cell killing through an additional mechanism. When AuNPs are heated by surface plasmon excitation, the temperature on the particle's surface can become hot enough to produce microbubbles.[329] This is particularly the case when the laser light is provided in short (femtosecond) pulses where cavitations can occur. When the nanoparticles are then located within cells or on the plasma membrane, the microbubbles can cause mechanical damage. The result is organelle damage, increased plasma membrane permeability and membrane blebbing.[330-333] This advantage of localizing the particles on the cell's plasma membrane is therefore taken advantage of when active targeting is employed where greater cell death due to increased membrane blebbing occurs.[334-336]

With respect to the types of AuNPs available for PPTT, a wide variety of designs exists. The most important of these relates to the particle's size and shape. AuNPs which are either very small (< 5 nm) or very large (>1 μm) do not typically exhibit strong plasmon light absorption nor favorable biodistribution and are therefore not commonly used. Therefore, most fall within this size range. The particle's shape is an important parameter in terms of its biodistribution, but more importantly its light extinction cross-section. Gold nanospheres, for example, typically have an SPR peak around 550 nm whereas GNRs and gold nanoshells are typically within the NIR spectra. Because light

penetrates most tissue maximally in the NIR range,[302] gold nanospheres are not typically used for PPTT. When comparing GNRs with gold nanoshells, the two most commonly used nanoparticles for PPTT, GNRs exhibit higher light absorption in the NIR spectra per unit size as well as faster heating dynamics.[307, 337] Many other AuNP shapes exist such as stars, cages, triangles, rattles, etc.,[338] and future work comparing their utility in tumor therapy against GNRs and nanoshells will be intriguing.

Clinical translation of PPTT will likely face many challenges and opportunities. Since their initial paper in 2003, West and colleagues have started a company (Nanospectra Biosciences, Inc., Houston, Texas) using gold nanoshells to treat patients with head and neck cancer in a Phase I trial. One preclinical study using a naturally occurring canine brain tumor model provided initial and encouraging results that such therapy may ultimately be useful.[339] However, concerns over patient long term toxicity due to AuNPs in the liver and spleen will need to be thoroughly addressed.

2.5.4 PPTT and combination therapy

The majority of studies applying PPTT for tumor therapy have been done with tissue ablative intentions. Tumor heating above 50°C, well above the temperature required to ablate its vasculature, is not difficult to achieve using low-powered laser diodes and therefore cure of subcutaneous tumor models is widely reported.[308, 323-324, 327] Of interest, however, is the possibility of using the precise control over heating to modulate the tumor microenvironment to facilitate the potency of other therapeutics. As mentioned in Section 2.4.4, several labs have used hyperthermia for this purpose to improve the delivery of liposomes.[280, 285-287, 340] The methods these groups have used to

treat the tumors with heat do not offer tissue selective control of heating in a well defined manner. Heating with a water bath provides a source of heat exterior to the skin at a predefined temperature, though direct control of temperature within the tumor core cannot be easily manipulated. Also, this method for delivering heat is not a clinically viable approach to heat most tumors. Treatment with high-energy radiofrequency probes can injure the tissue upon insertion of the probe and produces regions of high heat or hot spots immediately adjacent to the probe's surface and is not selective towards the cancerous tissue.[341] For these reasons, PPTT may offer an advantage due to its selectivity towards cancerous tissue, depth of heat generation in tumors less than a few centimeter and precise control of heat delivery by modulating laser power output. Additionally, because the AuNPs do not permeate far from the tumor's leaky vasculature, providing the sources of heat directly near blood vessels may offer better control of blood flow and vascular permeability.

There are a few studies where mild PPTT was used to improve the outcome of other therapies. In one example, gold nanoshells were used to mildly heat colorectal tumors between 42-45°C in combination with radiotherapy.[342] The aim here was to increase overall blood perfusion in tumors using PPTT so that radiotherapy could be more effective. It was observed that treatment with mild PPTT does in fact increase the blood perfusion of tumors and that combined treatment with radiotherapy provides a greater outcome than either treatment alone. This study also observed significant vascular collapse when higher laser powers were used which could also improve overall outcome in the clinical setting.[342]

Three additional studies reported by the Bhatia and Sailor groups used GNR mediated PPTT to improve the delivery of liposomes, micelles and magnetic nanoworms.[343-345] In each of these experiments, GNRs were used to heat tumors between 43-45°C for up to 30 minutes. In the first of the three papers, they were able to improve the localization of doxorubicin-loaded liposomes as well as nanoworms by increasing the tumor's blood perfusion and permeability with PPTT.[343] Next, they replaced these with temperature sensitive liposomes and micelles so that the heating could also trigger drug release in addition to overall accumulation.[344] Similar to those findings by Dewhirst and others,[283] treatment of the tumors with heating by PPTT increased the extravasation and drug release from these temperature sensitive nanomedicines. Finally, by increasing the temperature to 45°C to ensure vascular damage and ultimately clot formation, they followed this therapy with fibrin binding nanoworms and liposomes to facilitate localization to the site of clot formation after PPTT.[345] Each of these studies, in addition to the previously described study, highlights the potential role of PPTT to act synergistically with both chemo and radiation therapy.

2.5.5 Advantages and disadvantages

Compared to current methods for delivering heat to tumors for treatment with hyperthermia, PPTT offers many advantages which have already been discussed. The extravasation of nanoparticles through the leaky vasculature of tumors provides some selectivity towards cancerous tissue. This is in contrast to radiofrequency and ultrasound based ablation technologies where the tumor margins must be known in order to avoid healthy tissue damage. The use of laser light to deliver heat is also advantageous as the

power output and site of illumination is easy to control using standard fiber optics which are already used in the clinic for laser light surgery. Also, direct heating of cells and tissue using nano-antennas as energy converters localizes the heat directly within the site of interest. All of these advantages among others make this technology promising.

There are several major disadvantages of PPTT that are worth discussing. First, intravenously administered AuNPs over 10 nm ultimately distribute mainly to the liver and spleen.[346] This highlights a significant concern over their safety as they are non-degradable and not readily excreted. Second, the limited penetration depth of NIR light (< 2 cm) limits PPTT to tumors which are small in size and easily accessible with a fiber optic. Similarly, though the AuNPs are typically injected intravenously, PPTT is a localized therapy and may not be valuable to treat distant metastases. Finally, heterogeneous nanoparticle distribution in the tumor and limited access of tumor margins with the laser light increases the possibility of nonablative rims existing after therapy which may ultimately recur. Each of these disadvantages represents significant barriers to success which will likely limit this technology from existing as a standalone form of therapy.

2.6 Conclusions and Implications for Prostate Cancer Therapy

When a patient is presented with locally advanced prostate cancer that is unresectable, radiotherapy represents the primary form of care. Chemotherapy is an attractive means of treating these tumors, however the toxicity profile of the available drugs outweigh the benefits and is therefore not used until the disease has formed distant metastases. Strategies to alter drug pharmacokinetics using nanocarriers are under heavy

development and it is anticipated that these efforts will yield substantial benefits for patients with prostate cancer. The challenges which this field faces have been discussed in detail, and it is clear that alternations in carrier chemistry and delivery strategies will provide the best outcome. Also, as it remains unlikely that a single form of therapy will provide the desired outcome alone, understanding the potential of future combination therapies remains an important area of study. With this in mind, treatment designs which aim to improve drug delivery using a combination therapy approach are likely to be of significant future value.

As PPTT matures and enters clinical evaluation, its potential use when used in combination with other therapies is worth investigating. Hyperthermia has long been known to be synergistic with both chemo and radiation therapy, and given PPTT's advantages, it is likely that the same will also be true for it. Therefore, it is natural to consider PPTT as a combination therapy tool to synergistically improve the therapeutic ratio of nanomedicines including polymer therapeutics. This approach may in the future help those suffering from prostate cancer and other diseases where localized hyperthermia can improve treatment outcome.

2.7 References

1. Howlader, N.; Noone, A. M.; Krapcho, M.; Neyman, N.; Aminou, R.; Altekruse, S. F.; Kosary, C. L.; Ruhl, J.; Tatalovich, Z.; Cho, H.; Mariotto, A.; Eisner, M. P.; Lewis, D. R.; Chen, H. S.; Feuer, E. J.; Chronin, K. A., *SEER Cancer Statistics Review 1975-2009 (Vintage 2009 Populations)*. National Cancer Institute: Bethesda, MD, 2012.

2. ACS, *Cancer Facts and Figures 2012*. American Cancer Society: Atlanta, GA, 2012.

3. Murphy, S. L.; Xu, J.; Kochanek, K. D. Deaths: Preliminary data for 2010. *National Vital Statistics Reports* **2012,** 60, 1-69.

4. Kalaitzi, C.; Kalantzis, A.; Gravas, S.; Georgiadis, J.; Christodoulou, C. State anxiety during watchful waiting for urinary lithiasis. *Int. J. Psychiatry Med.* **2006,** 36, 323-331.

5. Massie, M. J. Prevalence of depression in patients with cancer. *J. Natl. Cancer Inst. Monogr.* **2004,** 2004, 57-71.

6. Tangka, F.; Trogdon, J.; Richardson, L.; Howard, D.; Sabatino, S.; Finkelstein, E. Cancer treatment cost in the United States: has the burden shifted over time? *Cancer* **2010,** 116, 3477-3484.

7. Rubenstein, E. Costs and benefits of outpatient therapy. *Support. Care Cancer* **1994,** 2, 307-311.

8. Grönberg, H. Prostate cancer epidemiology. *Lancet* **2003,** 361, 859-864.

9. Sakr, W.; Haas, G.; Cassin, B.; Pontes, J.; Crissman, J. The frequency of carcinoma and intraepithelial neoplasia of the prostate in young male patients. *J. Urol.* **1993,** 150, 379-385.

10. Dong, J. Prevalent mutations in prostate cancer. *J. Cell. Biochem.* **2006,** 97, 433-47.

11. Damber, J.; Aus, G. Prostate cancer. *Lancet* **2008,** 371, 1710-1721.

12. Amundadottir, L. T.; Sulem, P.; Gudmundsson, J.; Helgason, A.; Baker, A.; Agnarsson, B. A.; Sigurdsson, A.; Benediktsdottir, K. R.; Cazier, J. B.; Sainz, J. A common variant associated with prostate cancer in European and African populations. *Nat. Genet.* **2006,** 38, 652-658.

13. Lilja, H.; Ulmert, D.; Vickers, A. J. Prostate-specific antigen and prostate cancer: prediction, detection and monitoring. *Nat. Rev. Cancer* **2008,** 8, 268-278.

14. Johansson, J. E.; Andrén, O.; Andersson, S. O.; Dickman, P. W.; Holmberg, L.; Magnuson, A.; Adami, H. O. Natural history of early, localized prostate cancer. *JAMA* **2004,** 291, 2713-2719.

15. Albertsen, P. C.; Hanley, J. A.; Fine, J. 20-year outcomes following conservative management of clinically localized prostate cancer. *JAMA* **2005,** 293, 2095-2101.

16. Bill-Axelson, A.; Holmberg, L.; Ruutu, M.; Häggman, M.; Andersson, S. O.; Bratell, S.; Spångberg, A.; Busch, C.; Nordling, S.; Garmo, H. Radical

prostatectomy versus watchful waiting in early prostate cancer. *N. Engl. J. Med.* **2005,** 352, 1977-1984.

17. Denmeade, S. R.; Isaacs, J. T. A history of prostate cancer treatment. *Nat. Rev. Cancer* **2002,** 2, 389-396.

18. Walsh, P. C.; Marschke, P.; Ricker, D.; Burnett, A. L. Patient-reported urinary continence and sexual function after anatomic radical prostatectomy. *Urology* **2000,** 55, 58-61.

19. Herrmann, T.; Rabenalt, R.; Stolzenburg, J.; Liatsikos, E.; Imkamp, F.; Tezval, H.; Gross, A.; Jonas, U.; Burchardt, M. Oncological and functional results of open, robot-assisted and laparoscopic radical prostatectomy: does surgical approach and surgical experience matter? *World J. Urol.* **2007,** 25, 149-160.

20. Mangar, S.; Huddart, R.; Parker, C.; Dearnaley, D.; Khoo, V.; Horwich, A. Technological advances in radiotherapy for the treatment of localised prostate cancer. *Eur. J. Cancer* **2005,** 41, 908-921.

21. D'Amico, A.; Whittington, R.; Malkowicz, S.; Schultz, D.; Blank, K.; Broderick, G.; Tomaszewski, J.; Renshaw, A.; Kaplan, I.; Beard, C. Biochemical outcome after radical prostatectomy, external beam radiation therapy, or interstitial radiation therapy for clinically localized prostate cancer. *JAMA* **1998,** 280, 969-974.

22. Peeters, S. T. H.; Heemsbergen, W. D.; van Putten, W. L. J.; Slot, A.; Tabak, H.; Mens, J. W.; Lebesque, J. V.; Koper, P. Acute and late complications after radiotherapy for prostate cancer: results of a multicenter randomized trial comparing 68 Gy to 78 Gy. *Int. J. Radiat. Biol.* **2005,** 61, 1019-1034.

23. Simmons, M.; Stephenson, A.; Klein, E. Natural history of biochemical recurrence after radical prostatectomy: risk assessment for secondary therapy. *Eur. Urol.* **2007,** 51, 1175-1184.

24. Huggins, C.; Stephens, R. C.; Hodges, C. V. Studies on prostatic cancer: 2. The effects of castration on advanced carcinoma of the prostate gland. *Arch. Surg.* **1941,** 43, 209-223.

25. Heinlein, C. A.; Chang, C. Androgen receptor in prostate cancer. *Endocr. Rev.* **2004,** 25, 276-308.

26. Culig, Z.; Hobisch, A.; Hittmair, A.; Peterziel, H.; Cato, A. C.; Bartsch, G.; Klocker, H. Expression, structure, and function of androgen receptor in advanced prostatic carcinoma. *Prostate* **1998,** 35, 63-70.

27. Feldman, B.; Feldman, D. The development of androgen-independent prostate cancer. *Nat. Rev. Cancer* **2001,** 1, 34-45.

28. Sharifi, N.; Gulley, J. L.; Dahut, W. L. Androgen deprivation therapy for prostate cancer. *JAMA* **2005,** 294, 238-244.

29. Yagoda, A.; Petrylak, D. Cytotoxic chemotherapy for advanced hormone-resistant prostate cancer. *Cancer* **1993,** 71, 1098-1109.

30. Eisenberger, M.; Simon, R.; O'Dwyer, P.; Wittes, R.; Friedman, M. A reevaluation of nonhormonal cytotoxic chemotherapy in the treatment of prostatic carcinoma. *J. Clin. Oncol.* **1985,** 3, 827-841.

31. Stein, C. Mechanisms of action of taxanes in prostate cancer. *Semin. Oncol.* **1999,** 26, 3-7.

32. Pienta, K. J. Preclinical mechanisms of action of docetaxel and docetaxel combinations in prostate cancer. *Semin. Oncol.* **2001,** 28, 3-7.

33. Tannock, I. F.; De Wit, R.; Berry, W. R.; Horti, J.; Pluzanska, A.; Chi, K. N.; Oudard, S.; Théodore, C.; James, N. D.; Turesson, I. Docetaxel plus prednisone or mitoxantrone plus prednisone for advanced prostate cancer. *N. Engl. J. Med.* **2004,** 351, 1502-1512.

34. Petrylak, D. P.; Tangen, C. M.; Hussain, M. H. A.; Lara Jr, P. N.; Jones, J. A.; Taplin, M. E.; Burch, P. A.; Berry, D.; Moinpour, C.; Kohli, M. Docetaxel and estramustine compared with mitoxantrone and prednisone for advanced refractory prostate cancer. *N. Engl. J. Med.* **2004,** 351, 1513-1520.

35. Heidenreich, A.; Aus, G.; Bolla, M.; Joniau, S.; Matveev, V.; Schmid, H.; Zattoni, F. EAU guidelines on prostate cancer. *Eur. Urol.* **2008,** 53, 68-80.

36. Pienta, K. J.; Smith, D. C. Advances in prostate cancer chemotherapy: A new era begins. *CA Cancer J. Clin.* **2005,** 55, 300-318.

37. Canil, C.; Tannock, I. Is there a role for chemotherapy in prostate cancer? *Br. J. Cancer* **2004,** 91, 1005-1011.

38. Hildebrandt, B.; Wust, P.; Ahlers, O.; Dieing, A.; Sreenivasa, G.; Kerner, T.; Felix, R.; Riess, H. The cellular and molecular basis of hyperthermia. *Crit. Rev. Oncol. Hematol.* **2002,** 43, 33-56.

39. Sreedhar, A. S. Hyperthermia and pharmacological intervention of heat shock proteins in anticancer treatments. *Jpn. J. Hyperthermic Oncol.* **2006,** 22, 211-227.

40. Harmon, B.; Corder, A.; Collins, R.; Gobé, G.; Allen, J.; Allan, D.; Kerr, J. Cell death induced in a murine mastocytoma by 42-47 degrees C heating in vitro: evidence that the form of death changes from apoptosis to necrosis above a critical heat load. *Int. J. Radiat. Biol.* **1990,** 58, 845-858.

41. Giovanella, B. C.; Stehlin, J. S.; Morgan, A. C. Selective lethal effect of supranormal temperatures on human neoplastic cells. *Cancer Res.* **1976,** 36, 3944-3950.

42. Jain, R. K. Determinants of tumor blood flow: a review. *Cancer Res.* **1988,** 48, 2641-2658.

43. Jain, R. K. Normalization of tumor vasculature: an emerging concept in antiangiogenic therapy. *Science* **2005,** 307, 58-62.

44. Jain, R. Transport of molecules across tumor vasculature. *Cancer Metastasis Rev.* **1987,** 6, 559-593.

45. Horsman, M. R. Tissue physiology and the response to heat. *Int. J. Hyperthermia* **2006,** 22, 197-203.

46. Song, C. W.; Lokshina, A.; Rhee, J. G.; Patten, M.; Levitt, S. H. Implication of blood flow in hyperthermic treatment of tumors. *IEEE Trans. Biomed. Eng.* **1984,** 31, 9-16.

47. Song, C. W.; Kang, M. S.; Rhee, J. G.; Levitt, S. H. Effect of hyperthermia on vascular function in normal and neoplastic tissues. *Ann. NY Acad. Sci.* **1980,** 335, 35-47.

48. Dudar, T. E.; Jain, R. K. Differential response of normal and tumor microcirculation to hyperthermia. *Cancer Res.* **1984,** 44, 605-612.

49. Song, C.; Kang, M.; Rhee, J.; Levitt, S. The effect of hyperthermia on vascular function, pH, and cell survival. *Radiology* **1980,** 137, 795-803.

50. Vaupel, P.; Müller-Klieser, W.; Otte, J.; Manz, R.; Kallinowski, F. Blood flow, tissue oxygenation, and pH-distribution in malignant tumors upon localized hyperthermia. Basic pathophysiological aspects and the role of various thermal doses. *Strahlentherapie* **1983,** 159, 73-81.

51. Wust, P.; Hildebrandt, B.; Sreenivasa, G.; Rau, B.; Gellermann, J.; Riess, H.; Felix, R.; Schlag, P. M. Hyperthermia in combined treatment of cancer. *Lancet Oncol.* **2002,** 3, 487-497.

52. Servadio, C.; Leib, Z. Hyperthermia in the treatment of prostate cancer. *Prostate* **1984,** 5, 205-211.

53. Bull, J. M. An update on the anticancer effects of a combination of chemotherapy and hyperthermia. *Cancer Res.* **1984,** 44, 4853s-4856s.

54. Issels, R. Hyperthermia combined with chemotherapy–biological rationale, clinical application, and treatment results. *Onkologie* **2000,** 22, 374-381.

55. Hettinga, J.; Lemstra, W.; Meijer, C.; Dam, W.; Uges, D.; Konings, A.; De Vries, E.; Kampinga, H. Mechanism of hyperthermic potentiation of cisplatin action in cisplatin-sensitive and-resistant tumour cells. *Br. J. Cancer* **1997,** 75, 1735-1743.

56. Bates, D. A.; Mackillop, W. J. Hyperthermia, adriamycin transport, and cytotoxicity in drug-sensitive and-resistant Chinese hamster ovary cells. *Cancer Res.* **1986,** 46, 5477-5481.

57. Hahn, G. M.; Braun, J.; Har-Kedar, I. Thermochemotherapy: synergism between hyperthermia (42-43 degrees) and adriamycin (or bleomycin) in mammalian cell inactivation. *Proc. Natl. Acad. Sci. USA.* **1975,** 72, 937-940.

58. Nagaoka, S.; Kawasaki, S.; Sasaki, K.; Nakanishi, T. Intracellular uptake, retention and cytotoxic effect of adriamycin combined with hyperthermia in vitro. *Jpn. J. Cancer Res.* **1986,** 77, 205-211.

59. Overgaard, J. Combined adriamycin and hyperthermia treatment of a murine mammary carcinoma in vivo. *Cancer Res.* **1976,** 36, 3077-3081.

60. Rietbroek, R. C.; Katschinski, D. M.; Reijers, M. H. E.; Robins, H. I.; Geerdink, A.; Tutsch, K.; d'Oleire, F.; Haveman, J. Lack of thermal enhancement for taxanes in vitro. *Int. J. Hyperthermia* **1997,** 13, 525-533.

61. Mohamed, F.; Stuart, O. A.; Glehen, O.; Urano, M.; Sugarbaker, P. H. Docetaxel and hyperthermia: factors that modify thermal enhancement. *J. Surg. Oncol.* **2004,** 88, 14-20.

62. Witkamp, A. J.; de Bree, E.; Van Goethem, R.; Zoetmulder, F. A. N. Rationale and techniques of intra-operative hyperthermic intraperitoneal chemotherapy. *Cancer Treat Rev.* **2001,** 27, 365-374.

63. Ryu, K. S.; Kim, J. H.; Ko, H. S.; Kim, J. W.; Ahn, W. S.; Park, Y. G.; Kim, S. J.; Lee, J. M. Effects of intraperitoneal hyperthermic chemotherapy in ovarian cancer. *Gynecol. Oncol.* **2004,** 94, 325-332.

64. Stewart, J. H.; Shen, P.; Levine, E. A. Intraperitoneal hyperthermic chemotherapy for peritoneal surface malignancy: current status and future directions. *Ann. Surg. Oncol.* **2005,** 12, 765-777.

65. Baronzio, G.; Gramaglia, A.; Fiorentini, G. Current role and future perspectives of hyperthermia for prostate cancer treatment. *In vivo* **2009,** 23, 143-146.

66. Kampinga, H.; Dikomey, E. Hyperthermic radiosensitization: mode of action and clinical relevance. *Int. J. Radiat. Biol.* **2001,** 77, 399-408.

67. Horsman, M.; Overgaard, J. Hyperthermia: a potent enhancer of radiotherapy. *Clin . Oncol.* **2007,** 19, 418-426.

68. Algan, O.; Fosmire, H.; Hynynen, K.; Dalkin, B.; Cui, H.; Drach, G.; Stea, B.; Cassady, J. External beam radiotherapy and hyperthermia in the treatment of patients with locally advanced prostate carcinoma. *Cancer* **2000,** 89, 399-403.

69. Van Vulpen, M.; De Leeuw, A.; Raaymakers, B.; Van Moorselaar, R.; Hofman, P.; Lagendijk, J.; Battermann, J. Radiotherapy and hyperthermia in the treatment of patients with locally advanced prostate cancer: preliminary results. *BJU Int.* **2004,** 93, 36-41.

70. Anscher, M. S.; Samulski, T. V.; Dodge, R.; Prosnitz, L. R.; Dewhirst, M. W. Combined external beam irradiation and external regional hyperthermia for locally advanced adenocarcinoma of the prostate. *Int. J. Radiat. Oncol. Biol. Phys.* **1997,** 37, 1059-1065.

71. Tilly, W.; Gellermann, J.; Graf, R.; Hildebrandt, B.; Weissbach, L.; Budach, V.; Felix, R.; Wust, P. Regional hyperthermia in conjunction with definitive radiotherapy against recurrent or locally advanced prostate cancer T3 pN0 M0. *Strahlenther. Onkol.* **2005,** 181, 35-41.

72. Strebhardt, K.; Ullrich, A. Paul Ehrlich's magic bullet concept: 100 years of progress. *Nat. Rev. Cancer* **2008,** 8, 473-480.

73. Ringsdorf, H. Structure and properties of pharmacologically active polymers. *J. Polym. Sci. Polym. Symp.* **1975,** 51, 135-153.

74. Wagner, V.; Dullaart, A.; Bock, A.; Zweck, A. The emerging nanomedicine landscape. *Nat. Biotechnol.* **2006,** 24, 1211-1217.

75. Gommersall, L.; Shergill, I. S.; Ahmed, H. U.; Hayne, D.; Arya, M.; Patel, H. R.; Hashizume, M.; Gill, I. S. Nanotechnology and its relevance to the urologist. *Eur. Urol.* **2007,** 52, 368-375.

76. Ratner, B. D.; Hoffman, A. S.; Schoen, F. J.; Lemons, J. E., *Biomaterials Science: an Introduction to Materials in Medicine*. 2nd ed.; Elsevier Academic Press: London, 2004.

77. Duncan, R. The dawning era of polymer therapeutics. *Nat. Rev. Drug Discov.* **2003,** 2, 347-360.

78. Etrych, T.; Šírová, M.; Starovoytova, L.; Říhová, B.; Ulbrich, K. HPMA copolymer conjugates of paclitaxel and docetaxel with pH-controlled drug release. *Mol. Pharm.* **2010,** 7, 1015-1026.

79. Rabinow, B. E. Nanosuspensions in drug delivery. *Nat. Rev. Drug Discov.* **2004,** 3, 785-796.

80. Lipinski, C. A. Drug-like properties and the causes of poor solubility and poor permeability. *J. Pharmacol. Toxicol. Methods* **2000,** 44, 235-249.

81. Chipman, S. D.; Oldham, F. B.; Pezzoni, G.; Singer, J. W. Biological and clinical characterization of paclitaxel poliglumex (PPX, CT-2103), a macromolecular polymer–drug conjugate. *Int. J. Nanomedicine* **2006,** 1, 375-383.

82. Hashizume, H.; Baluk, P.; Morikawa, S.; McLean, J. W.; Thurston, G.; Roberge, S.; Jain, R. K.; McDonald, D. M. Openings between defective endothelial cells explain tumor vessel leakiness. *Am. J. Pathol.* **2000,** 156, 1363-1380.

83. Kopecek, J. Controlled biodegradability of polymers--a key to drug delivery systems. *Biomaterials* **1984,** 5, 19-25.

84. Peer, D.; Karp, J. M.; Hong, S.; Farokhzad, O. C.; Margalit, R.; Langer, R. Nanocarriers as an emerging platform for cancer therapy. *Nat. Nanotechnol.* **2007,** 2, 751-760.

85. Sumer, B.; Gao, J. Theranostic nanomedicine for cancer. *Nanomedicine* **2008,** 3, 137-140.

86. Duncan, R.; Gaspar, R. Nanomedicine (s) under the microscope. *Mol. Pharm.* **2011,** 8, 2101-2141.

87. Duncan, R. Polymer conjugates as anticancer nanomedicines. *Nat. Rev. Cancer* **2006,** 6, 688-701.

88. Nagle, T.; Berg, C.; Nassr, R.; Pang, K. The further evolution of biotech. *Nat. Rev. Drug Discov.* **2003,** 2, 75-79.

89. Muller, R. H.; Keck, C. M. Challenges and solutions for the delivery of biotech drugs–a review of drug nanocrystal technology and lipid nanoparticles. *J. Biotechnol.* **2004,** 113, 151-170.

90. Roberts, M.; Bentley, M.; Harris, J. Chemistry for peptide and protein PEGylation. *Adv. Drug Deliv. Rev.* **2002,** 54, 459-476.

91. Veronese, F. M. Peptide and protein PEGylation: a review of problems and solutions. *Biomaterials* **2001,** 22, 405-417.

92. Caliceti, P.; Veronese, F. M. Pharmacokinetic and biodistribution properties of poly (ethylene glycol)-protein conjugates. *Adv. Drug Deliv. Rev.* **2003,** 55, 1261-1277.

93. Matsumura, Y.; Maeda, H. A new concept for macromolecular therapeutics in cancer chemotherapy: mechanism of tumoritropic accumulation of proteins and the antitumor agent smancs. *Cancer Res.* **1986,** 46, 6387-6392.

94. Hey, T.; Knoller, H.; Vorstheim, P., Half-life extension through HESylation®. In *Therapeutic Proteins: Strategies to Modulate Their Plasma Half-Lives*, Kontermann, R., Ed. Wiley-VCH Verlag GmbH Co.: Weinheim, Germany, 2012; pp 117-140.

95. Hardwicke, J.; Ferguson, E. L.; Moseley, R.; Stephens, P.; Thomas, D. W.; Duncan, R. Dextrin-rhEGF conjugates as bioresponsive nanomedicines for wound repair. *J. Control. Release* **2008,** 130, 275-283.

96. Wiethoff, C. M.; Middaugh, C. R. Barriers to nonviral gene delivery. *J. Pharm. Sci.* **2003,** 92, 203-217.

97. Pack, D. W.; Hoffman, A. S.; Pun, S.; Stayton, P. S. Design and development of polymers for gene delivery. *Nat. Rev. Drug Discov.* **2005,** 4, 581-593.

98. De Smedt, S. C.; Demeester, J.; Hennink, W. E. Cationic polymer based gene delivery systems. *Pharm. Res.* **2000,** 17, 113-126.

99. Tang, M.; Szoka, F. The influence of polymer structure on the interactions of cationic polymers with DNA and morphology of the resulting complexes. *Gene Ther.* **1997,** 4, 823-832.

100. Choi, Y. H.; Liu, F.; Kim, J. S.; Choi, Y. K.; Park, J. S.; Kim, S. W. Polyethylene glycol-grafted poly-L-lysine as polymeric gene carrier. *J. Control. Release* **1998,** 54, 39-48.

101. Ahn, C. H.; Chae, S. Y.; Bae, Y. H.; Kim, S. W. Biodegradable poly (ethylenimine) for plasmid DNA delivery. *J. Control. Release* **2002,** 80, 273-282.

102. Braun, C. S.; Vetro, J. A.; Tomalia, D. A.; Koe, G. S.; Koe, J. G.; Russell Middaugh, C. Structure/function relationships of polyamidoamine/DNA dendrimers as gene delivery vehicles. *J. Pharm. Sci.* **2005,** 94, 423-436.

103. Park, T. G.; Jeong, J. H.; Kim, S. W. Current status of polymeric gene delivery systems. *Adv. Drug Deliv. Rev.* **2006,** 58, 467-486.

104. Torchilin, V. P. Structure and design of polymeric surfactant-based drug delivery systems. *J. Control. Release* **2001,** 73, 137-172.

105. Mukerjee, P.; Mysels, K. J. *Critical Micelle Concentrations of Aqueous Surfactant Systems*; DTIC Document: 1971.

106. Yoo, H. S.; Park, T. G. Biodegradable polymeric micelles composed of doxorubicin conjugated PLGA–PEG block copolymer. *J. Control. Release* **2001,** 70, 63-70.

107. Torchilin, V. P. PEG-based micelles as carriers of contrast agents for different imaging modalities. *Adv. Drug Deliv. Rev.* **2002,** 54, 235-252.

108. Chung, J.; Yokoyama, M.; Yamato, M.; Aoyagi, T.; Sakurai, Y.; Okano, T. Thermo-responsive drug delivery from polymeric micelles constructed using block copolymers of poly (N-isopropylacrylamide) and poly (butylmethacrylate). *J. Control. Release* **1999,** 62, 115-127.

109. Kohori, F.; Sakai, K.; Aoyagi, T.; Yokoyama, M.; Sakurai, Y.; Okano, T. Preparation and characterization of thermally responsive block copolymer micelles comprising poly (N-isopropylacrylamide- b-DL-lactide). *J. Control. Release* **1998,** 55, 87-98.

110. Benahmed, A.; Ranger, M.; Leroux, J. C. Novel polymeric micelles based on the amphiphilic diblock copolymer poly (N-vinyl-2-pyrrolidone)-block-poly (D, L-lactide). *Pharm. Res.* **2001,** 18, 323-328.

111. Jeong, B.; Han Bae, Y.; Wan Kim, S. Biodegradable thermosensitive micelles of PEG-PLGA-PEG triblock copolymers. *Colloids Surf B Interfaces* **1999,** 16, 185-193.

112. Wilhelm, M.; Zhao, C. L.; Wang, Y.; Xu, R.; Winnik, M. A.; Mura, J. L.; Riess, G.; Croucher, M. D. Poly (styrene-ethylene oxide) block copolymer micelle formation in water: a fluorescence probe study. *Macromolecules* **1991,** 24, 1033-1040.

113. Rapoport, N. Stabilization and activation of Pluronic micelles for tumor-targeted drug delivery. *Colloids Surf B Interfaces* **1999,** 16, 93-111.

114. Cheon Lee, S.; Kim, C.; Chan Kwon, I.; Chung, H.; Young Jeong, S. Polymeric micelles of poly (2-ethyl-2-oxazoline)-block-poly (ε-caprolactone) copolymer as a carrier for paclitaxel. *J. Control. Release* **2003,** 89, 437-446.

115. Kabanov, A. V.; Alakhov, V. Y. Pluronic block copolymers in drug delivery: from micellar nanocontainers to biological response modifiers. *CRit. Rev. Ther. Drug Carrier Syst.* **2002,** 19, 1-72.

116. Torchilin, V. Micellar nanocarriers: pharmaceutical perspectives. *Pharm. Res.* **2007,** 24, 1-16.

117. Matsumura, Y.; Kataoka, K. Preclinical and clinical studies of anticancer agent-incorporating polymer micelles. *Cancer Sci.* **2009,** 100, 572-579.

118. Hamaguchi, T.; Matsumura, Y.; Suzuki, M.; Shimizu, K.; Goda, R.; Nakamura, I.; Nakatomi, I.; Yokoyama, M.; Kataoka, K.; Kakizoe, T. NK105, a paclitaxel-incorporating micellar nanoparticle formulation, can extend in vivo antitumour activity and reduce the neurotoxicity of paclitaxel. *Br. J. Cancer* **2005,** 92, 1240-1246.

119. Plummer, R.; Wilson, R.; Calvert, H.; Boddy, A.; Griffin, M.; Sludden, J.; Tilby, M.; Eatock, M.; Pearson, D.; Ottley, C. A Phase I clinical study of cisplatin-incorporated polymeric micelles (NC-6004) in patients with solid tumours. *Br. J. Cancer* **2011,** 104, 593-598.

120. Matsumura, Y. Preclinical and clinical studies of NK012, an SN-38-incorporating polymeric micelles, which is designed based on EPR effect. *Adv. Drug Deliv. Rev.* **2011,** 63, 184-192.

121. Danson, S.; Ferry, D.; Alakhov, V.; Margison, J.; Kerr, D.; Jowle, D.; Brampton, M.; Halbert, G.; Ranson, M. Phase I dose escalation and pharmacokinetic study of pluronic polymer-bound doxorubicin (SP1049C) in patients with advanced cancer. *Br. J. Cancer* **2004,** 90, 2085-2091.

122. Larson, N.; Ghandehari, H. Polymeric conjugates for drug delivery. *Chem. Mater.* **2012,** 24, 840-853.

123. Kope ek, J.; Kope ková, P.; Minko, T.; Lu, Z. R. HPMA copolymer–anticancer drug conjugates: design, activity, and mechanism of action. *Eur. J. Pharm. Biopharm.* **2000,** 50, 61-81.

124. Schoenmakers, R. G.; van de Wetering, P.; Elbert, D. L.; Hubbell, J. A. The effect of the linker on the hydrolysis rate of drug-linked ester bonds. *J. Control. Release* **2004,** 95, 291-300.

125. Ulbrich, K.; Šubr, V. Polymeric anticancer drugs with pH-controlled activation. *Adv. Drug Deliv. Rev.* **2004,** 56, 1023-1050.

126. Meerum Terwogt, J. M.; ten Bokkel Huinink, W. W.; Schellens, J. H. M.; Schot, M.; Mandjes, I. A. M.; Zurlo, M. G.; Rocchetti, M.; Rosing, H.; Koopman, F. J.;

Beijnen, J. H. Phase I clinical and pharmacokinetic study of PNU166945, a novel water-soluble polymer-conjugated prodrug of paclitaxel. *Anticancer Drugs* **2001,** 12, 315-323.

127. Ulbrich, K.; Zacharieva, E.; Obereigner, B.; Kopecek, J. Polymers containing enzymatically degradable bonds V. Hydrophilic polymers degradable by papain. *Biomaterials* **1980,** 1, 199-204.

128. Kopeček, J.; Rejmanová, P.; Chytrý, V. Polymers containing enzymatically degradable bonds, 1. Chymotrypsin catalyzed hydrolysis of p-nitroanilides of phenylalanine and tyrosine attached to side-chains of copolymers of *N*-(2-hydroxypropyl) methacrylamide. *Die Makromolekulare Chemie* **1981,** 182, 799-809.

129. Rejmanová, P.; Obereigner, B.; Kopeček, J. Polymers containing enzymatically degradable bonds, 2. Poly [*N*-(2-hydroxypropyl) methacrylamide] chains connected by oligopeptide sequences cleavable by chymotrypsin. *Die Makromolekulare Chemie* **1981,** 182, 1899-1915.

130. Ulbrich, K.; Strohalm, J.; Kopeček, J. Polymers containing enzymatically degradable bonds, 3. Poly [*N*-(2-hydroxypropyl) methacrylamide] chains connected by oligopeptide sequences cleavable by trypsin. *Die Makromolekulare Chemie* **1981,** 182, 1917-1928.

131. Kopeček, J.; Cífková, I.; Rejmanová, P.; Strohalm, J.; Obereigner, B.; Ulbrich, K. Polymers containing enzymatically degradable bonds, 4. Preliminary experiments in vivo. *Die Makromolekulare Chemie* **1981,** 182, 2941-2949.

132. Duncan, R.; Cable, H. C.; Lloyd, J. B.; Rejmanová, P.; Kopeček, J. Polymers containing enzymatically degradable bonds, 7. Design of oligopeptide side-chains in poly [*N*-(2-hydroxypropyl) methacrylamide] copolymers to promote efficient degradation by lysosomal enzymes. *Die Makromolekulare Chemie* **1983,** 184, 1997-2008.

133. Rejmanová, P.; Kopeček, J.; Pohl, J.; Baudyš, M.; Kostka, V. Polymers containing enzymatically degradable bonds, 8. Degradation of oligopeptide sequences in *N*-(2-hydroxypropyl) methacrylamide copolymers by bovine spleen cathepsin B. *Die Makromolekulare Chemie* **1983,** 184, 2009-2020.

134. Ulbrich, K.; Strohalm, J.; Kopeček, J. Polymers containing enzymatically degradable bonds. VI. Hydrophilic gels cleavable by chymotrypsin. *Biomaterials* **1982,** 3, 150-154.

135. Greenwald, R. B.; Choe, Y. H.; McGuire, J.; Conover, C. D. Effective drug delivery by PEGylated drug conjugates. *Adv. Drug Deliv. Rev.* **2003,** 55, 217-250.

136. Rowinsky, E. K.; Rizzo, J.; Ochoa, L.; Takimoto, C. H.; Forouzesh, B.; Schwartz, G.; Hammond, L. A.; Patnaik, A.; Kwiatek, J.; Goetz, A. A phase I and pharmacokinetic study of pegylated camptothecin as a 1-hour infusion every 3 weeks in patients with advanced solid malignancies. *J. Clin. Oncol.* **2003,** 21, 148-157.

137. Li, C. Poly(L-glutamic acid)-anticancer drug conjugates. *Adv. Drug Deliv. Rev.* **2002,** 54, 695-713.

138. Zunino, F.; Pratesi, G.; Micheloni, A. Poly (carboxylic acid) polymers as carriers for anthracyclines. *J. Control. Release* **1989,** 10, 65-73.

139. Beer, T. M.; Ryan, C.; Alumkal, J.; Ryan, C. W.; Sun, J.; Eilers, K. M. A phase II study of paclitaxel poliglumex in combination with transdermal estradiol for the treatment of metastatic castration-resistant prostate cancer after docetaxel chemotherapy. *Anticancer Drugs* **2010,** 21, 433-438.

140. Mita, M.; Mita, A.; Sarantopoulos, J.; Takimoto, C. H.; Rowinsky, E. K.; Romero, O.; Angiuli, P.; Allievi, C.; Eisenfeld, A.; Verschraegen, C. F. Phase I study of paclitaxel poliglumex administered weekly for patients with advanced solid malignancies. *Cancer Chemother. Pharmacol.* **2009,** 64, 287-295.

141. Sabbatini, P.; Sill, M. W.; O'Malley, D.; Adler, L.; Secord, A. A. A phase II trial of paclitaxel poliglumex in recurrent or persistent ovarian or primary peritoneal cancer (EOC): a Gynecologic Oncology Group Study. *Gynecol. Oncol.* **2008,** 111, 455-460.

142. O'Brien, M. E. R.; Socinski, M. A.; Popovich, A. Y.; Bondarenko, I. N.; Tomova, A.; Bilynsky, B. T.; Hotko, Y. S.; Ganul, V. L.; Kostinsky, I. Y.; Eisenfeld, A. J. Randomized phase III trial comparing single-agent paclitaxel Poliglumex (CT-2103, PPX) with single-agent gemcitabine or vinorelbine for the treatment of PS 2 patients with chemotherapy-naive advanced non-small cell lung cancer. *J. Thorac. Oncol.* **2008,** 3, 728-734.

143. Langer, C. J.; O'Byrne, K. J.; Socinski, M. A.; Mikhailov, S. M.; Lesniewski-Kmak, K.; Smakal, M.; Ciuleanu, T. E.; Orlov, S. V.; Dediu, M.; Heigener, D. Phase III trial comparing paclitaxel poliglumex (CT-2103, PPX) in combination with carboplatin versus standard paclitaxel and carboplatin in the treatment of PS 2 patients with chemotherapy-naive advanced non-small cell lung cancer. *J. Thorac. Oncol.* **2008,** 3, 623-630.

144. Hardwicke, J.; Moseley, R.; Stephens, P.; Harding, K.; Duncan, R.; Thomas, D. W. Bioresponsive dextrin− rhEGF conjugates: In vitro evaluation in models relevant to its proposed use as a treatment for chronic wounds. *Mol. Pharm.* **2010,** 7, 699-707.

145. Besheer, A.; Hertel, T. C.; Kressler, J.; Mäder, K.; Pietzsch, M. Enzymatically catalyzed HES conjugation using microbial transglutaminase: Proof of feasibility. *J. Pharm. Sci.* **2009,** 98, 4420-4428.

146. Hreczuk-Hirst, D.; Chicco, D.; German, L.; Duncan, R. Dextrins as potential carriers for drug targeting: tailored rates of dextrin degradation by introduction of pendant groups. *Int. J. Pharm.* **2001,** 230, 57-66.

147. Liu, M.; Fréchet, J. M. J. Designing dendrimers for drug delivery. *Pharm. Sci. Technolo. Today* **1999,** 2, 393-401.

148. Esfand, R.; Tomalia, D. A. Poly(amidoamine)(PAMAM) dendrimers: from biomimicry to drug delivery and biomedical applications. *Drug Discov. Today* **2001,** 6, 427-436.

149. Twyman, L. J.; Beezer, A. E.; Esfand, R.; Hardy, M. J.; Mitchell, J. C. The synthesis of water soluble dendrimers, and their application as possible drug delivery systems. *Tetrahedron Lett.* **1999,** 40, 1743-1746.

150. Malik, N.; Evagorou, E. G.; Duncan, R. Dendrimer-platinate: a novel approach to cancer chemotherapy. *Anticancer Drugs* **1999,** 10, 767-776.

151. Zhu, S.; Hong, M.; Zhang, L.; Tang, G.; Jiang, Y.; Pei, Y. PEGylated PAMAM dendrimer-doxorubicin conjugates: in vitro evaluation and in vivo tumor accumulation. *Pharm. Res.* **2010,** 27, 161-174.

152. Thiagarajan, G.; Ray, A.; Malugin, A.; Ghandehari, H. PAMAM-camptothecin conjugate inhibits proliferation and induces nuclear fragmentation in colorectal carcinoma cells. *Pharm. Res.* **2010,** 27, 2307-2316.

153. Vijayalakshmi, N.; Ray, A.; Malugin, A.; Ghandehari, H. Carboxyl-terminated PAMAM-SN38 conjugates: synthesis, characterization, and in vitro evaluation. *Bioconjug. Chem.* **2010,** 21, 1804-1810.

154. Goldberg, D. S.; Vijayalakshmi, N.; Swaan, P. W.; Ghandehari, H. G3. 5 PAMAM dendrimers enhance transepithelial transport of SN38 while minimizing gastrointestinal toxicity. *J. Control. Release* **2011,** 150, 318-325.

155. Kukowska-Latallo, J. F.; Candido, K. A.; Cao, Z.; Nigavekar, S. S.; Majoros, I. J.; Thomas, T. P.; Balogh, L. P.; Khan, M. K.; Baker, J. R. Nanoparticle targeting of anticancer drug improves therapeutic response in animal model of human epithelial cancer. *Cancer Res.* **2005,** 65, 5317-5324.

156. Kitchens, K. M.; Foraker, A. B.; Kolhatkar, R. B.; Swaan, P. W.; Ghandehari, H. Endocytosis and interaction of poly (amidoamine) dendrimers with Caco-2 cells. *Pharm. Res.* **2007,** 24, 2138-2145.

157. Kitchens, K. M.; Kolhatkar, R. B.; Swaan, P. W.; Ghandehari, H. Endocytosis inhibitors prevent poly(amidoamine) dendrimer internalization and permeability across Caco-2 cells. *Mol. Pharm.* **2008,** 5, 364-369.

158. Kitchens, K. M.; El-Sayed, M. E.; Ghandehari, H. Transepithelial and endothelial transport of poly (amidoamine) dendrimers. *Adv. Drug Deliv. Rev.* **2005,** 57, 2163-2176.

159. El-Sayed, M.; Ginski, M.; Rhodes, C.; Ghandehari, H. Transepithelial transport of poly(amidoamine) dendrimers across Caco-2 cell monolayers. *J. Control. Release* **2002,** 81, 355-365.

160. El-Sayed, M.; Rhodes, C. A.; Ginski, M.; Ghandehari, H. Transport mechanism(s) of poly(amidoamine) dendrimers across Caco-2 cell monolayers. *Int. J. Pharm.* **2003,** 265, 151-157.

161. Kitchens, K. M.; Kolhatkar, R. B.; Swaan, P. W.; Eddington, N. D.; Ghandehari, H. Transport of poly(amidoamine) dendrimers across Caco-2 cell monolayers: Influence of size, charge and fluorescent labeling. *Pharm. Res.* **2006,** 23, 2818-2826.

162. Wiwattanapatapee, R.; Carreño-Gómez, B.; Malik, N.; Duncan, R. Anionic PAMAM dendrimers rapidly cross adult rat intestine in vitro: a potential oral delivery system? *Pharm. Res.* **2000,** 17, 991-998.

163. Jevprasesphant, R.; Penny, J.; Attwood, D.; McKeown, N. B.; D'Emanuele, A. Engineering of dendrimer surfaces to enhance transepithelial transport and reduce cytotoxicity. *Pharm. Res.* **2003,** 20, 1543-1550.

164. Greish, K.; Thiagarajan, G.; Herd, H.; Price, R.; Bauer, H.; Hubbard, D.; Burckle, A.; Sadekar, S.; Yu, T.; Anwar, A.; Ray, A.; Ghandehari, H. Size and surface charge significantly influence the toxicity of silica and dendritic nanoparticles. *Nanotoxicology* **2011**, Epub ahead of print.

165. Duncan, R.; Izzo, L. Dendrimer biocompatibility and toxicity. *Adv. Drug Deliv. Rev.* **2005,** 57, 2215-2237.

166. Jones, C. F.; Campbell, R. A.; Franks, Z.; Gibson, C. C.; Thiagarajan, G.; Vieira-de-Abreu, A.; Sukavaneshvar, S.; Mohammad, S. F.; Li, D. Y.; Ghandehari, H. Cationic PAMAM dendrimers disrupt key platelet functions. *Mol. Pharm.* **2012,** 9, 1599-1611.

167. Kopecek, J.; Kopecková, P. HPMA copolymers: origins, early developments, present, and future. *Adv. Drug Deliv. Rev.* **2010,** 62, 122-149.

168. Strohalm, J.; Kopecek, J. Poly *N*-(2-hydroxypropyl) methacrylamide. 4. Heterogeneous polymerization. *Angew. Makromol. Chem.* **1978,** 70, 109-118.

169. Kopecek, J.; Kopecková, P.; Minko, T.; Lu, Z. R. HPMA copolymer–anticancer drug conjugates: design, activity, and mechanism of action. *Eur. J. Pharm. Biopharm.* **2000,** 50, 61-81.

170. Duncan, R. Development of HPMA copolymer–anticancer conjugates: Clinical experience and lessons learnt. *Adv. Drug Deliv. Rev.* **2009,** 61, 1131-1148.

171. Vasey, P. A.; Kaye, S. B.; Morrison, R.; Twelves, C.; Wilson, P.; Duncan, R.; Thomson, A. H.; Murray, L. S.; Hilditch, T. E.; Murray, T. Phase I clinical and pharmacokinetic study of PK1 [*N*-(2-hydroxypropyl) methacrylamide copolymer doxorubicin]: first member of a new class of chemotherapeutic agents—drug-polymer conjugates. *Clin. Cancer Res.* **1999,** 5, 83-94.

172. Seymour, L. W.; Ferry, D. R.; Kerr, D. J.; Rea, D.; Whitlock, M.; Poyner, R.; Boivin, C.; Hesslewood, S.; Twelves, C.; Blackie, R. Phase II studies of polymer-doxorubicin (PK1, FCE28068) in the treatment of breast, lung and colorectal cancer. *Int. J. Oncol.* **2009,** 34, 1629-1636.

173. Seymour, L. W.; Ferry, D. R.; Anderson, D.; Hesslewood, S.; Julyan, P. J.; Poyner, R.; Doran, J.; Young, A. M.; Burtles, S.; Kerr, D. J. Hepatic drug targeting: phase I evaluation of polymer-bound doxorubicin. *J. Clin. Oncol.* **2002,** 20, 1668-1676.

174. Julyan, P. J.; Seymour, L. W.; Ferry, D. R.; Daryani, S.; Boivin, C. M.; Doran, J.; David, M.; Anderson, D.; Christodoulou, C.; Young, A. M. Preliminary clinical study of the distribution of HPMA copolymers bearing doxorubicin and galactosamine. *J. Control. Release* **1999,** 57, 281-290.

175. Bissett, D.; Cassidy, J.; De Bono, J.; Muirhead, F.; Main, M.; Robson, L.; Fraier, D.; Magne, M.; Pellizzoni, C.; Porro, M. Phase I and pharmacokinetic (PK) study of MAG-CPT (PNU 166148): a polymeric derivative of camptothecin (CPT). *Br. J. Cancer* **2004,** 91, 50-55.

176. Wachters, F.; Groen, H.; Maring, J.; Gietema, J.; Porro, M.; Dumez, H.; De Vries, E.; Van Oosterom, A. A phase I study with MAG-camptothecin intravenously administered weekly for 3 weeks in a 4-week cycle in adult patients with solid tumours. *Br. J. Cancer* **2004,** 90, 2261-2267.

177. Schoemaker, N.; Van Kesteren, C.; Rosing, H.; Jansen, S.; Swart, M.; Lieverst, J.; Fraier, D.; Breda, M.; Pellizzoni, C.; Spinelli, R. A phase I and pharmacokinetic study of MAG-CPT, a water-soluble polymer conjugate of camptothecin. *Br. J. Cancer* **2002,** 87, 608-614.

178. Campone, M.; Rademaker-Lakhai, J. M.; Bennouna, J.; Howell, S. B.; Nowotnik, D. P.; Beijnen, J. H.; Schellens, J. H. M. Phase I and pharmacokinetic trial of AP5346, a DACH–platinum–polymer conjugate, administered weekly for three out of every 4 weeks to advanced solid tumor patients. *Cancer Chemother. Pharmacol.* **2007,** 60, 523-533.

179. Rademaker-Lakhai, J. M.; Terret, C.; Howell, S. B.; Baud, C. M.; de Boer, R. F.; Pluim, D.; Beijnen, J. H.; Schellens, J. H. M.; Droz, J. P. A Phase I and pharmacological study of the platinum polymer AP5280 given as an intravenous infusion once every 3 weeks in patients with solid tumors. *Clin. Cancer Res.* **2004,** 10, 3386-3395.

180. Malone, D. C.; Tran, T. T.; Poordad, F. F. Cost-efficacy analysis of peginterferon alfa-2b plus ribavirin compared with peginterferon alfa-2a plus ribavirin for the treatment of chronic hepatitis C. *J. Manag. Care Pharm.* **2005,** 11, 687-694.

181. Tewey, M., Sigma-Tau Pharmaceuticals announces new ONCASPAR pricing. *Sigma-tau Pharmaceuticals, Inc.* 2011.

182. Nie, S. Understanding and overcoming major barriers in cancer nanomedicine. *Nanomedicine (London, England)* **2010,** 5, 523-528.

183. Cedervall, T.; Lynch, I.; Lindman, S.; Berggård, T.; Thulin, E.; Nilsson, H.; Dawson, K. A.; Linse, S. Understanding the nanoparticle–protein corona using methods to quantify exchange rates and affinities of proteins for nanoparticles. *Proc. Natl. Acad. Sci. USA.* **2007,** 104, 2050-2055.

184. Jain, R. K. Vascular and interstitial barriers to delivery of therapeutic agents in tumors. *Cancer Metastasis Rev.* **1990,** 9, 253-266.

185. Jain, R. K. Transport of molecules in the tumor interstitium: a review. *Cancer Res.* **1987,** 47, 3039-3051.

186. Peterson, H. I.; Appelgren, L. Tumour vessel permeability and transcapillary exchange of large molecules of different size. *Bibl. Anat.* **1977,** 15 Pt 1, 262-265.

187. Peterson, H. I., Vascular and extravascular spaces in tumors: tumor vascular permeability. In *Tumor Blood Circulation: Angiogenesis, Vascular Morphology and Blood Flow of Experimental and Human Tumors*, Peterson, H. I., Ed. CRS Press, Inc.: Boca Raton, 1979; pp 77-85.

188. Larson, S. M. In *Mechanisms of Localization of Gallium-67 in Tumors*, 1978; Elsevier: 1978; pp 193-203.

189. Pinsky, S. M.; Henkin, R. E. In *Gallium-67 Tumor Scanning*, 1976; Elsevier: 1976; pp 397-409.

190. Maeda, H.; Wu, J.; Sawa, T.; Matsumura, Y.; Hori, K. Tumor vascular permeability and the EPR effect in macromolecular therapeutics: a review. *J. Control. Release* **2000,** 65, 271-284.

191. Jain, R. K. Normalizing tumor vasculature with anti-angiogenic therapy: a new paradigm for combination therapy. *Nat. Med.* **2001,** 7, 987-989.

192. Konerdingi, M.; Fait, E.; Gaumann, A.; Dimitropouloui, C.; Malkusch, W., Scanning electron microscopy of corrosion casts in the study of tumor. In *Angiogenesis: models, modulators, and clinical applications*, Maragoudakis, M. E., Ed. Plenum Press: New York, USA, 1998; Vol. 298, pp 429-447.

193. Baish, J. W.; Jain, R. K. Fractals and cancer. *Cancer Res.* **2000,** 60, 3683-3688.

194. Jain, R. K.; Stylianopoulos, T. Delivering nanomedicine to solid tumors. *Nat. Rev. Clin. Oncol.* **2010,** 7, 653-664.

195. Sevick, E. M.; Jain, R. K. Viscous resistance to blood flow in solid tumors: effect of hematocrit on intratumor blood viscosity. *Cancer Res.* **1989,** 49, 3513-3519.

196. Boucher, Y.; Jain, R. K. Microvascular pressure is the principal driving force for interstitial hypertension in solid tumors: implications for vascular collapse. *Cancer Res.* **1992,** 52, 5110-5114.

197. Boucher, Y.; Baxter, L. T.; Jain, R. K. Interstitial pressure gradients in tissue-isolated and subcutaneous tumors: implications for therapy. *Cancer Res.* **1990,** 50, 4478-4484.

198. Netti, P. A.; Berk, D. A.; Swartz, M. A.; Grodzinsky, A. J.; Jain, R. K. Role of extracellular matrix assembly in interstitial transport in solid tumors. *Cancer Res.* **2000,** 60, 2497-2503.

199. Fukumura, D.; Jain, R. K. Tumor microenvironment abnormalities: causes, consequences, and strategies to normalize. *J. Cell. Biochem.* **2007,** 101, 937-949.

200. Hobbs, S. K.; Monsky, W. L.; Yuan, F.; Roberts, W. G.; Griffith, L.; Torchilin, V. P.; Jain, R. K. Regulation of transport pathways in tumor vessels: role of tumor type and microenvironment. *Proc. Natl. Acad. Sci. USA.* **1998,** 95, 4607-4612.

201. Ramanujan, S.; Pluen, A.; McKee, T. D.; Brown, E. B.; Boucher, Y.; Jain, R. K. Diffusion and convection in collagen gels: implications for transport in the tumor interstitium. *Biophys. J.* **2002,** 83, 1650-1660.

202. Yuan, F.; Dellian, M.; Fukumura, D.; Leunig, M.; Berk, D. A.; Torchilin, V. P.; Jain, R. K. Vascular permeability in a human tumor xenograft: molecular size dependence and cutoff size. *Cancer Res.* **1995,** 55, 3752-3756.

203. Yuan, F.; Leunig, M.; Huang, S. K.; Berk, D. A.; Papahadjopoulos, D.; Jain, R. K. Mirovascular permeability and interstitial penetration of sterically stabilized (stealth) liposomes in a human tumor xenograft. *Cancer Res.* **1994,** 54, 3352-3356.

204. Torchilin, V. Tumor delivery of macromolecular drugs based on the EPR effect. *Adv. Drug Deliv. Rev.* **2011,** 63, 131-135.

205. Adams, G. P.; Weiner, L. M. Monoclonal antibody therapy of cancer. *Nat. Biotechnol.* **2005,** 23, 1147-1157.

206. Mehren, M.; Adams, G. P.; Weiner, L. M. Monoclonal antibody therapy for cancer. *Annu. Rev. Med.* **2003,** 54, 343-369.

207. Loo, C.; Lowery, A.; Halas, N.; West, J.; Drezek, R. Immunotargeted nanoshells for integrated cancer imaging and therapy. *Nano Lett.* **2005,** 5, 709-711.

208. Park, J.; Kirpotin, D.; Hong, K.; Shalaby, R.; Shao, Y.; Nielsen, U.; Marks, J.; Papahadjopoulos, D.; Benz, C. Tumor targeting using anti-her2 immunoliposomes. *J. Control. Release* **2001,** 74, 95-113.

209. Nurunnabi, M.; Cho, K. J.; Choi, J. S.; Huh, K. M.; Lee, Y. Targeted near-IR QDs-loaded micelles for cancer therapy and imaging. *Biomaterials* **2010,** 31, 5436-5444.

210. Hattori, Y.; Maitani, Y. Enhanced in vitro DNA transfection efficiency by novel folate-linked nanoparticles in human prostate cancer and oral cancer. *J. Control. Release* **2004,** 97, 173-183.

211. Dixit, V.; Van den Bossche, J.; Sherman, D. M.; Thompson, D. H.; Andres, R. P. Synthesis and grafting of thioctic acid- PEG- folate conjugates onto Au nanoparticles for selective targeting of folate receptor-positive tumor cells. *Bioconjug. Chem.* **2006,** 17, 603-609.

212. Stella, B.; Arpicco, S.; Peracchia, M. T.; Desmaële, D.; Hoebeke, J.; Renoir, M.; D'Angelo, J.; Cattel, L.; Couvreur, P. Design of folic acid-conjugated nanoparticles for drug targeting. *J. Pharm. Sci.* **2000,** 89, 1452-1464.

213. Chithrani, B. D.; Chan, W. C. Elucidating the mechanism of cellular uptake and removal of protein-coated gold nanoparticles of different sizes and shapes. *Nano Lett.* **2007,** 7, 1542-1550.

214. Yang, P. H.; Sun, X.; Chiu, J. F.; Sun, H.; He, Q. Y. Transferrin-mediated gold nanoparticle cellular uptake. *Bioconjug. Chem.* **2005,** 16, 494–496.

215. Ishida, O.; Maruyama, K.; Tanahashi, H.; Iwatsuru, M.; Sasaki, K.; Eriguchi, M.; Yanagie, H. Liposomes bearing polyethyleneglycol-coupled transferrin with intracellular targeting property to the solid tumors in vivo. *Pharm. Res.* **2001,** 18, 1042-1048.

216. Kursa, M.; Walker, G. F.; Roessler, V.; Ogris, M.; Roedl, W.; Kircheis, R.; Wagner, E. Novel shielded transferrin-polyethylene glycol-polyethylenimine/DNA complexes for systemic tumor-targeted gene transfer. *Bioconjug. Chem.* **2003,** 14, 222-231.

217. Greish, K.; Ray, A.; Bauer, H.; Larson, N.; Malugin, A.; Pike, D. B.; Haider, M.; Ghandehari, H. Anticancer and antiangiogenic activity of HPMA copolymer-aminohexylgeldanamycin-RGDfK conjugates for prostate cancer therapy. *J. Control. Release* **2011,** 151, 263-270.

218. Gormley, A. J.; Malugin, A.; Ray, A.; Robinson, R.; Ghandehari, H. Biological evaluation of RGDfK-gold nanorod conjugates for prostate cancer treatment. *J. Drug Target.* **2011,** 19, 915-924.

219. Arosio, D.; Manzoni, L.; Araldi, E. M. V.; Scolastico, C. Cyclic RGD functionalized gold nanoparticles for tumor targeting. *Bioconjug. Chem.* **2011,** 22, 664-672.

220. Danhier, F.; Vroman, B.; Lecouturier, N.; Crokart, N.; Pourcelle, V.; Freichels, H.; Jérôme, C.; Marchand-Brynaert, J.; Feron, O.; Préat, V. Targeting of tumor endothelium by RGD-grafted PLGA-nanoparticles loaded with Paclitaxel. *J. Control. Release* **2009,** 140, 166-173.

221. Temming, K.; Schiffelers, R. M.; Molema, G.; Kok, R. J. RGD-based strategies for selective delivery of therapeutics and imaging agents to the tumour vasculature. *Drug Resistance Updates* **2005,** 8, 381-402.

222. Sapra, P.; Allen, T. M. Internalizing antibodies are necessary for improved therapeutic efficacy of antibody-targeted liposomal drugs. *Cancer Res.* **2002,** 62, 7190-7194.

223. Maruyama, K.; Ishida, O.; Takizawa, T.; Moribe, K. Possibility of active targeting to tumor tissues with liposomes. *Adv. Drug Deliv. Rev.* **1999,** 40, 89-102.

224. Allen, T. M.; Agrawal, A. K.; Ahmad, I.; Hansen, C. B.; Zalipsky, S. Antibody-mediated targeting of long-circulating (StealthR) liposomes. *J. Liposome Res.* **1994,** 4, 1-25.

225. Kamps, J.; Koning, G.; Velinova, M.; Morselt, H.; Wilkens, M.; Gorter, A.; Donga, J.; Scherphof, G. Uptake of long-circulating immunoliposomes, directed against colon adenocarcinoma cells, by liver metastases of colon cancer. *J. Drug Target.* **2000,** 8, 235-245.

226. Goren, D.; Horowitz, A.; Zalipsky, S.; Woodle, M.; Yarden, Y.; Gabizon, A. Targeting of stealth liposomes to erbB-2 (Her/2) receptor: in vitro and in vivo studies. *Br. J. Cancer* **1996,** 74, 1749-1756.

227. Bae, Y. H. Drug targeting and tumor heterogeneity. *J. Control. Release* **2009,** 133, 2-3.

228. Kirpotin, D. B.; Drummond, D. C.; Shao, Y.; Shalaby, M. R.; Hong, K.; Nielsen, U. B.; Marks, J. D.; Benz, C. C.; Park, J. W. Antibody targeting of long-circulating lipidic nanoparticles does not increase tumor localization but does increase internalization in animal models. *Cancer Res.* **2006,** 66, 6732-6740.

229. Trere, D.; Fiume, L.; De Giorgi, L. B.; Di Stefano, G.; Migaldi, M.; Derenzini, M. The asialoglycoprotein receptor in human hepatocellular carcinomas: its expression on proliferating cells. *Br. J. Cancer* **1999,** 81, 404-408.

230. Duncan, R.; Kopecek, J.; Rejmanova, P.; Lloyd, J. Targeting of *N*-(2-hydroxypropyl) methacrylamide copolymers to liver by incorporation of galactose residues. *Biochim. Biophys. Acta.* **1983,** 755, 518-521.

231. Duncan, R.; Seymour, L. C. W.; Scarlett, L.; Lloyd, J. B.; Rejmanova, P. Fate of *N*-(2-hydroxypropyl) methacrylamide copolymers with pendent galactosamine residues after intravenous administration to rats. *Biochim. Biophys. Acta.* **1986,** 880, 62-71.

232. Seymour, L.; Ulbrich, K.; Wedge, S.; Hume, I.; Strohalm, J.; Duncan, R. *N*-(2-hydroxypropyl) methacrylamide copolymers targeted to the hepatocyte galactose-receptor: pharmacokinetics in DBA2 mice. *Br. J. Cancer* **1991,** 63, 859-866.

233. Chauhan, V. P.; Stylianopoulos, T.; Boucher, Y.; Jain, R. K. Delivery of molecular and nanoscale medicine to tumors: Transport barriers and strategies. *Annu. Rev. Chem. Biomol. Eng.* **2011,** 2, 281-298.

234. Zlotecki, R. A.; Baxter, L. T.; Boucher, Y.; Jain, R. K. Pharmacologic modification of tumor blood flow and interstitial fluid pressure in a human tumor xenograft: network analysis and mechanistic interpretation. *Microvasc. Res.* **1995,** 50, 429-443.

235. Li, C.; Miyamoto, Y.; Kojima, Y.; Maeda, H. Augmentation of tumour delivery of macromolecular drugs with reduced bone marrow delivery by elevating blood pressure. *Br. J. Cancer* **1993,** 67, 975-980.

236. Nagamitsu, A.; Greish, K.; Maeda, H. Elevating blood pressure as a strategy to increase tumor-targeted delivery of macromolecular drug SMANCS: cases of advanced solid tumors. *Jpn. J. Clin. Oncol.* **2009,** 39, 756-766.

237. Zlotecki, R. A.; Boucher, Y.; Lee, I.; Baxter, L. T.; Jain, R. K. Effect of angiotensin II induced hypertension on tumor blood flow and interstitial fluid pressure. *Cancer Res.* **1993,** 53, 2466-2468.

238. Burton, M. A.; Gray, B. N.; Self, G. W.; Heggie, J. C.; Townsend, P. S. Manipulation of experimental rat and rabbit liver tumor blood flow with angiotensin II. *Cancer Res.* **1985,** 45, 5390-5393.

239. Suzuki, M.; Hori, K.; Abe, I.; Saito, S.; Sato, H. A new approach to cancer chemotherapy: selective enhancement of tumor blood flow with angiotensin II. *J. Natl. Cancer Inst.* **1981,** 67, 663-669.

240. Chaplin, D. J.; Hill, S. A.; Bell, K. M.; Tozer, G. M. Modification of tumor blood flow: Current status and future directions. *Semin. Radiat. Oncol.* **1998,** 8, 151-163.

241. Seki, T.; Fang, J.; Maeda, H. Enhanced delivery of macromolecular antitumor drugs to tumors by nitroglycerin application. *Cancer Sci.* **2009,** 100, 2426-2430.

242. Tozer, G. M.; Prise, V. E.; Chaplin, D. J. Inhibition of nitric oxide synthase induces a selective reduction in tumor blood flow that is reversible with L-arginine. *Cancer Res.* **1997,** 57, 948-955.

243. Chan, R.; Babbs, C.; Vetter, R.; Lamar, C. Abnormal response of tumor vasculature to vasoactive drugs. *J. Natl. Cancer Inst.* **1984,** 72, 145-150.

244. Brett, J.; Gerlach, H.; Nawroth, P.; Steinberg, S.; Godman, G.; Stern, D. Tumor necrosis factor/cachectin increases permeability of endothelial cell monolayers by a mechanism involving regulatory G proteins. *J. Exp. Med.* **1989,** 169, 1977-1991.

245. Aicher, K. P.; Dupon, J. W.; White, D. L.; Aukerman, S. L.; Moseley, M. E.; Juster, R.; Rosenau, W.; Winkelhake, J. L.; Brasch, R. C. Contrast-enhanced magnetic resonance imaging of tumor-bearing mice treated with human recombinant tumor necrosis factor α. *Cancer Res.* **1990,** 50, 7376-7381.

246. Paciotti, G. F.; Myer, L.; Weinreich, D.; Goia, D.; Pavel, N.; McLaughlin, R. E.; Tamarkin, L. Colloidal gold: a novel nanoparticle vector for tumor directed drug delivery. *Drug Deliv.* **2004,** 11, 169-183.

247. Farma, J. M.; Puhlmann, M.; Soriano, P. A.; Cox, D.; Paciotti, G. F.; Tamarkin, L.; Alexander, H. R. Direct evidence for rapid and selective induction of tumor

neovascular permeability by tumor necrosis factor and a novel derivative, colloidal gold bound tumor necrosis factor. *Int. J. Cancer* **2007,** 120, 2474-2480.

248. Zhao, L.; Ching, L. M.; Kestell, P.; Kelland, L. R.; Baguley, B. C. Mechanisms of tumor vascular shutdown induced by 5, 6-dimethylxanthenone-4-acetic acid (DMXAA): Increased tumor vascular permeability. *Int. J. Cancer* **2005,** 116, 322-326.

249. Galbraith, S. M.; Rustin, G. J. S.; Lodge, M. A.; Taylor, N. J.; Stirling, J. J.; Jameson, M.; Thompson, P.; Hough, D.; Gumbrell, L.; Padhani, A. R. Effects of 5, 6-dimethylxanthenone-4-acetic acid on human tumor microcirculation assessed by dynamic contrast-enhanced magnetic resonance imaging. *J. Clin. Oncol.* **2002,** 20, 3826-3840.

250. Sherwood, L. M.; Parris, E. E.; Folkman, J. Tumor angiogenesis: therapeutic implications. *N. Engl. J. Med.* **1971,** 285, 1182-1186.

251. Carmeliet, P.; Jain, R. K. Principles and mechanisms of vessel normalization for cancer and other angiogenic diseases. *Nat. Rev. Cancer* **2011,** 10, 417-427.

252. Winkler, F.; Kozin, S. V.; Tong, R. T.; Chae, S. S.; Booth, M. F.; Garkavtsev, I.; Xu, L.; Hicklin, D. J.; Fukumura, D.; di Tomaso, E. Kinetics of vascular normalization by VEGFR2 blockade governs brain tumor response to radiation:: Role of oxygenation, angiopoietin-1, and matrix metalloproteinases. *Cancer Cell* **2004,** 6, 553-563.

253. Wildiers, H.; Guetens, G.; De Boeck, G.; Verbeken, E.; Landuyt, B.; Landuyt, W.; De Bruijn, E.; van Oosterom, A. T. Effect of antivascular endothelial growth factor treatment on the intratumoral uptake of CPT-11. *Br. J. Cancer* **2003,** 88, 1979-1986.

254. Chauhan, V. P.; Stylianopoulos, T.; Martin, J. D.; Popović, Z.; Chen, O.; Kamoun, W. S.; Bawendi, M. G.; Fukumura, D.; Jain, R. K. Normalization of tumour blood vessels improves the delivery of nanomedicines in a size-dependent manner. *Nat. Nanotechnol.* **2012,** 7, 383-388.

255. Griffon-Etienne, G.; Boucher, Y.; Brekken, C.; Suit, H. D.; Jain, R. K. Taxane-induced apoptosis decompresses blood vessels and lowers interstitial fluid pressure in solid tumors. *Cancer Res.* **1999,** 59, 3776-3782.

256. Magzoub, M.; Jin, S.; Verkman, A. Enhanced macromolecule diffusion deep in tumors after enzymatic digestion of extracellular matrix collagen and its associated proteoglycan decorin. *FASEB J.* **2008,** 22, 276-284.

257. Wong, C.; Stylianopoulos, T.; Cui, J.; Martin, J.; Chauhan, V. P.; Jiang, W.; Popović, Z.; Jain, R. K.; Bawendi, M. G.; Fukumura, D. Multistage nanoparticle

delivery system for deep penetration into tumor tissue. *Proc. Natl. Acad. Sci. USA.* **2011,** 108, 2426-2431.

258. Serda, R. E.; Godin, B.; Blanco, E.; Chiappini, C.; Ferrari, M. Multi-stage delivery nano-particle systems for therapeutic applications. *Biochim. Biophys. Acta.* **2011,** 1810, 317-329.

259. Yavuz, M. S.; Cheng, Y.; Chen, J.; Cobley, C. M.; Zhang, Q.; Rycenga, M.; Xie, J.; Kim, C.; Song, K. H.; Schwartz, A. G.; Wang, L. V.; Xia, Y. Gold nanocages covered by smart polymers for controlled release with near-infrared light. *Nat. Mater.* **2009,** 8, 935-939.

260. ter Haar, G. Therapeutic ultrasound. *Eur. J. Ultrasound* **1999,** 9, 3-9.

261. Aus, G. Current status of HIFU and cryotherapy in prostate cancer–a review. *Eur. Urol.* **2006,** 50, 927-934.

262. Mitragotri, S. Healing sound: the use of ultrasound in drug delivery and other therapeutic applications. *Nat. Rev. Drug Discov.* **2005,** 4, 255-260.

263. Hancock, H. A.; Smith, L. H.; Cuesta, J.; Durrani, A. K.; Angstadt, M.; Palmeri, M. L.; Kimmel, E.; Frenkel, V. Investigations into pulsed high-intensity focused ultrasound–enhanced delivery: Preliminary evidence for a novel mechanism. *Ultrasound Med. Biol.* **2009,** 35, 1722-1736.

264. Mitragotri, S.; Blankschtein, D.; Langer, R. Ultrasound-mediated transdermal protein delivery. *Science* **1995,** 269, 850-853.

265. Miller, D. L.; Pislaru, S. V.; Greenleaf, J. F. Sonoporation: mechanical DNA delivery by ultrasonic cavitation. *Somat. Cell Mol. Genet.* **2002,** 27, 115-134.

266. Deng, C. X.; Sieling, F.; Pan, H.; Cui, J. Ultrasound-induced cell membrane porosity. *Ultrasound Med. Biol.* **2004,** 30, 519-526.

267. Hynynen, K.; McDannold, N.; Sheikov, N. A.; Jolesz, F. A.; Vykhodtseva, N. Local and reversible blood-brain barrier disruption by noninvasive focused ultrasound at frequencies suitable for trans-skull sonications. *Neuroimage.* **2005,** 24, 12-20.

268. McDannold, N.; Vykhodtseva, N.; Hynynen, K. Targeted disruption of the blood–brain barrier with focused ultrasound: association with cavitation activity. *Phys. Med. Biol.* **2006,** 51, 793-807.

269. Larina, I. V.; Evers, B. M.; Ashitkov, T. V.; Bartels, C.; Larin, K. V.; Esenaliev, R. O. Enhancement of drug delivery in tumors by using interaction of

nanoparticles with ultrasound radiation. *Technol. Cancer Res. Treat.* **2005,** 4, 217-226.

270. Yuh, E. L.; Shulman, S. G.; Mehta, S. A.; Xie, J.; Chen, L.; Frenkel, V.; Bednarski, M. D.; Li, K. C. P. Delivery of systemic chemotherapeutic agent to tumors by using focused ultrasound: Study in a murine model. *Radiology* **2005,** 234, 431-437.

271. Frenkel, V.; Etherington, A.; Greene, M.; Quijano, J.; Xie, J.; Hunter, F.; Dromi, S.; Li, K. C. P. Delivery of liposomal doxorubicin (Doxil) in a breast cancer tumor model: investigation of potential enhancement by pulsed-high intensity focused ultrasound exposure. *Acad. Radiol.* **2006,** 13, 469-479.

272. Vega, V. L.; Charles, W.; De Maio, A. A new feature of the stress response: increase in endocytosis mediated by Hsp70. *Cell Stress Chaperones* **2009,** 15, 517-527.

273. Vega, V. L.; De Maio, A. Increase in phagocytosis after geldanamycin treatment or heat shock: role of heat shock proteins. *J. Immunol.* **2005,** 175, 5280-5287.

274. Song, C. W. Effect of local hyperthermia on blood flow and microenvironment: a review. *Cancer Res.* **1984,** 44, 4721s-4730s.

275. Fujiwara, K.; Watanabe, T. Effects of hyperthermia, radiotherapy and thermoradiotherapy on tumor microvascular permeability. *Pathol. Int.* **2008,** 40, 79-84.

276. Lefor, A. T.; Makohon, S.; Ackerman, N. B. The effects of hyperthermia on vascular permeability in experimental liver metastasis. *J. Surg. Oncol.* **1985,** 28, 297-300.

277. Fajardo, L.; Schreiber, A.; Kelly, N.; Hahn, G. Thermal sensitivity of endothelial cells. *Radiat. Res.* **1985,** 103, 276-285.

278. Chen, B.; Zhou, M.; Xu, L. Study of vascular endothelial cell morphology during hyperthermia. *J. Therm. Biol.* **2005,** 30, 111-117.

279. Xu, L.; Chen, B.; Zhou, M. Change of individual vascular endothelial calcium during hyperthermia. *J. Therm. Biol.* **2006,** 31, 302-306.

280. Kong, G.; Dewhirst, M. W. Hyperthermia and liposomes. *Int. J. Hyperthermia* **1999,** 15, 345-370.

281. Huang, S. K.; Stauffer, P. R.; Hong, K.; Guo, J. W. H.; Phillips, T. L.; Huang, A.; Papahadjopoulos, D. Liposomes and hyperthermia in mice: increased tumor

uptake and therapeutic efficacy of doxorubicin in sterically stabilized liposomes. *Cancer Res.* **1994,** 54, 2186-2191.

282. Weinstein, J.; Magin, R.; Yatvin, M.; Zaharko, D. Liposomes and local hyperthermia: selective delivery of methotrexate to heated tumors. *Science* **1979,** 204, 188-191.

283. Gaber, M. H.; Wu, N. Z.; Hong, K.; Huang, S. K.; Dewhirst, M. W.; Papahadjopoulos, D. Thermosensitive liposomes: extravasation and release of contents in tumor microvascular networks. *Int. J. Radiat. Oncol. Biol. Phys.* **1996,** 36, 1177-1187.

284. Lammers, T.; Peschke, P.; Kühnlein, R.; Subr, V.; Ulbrich, K.; Debus, J.; Huber, P.; Hennink, W.; Storm, G. Effect of radiotherapy and hyperthermia on the tumor accumulation of HPMA copolymer-based drug delivery systems. *J. Control. Release* **2007,** 117, 333-341.

285. Kong, G.; Braun, R. D.; Dewhirst, M. W. Hyperthermia enables tumor-specific nanoparticle delivery: effect of particle size. *Cancer Res.* **2000,** 60, 4440-4445.

286. Matteucci, M. L.; Anyarambhatla, G.; Rosner, G.; Azuma, C.; Fisher, P. E.; Dewhirst, M. W.; Needham, D.; Thrall, D. E. Hyperthermia increases accumulation of technetium-99m-labeled liposomes in feline sarcomas. *Clin. Cancer Res.* **2000,** 6, 3748-3755.

287. Kong, G.; Braun, R. D.; Dewhirst, M. W. Characterization of the effect of hyperthermia on nanoparticle extravasation from tumor vasculature. *Cancer Res.* **2001,** 61, 3027-3032.

288. Chen, Q.; Krol, A.; Wright, A.; Needham, D.; Dewhirst, M.; Yuan, F. Tumor microvascular permeability is a key determinant for antivascular effects of doxorubicin encapsulated in a temperature sensitive liposome. *Int. J. Hyperthermia* **2008,** 24, 475-482.

289. Liu, P.; Zhang, A.; Xu, Y.; Xu, L. X. Study of non-uniform nanoparticle liposome extravasation in tumour. *Int. J. Hyperthermia* **2005,** 21, 259-270.

290. Rewcastle, J. High intensity focused ultrasound for prostate cancer: a review of the scientific foundation, technology and clinical outcomes. *Technol. Cancer Res. Treat.* **2006,** 5, 619-625.

291. Ripert, T.; Azémar, M. D.; Ménard, J.; Bayoud, Y.; Messaoudi, R.; Duval, F.; Staerman, F. Transrectal high-intensity focused ultrasound (HIFU) treatment of localized prostate cancer: review of technical incidents and morbidity after 5 years of use. *Prostate Cancer Prostatic Dis.* **2010,** 13, 132-137.

292. Huang, X.; Jain, P. K.; El-Sayed, I. H.; El-Sayed, M. A. Gold nanoparticles: interesting optical properties and recent applications in cancer diagnostics and therapy. *Nanomed.* **2007,** 2, 681-693.

293. Jain, P. K.; El-Sayed, I. H.; El-Sayed, M. A. Au nanoparticles target cancer. *Nano Today* **2007,** 2, 18-29.

294. Huang, X.; Jain, P. K.; El-Sayed, I. H.; El-Sayed, M. A. Plasmonic photothermal therapy (PPTT) using gold nanoparticles. *Lasers Med. Sci.* **2008,** 23, 217-228.

295. Faraday, M. The Bakerian Lecture: Experimental relations of gold (and other metals) to light. *Phil. Trans.* **1857,** 147, 145-181.

296. Link, S.; El-Sayed, M. A. Shape and size dependence of radiative, non-radiative and photothermal properties of gold nanocrystals. *Int. Rev. Phys. Chem.* **2000,** 19, 409-453.

297. Vollmer, M.; Kreibig, U. Optical properties of metal clusters. *Springer Ser. Mat. Sci* **1995,** 25.

298. Mie, G. Contributions to the optics of diffusing media. *Ann physik* **1908,** 25.

299. Link, S.; El-Sayed, M. A. Size and temperature dependence of the plasmon absorption of colloidal gold nanoparticles. *J. Phys. Chem. B* **1999,** 103, 4212-4217.

300. Gans, R. Propagation of light through an inhomogeneous medium. *Ann. Physik* **1915,** 47, 709-738.

301. Link, S.; Mohamed, M.; El-Sayed, M. Simulation of the optical absorption spectra of gold nanorods as a function of their aspect ratio and the effect of the medium dielectric constant. *J. Phys. Chem. B* **1999,** 103, 3073-3077.

302. Taroni, P.; Pifferi, A.; Torricelli, A.; Comelli, D.; Cubeddu, R. In vivo absorption and scattering spectroscopy of biological tissues. *Photochem. Photobiol. Sci.* **2003,** 2, 124-129.

303. Petrova, H.; Hu, M.; Hartland, G. Photothermal properties of gold nanoparticles. *Z. Phys. Chem* **2007,** 221, 361-376.

304. Voisin, C.; Del Fatti, N.; Christofilos, D.; Vallée, F. Ultrafast electron dynamics and optical nonlinearities in metal nanoparticles. *J. PHys. Chem. B* **2001,** 105, 2264-2280.

305. Arbouet, A.; Voisin, C.; Christofilos, D.; Langot, P.; Fatti, N. D.; Vallée, F.; Lermé, J.; Celep, G.; Cottancin, E.; Gaudry, M. Electron-phonon scattering in metal clusters. *Phys. Rev. Lett.* **2003,** 90, 177401.1-177401.4.

306. Sassaroli, E.; Li, K.; O'Neill, B. Numerical investigation of heating of a gold nanoparticle and the surrounding microenvironment by nanosecond laser pulses for nanomedicine applications. *Phys. Med. Biol.* **2009,** 54, 5541-5560.

307. Cole, J. R.; Mirin, N. A.; Knight, M. W.; Goodrich, G. P.; Halas, N. J. Photothermal efficiencies of nanoshells and nanorods for clinical therapeutic applications. *J. Phys. Chem. C* **2009,** 113, 12090-12094.

308. Dickerson, E. B.; Dreaden, E. C.; Huang, X.; El-Sayed, I. H.; Chu, H.; Pushpanketh, S.; McDonald, J. F.; El-Sayed, M. A. Gold nanorod assisted near-infrared plasmonic photothermal therapy (PPTT) of squamous cell carcinoma in mice. *Cancer Lett.* **2008,** 269, 57-66.

309. Arnida; Malugin, A.; Ghandehari, H. Cellular uptake and toxicity of gold nanoparticles in prostate cancer cells: a comparative study of rods and spheres. *J. Appl. Toxicol.* **2009,** 30, 212-217.

310. Gratton, S. E.; Ropp, P. A.; Pohlhaus, P. D.; Luft, J. C.; Madden, V. J.; Napier, M. E.; DeSimone, J. M. The effect of particle design on cellular internalization pathways. *Proc. Natl. Acad. Sci. USA.* **2008,** 105, 11613-11618.

311. Jiang, W.; Kim, B. Y. S.; Rutka, J. T.; Chan, W. C. Nanoparticle-mediated cellular response is size-dependent. *Nat. Nanotechnol.* **2008,** 3, 145-150.

312. Pan, Y.; Neuss, S.; Leifert, A.; Fischler, M.; Wen, F.; Simon, U.; Schmid, G.; Brandau, W.; Jahnen-Dechent, W. Size-dependent cytotoxicity of gold nanoparticles. *Small* **2007,** 3, 1941-1949.

313. Takahashi, H.; Niidome, Y.; Niidome, T.; Kaneko, K.; Kawasaki, H.; Yamada, S. Modification of gold nanorods using phosphatidylcholine to reduce cytotoxicity. *Langmuir* **2006,** 22, 2-5.

314. Goodman, C. M.; McCusker, C. D.; Yilmaz, T.; Rotello, V. M. Toxicity of gold nanoparticles functionalized with cationic and anionic side chains. *Bioconjug. Chem.* **2004,** 15, 897-900.

315. Arnida, M.; Janat-Amsbury, M.; Ray, A.; Peterson, C.; Ghandehari, H. Geometry and surface characteristics of gold nanoparticles influence their biodistribution and uptake by macrophages. *Eur. J. Pharm. Biopharm.* **2011,** 77, 417-423.

316. Aggarwal, P.; Hall, J. B.; McLeland, C. B.; Dobrovolskaia, M. A.; McNeil, S. E. Nanoparticle interaction with plasma proteins as it relates to particle

biodistribution, biocompatibility and therapeutic efficacy. *Adv. Drug Deliv. Rev.* **2009,** 61, 428-437.

317. Dobrovolskaia, M. A.; Patri, A. K.; Zheng, J.; Clogston, J. D.; Ayub, N.; Aggarwal, P.; Neun, B. W.; Hall, J. B.; McNeil, S. E. Interaction of colloidal gold nanoparticles with human blood: effects on particle size and analysis of plasma protein binding profiles. *Nanomedicine* **2009,** 5, 106-117.

318. Lacerda, S. H. D. P.; Park, J. J.; Meuse, C.; Pristinski, D.; Becker, M. L.; Karim, A.; Douglas, J. F. Interaction of gold nanoparticles with common human blood proteins. *ACS Nano* **2009,** 4, 365-379.

319. Jeon, S.; Lee, J.; Andrade, J.; De Gennes, P. Protein--surface interactions in the presence of polyethylene oxide: I. Simplified theory. *J. Colloid Interface. Sci.* **1991,** 142, 149-158.

320. Niidome, T.; Yamagata, M.; Okamoto, Y.; Akiyama, Y.; Takahashi, H.; Kawano, T.; Katayama, Y.; Niidome, Y. PEG-modified gold nanorods with a stealth character for in vivo applications. *J. Control. Release* **2006,** 114, 343-347.

321. Park, J.; Estrada, A.; Schwartz, J. A.; Diagaradjane, P.; Krishnan, S.; Dunn, A. K.; Tunnell, J. W. Intra-organ biodistribution of gold nanoparticles using intrinsic two-photon-induced photoluminescence. *Lasers Surg. Med.* **2010,** 42, 630-639.

322. Feng, Y.; Fuentes, D.; Hawkins, A.; Bass, J.; Rylander, M. N.; Elliott, A.; Shetty, A.; Stafford, R. J.; Oden, J. T. Nanoshell-mediated laser surgery simulation for prostate cancer treatment. *Eng. Comput.* **2009,** 25, 3-13.

323. Hirsch, L. R.; Stafford, R. J.; Bankson, J. A.; Sershen, S. R.; Rivera, B.; Price, R. E.; Hazle, J. D.; Halas, N. J.; West, J. L. Nanoshell-mediated near-infrared thermal therapy of tumors under magnetic resonance guidance. *Proc. Natl. Acad. Sci. USA.* **2003,** 100, 13549-13554.

324. O'Neal, D. P.; Hirsch, L. R.; Halas, N. J.; Payne, J. D.; West, J. L. Photo-thermal tumor ablation in mice using near infrared-absorbing nanoparticles. *Cancer Lett.* **2004,** 209, 171-176.

325. Stern, J. M.; Stanfield, J.; Lotan, Y.; Park, S.; Hsieh, J. T.; Cadeddu, J. A. Efficacy of laser-activated gold nanoshells in ablating prostate cancer cells in vitro. *J. Endourol.* **2007,** 21, 939-943.

326. Stern, J. M.; Stanfield, J.; Kabbani, W.; Hsieh, J. T.; Cadeddu, J. A. Selective prostate cancer thermal ablation with laser activated gold nanoshells. *J. Urol.* **2008,** 179, 748-753.

327. von Maltzahn, G.; Park, J. H.; Agrawal, A.; Bandaru, N. K.; Das, S. K.; Sailor, M. J.; Bhatia, S. N. Computationally guided photothermal tumor therapy using long-circulating gold nanorod antennas. *Cancer Res.* **2009,** 69, 3892-3900.

328. Huang, X.; El-Sayed, I. H.; Qian, W.; El-Sayed, M. A. Cancer cell imaging and photothermal therapy in the near-infrared region by using gold nanorods. *J. Am. Chem. Soc.* **2006,** 128, 2115-2120.

329. Zharov, V. P.; Letfullin, R. R.; Galitovskaya, E. N. Microbubbles-overlapping mode for laser killing of cancer cells with absorbing nanoparticle clusters. *J. Phys. D: Appl. Phys.* **2005,** 38, 2571-2581.

330. Yao, C.; Rahmanzadeh, R.; Endl, E.; Zhang, Z.; Gerdes, J.; Hüttmann, G. Elevation of plasma membrane permeability by laser irradiation of selectively bound nanoparticles. *J. Biomed. Opt.* **2005,** 10, 064012.1-064012.8.

331. Tong, L.; Cheng, J. X. Gold nanorod-mediated photothermolysis induces apoptosis of macrophages via damage of mitochondria. *Nanomedicine* **2009,** 4, 265-276.

332. Tong, L.; Zhao, Y.; Huff, T. B.; Hansen, M. N.; Wei, A.; Cheng, J. X. Gold nanorods mediate tumor cell death by compromising membrane integrity. *Adv. Mater. Deerfield* **2007,** 19, 3136-3141.

333. Lapotko, D. O.; Lukianova, E.; Oraevsky, A. A. Selective laser nano-thermolysis of human leukemia cells with microbubbles generated around clusters of gold nanoparticles. *Lasers Surg. Med.* **2006,** 38, 631-642.

334. Huang, X.; Jain, P. K.; El-Sayed, I. H.; El-Sayed, M. A. Determination of the minimum temperature required for selective photothermal destruction of cancer cells with the use of immunotargeted gold nanoparticles. *Photochem. Photobiol.* **2006,** 82, 412-417.

335. Huff, T. B.; Tong, L.; Zhao, Y.; Hansen, M. N.; Cheng, J. X.; Wei, A. Hyperthermic effects of gold nanorods on tumor cells. *Nanomedicine* **2007,** 2, 125-132.

336. Lapotko, D.; Lukianova, E.; Potapnev, M.; Aleinikova, O.; Oraevsky, A. Method of laser activated nano-thermolysis for elimination of tumor cells. *Cancer Lett.* **2006,** 239, 36-45.

337. Jain, P. K.; Lee, K. S.; El-Sayed, I. H.; El-Sayed, M. A. Calculated absorption and scattering properties of gold nanoparticles of different size, shape, and composition: applications in biological imaging and biomedicine. *J. Phys. Chem. B* **2006,** 110, 7238-7248.

338. Sun, Y.; Xia, Y. Shape-controlled synthesis of gold and silver nanoparticles. *Science* **2002,** 298, 2176-2179.

339. Schwartz, J. A.; Shetty, A. M.; Price, R. E.; Stafford, R. J.; Wang, J. C.; Uthamanthil, R. K.; Pham, K.; McNichols, R. J.; Coleman, C. L.; Payne, J. D. Feasibility study of particle-assisted laser ablation of brain tumors in orthotopic canine model. *Cancer Res.* **2009,** 69, 1659-1667.

340. Ponce, A. M.; Vujaskovic, Z.; Yuan, F.; Needham, D.; Dewhirst, M. W. Hyperthermia mediated liposomal drug delivery. *Int. J. Hyperthermia* **2006,** 22, 205-213.

341. Tungjitkusolmun, S.; Staelin, S. T.; Haemmerich, D.; Tsai, J. Z.; Cao, H.; Webster, J. G.; Lee Jr, F. T.; Mahvi, D. M.; Vorperian, V. R. Three-dimensional finite-element analyses for radio-frequency hepatic tumor ablation. *Biomedical Engineering, IEEE Transactions on* **2002,** 49, 3-9.

342. Diagaradjane, P.; Shetty, A.; Wang, J. C.; Elliott, A. M.; Schwartz, J.; Shentu, S.; Park, H. C.; Deorukhkar, A.; Stafford, R. J.; Cho, S. H. Modulation of in vivo tumor radiation response via gold nanoshell-mediated vascular-focused hyperthermia: characterizing an integrated antihypoxic and localized vascular disrupting targeting strategy. *Nano Lett.* **2008,** 8, 1492-1500.

343. Park, J. H.; von Maltzahn, G.; Xu, M. J.; Fogal, V.; Kotamraju, V. R.; Ruoslahti, E.; Bhatia, S. N.; Sailor, M. J. Cooperative nanomaterial system to sensitize, target, and treat tumors. *Proc. Natl. Acad. Sci. USA.* **2010,** 107, 981-986.

344. Park, J. H.; Maltzahn, G. v.; Ong, L. L.; Centrone, A.; Hatton, T. A.; Ruoslahti, E.; Bhatia, S. N.; Sailor, M. J. Cooperative nanoparticles for tumor detection and photothermally triggered drug delivery. *Adv. Mater.* **2010,** 22, 880-885.

345. Von Maltzahn, G.; Park, J. H.; Lin, K. Y.; Singh, N.; Schwöppe, C.; Mesters, R.; Berdel, W. E.; Ruoslahti, E.; Sailor, M. J.; Bhatia, S. N. Nanoparticles that communicate in vivo to amplify tumour targeting. *Nat. Mater.* **2011,** 10, 545-552.

346. Sonavane, G.; Tomoda, K.; Makino, K. Biodistribution of colloidal gold nanoparticles after intravenous administration: Effect of particle size. *Colloids Surf. B Interfaces* **2008,** 66, 274-280.

CHAPTER 3

GOLD NANOROD MEDIATED PLASMONIC PHOTOTHERMAL THERAPY: A TOOL TOENHANCE MACROMOLECULAR DELIVERY

3.1 Introduction

It is well known that the permeability of tumor blood vessels is higher than that of tissues with a healthy morphology.[1] EPR mainly due to large intercellular gaps between endothelial cells in tumor blood vessels allow for the diffusion of macromolecules out of the bloodstream enabling nanocarriers to deliver therapeutic anticancer drugs to cancerous cells.[2-3] Under conditions of elevated temperatures and increased blood perfusion, it has been found that this tumor microvascular permeability is significantly increased.[4-5] For example, the extravasation of Evans blue dye (EBD), a dye with high albumin affinity and therefore serving as a macromolecule indicator, as well as liposomes have been shown to be enhanced under conditions of hyperthermia.[4, 6-10] This is believed to be due to endothelial cell injury and can therefore be used to enhance the passive delivery of nanocarriers.[11-14]

Despite the apparent advantages of using heat for either tumor ablation or enhancing the delivery of macromolecules, clinical use of tumor hyperthermia is difficult

---

Reprinted with permission from the International Journal of Pharmaceutics
Reference: Gormley, A. J.; et al., *Int. J. Pharm.* **2011,** 415, 315-318.

due to limited ability to deliver sufficient heat in target regions without harming native tissue.[15] More recently several laboratories have taken advantage of unique nanoscale events that occur when light is absorbed by plasmonic gold nanostructures. In brief, when light with a wavelength that matches the tunable SPR of gold nanostructures meets these particles, coherent oscillations of electrons in the conduction band allow the light to be absorbed and photothermal conversion to occur.[16] When such particles are localized within tissue with the intention of using this technique as a tool to induce hyperthermia, termed PPTT, effective heating is possible.[17] With PPTT, many groups have achieved tumor selective temperatures from 50°C to over 70°C, well above the threshold required for vascular damage.[18-22]

In this chapter, PPTT is used as a tool to induce both severe (46°C) and moderate hyperthermia (43°C). GNRs were used in this study as they are known to have higher absorption and scattering coefficients per unit size when compared to other architectures such as spheres or shells.[23] By quantifying EBD extravasation in tumors receiving PPTT, it is shown that such a technique may be used as a means of enhancing the permeability of tumor vessels and therefore enhancing the delivery of nanocarriers.

3.2 Materials and Methods

GNRs were synthesized with an SPR peak between 800-810 nm using the seed-mediated growth method.[24] After centrifugation and washing three times with deionized (DI) water, PEG (methoxy-PEG-thiol, 5 kD, Creative PEGWorks #PLS-604) was added to the GNR suspension (optical density (OD) = 10) at a final PEG concentration of 100 μM and stirred for 1 hour. The PEG-GNR mixture was then dialyzed (3.5 K MWCO,

Spectrum Labs #132594), centrifuged, washed and concentrated to remove unreacted PEG.

Mouse sarcoma S-180 cells were propagated by intraperitoneal injection (5×10^6 S-180 cells in 1 ml phosphate buffered saline (PBS)) in female CD-1 mice (4-6 weeks old) and allowed to grow until 15% weight gain was observed. Animals were then euthanized by CO_2 gas inhalation and the cells were harvested from the abdominal cavity. The cells were then washed to remove blood, diluted and subcutaneously injected into each flank of the animal (2×10^6 cells/flank in 200 µl PBS) while anesthetized with isofluorane. Tumors were then allowed to grow until average tumor volume reached 50-100 mm^3 (usually 7-10 days).

The animals were separated randomly into groups. Half received 200 µl of GNRs (9.6 mg/kg, OD = 120) and the other half saline by intravenous injection through the tail vein. After 24 hours, enough time for the GNRs to accumulate in the tumor at 1.22% injected dosed based on previous experiments and other reports in the literature,[19] the animals were anesthetized and the areas around the tumors were shaved and swabbed with 50% propylene glycol to facilitate laser penetration.[25] After 20 minutes, EBD (10 mg/kg in 200 µl saline) was injected intravenously and a 33 gauge needle thermocouple (Omega #HYP0-33-1-T-G-60-SMPW-M) was inserted into the center of the tumor to record temperatures. Then, an 808 nm fiber coupled laser diode (Oclaro #BMU6-808-02-R01) with collimating lens (Thorlabs #F810SMA-780, spot size = 7 mm) was directed over the right tumor and radiated. Two different laser powers were used in this study (1.6 and 1.2 W/cm^2) such that one group received severe and the other moderate tumor hyperthermia. After 10 minutes of radiation, the laser was turned off and tumors were

allowed to cool for two minutes before removal of the temperature probe. The left tumor did not receive laser treatment to serve as an internal control.

The thermal doses in these experiments were chosen based on reports in the literature. It is known that tumor vascular perfusion and permeability occurs maximally between 42-43°C.[27] Above this temperature range, damage to the microvascular network occurs leading to vascular ablation. Because of this, the experiment sought to test delivery when the temperature was between 42-43°C (1.2 W/cm^2). Because enhanced delivery is also expected even with tumor ablation, the experiment also tested 46°C (1.6 W/cm^2). This test was important to confirm ablation at this temperature. The length of laser treatment (10 min) was chosen based on results using a similar model which shows that 10 minutes of heating at 42°C is enough to enhance the delivery of albumin.[8]

After the animals were allowed to rest for 5 hours, enough time for the EBD to be cleared from the blood,[26] the animals were sacrificed by CO_2 inhalation. Both tumors were collected, weighed and the EBD was extracted in 1.5 ml of formamide for 48 hrs at 60°C. The EBD content was then measured spectrophotometrically at 620 nm and divided by the weight of the tumor.[26] The extravasation of EBD was then calculated as a ratio of the right (treated) to left (untreated) tumor and expressed as a TER.

3.3 Results and Discussion

The injection of PEGylated GNRs (60 x 15 nm ± 6 x 2 nm, SPR = 800 nm, Figure 3.1) in mice is well tolerated and no signs of distress or toxicity have been observed in this and other experiments. Immediately after initiation of laser treatment, temperatures inside the tumor climb rapidly and reach equilibrium within a few minutes (Figure 3.2).

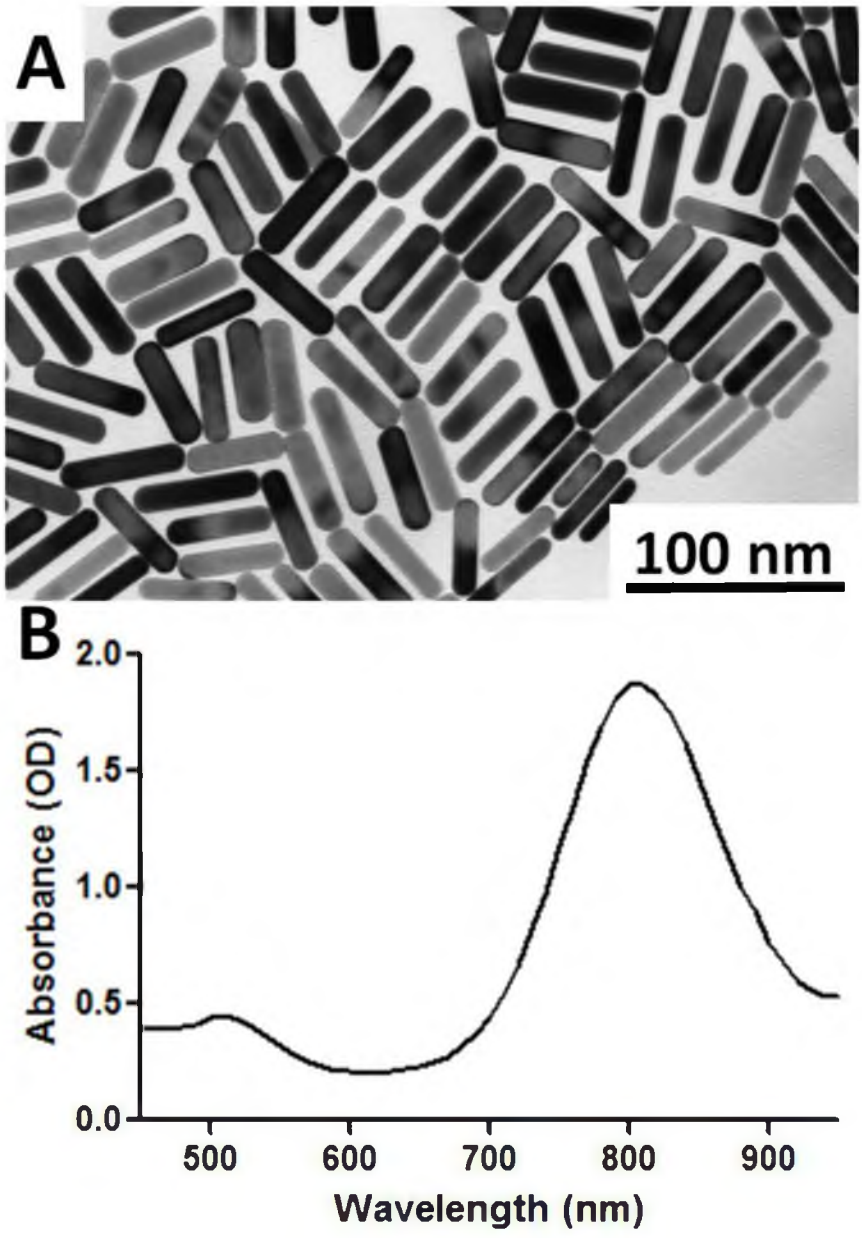

Figure 3.1: Characterization of GNRs. (A) Transmission electron micrograph (TEM) of GNRs; and (B) light absorption profile of GNRs (20 μg/ml) with SPR peak at 800 nm.

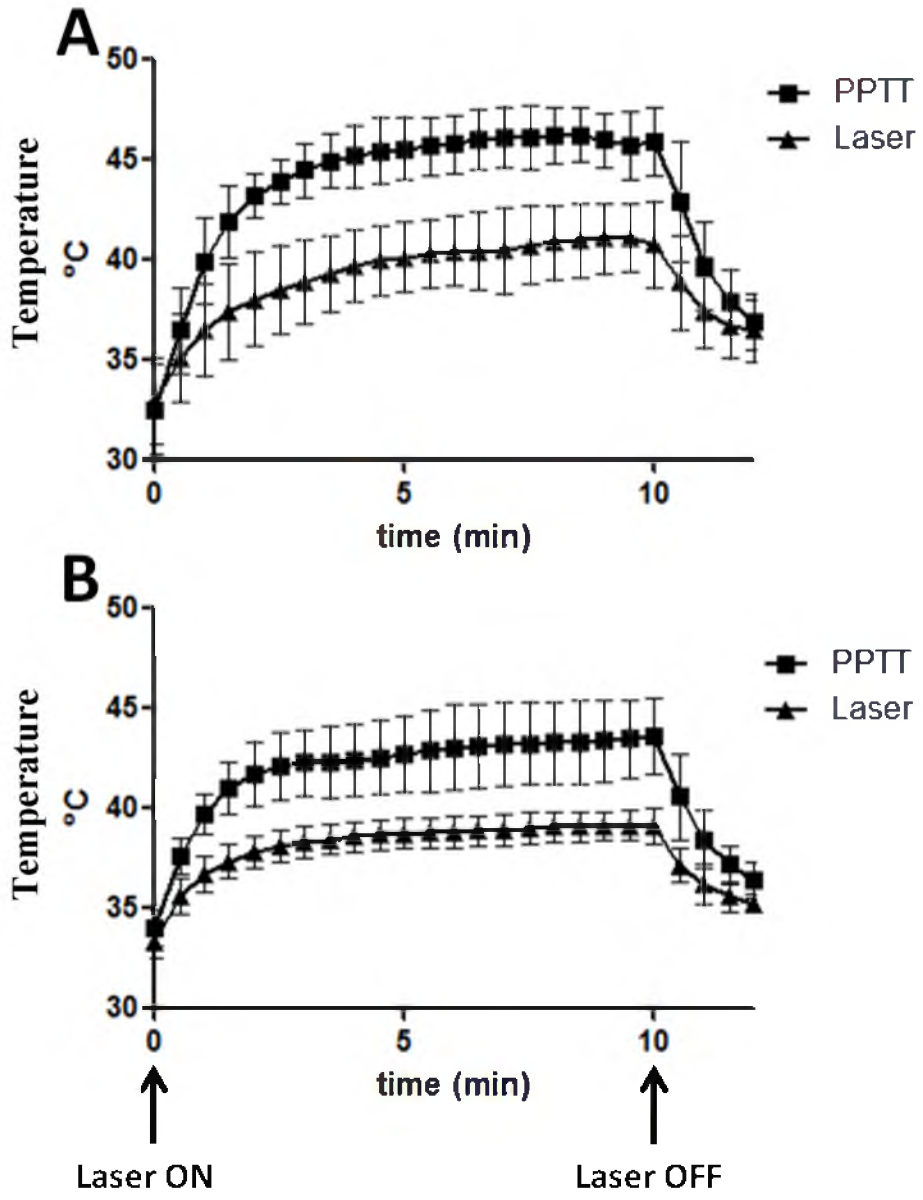

Figure 3.2: Intratumoral temperatures during PPTT or laser alone. Laser power = 1.6 W/cm^2 (A) and 1.2 W/cm^2 (B). Error bars represented as ±standard deviation.

Though treatment with laser alone (absence of GNRs) does result in some tissue heating, the presence of GNRs significantly amplifies the degree of heat generation at both laser powers tested. The temperatures inside the tumors in the last 10 seconds of laser treatment were averaged and the changes in temperatures as well as final temperatures are listed in Table 3.1. When groups were treated with PPTT using a laser power equal to 1.6 W/cm^2 and 1.2 W/cm^2, the average equilibrium temperature inside the tumors reaches 46.3°C and 43.6°C, respectively. Therefore, by changing the laser power alone, severe and moderate hyperthermia was able to be achieved.

After animal sacrifice five hours post laser treatment, the tumors were dissected out. In the animals receiving PPTT at 1.6 W/cm^2, significant bleeding was observed in most tumors due to conditions of severe hyperthermia. Additionally, the areas around the tumor were deeply colored in EBD indicating that the heat generated in the tumors caused the surrounding tissue to also heat. Though definitive conclusions cannot be made as to why this heating of normal tissue results in increased delivery of EBD, it is probable that the vessels dilated in response to insult and therefore the resulting increase in blood perfusion aided the delivery of EBD. In all other experimental groups, including animals treated with PPTT at 1.2 W/cm^2, no obvious hemorrhaging and local discoloration of surrounding tissue was observed.

Quantification of EBD in treated and untreated tumors, expressed as a ratio, indicates that PPTT does in fact enhance the delivery of macromolecules (Table 3.1 and Figure 3.3). When the average tumor temperature during PPTT was 46.3°C and 43.6°C, the extravasation of EBD was enhanced 1.82 and 1.68-fold respectively. Though the TER is statistically different between groups with and without GNRs ($p<0.01$), no

Table 3.1: Thermal enhancement ratio (TER)

Group	ΔT (°C)	Max T (°C)	TER
[a]PPTT, 1.6 W/cm^2	13.7 ± 2.9	46.3 ± 1.3	1.82 ± 0.40
[b]Laser, 1.6 W/cm^2	8.3 ± 1.8	41.2 ± 1.7	1.05 ± 0.15
[b]PPTT, 1.2 W/cm^2	9.6 ± 2.3	43.6 ± 1.9	1.68 ± 0.65
[c]Laser, 1.2 W/cm^2	6.0 ± 1.1	39.3 ± 0.8	0.94 ± 0.25

Numbers expressed as: mean ± standard deviation

[a] N = 7

[b] N = 6

[c] N = 10

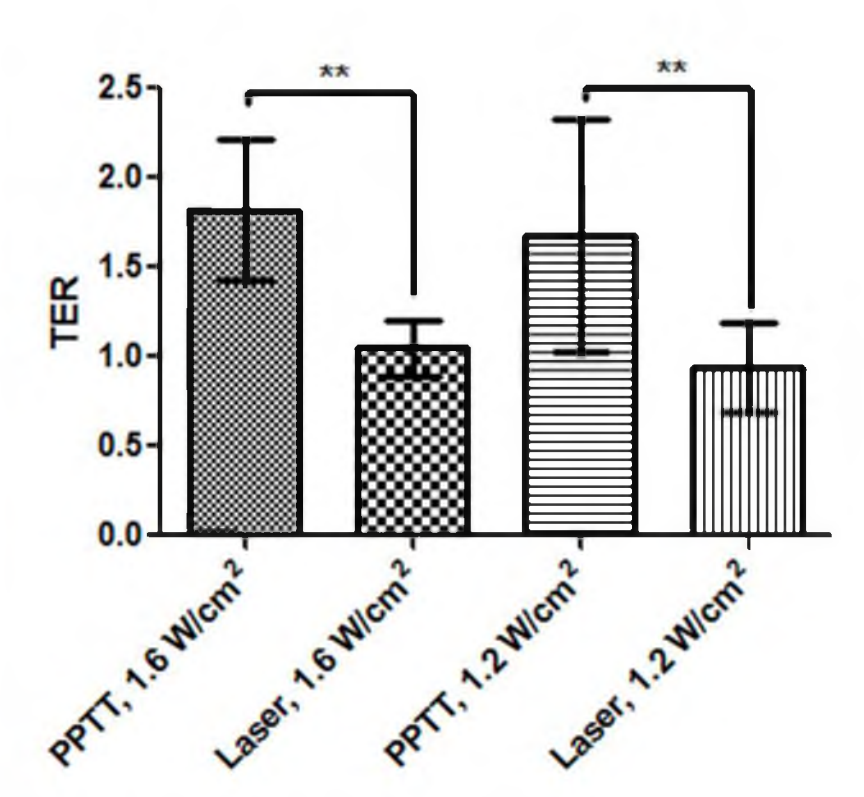

Figure 3.3: Evans blue dye (EBD) delivery TER. **Indicates a statistically significant difference ($p<0.01$) by one-way analysis of variance (ANOVA). Error bars represented as ±standard deviation

statistical difference is observed between both groups that received PPTT at different laser intensities. As expected, when laser treatment was applied without the presence of GNRs, the TER was around 1.0, indicating that the heat generated by laser alone, used under these study conditions, did not increase tumor microvascular permeability.

Hyperthermia enabled drug delivery has several limitations. There exists a very narrow window (roughly $42°C \leq T \leq 43°C$) where increased blood perfusion and permeability is observed without severe vascular damage.[27] This is supported by the fact that in the present study, at 1.6 W/cm^2 without the presence of GNRs, the tumor temperature reached 41.2°C but did not result in any increased EBD delivery. Therefore, using standard techniques of inducing hyperthermia in the clinic, maintaining a tumor temperature within this therapeutic window is difficult. Also, non-specific heating of surrounding healthy tissue may increase the probability of drug delivery within those regions where undesired toxicity is likely to occur.

PPTT has the potential to partially address these issues. Control of laser beam power and alignment may enable clinicians to precisely control thermal dose in a directed way. Also, PPTT represents a targeted approach to hyperthermia. As GNRs primarily partition out of the blood due to EPR, it is unlikely that GNRs will reside in surrounding, healthy tissue. This provides a degree of safety if the laser beam were to radiate such tissue. This can be further improved with the attachment of targeting moieties such as peptides and antibodies. Unfortunately, because the heat distribution is dependent on GNR localization, a significant disadvantage is that tumor tissue without GNRs will not receive thermal therapy.

A mouse sarcoma model was used in this study because of its known and well characterized permeability to albumin. Indeed, much of the work characterizing the EPR effect using EBD was performed using this animal model.[1] This model was also chosen for practical reasons due to its low cost, ease of tumor production and availability in the lab at the time of the experiment. However, because the intention of this dissertation is to treat prostate cancer, differences in animal models must be considered. It is possible that the inherent leaky nature of this model will provide artificially high values of enhanced delivery. Therefore, all future studies will be performed using prostate tumor models.

3.4 Conclusions

Using PPTT as a tool to induce hyperthermia and therefore increase the perfusion and permeability of tumor blood vessels may represent a new approach to augmenting macromolecular drug delivery. It has been shown that PPTT can be used to precisely control tumor temperature so that either moderate or severe tumor hyperthermia is obtained. This approach can therefore be used to increase the delivery of macromolecules such as albumin in the present paper. More detailed studies of resulting vascular events and delivery of macromolecular therapeutics for treatment of solid tumors is necessary.

3.5 References

1. Maeda, H.; Wu, J.; Sawa, T.; Matsumura, Y.; Hori, K. Tumor vascular permeability and the EPR effect in macromolecular therapeutics: a review. *J. Control. Release* **2000,** 65, 271-284.

2. Hashizume, H.; Baluk, P.; Morikawa, S.; McLean, J.; Thurston, G.; Roberge, S.; Jain, R.; McDonald, D. Openings between defective endothelial cells explain tumor vessel leakiness. *Am. J. Pathol.* **2000,** 156, 1363-1380.

3. Maeda, H.; Greish, K.; Fang, J. The EPR effect and polymeric drugs: A paradigm shift for cancer chemotherapy in the 21 st century. *Adv. Polymer Sci.* **2006,** 193, 103-121.

4. Lefor, A. T.; Makohon, S.; Ackerman, N. B. The effects of hyperthermia on vascular permeability in experimental liver metastasis. *J. Surg. Oncol.* **1985,** 28, 297-300.

5. Fujiwara, K.; Watanabe, T. Effects of hyperthermia, radiotherapy and thermoradiotherapy on tumor microvascular permeability. *Pathol. Int.* **2008,** 40, 79-84.

6. Gnant, M.; Noll, L.; Terrill, R.; Wu, P.; Berger, A.; Nguyen, H.; Lans, T.; Flynn, B.; Libutti, S.; Bartlett, D. Isolated hepatic perfusion for lapine liver metastases: impact of hyperthermia on permeability of tumor neovasculature. *Surgery* **1999,** 126, 890-899.

7. Kong, G.; Braun, R. D.; Dewhirst, M. W. Characterization of the effect of hyperthermia on nanoparticle extravasation from tumor vasculature. *Cancer Res.* **2001,** 61, 3027-3032.

8. Kong, G.; Braun, R. D.; Dewhirst, M. W. Hyperthermia enables tumor-specific nanoparticle delivery: effect of particle size. *Cancer Res.* **2000,** 60, 4440-4445.

9. Matteucci, M. L.; Anyarambhatla, G.; Rosner, G.; Azuma, C.; Fisher, P. E.; Dewhirst, M. W.; Needham, D.; Thrall, D. E. Hyperthermia increases accumulation of technetium-99m-labeled liposomes in feline sarcomas. *Clin. Cancer Res.* **2000,** 6, 3748-3755.

10. Chen, Q.; Krol, A.; Wright, A.; Needham, D.; Dewhirst, M.; Yuan, F. Tumor microvascular permeability is a key determinant for antivascular effects of doxorubicin encapsulated in a temperature sensitive liposome. *Int. J. Hyperthermia* **2008,** 24, 475-482.

11. Hildebrandt, B.; Wust, P.; Ahlers, O.; Dieing, A.; Sreenivasa, G.; Kerner, T.; Felix, R.; Riess, H. The cellular and molecular basis of hyperthermia. *Crit. Rev. Oncol. Hematol.* **2002,** 43, 33-56.

12. Xu, L.; Chen, B.; Zhou, M. Change of individual vascular endothelial calcium during hyperthermia. *J. Therm. Biol.* **2006,** 31, 302-306.

13. Chen, B.; Zhou, M.; Xu, L. Study of vascular endothelial cell morphology during hyperthermia. *J. Therm. Biol.* **2005,** 30, 111-117.

14. Fajardo, L.; Schreiber, A.; Kelly, N.; Hahn, G. Thermal sensitivity of endothelial cells. *Radiat. Res.* **1985,** 103, 276-285.

15. Wust, P.; Hildebrandt, B.; Sreenivasa, G.; Rau, B.; Gellermann, J.; Riess, H.; Felix, R.; Schlag, P. M. Hyperthermia in combined treatment of cancer. *Lancet Oncol.* **2002,** 3, 487-497.

16. Link, S.; El-Sayed, M. A. Shape and size dependence of radiative, non-radiative and photothermal properties of gold nanocrystals. *Int. Rev. Phys. Chem.* **2000,** 19, 409-453.

17. Huang, X.; Jain, P. K.; El-Sayed, I. H.; El-Sayed, M. A. Plasmonic photothermal therapy (PPTT) using gold nanoparticles. *Lasers Med. Sci.* **2008,** 23, 217-228.

18. von Maltzahn, G.; Park, J. H.; Agrawal, A.; Bandaru, N. K.; Das, S. K.; Sailor, M. J.; Bhatia, S. N. Computationally guided photothermal tumor therapy using long-circulating gold nanorod antennas. *Cancer Res.* **2009,** 69, 3892-3900.

19. Dickerson, E. B.; Dreaden, E. C.; Huang, X.; El-Sayed, I. H.; Chu, H.; Pushpanketh, S.; McDonald, J. F.; El-Sayed, M. A. Gold nanorod assisted near-infrared plasmonic photothermal therapy (PPTT) of squamous cell carcinoma in mice. *Cancer Lett.* **2008,** 269, 57-66.

20. Hirsch, L. R.; Stafford, R. J.; Bankson, J. A.; Sershen, S. R.; Rivera, B.; Price, R. E.; Hazle, J. D.; Halas, N. J.; West, J. L. Nanoshell-mediated near-infrared thermal therapy of tumors under magnetic resonance guidance. *Proc. Natl. Acad. Sci. USA.* **2003,** 100, 13549-13554.

21. O'Neal, D. P.; Hirsch, L. R.; Halas, N. J.; Payne, J. D.; West, J. L. Photo-thermal tumor ablation in mice using near infrared-absorbing nanoparticles. *Cancer Lett.* **2004,** 209, 171-176.

22. Stern, J. M.; Stanfield, J.; Kabbani, W.; Hsieh, J. T.; Cadeddu, J. A. Selective prostate cancer thermal ablation with laser activated gold nanoshells. *J. Urol.* **2008,** 179, 748-753.

23. Jain, P. K.; Lee, K. S.; El-Sayed, I. H.; El-Sayed, M. A. Calculated absorption and scattering properties of gold nanoparticles of different size, shape, and composition: applications in biological imaging and biomedicine. *J. Phys. Chem. B* **2006,** 110, 7238-7248.

24. Nikoobakht, B.; El-Sayed, M. A. Preparation and growth mechanism of gold nanorods (NRs) using seed-mediated growth method. *Chem. Mater.* **2003,** 15, 1957-1962.

25. Wang, R. K.; Tuchin, V. V. Enhance light penetration in tissue for high resolution optical imaging techniques by the use of biocompatible chemical agents. *J. X Ray Sci. Tech.* **2002,** 10, 167-176.

26. Matsumura, Y.; Maeda, H. A new concept for macromolecular therapeutics in cancer chemotherapy: mechanism of tumoritropic accumulation of proteins and the antitumor agent smancs. *Cancer Res.* **1986,** 46, 6387-6392.

27. Horsman, M. R. Tissue physiology and the response to heat. *Int. J. Hyperthermia* **2006,** 22, 197-203.

CHAPTER 4

BIOLOGICAL EVALUATION OF RGDFK-GOLD NANOROD CONJUGATES FOR PROSTATE CANCER TREATMENT

4.1 Introduction

The ability to precisely control material geometries with nanoscale dimension has enabled researchers with new and powerful tools not available when the same materials are in their bulk form. Examples of this include self-assembled structures from nanoparticle precursors,[1] precise control of reaction catalysis by modulation of nanoparticle shape and size,[2] as well as the fabrication of materials from nanotubes with unprecedented tensile strength and moduli.[3] The unique optical properties of metal colloids whose dimensions are significantly smaller than the wavelength of light are a particular example as particle vibrations give rise to size and shape dependent light absorption and scattering phenomenon.[4] For this reason, AuNPs have received significant attention in medicine due to their utility in disease detection and therapy.[5]

AuNPs in a variety of shapes, e.g., spheres, shells, and cages can act as multifunctional platforms. In addition to their use as optical imaging based contrast agents,[6-8] AuNPs are able to serve as delivery vehicles for drugs[9-10] and antennas for

---

Reprinted with permission from the Journal of Drug Targeting
Reference: Gormley, A. J.; et al., *J. Drug Target.* **2011,** 19, 915-924.

PPTT.[11-14] Current methods for tumor delivery leverage the vasculature's EPR which occurs due to both enlarged endothelial intercellular gaps as well as the lack of a functioning lymphatic system.[15-16] This technique for delivery is ubiquitous in drug delivery to solid tumors and is partially responsible for much of the success observed in that field.[17-19]

One approach to improve the delivery and tumor retention of AuNPs is to employ active targeting by conjugation of targeting moieties to their surface. Examples of such targeting strategies include conjugation of anti-EGFR and anti-HER2 antibodies,[20-21] folic acid,[22] as well as nuclear localizing peptides.[23] In this way selective delivery to tumor specific markers can potentially improve the degree of tumor localization compared to passive strategies.

One set of targets that have received significant attention in the last decade are the $\alpha_v\beta_3$ integrins which regulate cell adhesion to extracellular matrix proteins. Able to bind with high affinity to the RGD sequence of matrix proteins such as fibronectin and vitronectin,[24] $\alpha_v\beta_3$ integrins coating the angiogenic endothelium can be used as targets for nanoconstructs with surface modified variations of the RGD peptide.[25] Of particular interest in this regard is use of the monocyclic RGDfK peptide which has higher affinity for $\alpha_v\beta_3$ integrins and greater tumor targeting characteristics than linear RGD.[26-27] This technique for tumor targeting has been well characterized and validated using HPMA copolymers[28-35] and has resulted in significant prostate tumor efficacy with both geldanamycin[36] and docetaxel[37] attached to the side chains.

In the context of using GNRs as antennaes for PPTT,[38] their active delivery to sites of tumor angiogenesis by RGDfK targeting may be advantageous. The vasculature

which feeds cancerous cells has minimal organization and is devoid of smooth muscle ultimately impeding the capacity of this tissue to respond to heat stress. Transient increases in blood flow and vascular permeability up to 43°C is typically followed by vascular collapse, hemorrhage and circulatory stasis as temperatures rise above this threshold level.[39-41] During conventional hyperthermia or that induced by PPTT using passive delivery approaches, tumor mass heating ultimately causes vascular damage once the whole tumor volume has been heated above 43°C. We ultimately hypothesize, however, that by directing GNRs to the tumor's vasculature using cyclic RGD, greater control of vascular dynamics during heating is possible (Figure 4.1). To begin testing this hypothesis, in the present Chapter we first evaluated the *in vitro* cellular uptake and *in vivo* biodistribution of PEGylated GNRs functionalized with RGDfK.

4.2 Materials and Methods

4.2.1GNR synthesis and characterization

GNRs were synthesized using the seed-mediated growth method.[42] Optimization of silver nitrate content and seed amount yielded GNRs with an aspect ratio such that the SPR peak was between 800-810 nm. GNRs were then centrifuged (6,000 rcf, 30 minutes) and washed three times with DI water to remove excess CTAB. For the untargeted GNRs, PEG (50 mg, methoxy-PEG-thiol, 5 kD, Creative PEGWorks #PLS-604) was added to the GNR suspension (100 ml, 100 μg/ml, OD = 10) at a final PEG concentration of 100 μM and stirred for 1 hour. This was done to reduce the extent of protein adsorption and improve circulation time.[43] The PEG-GNR suspension was then thoroughly dialyzed (3.5 K MWCO, Spectrum Labs #132594) and sterile filtered.

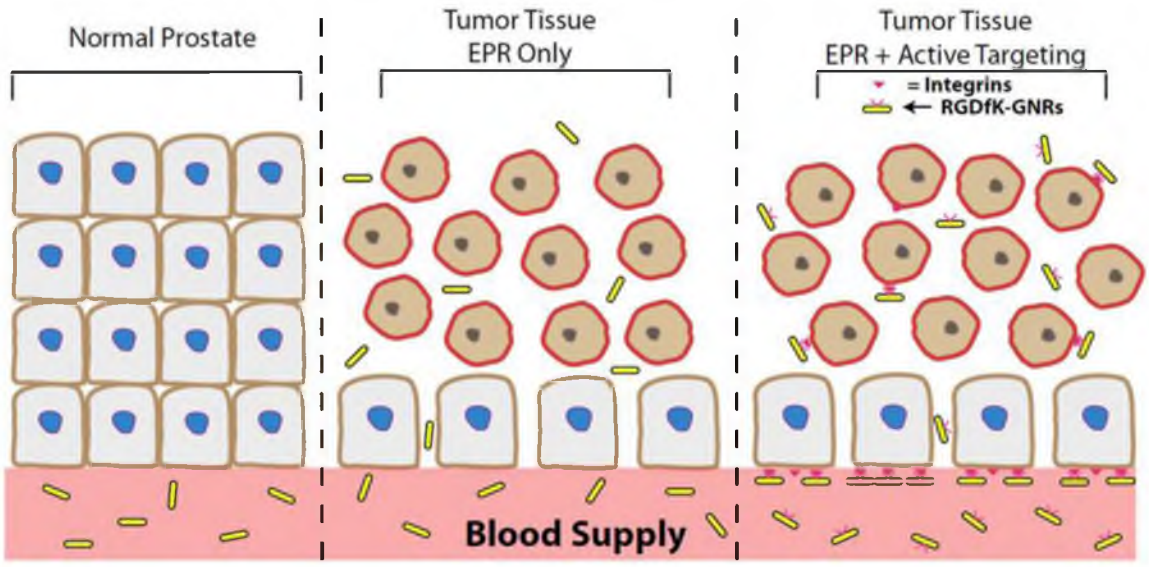

Figure 4.1: Scheme of GNR delivery mechanism. (A) GNRs do not accumulate in normal tissue due to tight endothelial gaps in the vasculature. (B) GNRs can passively diffuse in malignant tissue by EPR effect. (C) Active targeting may increase GNR concentration at the vascular bed and localize them to heat sensitive vasculature.

Finally, the GNR suspension was centrifuged, washed three times with DI water to remove unreacted PEG and concentrated to a final concentration of 1.2 mg/ml (OD = 120). Final product was stored at 4°C for a maximum of 2 months due to polymer shedding over time before use.

Targeted GNRs were synthesized by first reacting ortho-pyridyl-disulfide-PEG-succinimidyl ester (OPSS-PEG-NHS, 5 kD, Creative PEGWorks #PHB-997, 50 mg) with RGDfK (New England Peptide, Inc., 6 mg) in anhydrous DMSO (5 ml) and three drops of diisopropylethylamine (DIPEA) while stirring for 24 hours at room temperature. Dithiothreitol (DTT, 7 mg) was then added to the reaction mixture and stirred for an additional 2 hours to reduce the disulfide and obtain a free thiol at the end of the PEG-RGDfK polymer. The mixture was then dialyzed (3.5 K MWCO, Spectrum Labs #132594) and lyophilized to obtain the final product followed by confirmation of peptide attachment by amino acid analysis. Finally, the thiol-PEG-RGDfK polymer was grafted to the gold surface in the same way as the untargeted GNR conjugate.

GNR size and shape were measured by TEM (FEI Tecnai T12) after drop-casting the GNR suspension onto a copper grid. The GNR light absorption profile was measured before and after PEGylation using a spectrophotometer (Jasco V-650) and the stability of these conjugates was measured the same way after 30 minutes in 3.5% NaCl. GNR concentration was determined by inductively coupled plasma mass spectrometry (ICP-MS, Agilent 7500ce) against a gold and internal (irradium) standard. The zeta potential of the conjugates was measured in DI water by measuring the particle's electrophoretic mobility using laser doppler velocimetry (Malvern Instruments Zetasizer Nano-ZS). Finally the RGDfK content on the gold was determined by amino acid analysis.

4.2.2 Cell culture

The binding and uptake was evaluated for targeted (RGDfK) and untargeted GNRs in two cell lines obtained from ATCC (Manassas, VA); DU145 prostate cancer and human umbilical vein endothelial cells (HUVEC). DU145 cell lines were cultured in Eagle's Minimum Essential Medium with Earle's Balanced Salt Solution (ATCC) supplemented with 10% (v/v) fetal bovine serum (FBS) (Thermo Scientific HyClone, Logan, UT). HUVEC cell lines were cultured in Clonetics Endothelial Cell Basal Medium-2 supplemented with 2% FBS, hydrocortisone, hFGF-B, VEGF, R3-IGF-1, ascorbic acid, hEGF, GA-1000 and heparin (Lonza EGM-2 BulletKit). Cell lines were cultured at 37°C in 100% humidity with 5% CO_2. All cells were kept within logarithmic growth and while DU145 cells were kept under 20 passages, HUVEC cells were discarded after seven.

4.2.3 Dark field microscopy

Cells were plated on sterile cover slips coated with fibronectin and allowed to grow until 50% confluent. The media was then replaced with either fresh media or media containing either the RGDfK or untargeted GNRs (10 μg/ml). Cells were allowed to incubate for 24 hours followed by aspiration of GNR containing media and three washing steps with PBS followed by fixation for 10 minutes with 4% paraformaldehyde before mounting to a slide with mounting medium. To detect association (binding and uptake) of GNRs with the cells, slides were then imaged with an Olympus BX41 microscope coupled to the CytoViva 150 Ultra Resolution Imaging (URI) System (CytoViva Inc.,

Auburn, AL) using a 100x oil objective.[44-45] A DAGE XLM (DAGE-MTI, Michigan City, IN) digital camera and software was used to capture and store images.

4.2.4 ICP-MS

To quantify binding and uptake, cells were plated in 24-well plates and allowed to grow to 70% confluency. After incubation with GNRs and washing with PBS as described above, cells were lysed with 100 mM sodium hydroxide for 20 minutes while shaking and the protein content for each well was determined using a bicinchoninic (BCA) protein assay (Micro BCA Protein Assay Kit, Thermo Scientific Inc., Rockford, IL). The lysate was then transferred to Teflon vials, digested and evaporated three times with fresh trace-metal grade aqua regia, then resuspended in 5% trace-metal grade nitric acid before being analyzed by ICP-MS for gold content quantification against a gold and internal standard. All groups were done in triplicates.

4.2.5 TEM

For visualization of uptake by TEM, cells were grown to 50% confluency on fibronectin coated ACLAR® plastic films before 24 hr incubation with GNRs. Cells were then washed three times with PBS and fixed with 2.5% glutaraldehyde and 1% paraformaldehyde in 0.1M sodium cacodylate with sucrose and calcium chloride. Samples were then dehydrated with washes of increasing concentrations of ethanol and embedded in an epoxy resin before sectioning with an ultramicrotome. All samples were then imaged using a FEI Tecnai T12 microscope (University of Utah Core Research Facilities, Salt Lake City, UT).

4.2.6 Competitive inhibition of binding

Confirmation of RGDfK-GNR specificity to $\alpha_v\beta_3$ integrins was performed by competitive inhibition of binding with echistatin. In brief, HUVEC cells were grown to 50% confluency on fibronectin coated cover slips. The media was then removed and replaced with cold binding buffer (20 mmol/L Tris, pH 7.4, 150 mmol/L NaCl, 2 mmol/L $CaCl_2$, 1 mmol/L $MgCl_2$, 1 mmol/L $MnCl_2$, 0.1% bovine serum albumin) containing RGDfK-GNRs (10 μg/ml) and HUVECs were co-incubated at 4°C for 2 hours with or without 50 nM echistatin (Sigma-Aldrich). Cells were then washed three times with cold binding buffer, mounted to a slide and imaged by high-resolution dark field microscopy.

4.2.7 Biodistribution in prostate tumor bearing mice

Six-week-old female athymic (nu/nu) mice were obtained from Charles River Laboratories (Davis, CA) and used in accordance with the Institutional Animal Care and Use Committee (IACUC) of the University of Utah. To initiate prostate cancer xenografts, mice were anesthetized using 4% isofluorane and 10^7 DU145 cells in 200 μl PBS were injected bilaterally on the flank of each animal. Tumors were then allowed to grow until average tumor volume reached 50-100 mm^3 (usually 10-21 days).

The animals were separated randomly into two groups. Half received untargeted GNRs and the other half RGDfK-GNRs (9.6 mg/kg in 200 μl, OD = 120) by intravenous injection through the tail vein. The animals were allowed to rest for 6, 24 and 48 hours before sacrifice by CO_2 inhalation. After sacrifice, blood was collected using a heparinized needle from the inferior vena cava and the animals were perfused with at least 20 ml of saline by cardiac puncture. Blood and organs such as the liver, spleen,

lungs, heart and kidneys were collected and weighed as well as the tumors. Each sample was refluxed in 4 ml of fresh trace-metal grade aqua regia at 90°C for 24 hrs, and then dried at 130°C. Subsequently, samples were dissolved in 4 ml of 5% trace-metal grade nitric acid before quantification of gold content by ICP-MS against a gold and internal standard.

4.3 Results

4.3.1 GNR synthesis and characterization

GNRs were synthesized with an SPR peak at 800 nm corresponding to a size of 60.5 x 15.0 ± 6.4 x 2.0 nm with an aspect ratio equal to 4.0 (Figure 4.2, Table 4.1). After PEGylation, with or without RGDfK, there was minimal change in absorption profile and the nanoparticles had strong stability in the presence of 3.5% NaCl. Zeta potential measurements indicate that while the untargeted (methoxy terminated) GNRs had a slight negative charge (-10.0 mV), the RGDfK-GNRs had a strong negative charge (-44.1 mV). Amino acid analysis confirmed the presence of RGDfK on the targeted GNRs with a concentration equal to 5.6×10^{-11} M_{RGDfK} / μg_{Au} or roughly 3.0×10^{3} RGDfKs per GNR.

4.3.2 Binding and uptake by dark field microscopy and ICP-MS

Because GNRs scatter light to a very high extent, the binding and uptake of both the untargeted and targeted (RGDfK) GNRs were visualized by high-resolution dark field microscopy (Figure 4.3 A). Captured images show that GNRs were associated with cultured cells to a different extent and do not affect overall cell morphology and the confluency of the culture. The untargeted GNRs showed some binding and uptake in

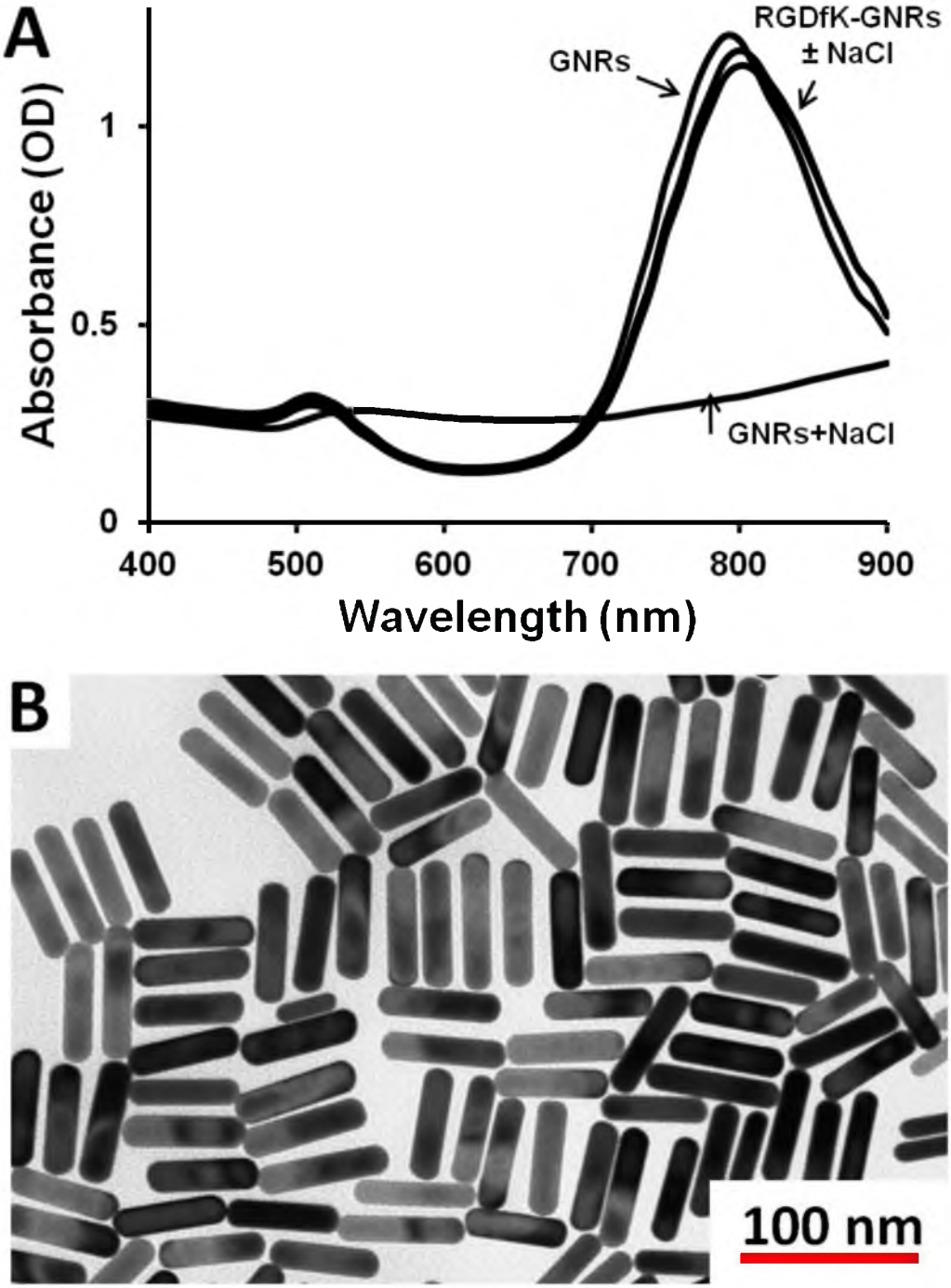

Figure 4.2: Characterization of GNRs. (A) Light absorption profile and (B) TEM of GNRs. Panel A shows the absorbance profile of CTAB stabilized GNRs (GNRs), CTAB stabilized GNRs with 3.5% NaCl (GNRs + NaCl) as well as RGDfK-PEG-GNRs with and without 3.5% NaCl (RGDfK-GNRs ± NaCl). Without the polymer coating, GNRs aggregate in the presence of NaCl, whereas those stabilized with PEG-RGDfK are stable in the presence of salt.

Table 4.1: Physicochemical characteristics of GNRs.

Size (nm)	SPR		Charge	Peptide Content
60.5 x 15.0 ± 6.5 x 2.0	800 nm	Untargeted	-10.0 mV	NA
		RGDfK	-44.1 mV	5.6×10^{-11} M_{RGDfK} / µg (Au)

both cell lines tested (DU145 and HUVEC).Internalized GNRs were primarily located in the perinuclear regions of the cells. Similarly, it appeared that the RGDfK-GNRs had slightly more uptake in DU145 cells than the untargeted GNRs, though this difference was not statistically significant after quantification by ICP-MS (Figure 4.3 B). After incubation of the targeted (RGDfK) GNRs with HUVECs however, significant binding and uptake was observed. ICP-MS analysis revealed that these binding and uptake events were roughly 20-fold higher for the targeted GNRs than the untargeted GNRs for HUVECs (Figure 4.3 B).

4.3.3 Binding and uptake by TEM

GNR uptake patterns by cells were typically as agglomerates and within membrane enclosed vacuoles (Figure 4.4). In some cases, the agglomerates were found in vesicles with multiple membranes suggesting possible association within the endoplasmic reticulum (ER). Despite significant uptake and GNR loading within the cells no obvious evidence of intracellular structure and organelle damage was observed. These observations and the fact that there were no visible changes of cell culture confluence after incubation with GNRs, provide evidence related to the overall biocompatibility of the nanoparticles. Though in all cases uptake was observed by cells, the uptake of RGDfK-GNRs in HUVECs was significantly higher than that of any other cell line and particle combination.

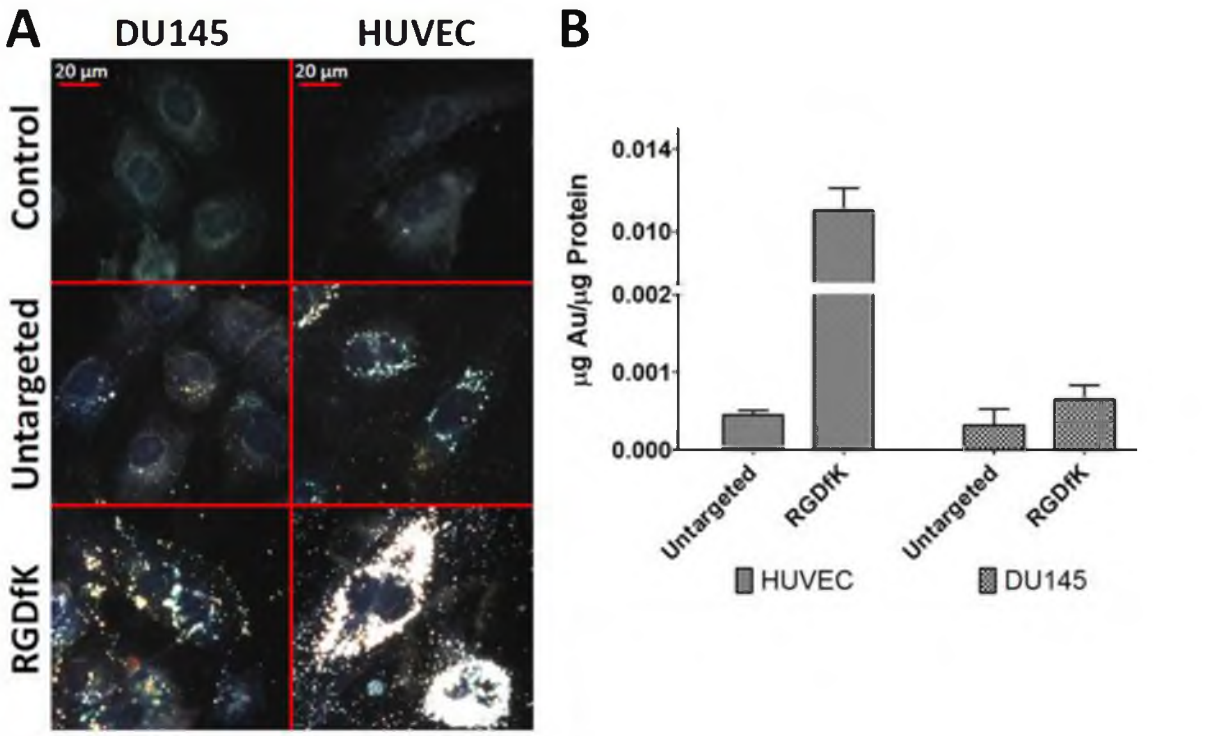

Figure 4.3: GNR binding and uptake. (A) high-resolution dark field microscopy and (B) ICP-MS after 24 h incubation with either RGDfK modified or untargeted GNRs (10 µg/mL). RGDfK-GNRs show increased binding and uptake relative to untargeted GNRs in both cell lines; however, this difference was most significant (roughly 20-fold) with HUVECs. Error bas represented as ±standard deviation (N = 3).

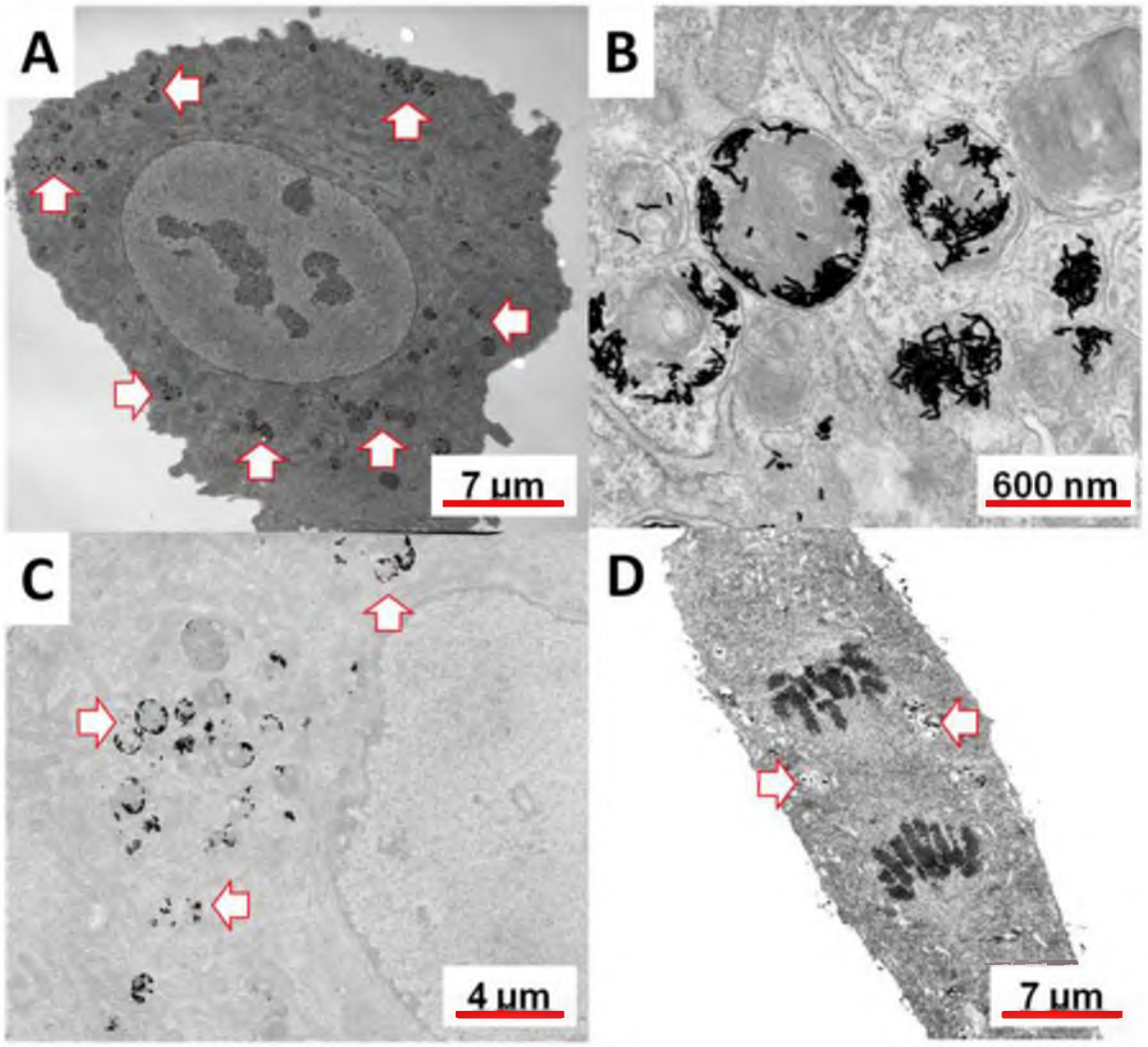

Figure 4.4: GNR uptake by TEM. Representative images of RGDfK (A-C) and untargeted (D) GNRs in HUVECs after 24 hours incubation. Arrows point to location of GNRs within the cell. Some GNRs were found within multiple membranes (panel B) near the nucleus.

4.3.4 Competitive inhibition of binding

As echistatin is known to bind to $\alpha_v\beta_3$ cell adhesion integrins with very high affinity,[46] competitive binding inhibition of the RGDfK targeted receptors with this protein is possible. Incubation of HUVECs with RGDfK-GNRs at 4°C for 2 hours in binding buffer alone resulted in some GNR binding along the cell's surface as visualized as small green-yellow dots observable by dark field microscopy (Figure 4.5 A). To confirm the specificity of this binding, co-incubation with echistatin (50 nM) resulted in almost complete inhibition of GNR binding to the cell's surface (Figure 4.5 B).

4.3.5 Biodistribution in prostate tumor bearing mice

To test the fate of the angiogenesis targeted GNRs compared to untargeted GNRs, their biodistribution was evaluated in prostate tumor bearing mice. Results indicate that while much of the untargeted GNRs remained in circulation after 6 hrs, the targeted (RGDfK) GNRs were no longer circulating (Figure 4.6 A). When comparing the tumor accumulation of both particle types, the untargeted GNRs had 7.6-fold higher tumor localization (1.22% injected dose) compared to the RGDfK conjugated GNRs (0.16% injected dose) at all time points (Figure 4.6 B). Gold analysis of other organs revealed that while the untargeted GNRs showed significant uptake by the liver and spleen, this effect was more pronounced with the targeted GNRs, particularly by the spleen (Figure 4.7). Over time the untargeted GNRs were increasingly found in both of these organs due to their longer circulation time whereas the targeted GNRs had maximal organ accumulation at 6 hours followed by a gradual decrease due to fast clearance from the

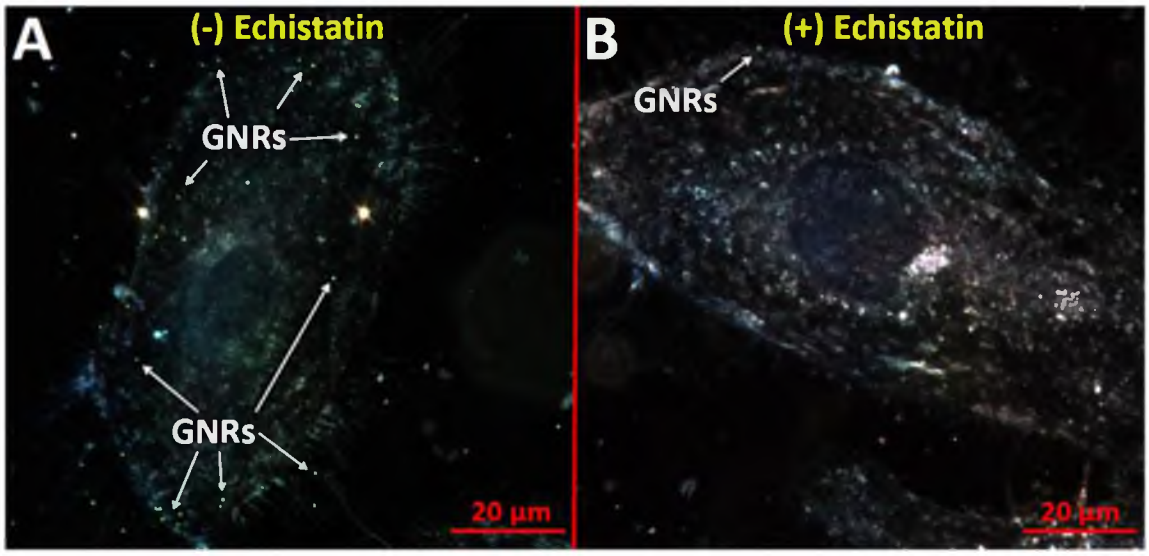

Figure 4.5: Binding inhibition with echistatin. RGDfK-GNRs binding to HUVECs in (A) absence and (B) presence of the $\alpha_v\beta_3$ inhibitor echistatin (50 nM) at 4°C for 2 h in binding buffer. Small green-yellow dots indicate presence of GNRs on the cell surface.

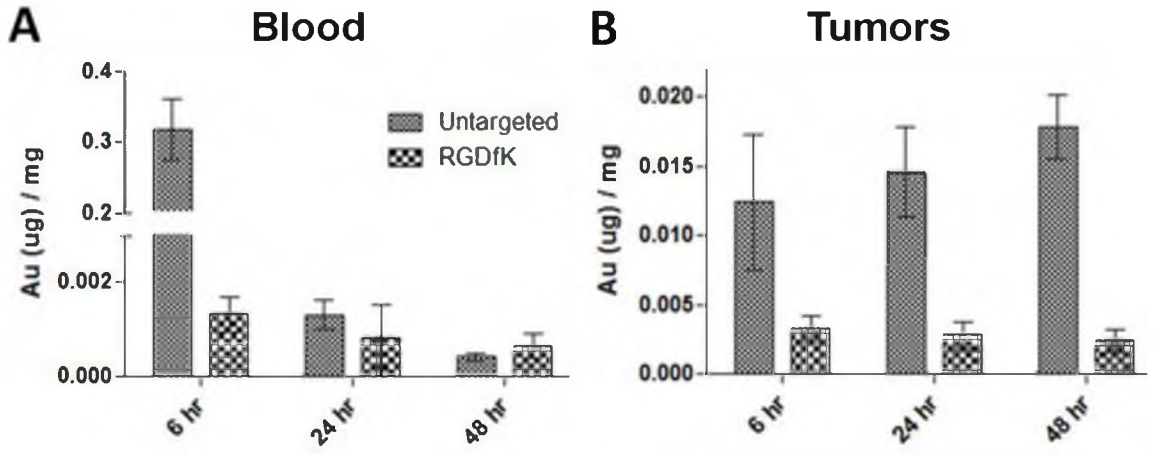

Figure 4.6: Tumor and blood accumulation of GNRs. Comparison of targeted (RGDfK) and untargeted gold content by ICP-MS in (A) blood and (B) tumors of mice bearing prostate cancer xenografts at 6, 24 and 48 hours postinjection. After 6 hours, the RGDfK-GNRs were mostly removed from the blood, while the same was true for untargeted GNRs after 24 hours. Error bars represented as ±standard deviation (N = 3).

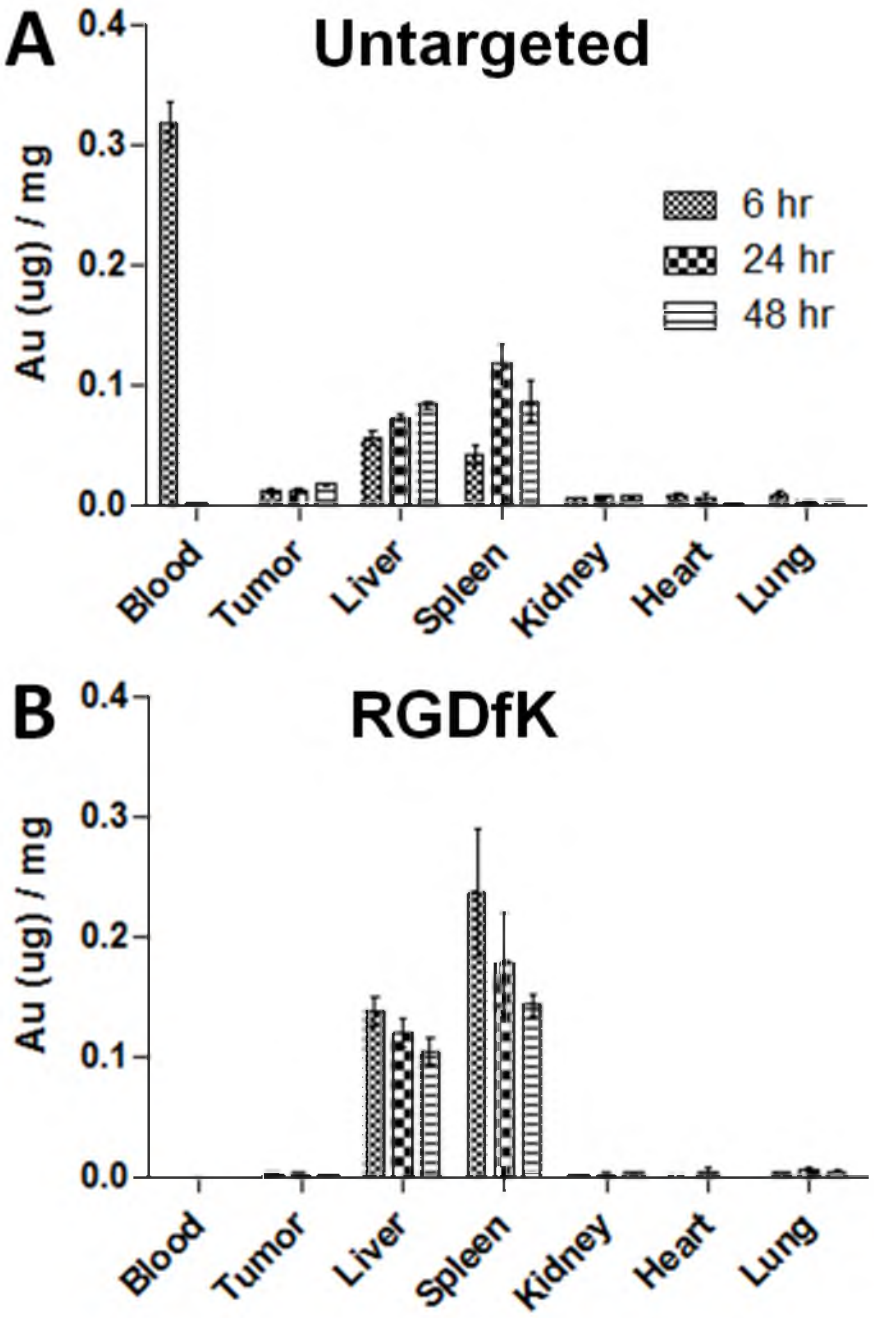

Figure 4.7: Biodistribution of gold content by ICP-MS: (A) untargeted and (B) targeted (RGDfK) GNRs in prostate cancer bearing mice. Error bars represented as ±standard deviation (N = 3).

blood. Upon dissection of the animals, the differences in hepatic and splenic uptake of the two GNR types were apparent as the liver and spleen from animals receiving RGDfK-GNRs were visibly darker than their untargeted counterparts.

4.4 Discussion

Among the many varieties of inorganic nanoparticles investigated for use in nanomedicine, AuNPs have been applied extensively.[47] Reasons for this include their ease of synthesis and surface modification with low cost materials, their stability in most environments, as well as their safety and unique optical properties. Such characteristics make these attractive nanoparticle platforms which have been used as drug delivery carriers for TNF-α[9] and antennas for PPTT.[48]

The use of ligand-directed delivery of nanoparticles to solid tumors over passive delivery mechanisms is desired. In most cases, maximizing the tumor localized percent injected dose represents the main value for this approach. Directed delivery to specific cells is advantageous as the imaging or therapy system may be specific to those cells. In drug delivery using water soluble polymers such as HPMA copolymers, for example, the attached anticancer drug may be specific for the target cells.[49] The same is true for imaging modalities such as quantum dots, where labeling of tumor vasculature may be desired, and therefore vascular targeting approaches are used.[50]

Likewise efforts aimed at directed delivery of GNRs to the tumor vasculature would be advantageous. During hyperthermia the impact of heat on the ill-formed tumor vasculature is significant and results in damage.[41] By localizing GNRs to the plasma membrane (by $\alpha_v\beta_3$ integrin targeting) of endothelial cells lining the neovasculature, these

cells are particularly susceptible to damage by light activation. This is because direct contact with the membrane limits the amount of heat needed for photothermolysis despite the heat sink nature of the surrounding blood and interstitial fluid. Additionally, if one chooses to administer a subtherapeutic dose of heat to modulate the tumor's vascular permeability and facilitate the passive delivery of other nanomedicines, directed PPTT to the tumor's vasculature may dramatically reduce the light energy required for this approach.[51]

In our previous studies we demonstrated the utility of HPMA copolymer – cyclic RGDfK conjugates for targeted delivery of drugs and imaging agents to solid tumors.[28, 30-35] Compared to nontargetable systems, HPMA copolymer-RGD4C and –RGDfK conjugates have shown increased accumulation in a variety of tumors including prostate, lung and breast cancer xenografts. This increased localization has been correlated with enhanced treatment efficacy and anti-angiogenic activity of both geldanamycin and docetaxel.[36-37]

In addition to the presence of targeting moiety, however, other factors that influence biodistribution and tumor uptake are the size, charge, surface modification and architecture of nanocarriers. In many cases use of a targeting moiety does not necessarily guarantee better tumor accumulation. For example a variety of active delivery approaches for liposomes have been tested *in vivo* and many of the parameters which govern their blood clearance and tumor targeting have been identified.[52] Physicochemical properties such as particle charge and PEG length are known to influence the blood clearance kinetics of liposomes.[53] Choice of targeting moiety and its structure also play a key role. For example, whole antibodies may be recognized by the

RES to a higher extent than if antibody fragments are used.[54-55] Finally, the architecture of the nanomedicine may play a significant role when comparing two systems. Besides the fact that carrier architecture and geometry influences biodistribution and passive tumor localization,[56-57] it is likely that the biorecognition of the same peptide for its ligand on two very different platforms will be different.

In the context of angiogenesis targeting of AuNPs, there exists conflicting reports. Besides examples providing evidence of targeting *in vitro* alone,[58] two other studies have validated this approach *in vivo*.[59-60] In one study, RGDfK was attached to gold nanoshells which resulted in a slight increase in nanoshell delivery compared to the untargeted nanoshells alone.[59] Also, when linear RGD functionalized dendrimer-GNRs were tested for tumor targeting, a very high (17% of the injected dose) amount of the targeted nanoparticles localized within the tumors.[60] Alternatively, a recent study investigating the targeting potential of GNRs with a variety of targeting peptides including RGD provided evidence that such functionalization does not enable better tumor delivery when compared to untargeted GNRs alone.[61] While attachment of moieties such as single-chain variable fragment (ScFv) and amino-terminal fragment (ATF) peptides resulted in a very slight increase in tumor delivery, use of the RGD peptide had a negative impact on tumor delivery.

When the binding and uptake of the RGDfK-GNRs was evaluated with both DU145 and HUVEC cells, the system performed as intended. GNRs with the RGDfK peptide on their surface had increased binding to cells which express $\alpha_v\beta_3$ integrins. Given that the expression profile of these receptors is highly dependent on cell type, it is expected that cells which have more $\alpha_v\beta_3$ integrins will have higher binding and uptake of

the RGDfK modified GNRs. This was indeed the case where RGDfK-GNRs had more binding to both cell types relative to the untargeted nanoparticles, but that this difference was more pronounced with HUVECs (roughly 20-fold increase). This is related to the fact that HUVEC cells have significant expression of $\alpha_v\beta_3$ integrins due to their angiogenic phenotype.[62-64] The fact that the RGDfK-GNRs had higher binding to the DU145 cells than the untargeted nanoparticles is also not surprising considering that these cells do have some expression profile of $\alpha_v\beta_3$ integrins, though not to the same extent as HUVECs.

Because there is always some concern that such binding and uptake events could be due to nonspecific interactions such as surface charge, inhibition of binding by co-incubation with echistatin was performed and visualized by dark field microscopy. After 2 hours incubation at 4°C, it is expected that minimal non-specific binding and uptake would occur. Because RGD-ligand binding is not an energy dependent process, such conditions should still result in some cell surface binding. In this way, peptide-ligand specificity was confirmed as HUVEC cells co-incubated with echistatin showed very little GNR binding while those cells without echistatin had GNRs decorating the cell's surface.

Dark field microscopy in this case was used as a visualization tool as it is very efficient at detecting the presence of nanoparticles which scatter light to a high extent. However, since this imaging tool is unable to distinguish GNRs which are bound to the plasma membrane and those that are located intracellularly, it has some limitations. To address this, TEM images of the uptaken particles in HUVEC cells were acquired. The information gathered from the TEM images were not surprising based on previous

findings.[65-71] Large nanoparticle agglomerates were found within single membrane vesicles indicative of endosomes and lysosomes (Figure 4.4 A, C). However, in some cases these agglomerates were found within multiple membranes which may be suggestive of their presence within the ER (Figure 4.4 B).

Despite confirming the capacity of the RGDfK-GNRs to bind to cells undergoing angiogenesis, when the system was tested *in vivo* fast clearance of the targeted GNRs prevented effective targeting from occurring. Because RGD targeting of nanoparticles has been validated previously, we hypothesize that the fast clearance is related to the strong negative charge of the RGDfK-GNRs (-44.1 mV). As the presence of strong net negative charges is known to facilitate nanoparticle biorecognition,[72] it is very possible that this physicochemical parameter alone may have initiated quick GNR uptake by the liver and spleen. Such quick RES clearance of negatively charged conjugates has been observed with several different nanomedicines. For example, the presence of strong negative charges was previously identified as the reason for quick clearance of RGDfK conjugated HPMA copolymers due to the presence of negatively charged ^{111}In chelators attached to the side chains.[29] Similar observations have also been made with liposomal systems,[73] micelles,[74] dendrimers,[57] as well as AuNPs.[56] Therefore, for successful targeting to occur lessons learned from nanoparticle systems with large surface charges necessitates careful consideration of particle charge in addition to other parameters such as targeting moiety content, as well as size and shape.

To reduce the presence of these surface charges, the number of PEG-RGDfKs on the gold surface may be decreased. However, because doing this alone has previously been shown to make little impact on the targetability of the system,[61] another possibility

is to change the PEG length to which the RGDfK moiety is attached. By attaching RGDfK or any other peptide to a PEG linker which is 2,000 Da in size and keeping the neutrally charged PEG (methoxy terminated) at 5,000 Da, a mixture of the two might hide the peptide and thus mask the surface charges. Of course there is a risk with this approach of not having the peptide available for binding to the ligand. In either case, an appropriate balance of enough peptide to achieve vascular targeting, but not so much that surface charges diminish blood circulation may be required to obtain a targeted system as designed.

4.5 Conclusions

In this chapter it was shown that surface modification of GNRs with the angiogenesis targeting peptide RGDfK results in effective targeting *in vitro* but not *in vivo*. Utilization of this peptide with GNRs shows excellent biorecognition with cells and their $\alpha_v\beta_3$ integrins, however the presence of strong negative charges likely accelerated the RES clearance of this system. In future designs, GNR surface modifications to maintain peptide-ligand bioactivity will need be balanced with particle surface charge to increase the targetability of this system. However, sufficient accumulation of nontargeted GNRs in the tumors was demonstrated to justify its use for further evaluation in PPTT and enhancing the delivery of polymeric systems.

4.6 References

1. Li, M.; Schnablegger, H.; Mann, S. Coupled synthesis and self-assembly of nanoparticles to give structures with controlled organization. *Phys. Rev. Lett.* **1999,** 82, 1345-1349.

2. Narayanan, R.; El-Sayed, M. A. Catalysis with transition metal nanoparticles in colloidal solution: Nanoparticle shape dependence and stability. *J. Phys. Chem. B* **2005,** 109, 12663-12676.

3. Breuer, O.; Sundararaj, U. Big returns from small fibers: A review of polymer/carbon nanotube composites. *Polymer Composites* **2004,** 25, 630-645.

4. Kelly, K. L.; Coronado, E.; Zhao, L. L.; Schatz, G. C. The optical properties of metal nanoparticles: the influence of size, shape, and dielectric environment. *J. Phys. Chem. B* **2003,** 107, 668-677.

5. Huang, X.; Jain, P. K.; El-Sayed, I. H.; El-Sayed, M. A. Gold nanoparticles: interesting optical properties and recent applications in cancer diagnostics and therapy. *Nanomed.* **2007,** 2, 681-693.

6. Chen, J.; Saeki, F.; Benjamin, J.; Cang, H.; Cobb, M. J.; Li, Z. Y.; Au, L.; Zhang, H.; Kimmey, M. B.; Li, X. Gold nanocages: bioconjugation and their potential use as optical imaging contrast agents. *Nano Lett.* **2005,** 5, 473-477.

7. Copland, J. A.; Eghtedari, M.; Popov, V. L.; Kotov, N.; Mamedova, N.; Motamedi, M.; Oraevsky, A. A. Bioconjugated gold nanoparticles as a molecular based contrast agent: implications for imaging of deep tumors using optoacoustic tomography. *Mol. Imaging Biol.* **2004,** 6, 341–349.

8. Tong, L.; Wei, Q.; Wei, A.; Cheng, J. X. Gold nanorods as contrast agents for biological imaging: Optical properties, surface conjugation and photothermal effects. *Photochem. Photobiol.* **2009,** 85, 21-32.

9. Paciotti, G. F.; Myer, L.; Weinreich, D.; Goia, D.; Pavel, N.; McLaughlin, R. E.; Tamarkin, L. Colloidal gold: a novel nanoparticle vector for tumor directed drug delivery. *Drug Deliv.* **2004,** 11, 169-183.

10. Yavuz, M. S.; Cheng, Y.; Chen, J.; Cobley, C. M.; Zhang, Q.; Rycenga, M.; Xie, J.; Kim, C.; Song, K. H.; Schwartz, A. G.; Wang, L. V.; Xia, Y. Gold nanocages covered by smart polymers for controlled release with near-infrared light. *Nat. Mater.* **2009,** 8, 935-939.

11. Dickerson, E. B.; Dreaden, E. C.; Huang, X.; El-Sayed, I. H.; Chu, H.; Pushpanketh, S.; McDonald, J. F.; El-Sayed, M. A. Gold nanorod assisted near-infrared plasmonic photothermal therapy (PPTT) of squamous cell carcinoma in mice. *Cancer Lett.* **2008,** 269, 57-66.

12. Hirsch, L. R.; Stafford, R. J.; Bankson, J. A.; Sershen, S. R.; Rivera, B.; Price, R. E.; Hazle, J. D.; Halas, N. J.; West, J. L. Nanoshell-mediated near-infrared thermal therapy of tumors under magnetic resonance guidance. *Proc. Natl. Acad. Sci. USA.* **2003,** 100, 13549-13554.

13. O'Neal, D. P.; Hirsch, L. R.; Halas, N. J.; Payne, J. D.; West, J. L. Photo-thermal tumor ablation in mice using near infrared-absorbing nanoparticles. *Cancer Lett.* **2004,** 209, 171-176.

14. Stern, J. M.; Stanfield, J.; Kabbani, W.; Hsieh, J. T.; Cadeddu, J. A. Selective prostate cancer thermal ablation with laser activated gold nanoshells. *J. Urol.* **2008,** 179, 748-753.

15. Maeda, H.; Greish, K.; Fang, J. The EPR effect and polymeric drugs: A paradigm shift for cancer chemotherapy in the 21 st century. *Adv. Polymer Sci.* **2006,** 193, 103-121.

16. Iyer, A. K.; Khaled, G.; Fang, J.; Maeda, H. Exploiting the enhanced permeability and retention effect for tumor targeting. *Drug Discov. Today* **2006,** 11, 812-818.

17. Duncan, R. The dawning era of polymer therapeutics. *Nat. Rev. Drug Discov.* **2003,** 2, 347-360.

18. O'Brien, M.; Wigler, N.; Inbar, M.; Rosso, R.; Grischke, E.; Santoro, A.; Catane, R.; Kieback, D.; Tomczak, P.; Ackland, S. Reduced cardiotoxicity and comparable efficacy in a phase III trial of pegylated liposomal doxorubicin HCl (CAELYX™/Doxil®) versus conventional doxorubicin for first-line treatment of metastatic breast cancer. *Ann. Oncol.* **2004,** 15, 440-449.

19. Matsumura, Y.; Kataoka, K. Preclinical and clinical studies of anticancer agent incorporating polymer micelles. *Cancer Sci.* **2009,** 100, 572-579.

20. El-Sayed, I. H.; Huang, X.; El-Sayed, M. A. Surface plasmon resonance scattering and absorption of anti-EGFR antibody conjugated gold nanoparticles in cancer diagnostics: applications in oral cancer. *Nano Lett.* **2005,** 5, 829-834.

21. Loo, C.; Lowery, A.; Halas, N.; West, J.; Drezek, R. Immunotargeted nanoshells for integrated cancer imaging and therapy. *Nano Lett.* **2005,** 5, 709-711.

22. Dixit, V.; Van den Bossche, J.; Sherman, D. M.; Thompson, D. H.; Andres, R. P. Synthesis and grafting of thioctic acid- PEG- folate conjugates onto Au nanoparticles for selective targeting of folate receptor-positive tumor cells. *Bioconjug. Chem.* **2006,** 17, 603-609.

23. Tkachenko, A. G.; Xie, H.; Liu, Y.; Coleman, D.; Ryan, J.; Glomm, W. R.; Shipton, M. K.; Franzen, S.; Feldheim, D. L. Cellular trajectories of peptide-modified gold particle complexes: comparison of nuclear localization signals and peptide transduction domains. *Bioconjug. Chem.* **2004,** 15, 482-490.

24. Ruoslahti, E.; Pierschbacher, M. D. New perspectives in cell adhesion: RGD and integrins. *Science* **1987,** 238, 491-497.

25. Pasqualini, R.; Koivunen, E.; Ruoslahti, E. Alpha v integrins as receptors for tumor targeting by circulating ligands. *Nat. Biotechnol.* **1997,** 15, 542-546.

26. Dijkgraaf, I.; Kruijtzer, J. A. W.; Liu, S.; Soede, A. C.; Oyen, W. J. G.; Corstens, F. H. M.; Liskamp, R. M. J.; Boerman, O. C. Improved targeting of the alpha v beta 3 integrin by multimerisation of RGD peptides. *Eur. J. Nucl. Med. Mol. Imaging* **2007,** 34, 267-273.

27. Thumshirn, G.; Hersel, U.; Goodman, S. L.; Kessler, H. Multimeric cyclic RGD peptides as potential tools for tumor targeting: Solid phase peptide synthesis and chemoselective oxime ligation. *Chemistry* **2003,** 9, 2717-2725.

28. Borgman, M.; Aras, O.; Geyser-Stoops, S.; Sausville, E. A.; Ghandehari, H. Biodistribution of HPMA copolymer-aminohexylgeldanamycin-RGDfK conjugates for prostate cancer drug delivery. *Mol. Pharm.* **2009,** 6, 1836-1847.

29. Borgman, M. P.; Coleman, T.; Kolhatkar, R. B.; Geyser-Stoops, S.; Line, B. R.; Ghandehari, H. Tumor-targeted HPMA copolymer-(RGDfK)-(CHX-A"-DTPA) conjugates show increased kidney accumulation. *J. Control. Release* **2008,** 132, 193-199.

30. Borgman, M. P.; Ray, A.; Kolhatkar, R. B.; Sausville, E. A.; Burger, A. M.; Ghandehari, H. Targetable HPMA copolymer-aminohexylgeldanamycin conjugates for prostate cancer therapy. *Pharm. Res.* **2009,** 26, 1407-1418.

31. Line, B. R.; Mitra, A.; Nan, A.; Ghandehari, H. Targeting tumor angiogenesis: comparison of peptide and polymer-peptide conjugates. *J. Nucl. Med.* **2005,** 46, 1552-1560.

32. Mitra, A.; Coleman, T.; Borgman, M.; Nan, A.; Ghandehari, H.; Line, B. R. Polymeric conjugates of mono-and bi-cyclic $a_V ß_3$ binding peptides for tumor targeting. *J. Control. Release* **2006,** 114, 175-183.

33. Mitra, A.; Mulholland, J.; Nan, A.; McNeill, E.; Ghandehari, H.; Line, B. R. Targeting tumor angiogenic vasculature using polymer-RGD conjugates. *J. Control. Release* **2005,** 102, 191-201.

34. Mitra, A.; Nan, A.; Papadimitriou, J. C.; Ghandehari, H.; Line, B. R. Polymer-peptide conjugates for angiogenesis targeted tumor radiotherapy. *Nucl. Med. Biol.* **2006,** 33, 43-52.

35. Zarabi, B.; Borgman, M. P.; Zhuo, J.; Gullapalli, R.; Ghandehari, H. Noninvasive monitoring of HPMA copolymer-RGDfK conjugates by magnetic resonance imaging. *Pharm. Res.* **2009,** 26, 1121-1129.

36. Greish, K.; Ray, A.; Bauer, H.; Larson, N.; Malugin, A.; Pike, D. B.; Haider, M.; Ghandehari, H. Anticancer and antiangiogenic activity of HPMA copolymer-aminohexylgeldanamycin-RGDfK conjugates for prostate cancer therapy. *J. Control. Release* **2011,** 151, 263-270.

37. Ray, A.; Larson, N.; Pike, D. B.; Gruner, M.; Naik, S.; Bauer, H.; Malugin, A.; Khaled, G.; Ghandehari, H. Comparison of active and passive targeting of docetaxel for prostate cancer therapy by HPMA copolymer-RGDfK conjugates. *Mol. Pharm.* **2011,** 8, 1090-1099.

38. Huang, X.; Jain, P. K.; El-Sayed, I. H.; El-Sayed, M. A. Plasmonic photothermal therapy (PPTT) using gold nanoparticles. *Lasers Med. Sci.* **2008,** 23, 217-228.

39. Dudar, T. E.; Jain, R. K. Differential response of normal and tumor microcirculation to hyperthermia. *Cancer Res.* **1984,** 44, 605-612.

40. Horsman, M. R. Tissue physiology and the response to heat. *Int. J. Hyperthermia* **2006,** 22, 197-203.

41. Song, C. W.; Kang, M. S.; Rhee, J. G.; Levitt, S. H. Effect of hyperthermia on vascular function in normal and neoplastic tissues. *Ann. NY Acad. Sci.* **1980,** 335, 35-47.

42. Nikoobakht, B.; El-Sayed, M. A. Preparation and growth mechanism of gold nanorods (NRs) using seed-mediated growth method. *Chem. Mater.* **2003,** 15, 1957-1962.

43. Niidome, T.; Yamagata, M.; Okamoto, Y.; Akiyama, Y.; Takahashi, H.; Kawano, T.; Katayama, Y.; Niidome, Y. PEG-modified gold nanorods with a stealth character for in vivo applications. *J. Control. Release* **2006,** 114, 343-347.

44. Vainrub, A.; Pustovyy, O.; Vodyanoy, V. Resolution of 90 nm (lambda/5) in an optical transmission microscope with an annular condenser. *Opt. Lett.* **2006,** 31, 2855-2857.

45. Skebo, J. E.; Grabinski, C. M.; Schrand, A. M.; Schlager, J. J.; Hussain, S. M. Assessment of metal nanoparticle agglomeration, uptake, and interaction using high-illuminating system. *Int. J. Toxicol.* **2007,** 26, 135-141.

46. Kumar, C.; Nie, H.; Rogers, C.; Malkowski, M.; Maxwell, E.; Catino, J.; Armstrong, L. Biochemical characterization of the binding of echistatin to integrin alphavbeta3 receptor. *J. Pharmacol. Exp. Ther.* **1997,** 283, 843-853.

47. Jain, P. K.; El-Sayed, I. H.; El-Sayed, M. A. Au nanoparticles target cancer. *Nano Today* **2007,** 2, 18-29.

48. Schwartz, J. A.; Shetty, A. M.; Price, R. E.; Stafford, R. J.; Wang, J. C.; Uthamanthil, R. K.; Pham, K.; McNichols, R. J.; Coleman, C. L.; Payne, J. D. Feasibility study of particle-assisted laser ablation of brain tumors in orthotopic canine model. *Cancer Res.* **2009,** 69, 1659-1667.

49. Kopecek, J.; Kopecková, P. HPMA copolymers: origins, early developments, present, and future. *Adv. Drug Deliv. Rev.* **2010,** 62, 122-149.

50. Cai, W.; Shin, D. W.; Chen, K.; Gheysens, O.; Cao, Q.; Wang, S. X.; Gambhir, S. S.; Chen, X. Peptide-labeled near-infrared quantum dots for imaging tumor vasculature in living subjects. *Nano Lett.* **2006,** 6, 669-676.

51. Gormley, A. J.; Greish, K.; Ray, A.; Robinson, R.; Gustafson, J. A.; Ghandehari, H. Gold nanorod mediated plasmonic photothermal therapy: A tool to enhance macromolecular delivery. *Int. J. Pharm.* **2011,** 415, 315-318.

52. Maruyama, K.; Ishida, O.; Takizawa, T.; Moribe, K. Possibility of active targeting to tumor tissues with liposomes. *Adv. Drug Deliv. Rev.* **1999,** 40, 89-102.

53. Levchenko, T. S.; Rammohan, R.; Lukyanov, A. N.; Whiteman, K. R.; Torchilin, V. P. Liposome clearance in mice: the effect of a separate and combined presence of surface charge and polymer coating. *Int. J. Pharm.* **2002,** 240, 95-102.

54. Aragnol, D.; Leserman, L. D. Immune clearance of liposomes inhibited by an anti-Fc receptor antibody in vivo. *Proc. Natl. Acad. Sci. USA.* **1986,** 83, 2699-2703.

55. Peeters, P. A. M.; Storm, G.; Crommelin, D. J. A. Immunoliposomes in vivo: state of the art. *Adv. Drug Deliv. Rev.* **1988,** 1, 249-266.

56. Arnida, M.; Janat-Amsbury, M.; Ray, A.; Peterson, C.; Ghandehari, H. Geometry and surface characteristics of gold nanoparticles influence their biodistribution and uptake by macrophages. *Eur J Pharm Biopharm* **2010,** 77, 417-23.

57. Sadekar, S.; Ray, A.; Jana t-Amsbury, M.; Peterson, C.; Ghandehari, H. Comparative ciodistribution of PAMAM dendrimers and HPMA copolymers in ovarian-tumor-bearing mice. *Biomacromolecules* **2010,** 12, 88-96.

58. Arosio, D.; Manzoni, L.; Araldi, E. M. V.; Scolastico, C. Cyclic RGD functionalized gold nanoparticles for tumor targeting. *Bioconjug. Chem.* **2011,** 22, 664-672.

59. Xie, H.; Diagaradjane, P.; Deorukhkar, A. A.; Goins, B.; Bao, A.; Phillips, W. T.; Wang, Z.; Schwartz, J.; Krishnan, S. Integrin alpha v beta 3-targeted gold nanoshells augment tumor vasculature-specific imaging and therapy. *Int. J. Nanomedicine* **2011,** 6, 259-269.

60. Li, Z.; Huang, P.; Zhang, X.; Lin, J.; Yang, S.; Liu, B.; Gao, F.; Xi, P.; Ren, Q.; Cui, D. RGD-conjugated dendrimer-modified gold nanorods for in vivo tumor targeting and photothermal therapy. *Mol. Pharm.* **2009,** 7, 94-104.

61. Huang, X.; Peng, X.; Wang, Y.; Shin, D. M.; El-Sayed, M. A.; Nie, S. A reexamination of active and passive tumor targeting by using rod-shaped gold nanocrystals and covalently conjugated peptide ligands. *ACS Nano* **2010,** 4, 5887-5896.

62. Rhim, J. S.; Tsai, W. P.; Chen, Z. Q.; Chen, Z.; Van Waes, C.; Burger, A. M.; Lautenberger, J. A. A human vascular endothelial cell model to study angiogenesis and tumorigenesis. *Carcinogenesis* **1998,** 19, 673-681.

63. Sakko, A. J.; Ricciardelli, C.; Mayne, K.; Suwiwat, S.; LeBaron, R. G.; Marshall, V. R.; Tilley, W. D.; Horsfall, D. J. Modulation of prostate cancer cell attachment to matrix by versican. *Cancer Res.* **2003,** 63, 4786-4791.

64. Romanov, V. I.; Goligorsky, M. S. RGD-recognizing integrins mediate interactions of human prostate carcinoma cells with endothelial cells in vitro. *Prostate* **1999,** 39, 108-118.

65. Shukla, R.; Bansal, V.; Chaudhary, M.; Basu, A.; Bhonde, R. R.; Sastry, M. Biocompatibility of gold nanoparticles and their endocytotic fate inside the cellular compartment: a microscopic overview. *Langmuir* **2005,** 21, 10644-10654.

66. Chithrani, B. D.; Ghazani, A. A.; Chan, W. C. Determining the size and shape dependence of gold nanoparticle uptake into mammalian cells. *Nano Lett.* **2006,** 6, 662-668.

67. Chithrani, B. D.; Chan, W. C. Elucidating the mechanism of cellular uptake and removal of protein-coated gold nanoparticles of different sizes and shapes. *Nano Lett.* **2007,** 7, 1542-1550.

68. Connor, E. E.; Mwamuka, J.; Gole, A.; Murphy, C. J.; Wyatt, M. D. Gold nanoparticles are taken up by human cells but do not cause acute cytotoxicity. *Small* **2005,** 1, 325-327.

69. Mao, Z.; Wang, B.; Ma, L.; Gao, C.; Shen, J. The influence of polycaprolactone coating on the internalization and cytotoxicity of gold nanoparticles. *Nanomedicine* **2007,** 3, 215-223.

70. Khan, J. A.; Pillai, B.; Das, T. K.; Singh, Y.; Maiti, S. Molecular effects of uptake of gold nanoparticles in HeLa cells. *Chembiochem* **2007,** 8, 1237-1240.

71. Salem, A. K.; Searson, P. C.; Leong, K. W. Multifunctional nanorods for gene delivery. *Nat. Mater.* **2003,** 2, 668-671.

72. Gormley, A. J.; Ghandehari, H., Evaluation of toxicity of nanostructures in biological systems. In *Nanotoxicity: From In Vivo and In Vitro Models to Health Risks*, Sahu, S. C.; Casciano, D. A., Eds. John Wiley & Sons, Ltd: West Sussex, 2009; pp 115-159.

73. Gabizon, A.; Papahadjopoulos, D. The role of surface charge and hydrophilic groups on liposome clearance in vivo. *Biochim. Biophys. Acta.* **1992,** 1103, 94-100.

74. Xiao, K.; Li, Y.; Luo, J.; Lee, J. S.; Xiao, W.; Gonik, A. M.; Agarwal, R. G.; Lam, K. S. The effect of surface charge on in vivo biodistribution of PEG-oligocholic acid based micellar nanoparticles. *Biomaterials* **2011,** 32, 3435-3446.

CHAPTER 5

GUIDED DELIVERY OF POLYMER THERAPEUTICS USING PLASMONIC PHOTOTHERMAL THERAPY

5.1 Introduction

Incorporation of anticancer agents within nanocarriers represents an effective way of delivering hydrophobic drugs in the blood as well as altering their organ distribution in the body.[1] These nanomedicines have been designed to target sites of disease and enhance delivery to solid tumors. Despite substantial progress, clinical translation has been slow due to limited accumulation in the target site.[2]

The delivery of targeted nanomedicines to solid tumors utilizes a two-pronged approach.[1] First, their nanoscale size (~5-500 nm) is leveraged to reduce the accumulation in healthy organs while maximizing extravasation into the tumor mass. While the junctions between vascular endothelial cells in healthy tissues are too small (~2-6 nm) to allow permeation, larger gaps (up to 1.2 μm), which are present in the tumor's poorly developed and leaky vasculature, allow them to partition out of the blood and into the tumor mass.[3] Described as the EPR effect,[4] this passive targeting approach has been applied ubiquitously in the delivery of nanomedicines.[5] Second, once in the tumor interstitial space, contact with receptors expressed on the cancer cell surface

---

Reprinted with permission from Nano Today
Reference: Gormley, A. J.; et al., *Nano Today.* **2012,** 7, 158-167.

immobilizes them and triggers their internalization via endocytosis followed by drug release.[6] This binding and uptake can be further increased through active targeting by conjugating receptor specific ligands to the nanocarriers.[7]

Polymer-based nanomedicines have the advantage of solubilizing hydrophobic drugs and exhibiting stealth-like characteristics thereby evading immune recognition.[8] In such systems drugs can be covalently linked to the polymer backbone and specifically released by enzymatic degradation or hydrolysis.[9] These polymer-drug conjugates are typically 5-15 nm in hydrodynamic diameter and can therefore be cleared by urinary excretion.[10] This is advantageous due to rising safety concerns of nanomedicines which are not eliminated from the body.[11-14] The small size however comes with a cost as rapid renal elimination reduces the availability of the conjugates to accumulate in tumors by the EPR effect.[15] With these advantages and limitations in mind, there is therefore a need to develop a strategy which maximizes the delivery of polymer therapeutics within the window of opportunity before renal clearance.

This need is particularly apparent considering conjugates, which aim to maximize tumor delivery, have to date demonstrated only moderate clinical benefit. For example, early generation polymer-drug conjugates such as HPMA copolymer-doxorubicin and PEG-camptothecin have not obtained the same success in the clinic as other nanomedicines such as Doxil® (liposome-doxorubicin) and Abraxane® (albumin-paclitaxel).[8] While much of this may be related to other variables such as drug release kinetics, the lack of sufficient delivery to the tumor (<<15% of the injected dose) represents the primary barrier to success. Recent efforts to improve this delivery such as using high molecular weight biodegradable polymers which exhibit prolonged blood

circulation as well as using polymers with different architectures (i.e., dendrimers and branched polymers) have achieved some success. However, greater control over both passive and active targeting strategies is desirable.[16]

One method which has been described as a temporary means of enhancing the delivery of macromolecules such as albumin, liposomes and other nanomedicines is by inducing tumor hyperthermia.[17-22] Under conditions of elevated temperatures and increased blood perfusion, it has been found that the tumor microvascular permeability and therefore EPR effect is significantly increased.[23] This is believed to be a result of cytoskeletal disaggregation in endothelial cells leading to further expansion of the fenestrae that already surround them.[24-27] Unfortunately, current techniques for inducing tumor hyperthermia such as radiofrequency ablation or hyperthermic intraperitoneal perfusion are restrictive in their capacity to selectively deliver heat towards cancerous tissue.[28]

More recently several laboratories have initiated hyperthermia by PPTT. In brief, when light with a wavelength that matches the tunable SPR of gold nanostructures interacts with these particles, coherent oscillations of electrons in the conduction band allow the light to be absorbed and photothermal conversion to occur.[29] When such particles are delivered to cancerous tissue by EPR, this phenomenon can be used as a tool to selectively induce hyperthermia.[30] Such PPTT has been used to achieve tumor selective temperatures varying from 50°C to over 70°C, well above the threshold required for vascular damage.[31-35] Previously, it has been shown in Chapter 3 of this dissertation as well as other works that this heat delivery technique at reduced temperatures (42-45°C) can be applied to selectively increase the perfusion and permeability of the tumor

vasculature and hence the delivery of nanomedicines during laser radiation.[36-40] In this way, the delivery of nanoworms, liposomes and micelles have shown to be recruited to the treatment site and sensitized for targeting and drug release.[38-40]

In this chapter, we aim to remotely modify the tumor microenvironment with laser mediated PPTT to increase both passive and active polymeric drug targeting. We use this technique immediately following injection of HPMA copolymers to augment EPR at the treatment site and drive their delivery into the tumor interstitial space while the copolymer is at its peak concentration in the blood (Figure 5.1). Once at the tumor site, we take advantage of the natural response of tissue to heat shock by conjugation of a targeting ligand which binds to HSPs. This is because the expression of HSPs is significantly increased following exposure to heat shock.[26] In this way, the targetability of these cancer cells can be elevated so that the copolymer is retained in the tumor and taken up by cells to a higher extent.

A technique is introduced wherein a laser can be used to direct the localization and retention of polymer therapeutics in solid tumors. With this technique, it is believed that polymer-drug conjugates can be administered to patients by clinicians and efficiently guided towards the location of disease to maximize treatment efficacy, while minimizing toxicity.

5.2 Materials and Methods

5.2.1 Synthesis and characterization of PEGylated GNRs

GNRs were synthesized using the seed-mediated growth method.[41] Optimization of silver nitrate content and seed amount yielded GNRs with an aspect ratio such that the

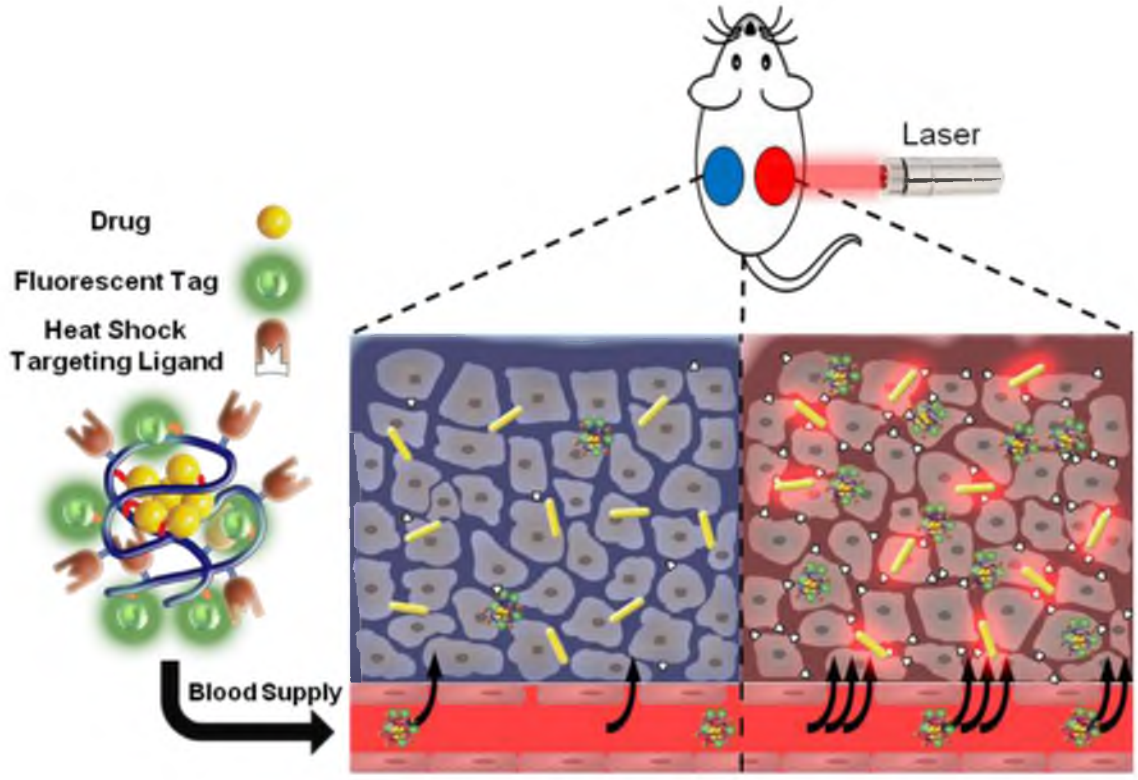

Figure 5.1: Schematic of laser guided approach. Following delivery of GNRs to tumors, a laser is applied to the right tumor to heat the GNRs and induce a heat shock response. This effectively increases the pore size in the tumor vasculature as well as the cell surface expression of HSPs, resulting in increased tumor accumulation and retention.

SPR peak was between 800 and 810 nm.The GNRs were then centrifuged and washed three times with DI water to remove excess CTAB. PEGylation was done by addition of methoxy-PEG-thiol (5 kD, Creative PEGWorks, Winston Salem, NC) to the GNR suspension. The suspension was then thoroughly dialyzed against DI water and sterile filtered. In the final step, the GNRs were centrifuged, washed three times with DI water to remove unreacted PEG and concentrated. The final product was stored at 4°C for a maximum of two months before use. The size and shape of the GNRs were determined by TEM and the light absorption profile was measured by UV spectrometry. Zeta potential was measured in DI water by measuring electrophoretic mobility using laser doppler velocimetry (Zetasizer Nano ZS, Malvern Instruments Ltd, Worcestershire, UK).

5.2.2 Synthesis and characterization of HPMA copolymer-drug conjugates

The comonomers were synthesized as described previously.[42-43] Precursor copolymer conjugates containing reactive carboxyl groups (thiazolidine-2-thione) were prepared by free radical copolymerization in methanol (50°C for 24 hours) using azobisisobutryonitrile (AIBN) as the initiator within a glass ampoule under N_2 gas. For these polymerizations, monomers, AIBN and methanol content were 15, 0.5 and 84.5 weight % respectively. Copolymerization with the monomer *N*-methacryloyl-tyrosinamide (MA-Tyr-$CONH_2$) allows for radiolabeling of the conjugates or 5-[3-(methacryloylaminopropyl)thioureidyl] fluorescein (APMA-FITC) for fluorescent tracking of cellular uptake in cells. Weight average molecular weight (M_w), number average molecular weight (M_n), and polydispersity (M_w/M_n) of the precursor copolymers were estimated by size exclusion chromatography (SEC) using HPMA homopolymer

fractions of known molecular weight. SEC was done on a Superose 12 column (10 mm x 30 cm) (GE Healthcare, Piscataway, NJ) using a Fast Protein Liquid Chromatography (FPLC) system (GE Healthcare). Heat shock targeted conjugates were obtained by aminolysis of precursor copolymers with the GRP78 targeting peptide (WIFPWIQL), synthesized by solid phase, in DMSO for 24 hrs. Untargeted conjugates were obtained by hydrolysis of precursor copolymers in the presence of aqueous sodium hydroxide. Following polymerization, product was obtained by precipitation into diethyl ether. Copolymer conjugates were purified by dialysis against DI water (3.5 KDa molecular weight cut-off), lyophilized, and stored at -20°C. The amount of GRP78 targeting peptide was quantified by amino acid analysis (HPLC method). ^{125}Iodine was conjugated to tyrosine residues to obtain radiolabeled copolymers using the Iodogen method with slight modification.[44] Each copolymer (2 mg) and 0.5 mCi Na-^{125}I were dissolved in 0.5M NaH_2PO_4 pH 7.0 and incubated at room temperature in Iodogen tubes for 10 minutes. Free radiolabel was removed by dialysis against saline and verified by SEC.

5.2.3 Cellular uptake of FITC-labeled conjugates

Cellular uptake was evaluated qualitatively by confocal microscopy. DU145 cells were exposed to heat shock (43°C / 30 min incubation) or control (37°C, continuous incubation). This thermal dose was chosen due to previous experiments which showed that treatment of cells with heat at 43°C for 30 minutes kills less than 5% of cells. Higher thermal doses, however, resulted in significantly more cell death. Therefore, this dose was chosen to minimize the impact of heat on cell viability. Eight hours post-heat shock, cells were incubated with 0.5 mg/mL of heat shock targeted or untargeted conjugates for

four hours. Cells were then washed, plasma membrane stained with TRITC-lectin (10 μg/ml, 10 minutes at 37°C, Sigma #L5266) and fixed with 4% paraformaldehyde in PBS. The cells were mounted to a slide using mounting medium containing DAPI and imaged using a confocal laser scanning microscope (Olympus FluoView® FV1000, Olympus, Center Valley, PA).

5.2.4 *In vivo* induction of heat shock via PPTT

Anesthetized 6-12 week old athymic nu/nu mice were subcutaneously injected with 10^7 DU145 cells on each flank and tumors were allowed to grow until approximately 5-7 mm in diameter. Animals were then administered PEGylated GNRs (9.6 mg/kg) via tail vein injection. After 48 hours, mice were anesthetized, and tumors were swabbed with 50% propylene glycol to enhance laser penetration depth.[45] Tumors on the right flank only were then radiated for 10 minutes using an 808 nm fiber coupled laser diode (Oclaro Inc., San Jose, CA) with collimating lens (Thorlabs, Newton, NJ). Intratumoral temperature was monitored using a 33 gauge needle thermocouple (Omega, Stamford, CT) and tumor temperature was maintained between 42°C and 43°C. This thermal dose (temperature and time) was chosen based on findings from Chapter 3. A more detailed discussion of this topic is also found in Section 3.2. Tumors on the left flank served as internal controls.

5.2.5 *In vivo* GRP78 expression in tumors following PPTT

Eight hours following induction of heat shock, mice were euthanized and tumors on the right (laser) and left (control) flanks were removed and snap frozen in liquid

nitrogen. Immunohistochemical (IHC) analysis of GRP78 expression was then performed on 4-micron thick sections of formalin-fixed, paraffin-embedded tissues using a goat polyclonal anti-GRP78 antibody (Santa Cruz Biotechnology, Santa Cruz, CA) and a polyclonal rabbit anti-goat biotinylated antibody. Positive signal was visualized using a streptavidin-HRP system, utilizing DAB (3-3' diaminobenzidine) as the chromogen. The sections were counterstained with hematoxylin. The sections were placed in iodine to remove any precipitates, and then dipped in sodium thiosulfate to clear the iodine. The sections were dehydrated in graded alcohols (70%, 95% x2 and 100% x2), cleared in xylene, coverslipped and imaged.

5.2.6 Tumor accumulation and biodistribution

Prior to induction of heat shock via PPTT, mice were intravenously administered via the tail vein a single bolus dose of 50 mg/kg ^{125}I radiolabeled conjugates (untargeted or heat shock targeted). At each time point, mice were euthanized, blood immediately collected, followed by blood perfusion with saline. Tumors and major organs were then collected and analyzed by gamma counting. Percent injected dose per gram of blood/tissue (%ID/g) was calculated and expressed as a function of time.

5.3 Results and Discussion

To begin, the HPMA copolymers were synthesized via free radical polymerization and characterized (Figure 5.2 A, Table 5.1, Figure A.1-4). Molecular weight for the conjugates varied from 60 – 80 kDa, and was maintained slightly above renal threshold to take advantage of the EPR effect by extending blood circulation. To

generate a targetable HPMA copolymer, the WIFPWIQL peptide was conjugated to the HPMA copolymer side chain via aminolysis of thiazolidine-2-thione side chains, resulting in copolymers with approximately 20% peptide content by weight or approximately 12 peptides per copolymer. This peptide was chosen due to its known affinity to GRP78, a member of the HSP70 family of proteins.[46] Previously, it was shown that this receptor-ligand approach can be used to effectively deliver HPMA copolymer-drug conjugates to prostate cancer cells.[42] Full details regarding the feed compositions and resulting polymer characteristics are given in Table 5.1.

GNRs were used in this study because they have a greater light absorption cross section per unit size relative to those with other geometries (i.e., shells and spheres),[47] and are capable of inducing heat shock in tissue upon laser excitation.[31, 35, 37-39, 48] Before use, the GNRs were grafted with a PEG surface coating to reduce the extent of protein adsorption and improve blood circulation time.[49] This resulted in a zeta potential of -10.0 mV. The aspect ratio (4.1), size (58.8 x 14.4 nm ± 6.5 x 2.1 nm) and therefore SPR peak at 800 nm was chosen as light at this wavelength is capable of penetrating tissue several centimeters (Figure 5.2 B-C). By this method, as determined in a previous study, 1.22% of the injected dose is delivered to the tumor.[50]

To determine if heat shock could be used to regulate the targetability of these conjugates, fluorescently labeled HPMA copolymers with and without the heat shock targeting peptide were introduced to cells eight hours post-heat shock (43°C, 30 min) or control (37°C, continuous incubation). Eight hours was chosen here because previous studies found that receptor expression peaks at this time following heat shock.[51] Visualization by confocal microscopy (four hour incubation, Figure 5.3) of uptake in

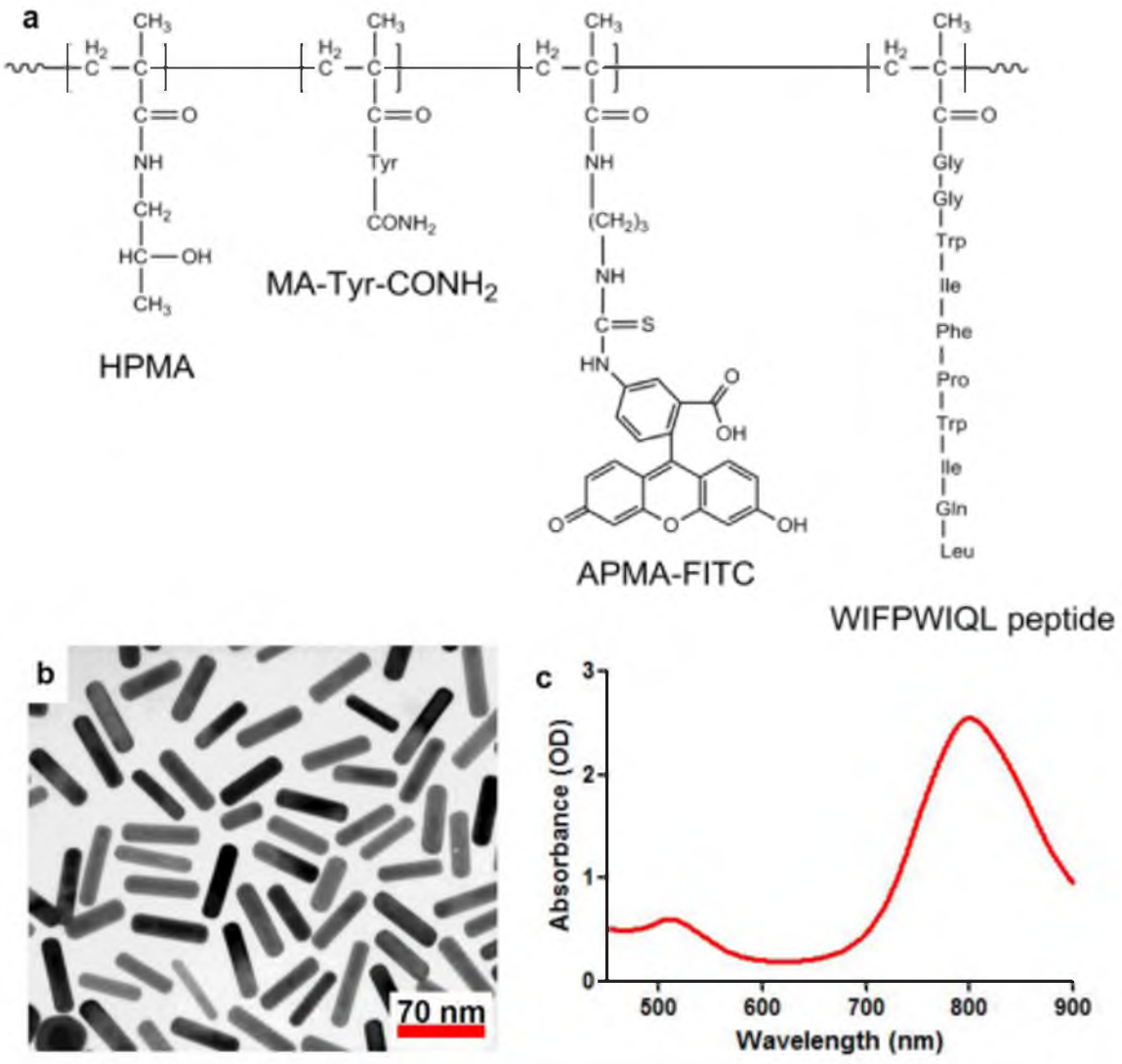

Figure 5.2: HPMA copolymer schematic and GNR characterization. (A) Representative HPMA copolymer with all monomers used in the study listed. For individual polymer composition, see Table 5.1. (B) TEM and (C) light absorption profile of synthesized GNRs.

Table 5.1: Characteristics of HPMA copolymer conjugates. Weight average molecular weight (M_w) and polydispersity (M_w/M_n) were estimated by SEC. The amount of the GRP78 targeting peptide was quantified by amino acid analysis (HPLC method).

Polymer	----------Feed composition (mol %) ----------				--------Polymer Characteristics ------		
	HPMA	MA-GG-TT	MA-Tyr-$CONH_2$	APMA-FITC	Apparent Mw (kDa)	M_w/M_n	WIFPWIQL content
HPMA	93	5	2	0	83.9	1.6	-
HPMA-WIFPWIQL	93	5	2	0	72.4	1.6	20.9 wt%
HPMA-FITC	93	5	0	2	62.4	1.4	-
HPMA-FITC-WIFPWIQL	93	5	0	2	64.4	1.4	18.0 wt%

cells indicates significantly increased binding and uptake of heat shock targeted conjugates which is in agreement with previous results.[42] This observation was much more pronounced, when the cells were first treated with heat shock due to increased receptor expression.

Next, the overall hypothesis of enhancing the delivery of these conjugates to laser radiated tissue was tested in mice bearing prostate tumors. Mice bearing two tumors, one on each flank, were intravenously (i.v.) administered PEG coated GNRs and allowed 48 hrs for the particles to accumulate in the tumors via EPR (Figure 5.4).[50] Radiolabeled conjugates (heat shock targeted and untargeted) were then administered i.v. followed immediately by laser radiation of the right tumor only for 10 minutes. During laser radiation the temperature in the right tumor was maintained between 42-43°C by controlling laser power such that only moderate hyperthermia was induced to avoid vascular collapse at higher temperatures (Figure 5.5).[52] It is important to note here that by directing the laser at the right tumor only, it is possible to directly compare the delivery of polymeric conjugates to tumors in the presence and absence of laser radiation in the same animal.

While the increased HSP expression profile of prostate cancer cells following heat shock was confirmed *in vitro*, it was necessary to confirm this phenomenon *in vivo*. The left (control) and right (laser treated) tumors were evaluated for GRP78 expression by immunohistochemistry. Heat shock treatment of the right tumors by laser resulted in increased HSP expression compared to the untreated tumors (Figure 5.6).

Following administration of the polymeric conjugates, a comparison of the laser radiated and control tumors 15 minutes and 4 hours following laser treatment indicates

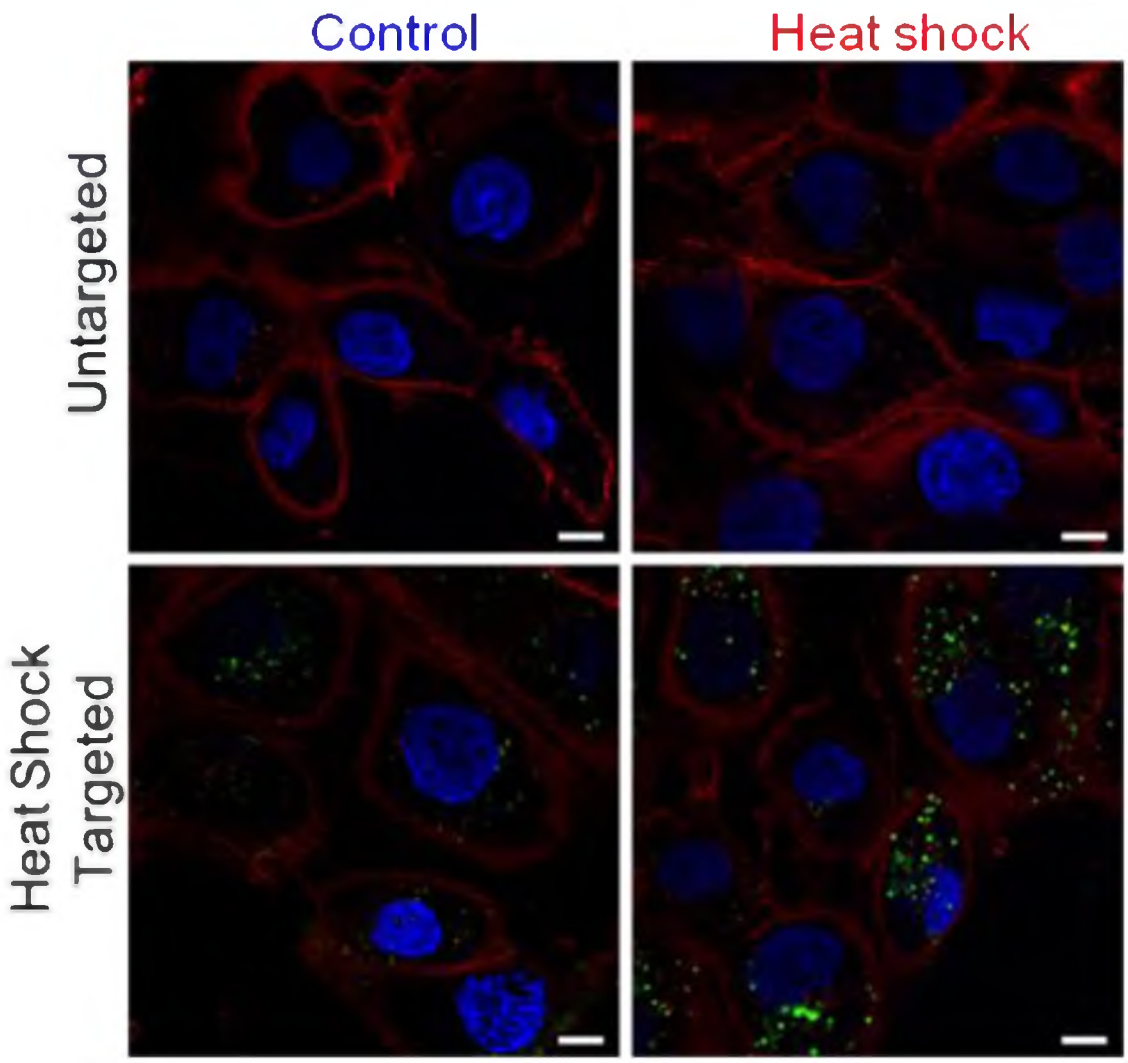

Figure 5.3: Visualization of cellular binding and uptake of fluorescently labeled (green) HPMA copolymers in cells by confocal microscopy. Blue stain is for nucleus (DAPI) and red stain is for plasma membrane (lectin-Rd). Scale bar, 10 μm.

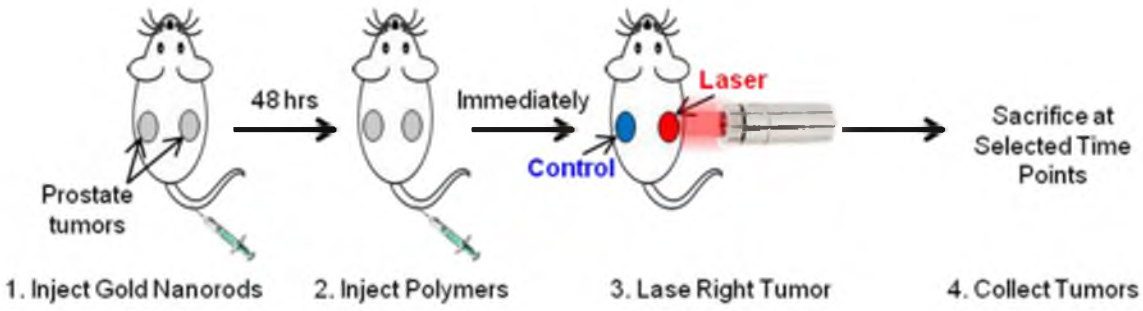

Figure 5.4: Schematic of experimental procedure.

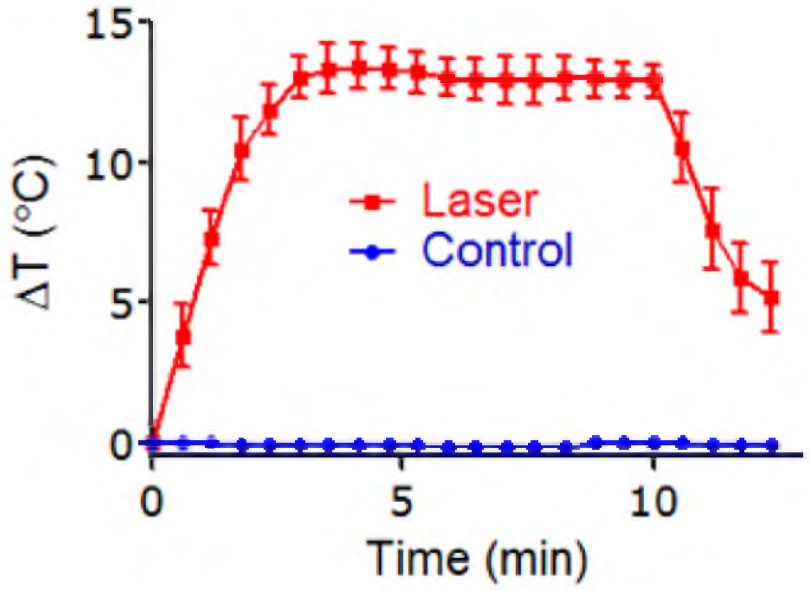

Figure 5.5: Changes in intratumoral temperatures during laser radiation (10 min) of left (control) and right (laser) tumors. Error bars represented as ±standard deviation.

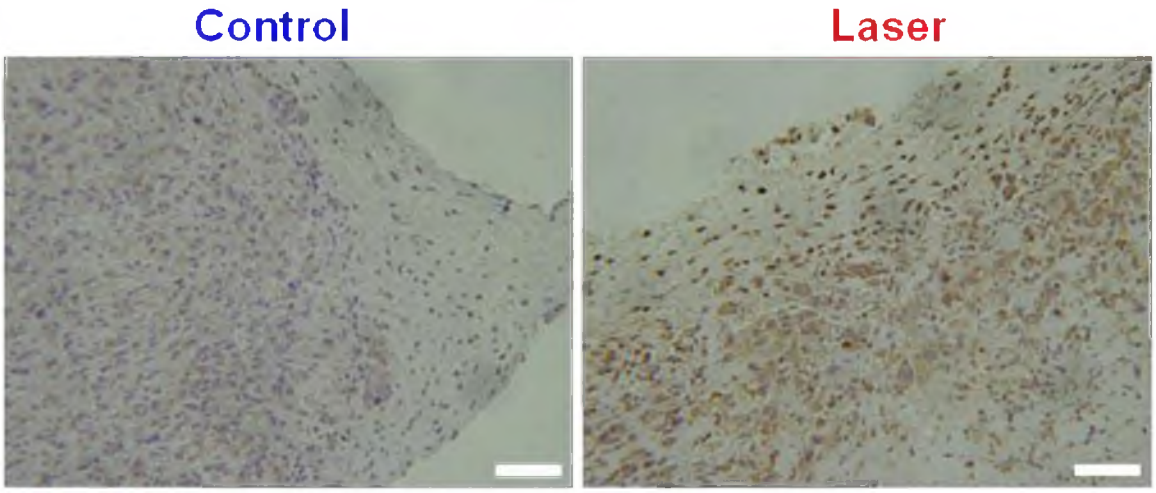

Figure 5.6: Cell expression of heat shock protein GRP78 (red color) in prostate tumors with or without laser treatment. Scale bar, 50 μm. Tumors which have been laser radiated have higher expression of GRP78.

that a two to three-fold increased burst accumulation occurred in the laser radiated tumors (Figure 5.7). This observation indicates that the treatment of tumors with heat causes increased tumor blood flow and augments the EPR effect by increasing vascular pore size.[19-20, 37] This burst accumulation was not maintained after four hours for the untargeted conjugates. As intended in the treatment design, the heat shock targeted conjugates were retained in the radiated tumor up to 12 hours after which elimination began to occur. This observation is supported by GRP78 expression data which shows that HSP expression is reduced after 12 hours.[51]

The biodistribution of the radiolabeled conjugates in major organs was also evaluated (Figure 5.8). Similar concentrations in the blood were observed over 72 hours for untargeted and heat shock targeted conjugates. However, significant accumulation was observed for the heat shock targeted conjugate in the liver, spleen, and kidneys. This non-specific accumulation is most likely due to the increased hydrophobic nature of the heat shock targeted conjugate due to the presence of the hydrophobic WIFPWIQL peptide (cLogP = 3.9). This increased hydrophobicity can potentiate interactions with biological tissues and increase uptake in RES organs.[53]

This nonspecific accumulation in healthy organs represents a significant disadvantage of the described therapy. It is very unlikely that such a therapy is useful its current form because of the expected side effects, a feature common to targeted therapeutics. It is anticipated that such non-specific interactions can be minimized by reducing the hydrophobic nature of the conjugates by either reducing the targeting peptide content or utilizing more hydrophilic targeting moieties. To test this, a new more hydrophilic peptide WDLAWMFRLPVG which also targets GRP78 is currently being

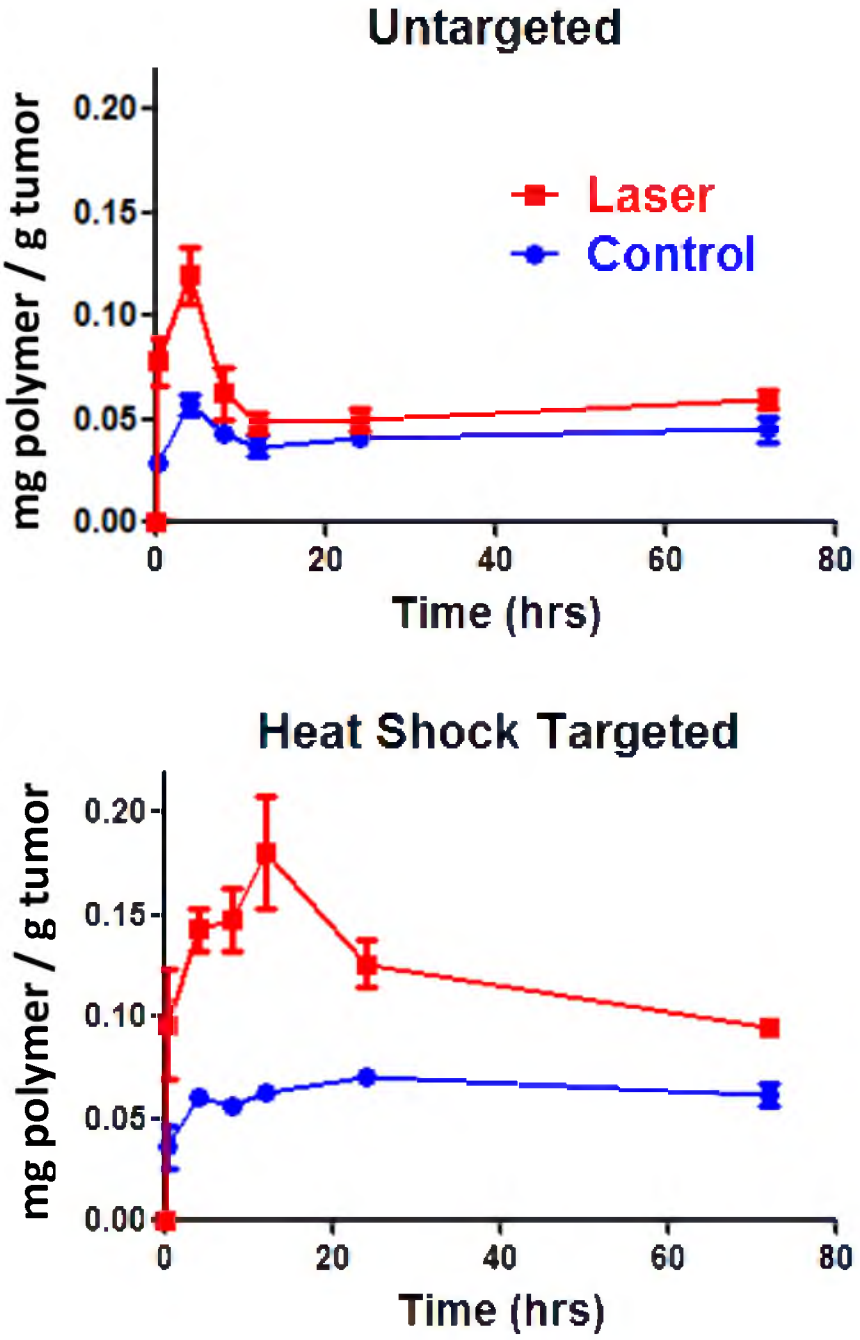

Figure 5.7: Tumor accumulation of radiolabeled polymers (untargeted and heat shock targeted) with or without laser treatment. Data expressed as experimental points with pharmacokinetic modeled lines. Laser radiation results in a burst accumulation (0-4 hours), which is only maintained (>24 hours) for the heat shock targeted polymers due to increased GRP78 expression. Error bars represented as ±standard error of the mean.

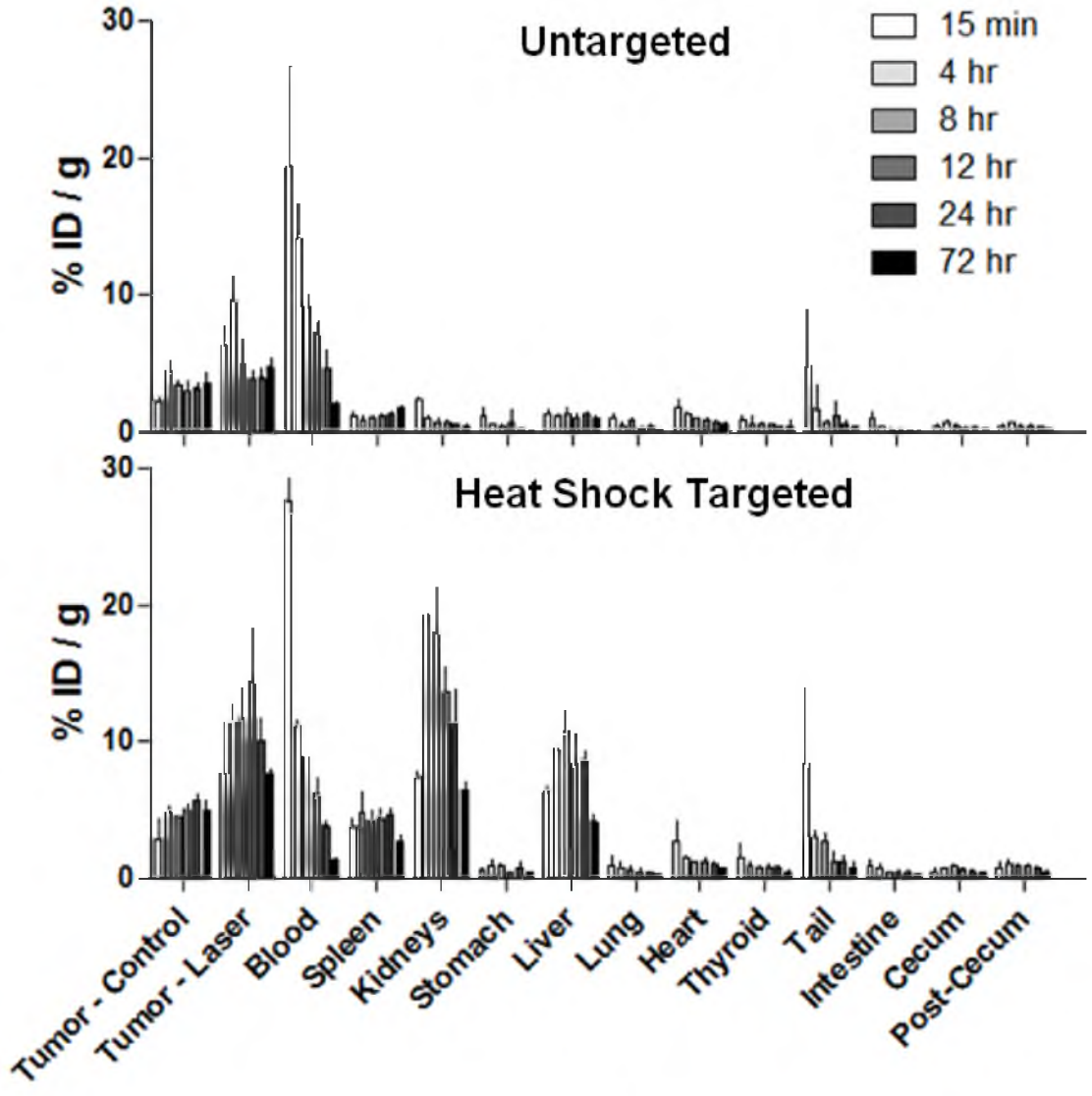

Figure 5.8: Biodistribution of radiolabeled (^{125}I) HPMA copolymers. Error bars represented as ±standard deviation.

evaluated. Preliminary biodistribution results provide some initial confirmation of this hypothesis in that an x-fold reduction in liver, kidney and spleen accumulation is observed using this new peptide. Targeting of this new conjugate has also been confirmed using the same *in vitro* experiments. Therefore, all future studies will likely utilize this new peptide to reduce the chances of toxicity to these organs.

5.4 Conclusions

In this chapter, it is demonstrated that it is possible to direct the delivery of targeted polymer therapeutics using PPTT by exploiting the physiologic response of tumors to heat. These findings help overcome one of the limitations of polymer therapeutics which is poor tumor accumulation. By using laser directed application of heat via GNRs, a burst accumulation of the therapeutics in the region of interest is possible while they are at their highest concentration in the blood. By incorporation of a heat shock targeting ligand in the copolymer design, high concentration can be maintained as the targeting receptors become increasingly available following heat induction. Ultimately, in a clinical setting, it is anticipated that clinicians will value this additional tool to help guide drug delivery to solid tumors.

5.5 References

1. Peer, D.; Karp, J. M.; Hong, S.; Farokhzad, O. C.; Margalit, R.; Langer, R. Nanocarriers as an emerging platform for cancer therapy. *Nat. Nanotechnol.* **2007,** 2, 751-760.

2. Vicent, M. J.; Ringsdorf, H.; Duncan, R. Polymer therapeutics: Clinical applications and challenges for development. *Adv. Drug Deliv. Rev.* **2009,** 61, 1117-1120.

3. Hobbs, S. K.; Monsky, W. L.; Yuan, F.; Roberts, W. G.; Griffith, L.; Torchilin, V. P.; Jain, R. K. Regulation of transport pathways in tumor vessels: role of tumor type and microenvironment. *Proc. Natl. Acad. Sci. USA.* **1998,** 95, 4607-4612.

4. Matsumura, Y.; Maeda, H. A new concept for macromolecular therapeutics in cancer chemotherapy: mechanism of tumoritropic accumulation of proteins and the antitumor agent smancs. *Cancer Res.* **1986,** 46, 6387-6392.

5. Maeda, H.; Wu, J.; Sawa, T.; Matsumura, Y.; Hori, K. Tumor vascular permeability and the EPR effect in macromolecular therapeutics: a review. *J. Control. Release* **2000,** 65, 271-284.

6. Lammers, T.; Hennink, W.; Storm, G. Tumour-targeted nanomedicines: principles and practice. *Br. J. Cancer* **2008,** 99, 392-397.

7. Pike, D. B.; Ghandehari, H. HPMA copolymer-cyclic RGD conjugates for tumor targeting. *Adv. Drug Deliv. Rev.* **2009,** 62, 167-183.

8. Duncan, R. The dawning era of polymer therapeutics. *Nat. Rev. Drug Discov.* **2003,** 2, 347-360.

9. Kopecek, J.; Kopeckovå, P. HPMA copolymers: origins, early developments, present, and future. *Adv. Drug Deliv. Rev.* **2010,** 62, 122-149.

10. Duncan, R. Polymer conjugates as anticancer nanomedicines. *Nat. Rev. Cancer* **2006,** 6, 688-701.

11. Oberdörster, G.; Oberdörster, E.; Oberdörster, J. Nanotoxicology: an emerging discipline evolving from studies of ultrafine particles. *Environ. Health Perspect.* **2005,** 113, 823-839.

12. Grainger, D. W. Nanotoxicity assessment: all small talk? *Adv. Drug Deliv. Rev.* **2009,** 61, 419.

13. Oberdörster, G. Safety assessment for nanotechnology and nanomedicine: concepts of nanotoxicology. *J. Intern. Med.* **2010,** 267, 89-105.

14. Sanhai, W. R.; Sakamoto, J. H.; Canady, R.; Ferrari, M. Seven challenges for nanomedicine. *Nat. Nanotechnol.* **2008,** 3, 242-244.

15. Seymour, L.; Miyamoto, Y.; Maeda, H.; Brereton, M.; Strohalm, J.; Ulbrich, K.; Duncan, R. Influence of molecular weight on passive tumour accumulation of a soluble macromolecular drug carrier. *Eur. J. Cancer* **1995,** 31, 766-770.

16. Duncan, R.; Gaspar, R. Nanomedicine (s) under the microscope. *Mol. Pharm.* **2011,** 8, 2101-2141.

17. Chen, Q.; Krol, A.; Wright, A.; Needham, D.; Dewhirst, M.; Yuan, F. Tumor microvascular permeability is a key determinant for antivascular effects of doxorubicin encapsulated in a temperature sensitive liposome. *Int. J. Hyperthermia* **2008,** 24, 475-482.

18. Gnant, M.; Noll, L.; Terrill, R.; Wu, P.; Berger, A.; Nguyen, H.; Lans, T.; Flynn, B.; Libutti, S.; Bartlett, D. Isolated hepatic perfusion for lapine liver metastases: impact of hyperthermia on permeability of tumor neovasculature. *Surgery* **1999,** 126, 890-899.

19. Kong, G.; Braun, R. D.; Dewhirst, M. W. Hyperthermia enables tumor-specific nanoparticle delivery: effect of particle size. *Cancer Res.* **2000,** 60, 4440-4445.

20. Kong, G.; Braun, R. D.; Dewhirst, M. W. Characterization of the effect of hyperthermia on nanoparticle extravasation from tumor vasculature. *Cancer Res.* **2001,** 61, 3027-3032.

21. Lefor, A. T.; Makohon, S.; Ackerman, N. B. The effects of hyperthermia on vascular permeability in experimental liver metastasis. *J. Surg. Oncol.* **1985,** 28, 297-300.

22. Matteucci, M. L.; Anyarambhatla, G.; Rosner, G.; Azuma, C.; Fisher, P. E.; Dewhirst, M. W.; Needham, D.; Thrall, D. E. Hyperthermia increases accumulation of technetium-99m-labeled liposomes in feline sarcomas. *Clin. Cancer Res.* **2000,** 6, 3748-3755.

23. Fujiwara, K.; Watanabe, T. Effects of hyperthermia, radiotherapy and thermoradiotherapy on tumor microvascular permeability. *Pathol. Int.* **2008,** 40, 79-84.

24. Chen, B.; Zhou, M.; Xu, L. Study of vascular endothelial cell morphology during hyperthermia. *J. Therm. Biol.* **2005,** 30, 111-117.

25. Fajardo, L.; Schreiber, A.; Kelly, N.; Hahn, G. Thermal sensitivity of endothelial cells. *Radiat. Res.* **1985,** 103, 276-285.

26. Hildebrandt, B.; Wust, P.; Ahlers, O.; Dieing, A.; Sreenivasa, G.; Kerner, T.; Felix, R.; Riess, H. The cellular and molecular basis of hyperthermia. *Crit. Rev. Oncol. Hematol.* **2002,** 43, 33-56.

27. Xu, L.; Chen, B.; Zhou, M. Change of individual vascular endothelial calcium during hyperthermia. *J. Therm. Biol.* **2006,** 31, 302-306.

28. Wust, P.; Hildebrandt, B.; Sreenivasa, G.; Rau, B.; Gellermann, J.; Riess, H.; Felix, R.; Schlag, P. M. Hyperthermia in combined treatment of cancer. *Lancet Oncol.* **2002,** 3, 487-497.

29. Link, S.; El-Sayed, M. A. Shape and size dependence of radiative, non-radiative and photothermal properties of gold nanocrystals. *Int. Rev. Phys. Chem.* **2000,** 19, 409-453.

30. Huang, X.; Jain, P. K.; El-Sayed, I. H.; El-Sayed, M. A. Plasmonic photothermal therapy (PPTT) using gold nanoparticles. *Lasers Med. Sci.* **2008,** 23, 217-228.

31. Dickerson, E. B.; Dreaden, E. C.; Huang, X.; El-Sayed, I. H.; Chu, H.; Pushpanketh, S.; McDonald, J. F.; El-Sayed, M. A. Gold nanorod assisted near-infrared plasmonic photothermal therapy (PPTT) of squamous cell carcinoma in mice. *Cancer Lett.* **2008,** 269, 57-66.

32. Hirsch, L. R.; Stafford, R. J.; Bankson, J. A.; Sershen, S. R.; Rivera, B.; Price, R. E.; Hazle, J. D.; Halas, N. J.; West, J. L. Nanoshell-mediated near-infrared thermal therapy of tumors under magnetic resonance guidance. *Proc. Natl. Acad. Sci. USA.* **2003,** 100, 13549-13554.

33. O'Neal, D. P.; Hirsch, L. R.; Halas, N. J.; Payne, J. D.; West, J. L. Photo-thermal tumor ablation in mice using near infrared-absorbing nanoparticles. *Cancer Lett.* **2004,** 209, 171-176.

34. Stern, J. M.; Stanfield, J.; Kabbani, W.; Hsieh, J. T.; Cadeddu, J. A. Selective prostate cancer thermal ablation with laser activated gold nanoshells. *J. Urol.* **2008,** 179, 748-753.

35. von Maltzahn, G.; Park, J. H.; Agrawal, A.; Bandaru, N. K.; Das, S. K.; Sailor, M. J.; Bhatia, S. N. Computationally guided photothermal tumor therapy using long-circulating gold nanorod antennas. *Cancer Res.* **2009,** 69, 3892-3900.

36. Diagaradjane, P.; Shetty, A.; Wang, J. C.; Elliott, A. M.; Schwartz, J.; Shentu, S.; Park, H. C.; Deorukhkar, A.; Stafford, R. J.; Cho, S. H. Modulation of in vivo tumor radiation response via gold nanoshell-mediated vascular-focused hyperthermia: characterizing an integrated antihypoxic and localized vascular disrupting targeting strategy. *Nano Lett.* **2008,** 8, 1492-1500.

37. Gormley, A. J.; Greish, K.; Ray, A.; Robinson, R.; Gustafson, J. A.; Ghandehari, H. Gold nanorod mediated plasmonic photothermal therapy: A tool to enhance macromolecular delivery. *Int. J. Pharm.* **2011,** 415, 315-318.

38. Park, J. H.; Maltzahn, G. v.; Ong, L. L.; Centrone, A.; Hatton, T. A.; Ruoslahti, E.; Bhatia, S. N.; Sailor, M. J. Cooperative nanoparticles for tumor detection and photothermally triggered drug delivery. *Adv. Mater.* **2010,** 22, 880-885.

39. Park, J. H.; von Maltzahn, G.; Xu, M. J.; Fogal, V.; Kotamraju, V. R.; Ruoslahti, E.; Bhatia, S. N.; Sailor, M. J. Cooperative nanomaterial system to sensitize, target, and treat tumors. *Proc. Natl. Acad. Sci. USA.* **2010,** 107, 981-986.

40. Von Maltzahn, G.; Park, J. H.; Lin, K. Y.; Singh, N.; Schwöppe, C.; Mesters, R.; Berdel, W. E.; Ruoslahti, E.; Sailor, M. J.; Bhatia, S. N. Nanoparticles that communicate in vivo to amplify tumour targeting. *Nat. Mater.* **2011,** 10, 545-552.

41. Nikoobakht, B.; El-Sayed, M. A. Preparation and growth mechanism of gold nanorods (NRs) using seed-mediated growth method. *Chem. Mater.* **2003,** 15, 1957-1962.

42. Larson, N.; Ray, A.; Malugin, A.; Pike, D. B.; Ghandehari, H. HPMA copolymer-aminohexylgeldanamycin conjugates targeting cell surface expressed GRP78 in prostate cancer. *Pharm. Res.* **2010,** 27, 2683-2693.

43. Omelyanenko, V.; Kopecková, P.; Gentry, C.; Kopecek, J. Targetable HPMA copolymer-adriamycin conjugates. Recognition, internalization, and subcellular fate. *J. Control. Release* **1998,** 53, 25-37.

44. Walker, J. M., *The Protein Protocols Handbook*. 2nd ed.; Humana Press Inc: Totowa, New Jersey, 1996.

45. Wang, R. K.; Tuchin, V. V. Enhance light penetration in tissue for high resolution optical imaging techniques by the use of biocompatible chemical agents. *J. X Ray Sci. Tech.* **2002,** 10, 167-176.

46. Arap, M. A.; Lahdenranta, J.; Mintz, P. J.; Hajitou, A.; Sarkis, Á.; Arap, W.; Pasqualini, R. Cell surface expression of the stress response chaperone GRP78 enables tumor targeting by circulating ligands. *Cancer Cell* **2004,** 6, 275-284.

47. Jain, P. K.; Lee, K. S.; El-Sayed, I. H.; El-Sayed, M. A. Calculated absorption and scattering properties of gold nanoparticles of different size, shape, and composition: applications in biological imaging and biomedicine. *J. Phys. Chem. B* **2006,** 110, 7238-7248.

48. Huang, X.; El-Sayed, I. H.; Qian, W.; El-Sayed, M. A. Cancer cell imaging and photothermal therapy in the near-infrared region by using gold nanorods. *J. Am. Chem. Soc.* **2006,** 128, 2115-2120.

49. Niidome, T.; Yamagata, M.; Okamoto, Y.; Akiyama, Y.; Takahashi, H.; Kawano, T.; Katayama, Y.; Niidome, Y. PEG-modified gold nanorods with a stealth character for in vivo applications. *J. Control. Release* **2006,** 114, 343-347.

50. Gormley, A. J.; Malugin, A.; Ray, A.; Robinson, R.; Ghandehari, H. Biological evaluation of RGDfK-gold nanorod conjugates for prostate cancer treatment. *J. Drug Target.* **2011,** 19, 915-924.

51. Gormley, A. J.; Larson, N.; Sadekar, S.; Robinson, R.; Ray, A.; Ghandehari, H. Guided delivery of polymer therapeutics using plasmonic photothermal therapy. *Nano Today* **2012,** 7, 158-167.

52. Dudar, T. E.; Jain, R. K. Differential response of normal and tumor microcirculation to hyperthermia. *Cancer Res.* **1984,** 44, 605-612.

53. Owens 3rd, D.; Peppas, N. Opsonization, biodistribution, and pharmacokinetics of polymeric nanoparticles. *Int. J. Pharm.* **2006,** 307, 93-102.

CHAPTER 6

PLASMONIC PHOTOTHERMAL THERAPY INCREASES THE TUMOR MASS PENETRATION OF HPMA COPOLYMERS

6.1 Introduction

The conjugation of hydrophobic anticancer drugs to water-soluble polymers represents an effective way of solubilizing them in blood plasma, prolonging their blood circulation half-life, targeting their biodistribution to tumors and overcoming multidrug resistance.[1] In this way, drugs can be retained in the blood and specifically delivered to the cancerous tissue with dramatically reduced accumulation in healthy organs. While the advantages of targeted delivery using polymer-drug conjugates are well known, clinical translation has been slow with no approved therapeutics to date. There are many reasons why this is the case, including poor drug release kinetics and carrier biocompatibility. However, the major barrier to obtaining favorable clinical outcome remains limited tumor and cancer cell delivery.[2]

There are many available techniques to improve the delivery of polymer-drug conjugates. The most obvious and widely used method involves tailoring the size of the conjugates so that the therapeutic takes advantage of the increased vascular permeability of tumors to macromolecules. Coined the EPR effect, large intercellular and transcellular

openings between endothelial cells that line the tumor vasculature allow macromolecules up to roughly 1 μm in size to partition from the blood and enter the tumor interstitial space with limited lymphatic drainage.[3-4] Another common approach involves the conjugation of biorecognizable motifs such as peptides or antibodies for cancer cell receptor-mediated targeting.[5] Such active targeting then enables drug carriers to specifically bind to cancer cells which express the targeted receptor and trigger internalization and drug release. Finally, a number of other pharmacologic based methods for improving delivery have been shown including treatment with angiotensin to raise the patient's blood pressure,[6-7] application of nitroglycerin,[8] pretreatment with vascular disrupting[9-10] or anti-angiogenic agents,[11-12] as well as direct injection of extracellular matrix enzymes to reduce the interstitial density.[13] Each of these tools provides greater selectivity of nanocarrier delivery to tumors.

Another technique which is shown to improve the delivery of nanocarriers involves treating the tumors with hyperthermia. Recent findings, for example, have shown that hyperthermia can increase the rate of both endo- and phagocytosis which may then potentiate macromolecular uptake and intracellular delivery.[14-15] At the vascular level, when tumors are heated up to 43°C, tumor blood flow can increase roughly two-fold.[16] This change in blood flow then increases the overall availability of macromolecules to extravasate. The resulting increased vascular pressure and heat-induced cytoskeletal injury then causes endothelial cell damage.[17-19] This causes further expansion of the intercellular openings and therefore increased vascular permeability to macromolecules.[20-21]

The observed changes in tumor vascular dynamics with heating have been leveraged to improve the delivery of various nanomedicines. In particular, tumor hyperthermia has been used to facilitate the delivery of liposomes.[22-26] The application of heat is shown to enhance the extravasation of liposomes in a thermal dose dependent manner for up to six hours after heat treatment.[27] Additionally, this effect was also dependent on nanoparticle size where the larger systems exhibited the greatest increase in overall delivery with heat.[28] Precise control over heating, however, is necessary as vascular collapse and blood flow stasis is probable when temperatures rise above 43°C.

A major challenge with treating tumors with hyperthermia lies in the ability to effectively deliver the appropriate thermal dose in a site specific manner. Evolving technologies such as radiofrequency ablation as well as HIFU have proven useful in this regard,[29] though these methods are not selective towards cancerous tissue and therefore rely on the physician to choose the regions which should receive thermal therapy. As the margins of tumor and normal tissue are often unknown, this adds greater risk of injury to healthy tissue. A recent method of selectively delivering heat to tumors takes advantage of the plasmonic properties of colloidal gold. Of special interest in this regard is the unique capacity of these colloids to scatter and absorb light. Under conditions of SPR, strong light absorption results in particle heating.[30] When located within a tumor mass, direct tissue heating can occur with laser light excitation by PPTT.[31-33] This heating process can be used as a means to selectively induce tumor hyperthermia with therapeutic intentions.[34-36]

Recent studies have shown the utility of PPTT to improve the delivery of other nanomedicines.[37-41] In each of these studies, PPTT was applied to heat tumors between

42-45°C and a resulting increase in conjugate accumulation was observed. In the previous Chapter, the tumor accumulation of heat shock targeted HPMA copolymers was evaluated in combination with PPTT.[38] A peptide which has known affinity for an extracellular heat shock protein was incorporated in the polymer design to specifically target cancer cells treated with hyperthermia. PPTT for 10 minutes at 43°C caused a burst accumulation of the conjugates for up to 4 hours. After 4 hours, while the untargeted conjugates diffused back out of the tumor, the heat shock targeted conjugates were retained for an extended period of time (up to 12 hours) due to cell specific targeting.[38] These results provided evidence for the utility of this approach.

What remains unknown, however, is the tumor tissue distribution of HPMA copolymers after delivery enhancement with PPTT. This information is important because drug delivery is not evenly distributed due to tumor vascular heterogeneity, particularly for nanomedicines which are large in size.[42-43] The objective of the study described in this Chapter was to visualize the distribution of HPMA copolymers in prostate tumors after treatment with PPTT.

6.2 Materials and Methods

6.2.1 Synthesis and characterization of PEGylated GNRs

GNRs were synthesized as described in Chapter 3, Section 3.2.[38] GNR size and shape were characterized by TEM and the light absorption profile was measured by UV spectrometry. Zeta potential was calculated in DI water by measuring its electrophoretic mobility using laser Doppler velocimetry (Zetasizer Nano ZS, Malvern Instruments Ltd, Worcestershire, UK).

6.2.2. Synthesis and characterization of HPMA copolymers

HPMA,[44] aminopropylmethacrylamide-benzyl-1,4,7,10 tetraazacyclododecane-1,4,7,10-tetraacetic acid (APMA-benzyl-DOTA),[45] APMA-FITC,[46] and 3-[(*N*-methacryloylglycyl)glycyl]thiazolidine-2-thione (MA-GG-TT)[47] comonomers were synthesized as described previously. The precursor copolymer conjugates contained the reactive carboxyl groups (thiazolidine-2-thione) so that future studies with the same copolymer could incorporate targeting peptides into their design. In the present study, these groups were hydrolyzed to obtain untargeted conjugates. Copolymerization was performed by reversible addition-fragmentation chain-transfer (RAFT) polymerization using 2-cyano-2-propyl dodecyl trithiocarbonate as the chain transfer agent (CTA) and VA-044 as the initiator in a DMF/MeOH (90:10) co-solvent at 50°C for 24 hours in a sealed ampoule under N_2 gas. Polymerization ratios were [monomers]:[CTA] = 450 and [CTA]:[VA-044] = 1.5. Following polymerization, product was obtained by precipitation into diethyl ether. The unpurified product was then dissolved in DI water with gadolinium (III) acetate hydrate (1.2 mol equivalent) and the pH was raised between 5.0-5.5. This solution was stirred overnight followed by addition of ethylenediaminetetraacetic acid (EDTA) to remove excess Gd (EDTA:GD, 1:1). The product was then filtered, dialyzed and lyophilized to obtain the final product. M_w, M_n, and M_w/M_n were estimated by SEC using HPMA homopolymer fractions of known molecular weight. SEC was done on a Superose 12 column (10 mm x 30 cm) (GE Healthcare, Piscataway, NJ) using a Fast Protein Liquid Chromatography (FPLC) system (GE Healthcare). The Gd content was quantified by ICP-MS against a standard curve. Fluorescently labeled polymers were synthesized as described in Chapter 5.[38]

To calculate the conjugate's longitudinal relaxivity, four different concentrations of copolymer (0.1 to 0.015 mM polymer) were prepared in DI water and placed in a Bruker BioSpec 7.1 T horizontal-bore MRI. T1 was measured by an inversion recovery fast spin-echo imaging sequence using inversion times of 50, 100, 300, 500, 800, 1000, 2000, 4000, 7000 and 8000 ms, echo time (TE) of 4.2 ms, and repetition time (TR) of 12000 ms. T1 for each vial was calculated using Bruker software and the relaxation rate (R1 = 1/T1) was plotted against Gd equivalent concentration. Relaxivity was measured as the slope of this plot.

6.2.3. Prostate tumor model

Animal experiments were performed in accordance with the IACUC of the University of Utah. Four-to-six week old female athymic (nu/nu) mice were anesthetized using 2% isoflurane and bilaterally inoculated with 10^7 DU145 cells in 200 µl PBS on the flank of each animal. Animals were used in the study once the average tumor volume reached 50-100 mm^3 (usually 10-21 days).

6.2.4. MR imaging

Prior to the experiment, those animals which were ultimately treated with PPTT received an intravenous dose of PEGylated GNRs roughly 48 hours before each experiment. This provided enough time for the GNRs to circulate and passively accumulate in the tumor tissue as discussed in chapter 4.[48] The animals in the laser only group did not receive GNRs. Each animal was then anesthetized with 2% isoflurane, placed within a Bruker BioSpec 7.1 T horizontal-bore MRI and an axial T1 flash pre-scan

was taken. Each tumor was then swabbed with 50% propylene glycol to enhance laser penetration depth,[49] and the Gd labeled HPMA copolymers were then intravenously administered (0.03 mmol Gd/kg) in saline. Immediately after injection, the right tumor was radiated for 10 minutes using an 808 nm fiber coupled laser diode (Oclaro Inc., San Jose, CA) with collimating lens (Thorlabs, Newton, NJ). Intratumoral temperature was monitored using a 33 gauge needle thermocouple (Omega, Stamford, CT), and the laser power was directly controlled so that tumor temperature was maintained between 42°C and 43°C when treated with PPTT. Tumors on the left flank served as internal controls.

Immediately following laser treatment, the bed was placed back into the MRI and axial section T1 flash images of both tumors were taken. Two hours after laser treatment, a series of multislice T1 flash images were taken to provide anatomical information. Also, quantitative T1 MR images were obtained using an inversion recovery fast spin-echo pulse imaging sequence (slice thickness = 1 mm, number of slices = 8). This was done using the same acquisition parameters when the conjugate's relaxivity was measured. In one animal, both T1 flash and T1 inversion recovery images were acquired before treatment (pre-scan), and then every 42 minutes for 5 hours after treatment. This was done to obtain time-dependent information on conjugate delivery.

6.2.5. Image analysis

The quantitative T1 relaxation maps were calculated from the inversion recovery data sets using QuickVol II, a plugin for Image J.[50] The images were then prepared in the following way. Using the T1 flash images, regions of interest (ROI) were drawn around both tumors and a mask was created for each slice. The mask was then used to isolate

only the tumor data from the T1 relaxation maps. Due to some noise in the data, pixel outliers were removed using Image J. Each map was then overlayed onto its respective T1 flash image and a montage was created to display the whole tumor volume or the time dependent information as well as a 3D surface plot.

To compare the accumulation of polymers in both tumors, the average relaxation (R1 = 1/T1) was calculated in the skin around the tumor as well as the tumor's center and periphery using Image J. This was done by first drawing ROIs on the T1 flash images (without the T1 map overlay) for both tumors. These ROIs were then used to calculate the average relaxation in each of these regions on the T1 relaxation map. The TER for each of these regions was then calculated by dividing R1 in the right tumor by R1 in the left tumor ($TER_{PPTT} = R1_{PPTT}/R1_{control}$, or $TER_{laser\ only} = R1_{laser\ only}/R1_{control}$). This was done for each mouse, tumor and slice. A normalized histogram of R1 values for whole tumors (center plus periphery) was also obtained using Image J software. This data was then graphically represented using GraphPad Prism.

6.2.6. Histology

After MR imaging, the animals were euthanized by CO_2 inhalation and the tumors were removed and fixed in neutral buffered formalin. Samples were then dehydrated, paraffin-embedded and cut into 4-micron thick sections. Immunohistochemical analysis of Factor VIII expression, an endothelial cell marker, was then performed on some sections using a Factor VIII rabbit polyclonal antibody (Dako, Carpinteria, CA) and a biotinylated rabbit IgG secondary antibody. Positive signal was visualized using a streptavidin-HRP system, utilizing DAB (3,3'-diaminobenzidine) as the chromogen. All

sections were then counterstained with hematoxylin. Washing with iodine, followed by sodium thiosulfate, removed any precipitates. Finally, sections were dehydrated in alcohol, cleared in xylene, coverslipped and imaged.

6.2.7. Fluorescence imaging

Prior to the experiment, animals received an intravenous dose of PEGylated GNRs (48 hrs before) and both tumors were swabbed with 50% propylene glycol (10 minutes before). Each animal (N = 4) was then intravenously administered 7.0 mg of FITC labeled HPMA copolymers and the right tumor was lased in the same way as the MRI experiment. Two hours after treatment with PPTT, each animal was then administered 5 mg of rhodamine labeled Concanavalin A (Vector Laboratories, Burlingame, CA) and euthanized 5 minutes later to visualize the vasculature. Both tumors were then collected, immediately placed in Tissue-Tek® OCT™ compound, frozen and cryo-sectioned into 12 μm thick sections (Leica CM3050, Wetzlar, Germany). Immediately before imaging, slides were dried and a cover slip was mounted using Cytoseal 60 diluted 1:5 in toluene. Large fluorescent imaging mosaics were acquired using a Nikon A1 confocal laser microscope system with a 10x objective.

6.2.8. Statistics

Statistical analyses were performed in GraphPad Prism. Comparisons between two groups (left vs. right tumors), were performed using a two-tailed, Welch-corrected unpaired t-test. P-values less than 0.05 were considered statistically significant. Data reported as mean ± SEM.

6.3 Results

6.3.1. GNR and HPMA copolymer synthesis and characterization

The GNRs were synthesized to be 58.6 x 15.4 ± 5.7 x 0.8 nm in size which corresponds to an aspect ratio of 3.8 and a SPR peak at 800 nm (Figure 6.1 A-B, Table 6.1). After PEGylation, the GNRs had a slightly negative zeta potential of -10 mV. These GNRs were found to be stable in a wide variety of buffers and solvents due to steric protection from aggregation.

The HPMA copolymers were synthesized by RAFT copolymerization to be roughly 65 kDa so that they were slightly above renal threshold to take advantage of the EPR effect (Figure 6.1 C, Table 6.1). In order for the copolymers to be imaged by MRI, they contained APMA-benzyl-DOTA comonomers which chelate Gd. For copolymers used for fluorescent imaging, APMA-FITC was used instead. An additional comonomer with a reactive carboxyl group, MA-GG-TT, was also incorporated so that future studies could incorporate receptor-mediated active targeting using the same copolymer if needed. In the present study, the TT group was hydrolyzed to obtain an untargeted conjugate. The copolymer Gd content was found to be similar to HPMA copolymer conjugates synthesized previously,[45] and the relaxivity of the conjugates was similar to Gd-diethylene-triamine penta-acetic acid (Gd-DTPA),[51] a common contrast agent used in clinical MRI imaging.

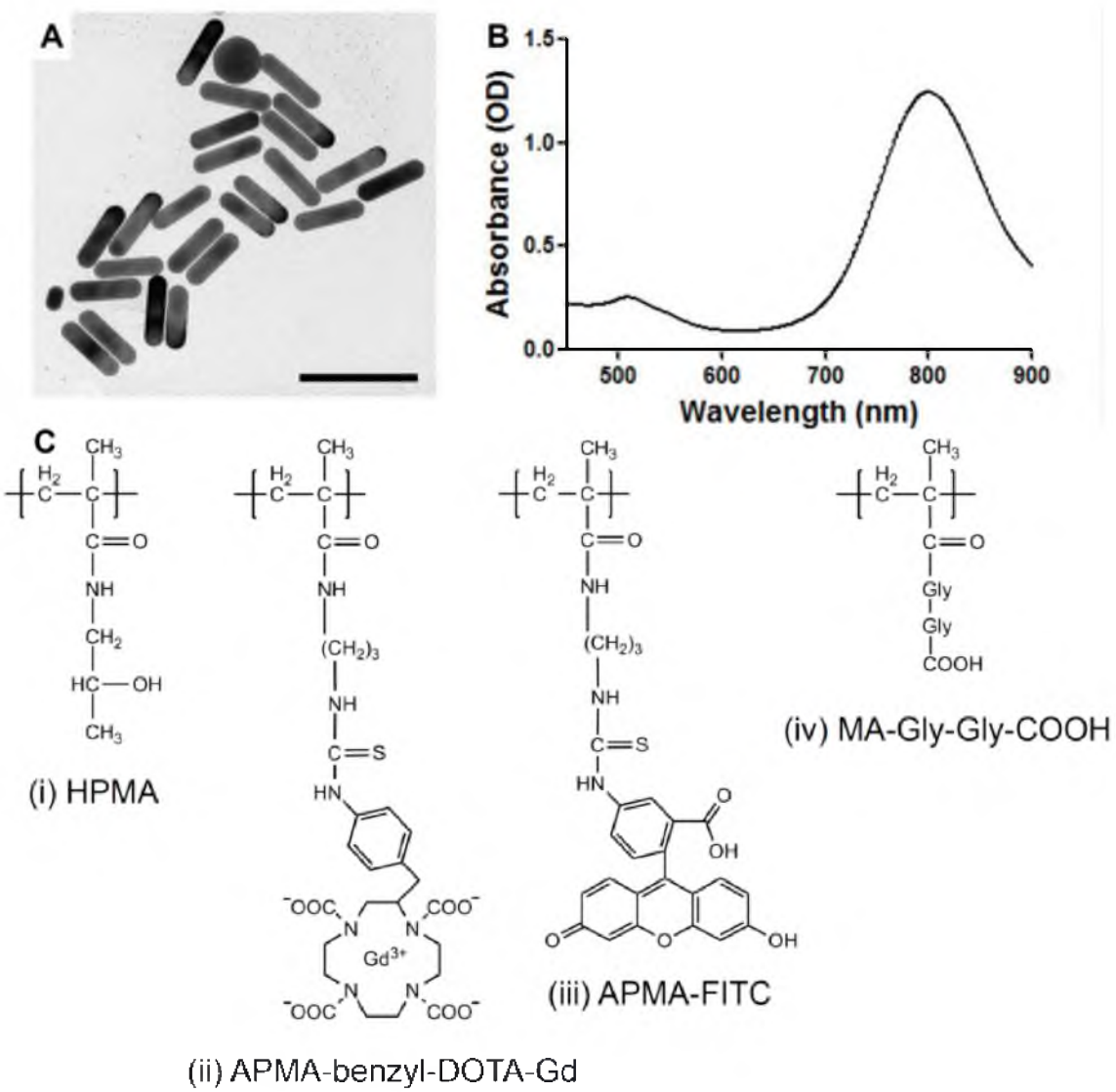

Figure 6.1. GNR characterization and HPMA copolymer schematic. GNRs were synthesized to be 60 x 15 nm in size (A) with an SPR peak at 800 nm (B). Scale bar, 100 nm. Two HPMA copolymers were synthesized for this study (C). The first was copolymerized with HPMA (i), DOTA to chelate Gd to provide MRI contrast (ii), and a hydrolyzed reactive carboxyl group to enable targeting in future studies using the same copolymer (iv). The other was copolymerized with HPMA (i), APMA-FITC for fluorescent imaging (iii), and a hydrolyzed reactive carboxyl group for the same reasons (iv).

Table 6.1. Physicochemical characteristics of GNRs and HPMA copolymers.

	Size (nm)	SPR (nm)	Zeta potential (mV)
GNRs	58.6 x 15.4 ± 5.7 x 0.8	800	-10

	HPMA (mol %)	APMA-benzyl-DOTA-Gd (mol %)	APMA-FITC (mol %)	MA-GG-TT (mol %)	Gd content (mmol Gd/g polymer)	Apparent Mw (kDa)	Mw/Mn	Relaxivity (s^{-1} mM Gd^{-1})
HPMA copolymer-Gd	85	10	0	5	0.37	64.9	1.3	7.1
HPMA copolymer-FITC	93	0	2	5	-	62.4	1.4	-

6.3.2. HPMA copolymer tumor delivery two hrs after treatment by MRI

In this experiment, half the animals were administered PEGylated GNRs (N = 3) and the other half saline (N = 3) 48 hours before MR imaging. On the day of the experiment, each animal was administered HPMA copolymer-Gd conjugates prior to laser radiation of the right tumor for 10 minutes. The tumors in animals which were previously given GNRs exhibited rapid heating which was maintained near 43°C. Animals without GNRs (laser alone) were slightly heated which is consistent with results described in Chapter 3.[37] Two hours after laser treatment, quantitative MR imaging shows significantly enhanced copolymer delivery to tumors treated with PPTT (Figure 6.2). While the left tumor (control) had some polymer accumulation, the right tumor (PPTT) displayed signs of greater copolymer accumulation. As expected, in both tumors the delivery was not evenly distributed likely due to vascular heterogeneity. However, the extent of distribution does appear greater in tumors treated with PPTT. In animals not previously given GNRs, differences between the laser radiated (right) and control (left) tumors were not apparent (Figure 6.2).

When the relaxation rate (R1) was quantified for the skin around the tumors as well as the tumor's center and periphery and expressed as a thermal enhancement ratio (TER, $R1_{PPTT}/R1_{control}$, or $R1_{laser\ only}/R1_{control}$), a clear trend was observed (Figure 6.3 A). Treatment with PPTT resulted in increased copolymer delivery to each of these regions. PPTT caused a 1.36-fold increase in delivery to the skin, though this difference was not statistically significant relative to the laser only group due to large variability in the data and some enhancement to the skin with laser alone (ns, $p = 0.434$). For the tumor's center, PPTT significantly raised the copolymer concentration by 1.42-fold relative to

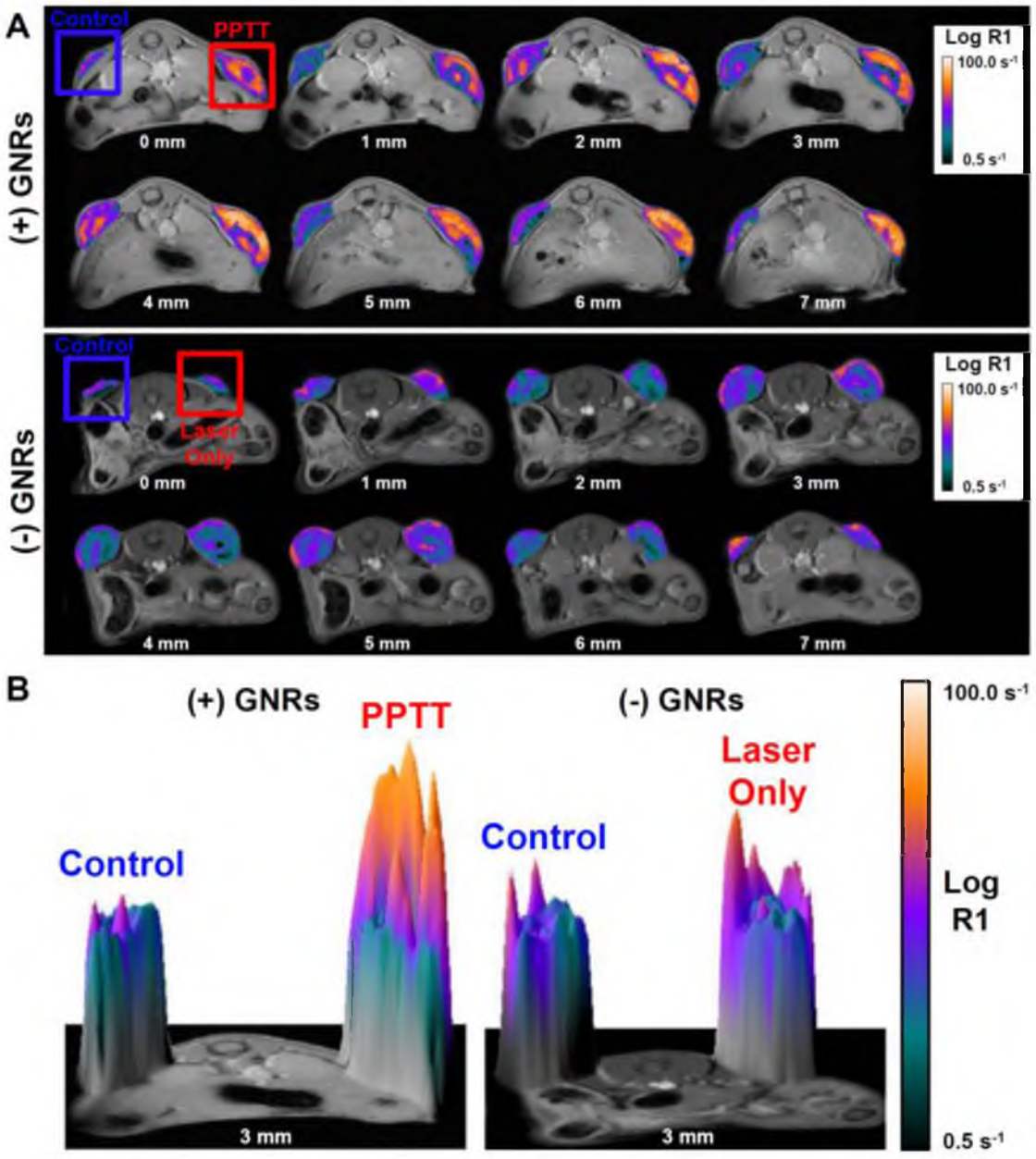

Figure 6.2. HPMA copolymer delivery two hours after treatment. Laser treatment of the right tumor in animals previously administered GNRs (PPTT) facilitated significant enhancement of HPMA copolymer delivery in terms of both accumulation and overall tumor distribution (A, top row). Laser alone did not cause any increased delivery (A, bottom row). A 3D surface plot provides better visualization of this effect at a single slice (B).

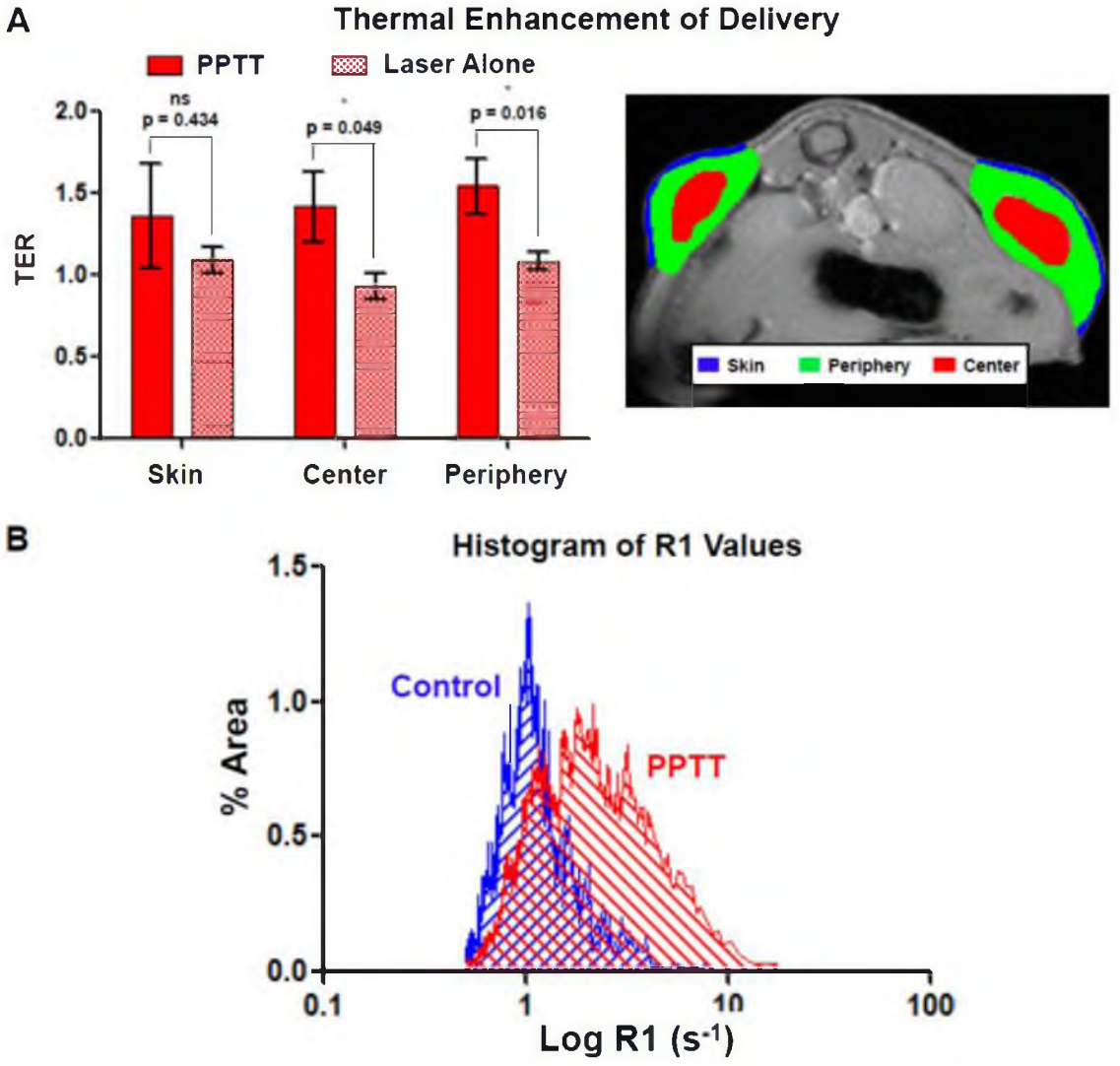

Figure 6.3. Image analysis of HPMA copolymer delivery. Treatment of tumors with PPTT was capable of significantly enhancing the delivery of HPMA copolymers to the tumor's center and periphery (A, left). Treatment with laser alone, absence of GNRs, did not increase delivery. Representative ROIs for this analysis is also shown (A, right). A histogram of R1 values of both control and PPTT treated tumors is shown (B). This data shows the capability of PPTT to increase tumor mass distribution. *Indicates a statistically significant difference ($p < 0.05$) by t-test. Error bars represented as ±standard error of the mean.

those animals treated with laser only (*, $p = 0.049$). The periphery of the tumors, regions of the tumors not including their center, saw the greatest thermal enhancement of 1.54-fold and was the most significant (*, $p = 0.016$). When the right tumors were treated with laser alone, i.e. no GNRs present, the same effect was not observed (Figure 6.3 A). Treatment with laser alone did not cause any appreciable increase in copolymer delivery to the skin, tumor center or periphery.

Plotting a histogram of R1 values for control and PPTT treated tumors provides some additional information (Figure 6.3 B). In control tumors, the majority of its volume comprised of relatively low R1 and therefore polymer concentration values. This distribution was Gaussian ($R^2 = 0.83$) and centered at roughly $R1_{mean} = 1.02\ s^{-1}$ with a narrow standard deviation of $\sigma = 0.28$. For tumors treated with PPTT, the distribution was less Gaussian ($R^2 = 0.67$), centered at $R1_{mean} = 2.31\ s^{-1}$ and exhibited a much broader distribution of $\sigma = 1.03$. This indicates that the majority of the tumor volume received a greater and more variable distribution of copolymer delivery, though overall its entire volume received more copolymers. All regions in the PPTT histogram that do not overlap with the control histogram received some benefit of delivery due to therapy.

6.3.3. HPMA copolymer tumor delivery over time

To better understand the kinetics of delivery, one animal was imaged for 5 hours after treatment with PPTT (Figure 6.4). Similar to findings described in chapter 5,[38] the majority of the dose was delivered to tumors within the first hour of treatment. 2 to 3 hours after treatment, accumulation did not show any appreciable increase with time. In the control tumor, copolymer delivery was observed as expected, though

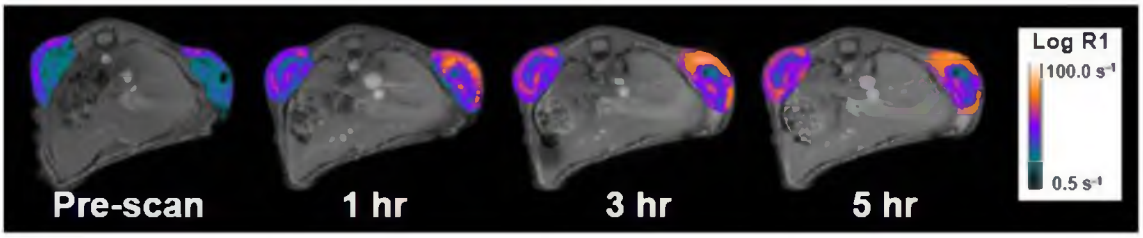

Figure 6.4. HPMA copolymer delivery over time. The majority of delivery occurs within the first hour of PPTT treatment.

the increase in R1 was slight. In the right tumor treated with PPTT, large differences in R1 were observed mostly within the first hour.

6.3.4. Fluorescence imaging of HPMA copolymer delivery

When the tumor delivery two hours after treatment was visualized by fluorescent imaging, a similar trend was observed (Figure 6.5). Treatment with PPTT facilitated more copolymer delivery overall. Delivery enhancement occurred mostly in the outer rim of the tumor, though increased delivery in the tumor's center was also observed. By this method, overall enhancement of delivery was less pronounced than those results obtained by MRI. In both tumors, vascularization density appeared the same. Interestingly, HPMA copolymer delivery did not directly correlate with location of blood vessels.

6.3.5. Histology of tumors after treatment with PPTT

After imaging, the right and left tumors were evaluated for damage by histology (Figure 6.6). In both the control and PPTT treated tumors, many blood and lymphatic vessels were observed throughout and appeared to be intact (Figure 6.6 A-D). There was, however, one major difference between the groups. In all PPTT treated tumors, areas of tissue damage and cell death were observed (Figure 6.6 E-F). These regions of damage were typically less than 20% of the tumor's total volume and were usually confined to the tumor's center. In some cases, intact blood vessels were found in these areas indicating that vessel injury was not necessarily the reason for damage (Figure 6.6F). Also, tumors

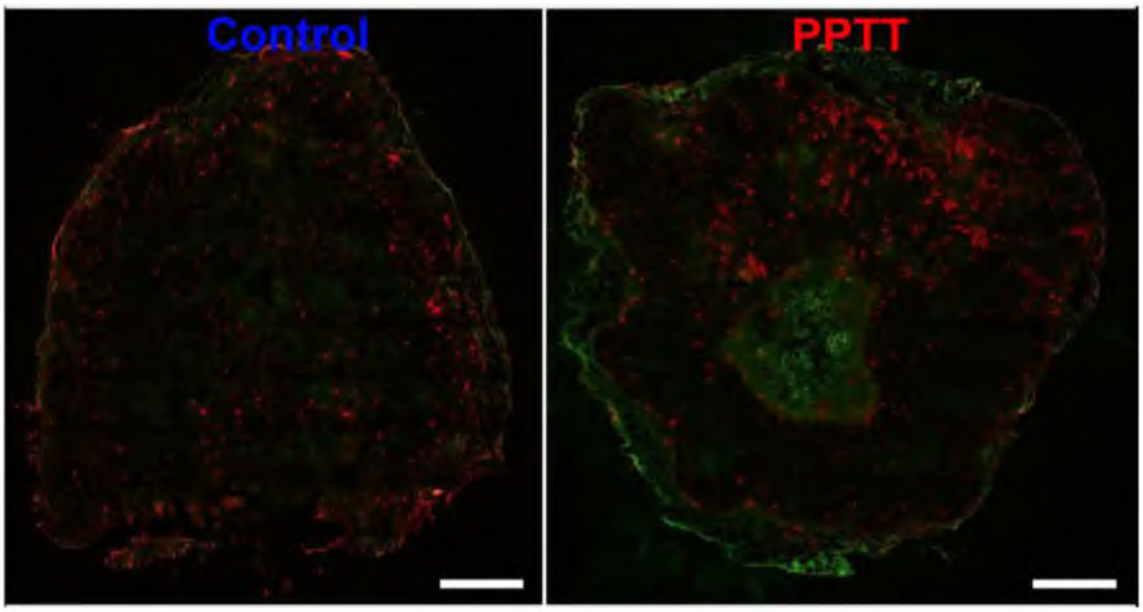

Figure 6.5. Fluorescent imaging of HPMA copolymer delivery. Two hours after treatment with PPTT, HPMA copolymer delivery (green) enhancement in the tumor's periphery and center is observed relative to untreated controls. This effect is most pronounced in the tumor's periphery. Blood vessel (red) density does not appear to be affected by treating with PPTT. Scale bar = 1 mm.

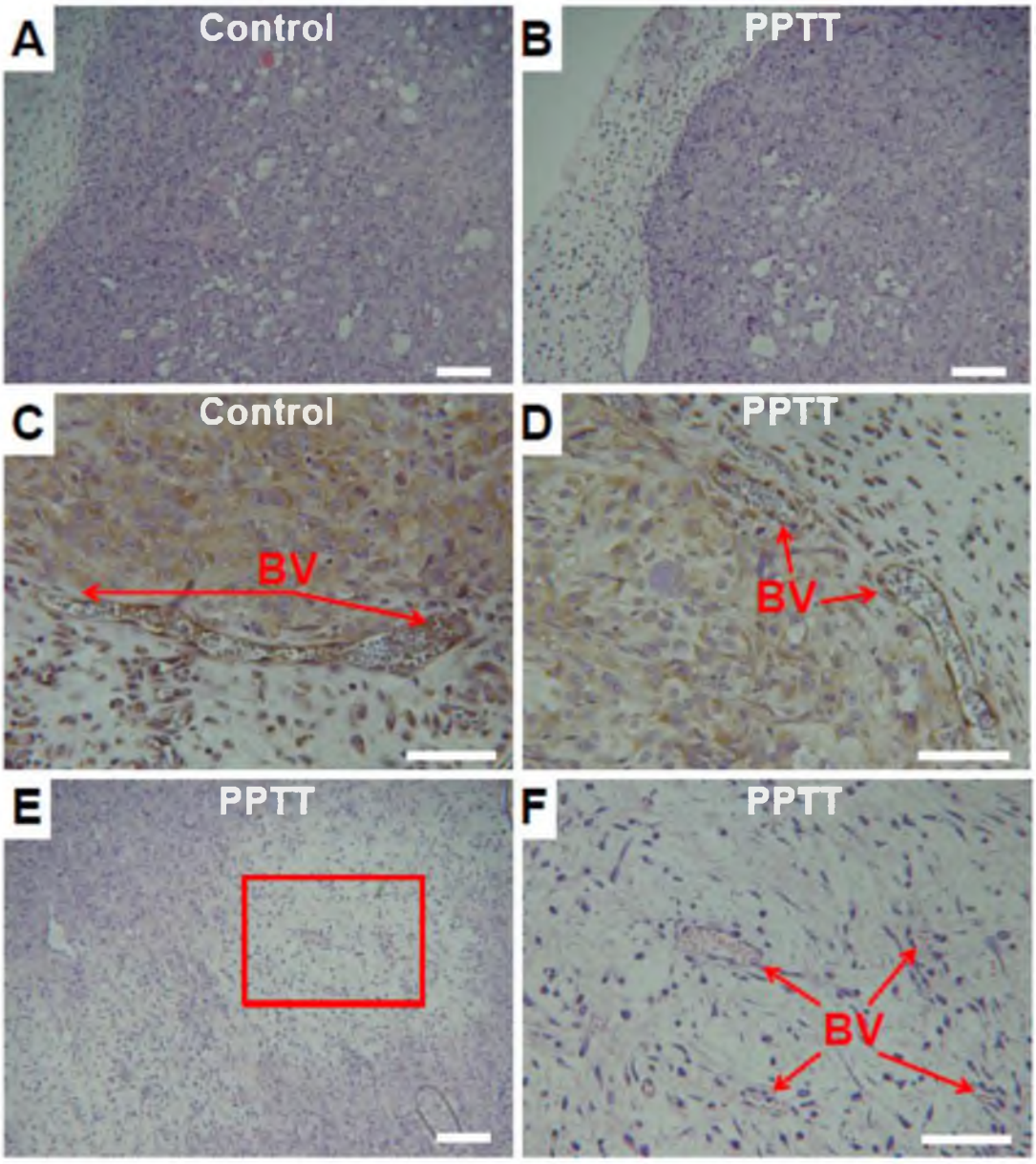

Figure 6.6. Histology of control and PPTT treated tumors. No differences between the tumor periphery of both control and PPTT treated tumors were observed (A-B, 10x objective, scale bar = 100 μm). IHC staining of blood vessels in the periphery did not provide evidence of damage in either group (C-D, 20x objective, scale bar = 50 μm). The center of tumors treated with PPTT had evidence of cell and tissue damage most likely due to excessive heating in this region (E, 10x objective, scale bar = 100 μm). A higher resolution view of this area shows the presence of capillary blood vessels which appear viable despite surrounding damage (F, 20x objective, scale bar = 50 μm).

treated with PPTT did not appear to have as many dividing cells further suggesting that some damage had occurred.

6.4 Discussion

It was shown previously that PPTT can be used to effectively deliver greater numbers of nanocarriers to solid tumors.[37-41] But simply delivering more drug to tumors may not necessary improve overall delivery to cancerous cells. For example, excessive delivery of drug to only perivascular regions and not areas that are distant from viable vasculature may not improve overall treatment outcome. For this reason, delivery strategies which also increase tumor mass penetration are equally important.[42]

There are many tumor tissue abnormalities that resist efficient transport of small and macromolecules to all cells. Most importantly, unregulated angiogenesis causes blood vessels to form with an abnormal and disorganized architecture.[52-53] The spatial distribution of blood vessels lacks order and continuity which ultimately generates a heterogenous distribution of tissue which is poorly perfused.[54] Upon entering the tumor microenivornment, efficient transport through the interstitium is further restricted due to several other abnormalities.[55] High ECM densities in the tumor interstitium prevent large objects such as nanocarriers from diffusing freely.[56] Also, poor lymphatic drainage and related high IFP restricts fluid transport, particularly to the tumor's center where pressure is the highest.[57] Finally, nonspecific binding to ECM or cellular components due to charge-charge or Van der Waals interactions restricts motion.

Using hyperthermia to improve the delivery of polymer-drug conjugates may offer distinct advantages towards maximizing nanocarrier delivery in the context of

interstitial transport. To describe interstitial transport or flux, J_i, one must consider the contributions to convective, J_c, and diffusive, J_d, molecule transport.[55, 58]:

$$J_i = J_d + J_c = -D\frac{\partial C}{\partial x} - CR_F K\frac{\partial p}{\partial x} \qquad \text{Equation 6.1}$$

where D is the diffusion coefficient of the nanocarrier, C and $\partial C/\partial x$ is the concentration and concentration gradient respectively, R_F is the retardation factor, K is the tissue's hydraulic conductivity, and $\partial p/\partial x$ is the pressure gradient in the tissue. During mild hyperthermia ($T \leq 43°C$), it is known that tumor blood flow increases most likely due to increases in blood flow from the host vessels or increased cardiac output.[16] The result is increased microvascular pressure and therefore passive dilation of tumor blood vessels. Also during hyperthermia it has been found that IFP decreases.[59] The result of these two phenomenon is an increase in $\partial p/\partial x$ and therefore interstitial convective transport.

Regarding how such a combination might be beneficial from a diffusive standpoint, one must look at the polymer's diffusion coefficient relative to other nanocarriers and the temperature of the environment. Using the Stokes-Einstein equation, D is calculated using the following relationship:

$$D = \frac{kT}{6\pi nR} \qquad \text{Equation 6.2}$$

where k is Boltzmann's constant, T is the absolute temperature, n is viscosity and R is the carrier's hydrodynamic radius. Here, it is shown that diffusive transport is higher for smaller nanocarriers (lower R) and at elevated temperatures (higher T, lower n). Also, as

shown in Chapter 5,[38] hyperthermia is able to increase the overall amount of copolymer delivery which therefore causes an increase in $\partial C/\partial x$.

The above highlights a) the importance of nanocarrier size on interstitial diffusive transport, and b) the advantages that mild hyperthermia provides for improving both convective and diffusive transport. In this context, using heat to drive the distribution of polymer-drug conjugates which are typically less than 15 nm in hydrodynamic diameter may offer the best opportunity to increase tumor tissue delivery. This may also be true as flexible, linear polymers such as HPMA copolymers have been shown to have greater transport properties than branched or rigid systems.[60-61] Of course, a balance between favorable mass penetration and unfavorable renal clearance for these polymers is a necessary consideration in therapy design.

In this study, PPTT was used to selectively heat prostate tumors between 42-43°C to facilitate the delivery of HPMA copolymers. Using PPTT in this way decreases the chances of heating healthy tissue due to tumor specific delivery of GNRs by EPR and provides a high degree of control over heating. It is also possible that using tissue embedded antennas for energy generation, similar to brachytherapy, provides an advantage in terms of heat distribution. Also, PPTT may have other unknown benefits as it has clearly been shown to improve the delivery of both albumin[37] and HPMA copolymers,[38] whereas previous studies using other methods to induce hyperthermia have not shown greater delivery of each of these.[28, 62]

When PPTT was used to direct the delivery of Gd labeled HPMA copolymers to the right tumor of the animal and imaged by MRI, a clear difference between the tumors was observed (Figure 6.2). The right tumor exhibited greater T1 contrast and therefore

polymer concentration than the left, untreated tumor. In these images, it is observed that these treated tumors did not just receive higher amount of copolymer accumulation. Rather, more of the tumor volume overall received greater delivery suggesting greater tumor mass penetration of these copolymers due to PPTT. This is in stark contrast to tumors treated with laser but not previously administered GNRs, showing that PPTT is in fact responsible and not just laser radiation itself. Though it would be ideal to have an even distribution of high copolymer concentrations throughout the whole tumor volume, the images show that this is not the case. There still exist regions in the tumor that did receive less copolymer. These regions are likely to be the necrotic core of the tumor and are thus difficult to reach.

When these images were analyzed for thermal enhancement of delivery based on region (skin, tumor center and periphery), in each case thermal enhancement was observed (Figure 6.3 A). For the skin, this difference was not statistically significant from laser alone though enhanced delivery to the skin is expected during heating. Both the tumor's center and periphery had a roughly 1.50-fold increase in delivery, where delivery to the center was barely significant and the periphery highly significant. This analysis further suggests that greater mass penetration to the tumor's center was achieved. This interpretation should be taken with a degree of caution however. Using MRI, it is very difficult to delineate the viable from the necrotic regions of the tumor. The ROIs were drawn based on what appeared to be the tumor's center and periphery, but this does not necessarily reflect the true location of the tumor's necrotic core. Vascular heterogeneity often makes the location of the tumor's core highly variable which explains why there is large variation in the data and limited significance in the tumor's center.

A better representation of mass penetration is found is Figure 6.3 B. In this histogram, it is easy to observe that PPTT caused more of the tumor to have higher concentrations of copolymer than the control tumor. For example, let us consider the total percent area of the tumor (area under the curve) less than and greater than R1 = 1.34 s^{-1} for both tumors. In the control (untreated) tumors, 83.3% of its area had R1 values less than 1.34 s^{-1}. In PPTT treated tumors, 46.5% of its area was less than 1.34 s^{-1} and 53.5% of its area had R1 values over this threshold. These data further suggest that higher concentrations of copolymers were able to more readily be transported through the tumor's interstitium when treated with PPTT.

The fact that the majority of delivery occurred within the first hour of laser radiation is not surprising (Figure 6.4). In the study described in the previous Chapter where HPMA copolymer delivery was quantified, roughly 60-70% of the copolymers were delivered within the first 15 minutes after laser radiation.[38] This is likely due to two main reasons. First, clearance of the HPMA copolymers from the blood via the kidneys or RES is likely due to the conjugate's size and negative charge which makes the window of opportunity for delivery within the first few hours. Second, the differential increase in pressure, $\partial p/\partial x$, which drives delivery during hyperthermia occurs over a short period of time (10-15 minutes). For this reason, future work aims to investigate longer periods of laser radiation to further improve delivery.

To corroborate the MRI results, FITC labeled HPMA copolymers were applied using the same experimental design to image distribution by fluorescence imaging. Because the location of copolymer delivery relative to vascularization is important, animals were administered rhodamine labeled lectin prior to euthanasia to stain the

tumor's vasculature. These results provide similar information in that PPTT increased delivery to both the tumor's periphery and center. This observation was however less pronounced than the MRI results which may be due to the relative small z-direction cross-section; 0.012 mm vs. 1.0 mm for fluorescence and MR imaging respectively. It was anticipated that the location of blood vessels would directly correlate with the location of copolymer delivery. While this was indeed the case in the tumor's outer rim where the blood vessels were of the greatest diameter (see Figure 6.6 C-D), the inner capillaries did not permit much delivery. This is likely because of their small and constricted nature due to high cellular density and interstitial pressure in these regions.

Histological evaluation of the tumors provides some insight into the impact of mild PPTT on tumor viability. In both tumors, control and PPTT treated, the tumor's periphery appeared undamaged with a high degree of vascularization (Figure 6.6 A-D). No signs of vascular damage was observed which is a concern when tumors are heated near the 43°C vascular damage threshold.[63] There was a difference though in the tumor's center. In each of the PPTT treated tumors, areas of tissue damage were observed (Figure 6.6 E-F). This is likely to be because of the inability of the tumor's center to dissipate heat effectively during hyperthermic treatment. Residual increases in temperature in these regions then causes direct cell death and tissue damage. What was interesting, however, was the presence of viable blood vessels found in these regions (Figure 6.6 F). These capillary blood vessels appeared to be intact, though further analysis of blood vessel viability in these regions is required to confirm this observation.

Effective transport of nanocarriers through the tumor's interstitium remains a major challenge in nanomedicine. Large nanoparticles such as liposomes, micelles and

inorganic nanoparticles are severely limited by this biological barrier, though strategies such as the one described in this study may help overcome this. An evolving and interesting concept to overcome the problem involves the design of multistage drug delivery platforms.[64] In these nanoparticle systems, large nanoparticles carry drugs to the site of the tumor followed by release of free drug in the interstitium due to external stimuli such as light and heat. In this way, such systems take full advantage of EPR and the high diffusivity of free drugs through the tumor's interstitium.

6.5 Conclusions

This study shows by MR and fluorescence imaging that PPTT is capable of improving the tumor distribution of HPMA copolymers. During laser radiation of the tumor, heating may facilitate both convective and diffusive interstitial transport of these conjugates. PPTT was capable of not only providing greater amounts of copolymer delivery, but also more pervasive distribution throughout the whole tumor mass. This observation is important for more effective drug delivery to cancerous cells. Necrotic and unavailable regions of the tumor were still present even after treatment with PPTT, and future studies improving delivery to these regions remains a significant challenge.

6.6 References

1. Duncan, R. Polymer conjugates as anticancer nanomedicines. *Nat. Rev. Cancer* **2006,** 6, 688-701.

2. Duncan, R.; Gaspar, R. Nanomedicine (s) under the microscope. *Mol. Pharm.* **2011,** 8, 2101-2141.

3. Maeda, H.; Wu, J.; Sawa, T.; Matsumura, Y.; Hori, K. Tumor vascular permeability and the EPR effect in macromolecular therapeutics: a review. *J. Control. Release* **2000,** 65, 271-284.

4. Hashizume, H.; Baluk, P.; Morikawa, S.; McLean, J. W.; Thurston, G.; Roberge, S.; Jain, R. K.; McDonald, D. M. Openings between defective endothelial cells explain tumor vessel leakiness. *Am. J. Pathol.* **2000,** 156, 1363-1380.

5. Peer, D.; Karp, J. M.; Hong, S.; Farokhzad, O. C.; Margalit, R.; Langer, R. Nanocarriers as an emerging platform for cancer therapy. *Nat. Nanotechnol.* **2007,** 2, 751-760.

6. Suzuki, M.; Hori, K.; Abe, I.; Saito, S.; Sato, H. A new approach to cancer chemotherapy: selective enhancement of tumor blood flow with angiotensin II. *J. Natl. Cancer Inst.* **1981,** 67, 663-669.

7. Li, C.; Miyamoto, Y.; Kojima, Y.; Maeda, H. Augmentation of tumour delivery of macromolecular drugs with reduced bone marrow delivery by elevating blood pressure. *Br. J. Cancer* **1993,** 67, 975-980.

8. Seki, T.; Fang, J.; Maeda, H. Enhanced delivery of macromolecular antitumor drugs to tumors by nitroglycerin application. *Cancer Sci.* **2009,** 100, 2426-2430.

9. Aicher, K. P.; Dupon, J. W.; White, D. L.; Aukerman, S. L.; Moseley, M. E.; Juster, R.; Rosenau, W.; Winkelhake, J. L.; Brasch, R. C. Contrast-enhanced magnetic resonance imaging of tumor-bearing mice treated with human recombinant tumor necrosis factor α. *Cancer Res.* **1990,** 50, 7376-7381.

10. Zhao, L.; Ching, L. M.; Kestell, P.; Kelland, L. R.; Baguley, B. C. Mechanisms of tumor vascular shutdown induced by 5, 6-dimethylxanthenone-4-acetic acid (DMXAA): Increased tumor vascular permeability. *Int. J. Cancer* **2005,** 116, 322-326.

11. Jain, R. K. Normalization of tumor vasculature: an emerging concept in antiangiogenic therapy. *Science* **2005,** 307, 58-62.

12. Chauhan, V. P.; Stylianopoulos, T.; Martin, J. D.; Popović, Z.; Chen, O.; Kamoun, W. S.; Bawendi, M. G.; Fukumura, D.; Jain, R. K. Normalization of tumour blood vessels improves the delivery of nanomedicines in a size-dependent manner. *Nat. Nanotechnol.* **2012,** 7, 383-388.

13. Magzoub, M.; Jin, S.; Verkman, A. Enhanced macromolecule diffusion deep in tumors after enzymatic digestion of extracellular matrix collagen and its associated proteoglycan decorin. *FASEB J.* **2008,** 22, 276-284.

14. Vega, V. L.; Charles, W.; De Maio, A. A new feature of the stress response: increase in endocytosis mediated by Hsp70. *Cell Stress Chaperones* **2009,** 15, 517-527.

15. Vega, V. L.; De Maio, A. Increase in phagocytosis after geldanamycin treatment or heat shock: role of heat shock proteins. *J. Immunol.* **2005,** 175, 5280-5287.

16. Song, C. W. Effect of local hyperthermia on blood flow and microenvironment: a review. *Cancer Res.* **1984,** 44, 4721s-4730s.

17. Hildebrandt, B.; Wust, P.; Ahlers, O.; Dieing, A.; Sreenivasa, G.; Kerner, T.; Felix, R.; Riess, H. The cellular and molecular basis of hyperthermia. *Crit. Rev. Oncol. Hematol.* **2002,** 43, 33-56.

18. Fajardo, L.; Schreiber, A.; Kelly, N.; Hahn, G. Thermal sensitivity of endothelial cells. *Radiat. Res.* **1985,** 103, 276-285.

19. Chen, B.; Zhou, M.; Xu, L. Study of vascular endothelial cell morphology during hyperthermia. *J. Therm. Biol.* **2005,** 30, 111-117.

20. Lefor, A. T.; Makohon, S.; Ackerman, N. B. The effects of hyperthermia on vascular permeability in experimental liver metastasis. *J. Surg. Oncol.* **1985,** 28, 297-300.

21. Fujiwara, K.; Watanabe, T. Effects of hyperthermia, radiotherapy and thermoradiotherapy on tumor microvascular permeability. *Pathol. Int.* **2008,** 40, 79-84.

22. Kong, G.; Dewhirst, M. W. Hyperthermia and liposomes. *Int. J. Hyperthermia* **1999,** 15, 345-370.

23. Huang, S. K.; Stauffer, P. R.; Hong, K.; Guo, J. W. H.; Phillips, T. L.; Huang, A.; Papahadjopoulos, D. Liposomes and hyperthermia in mice: increased tumor uptake and therapeutic efficacy of doxorubicin in sterically stabilized liposomes. *Cancer Res.* **1994,** 54, 2186-2191.

24. Weinstein, J.; Magin, R.; Yatvin, M.; Zaharko, D. Liposomes and local hyperthermia: selective delivery of methotrexate to heated tumors. *Science* **1979,** 204, 188-191.

25. Gaber, M. H.; Wu, N. Z.; Hong, K.; Huang, S. K.; Dewhirst, M. W.; Papahadjopoulos, D. Thermosensitive liposomes: extravasation and release of contents in tumor microvascular networks. *Int. J. Radiat. Oncol. Biol. Phys.* **1996,** 36, 1177-1187.

26. Matteucci, M. L.; Anyarambhatla, G.; Rosner, G.; Azuma, C.; Fisher, P. E.; Dewhirst, M. W.; Needham, D.; Thrall, D. E. Hyperthermia increases accumulation of technetium-99m-labeled liposomes in feline sarcomas. *Clin. Cancer Res.* **2000,** 6, 3748-3755.

27. Kong, G.; Braun, R. D.; Dewhirst, M. W. Characterization of the effect of hyperthermia on nanoparticle extravasation from tumor vasculature. *Cancer Res.* **2001,** 61, 3027-3032.

28. Kong, G.; Braun, R. D.; Dewhirst, M. W. Hyperthermia enables tumor-specific nanoparticle delivery: effect of particle size. *Cancer Res.* **2000,** 60, 4440-4445.

29. Ma, G.; Jiang, G. In *Review of tumor hyperthermia technique in biomedical engineering frontier*, 2010 3rd International Conference on Biomedical Engineering and Informatics (BMEI), 2010; IEEE: 2010; pp 1357-1359.

30. Link, S.; El-Sayed, M. A. Shape and size dependence of radiative, non-radiative and photothermal properties of gold nanocrystals. *Int. Rev. Phys. Chem.* **2000,** 19, 409-453.

31. Hirsch, L. R.; Stafford, R. J.; Bankson, J. A.; Sershen, S. R.; Rivera, B.; Price, R. E.; Hazle, J. D.; Halas, N. J.; West, J. L. Nanoshell-mediated near-infrared thermal therapy of tumors under magnetic resonance guidance. *Proc. Natl. Acad. Sci. USA.* **2003,** 100, 13549-13554.

32. O'Neal, D. P.; Hirsch, L. R.; Halas, N. J.; Payne, J. D.; West, J. L. Photo-thermal tumor ablation in mice using near infrared-absorbing nanoparticles. *Cancer Lett.* **2004,** 209, 171-176.

33. Stern, J. M.; Stanfield, J.; Kabbani, W.; Hsieh, J. T.; Cadeddu, J. A. Selective prostate cancer thermal ablation with laser activated gold nanoshells. *J. Urol.* **2008,** 179, 748-753.

34. Huang, X.; Jain, P. K.; El-Sayed, I. H.; El-Sayed, M. A. Gold nanoparticles: interesting optical properties and recent applications in cancer diagnostics and therapy. *Nanomed.* **2007,** 2, 681-693.

35. Jain, P. K.; El-Sayed, I. H.; El-Sayed, M. A. Au nanoparticles target cancer. *Nano Today* **2007,** 2, 18-29.

36. Huang, X.; Jain, P. K.; El-Sayed, I. H.; El-Sayed, M. A. Plasmonic photothermal therapy (PPTT) using gold nanoparticles. *Lasers Med. Sci.* **2008,** 23, 217-228.

37. Gormley, A. J.; Greish, K.; Ray, A.; Robinson, R.; Gustafson, J. A.; Ghandehari, H. Gold nanorod mediated plasmonic photothermal therapy: A tool to enhance macromolecular delivery. *Int. J. Pharm.* **2011,** 415, 315-318.

38. Gormley, A. J.; Larson, N.; Sadekar, S.; Robinson, R.; Ray, A.; Ghandehari, H. Guided delivery of polymer therapeutics using plasmonic photothermal therapy. *Nano Today* **2012,** 7, 158-167.

39. Park, J. H.; von Maltzahn, G.; Xu, M. J.; Fogal, V.; Kotamraju, V. R.; Ruoslahti, E.; Bhatia, S. N.; Sailor, M. J. Cooperative nanomaterial system to sensitize, target, and treat tumors. *Proc. Natl. Acad. Sci. USA.* **2010,** 107, 981-986.

40. Park, J. H.; Maltzahn, G. v.; Ong, L. L.; Centrone, A.; Hatton, T. A.; Ruoslahti, E.; Bhatia, S. N.; Sailor, M. J. Cooperative nanoparticles for tumor detection and photothermally triggered drug delivery. *Adv. Mater.* **2010,** 22, 880-885.

41. Von Maltzahn, G.; Park, J. H.; Lin, K. Y.; Singh, N.; Schwöppe, C.; Mesters, R.; Berdel, W. E.; Ruoslahti, E.; Sailor, M. J.; Bhatia, S. N. Nanoparticles that communicate in vivo to amplify tumour targeting. *Nat. Mater.* **2011,** 10, 545-552.

42. Jain, R. K.; Stylianopoulos, T. Delivering nanomedicine to solid tumors. *Nat. Rev. Clin. Oncol.* **2010,** 7, 653-664.

43. Yuan, F.; Leunig, M.; Huang, S. K.; Berk, D. A.; Papahadjopoulos, D.; Jain, R. K. Mirovascular permeability and interstitial penetration of sterically stabilized (stealth) liposomes in a human tumor xenograft. *Cancer Res.* **1994,** 54, 3352-3356.

44. Strohalm, J.; Kopecek, J. Poly *N*-(2-hydroxypropyl) methacrylamide. 4. Heterogeneous polymerization. *Angew. Makromol. Chem.* **1978,** 70, 109-118.

45. Zarabi, B.; Borgman, M. P.; Zhuo, J.; Gullapalli, R.; Ghandehari, H. Noninvasive monitoring of HPMA copolymer-RGDfK conjugates by magnetic resonance imaging. *Pharm. Res.* **2009,** 26, 1121-1129.

46. Omelyanenko, V.; Kopecková, P.; Gentry, C.; Kopecek, J. Targetable HPMA copolymer-adriamycin conjugates. Recognition, internalization, and subcellular fate. *J. Control. Release* **1998,** 53, 25-37.

47. Šubr, V.; Ulbrich, K. Synthesis and properties of new *N*-(2-hydroxypropyl) methacrylamide copolymers containing thiazolidine-2-thione reactive groups. *React. Funct. Polym.* **2006,** 66, 1525-1538.

48. Gormley, A. J.; Malugin, A.; Ray, A.; Robinson, R.; Ghandehari, H. Biological evaluation of RGDfK-gold nanorod conjugates for prostate cancer treatment. *J. Drug Target.* **2011,** 19, 915-924.

49. Wang, R. K.; Tuchin, V. V. Enhance light penetration in tissue for high resolution optical imaging techniques by the use of biocompatible chemical agents. *J. X Ray Sci. Tech.* **2002,** 10, 167-176.

50. Schmidt, K. F.; Ziu, M.; Ole Schmidt, N.; Vaghasia, P.; Cargioli, T. G.; Doshi, S.; Albert, M. S.; Black, P. M. L.; Carroll, R. S.; Sun, Y. Volume reconstruction techniques improve the correlation between histological and in vivo tumor volume measurements in mouse models of human gliomas. *J. Neurooncol.* **2004,** 68, 207-215.

51. Haar, P. J.; Broaddus, W. C.; Chen, Z.; Fatouros, P. P.; Gillies, G. T.; Corwin, F. D. Gd-DTPA T1 relaxivity in brain tissue obtained by convection-enhanced delivery, magnetic resonance imaging and emission spectroscopy. *Phys. Med. Biol.* **2010,** 55, 3451-3465.

52. Konerdingi, M.; Fait, E.; Gaumann, A.; Dimitropouloui, C.; Malkusch, W., Scanning electron microscopy of corrosion casts in the study of tumor. In *Angiogenesis: models, modulators, and clinical applications*, Maragoudakis, M. E., Ed. Plenum Press: New York, USA, 1998; Vol. 298, pp 429-447.

53. Folkman, J. Angiogenesis in cancer, vascular, rheumatoid and other disease. *Nat. Med.* **1995,** 1, 27-30.

54. Baish, J. W.; Jain, R. K. Fractals and cancer. *Cancer Res.* **2000,** 60, 3683-3688.

55. Jain, R. K. Transport of molecules in the tumor interstitium: a review. *Cancer Res.* **1987,** 47, 3039-3051.

56. Ramanujan, S.; Pluen, A.; McKee, T. D.; Brown, E. B.; Boucher, Y.; Jain, R. K. Diffusion and convection in collagen gels: implications for transport in the tumor interstitium. *Biophys. J.* **2002,** 83, 1650-1660.

57. Baxter, L. T.; Jain, R. K. Transport of fluid and macromolecules in tumors. I. Role of interstitial pressure and convection. *Microvasc. Res.* **1989,** 37, 77-104.

58. Swabb, E. A.; Wei, J.; Gullino, P. M. Diffusion and convection in normal and neoplastic tissues. *Cancer Res.* **1974,** 34, 2814-2822.

59. Leunig, M.; Goetz, A. E.; Dellian, M.; Zetterer, G.; Gamarra, F.; Jain, R. K.; Messmer, K. Interstitial fluid pressure in solid tumors following hyperthermia: possible correlation with therapeutic response. *Cancer Res.* **1992,** 52, 487-490.

60. Deen, W.; Bohrer, M.; Epstein, N. Effects of molecular size and configuration on diffusion in microporous membranes. *AIChE J.* **1981,** 27, 952-959.

61. Sadekar, S.; Ray, A.; Janat-Amsbury, M.; Peterson, C.; Ghandehari, H. Comparative biodistribution of PAMAM dendrimers and HPMA copolymers in ovarian-tumor-bearing mice. *Biomacromolecules* **2011,** 12, 88-96.

62. Lammers, T.; Peschke, P.; Kühnlein, R.; Subr, V.; Ulbrich, K.; Debus, J.; Huber, P.; Hennink, W.; Storm, G. Effect of radiotherapy and hyperthermia on the tumor accumulation of HPMA copolymer-based drug delivery systems. *J. Control. Release* **2007,** 117, 333-341.

63. Song, C. W.; Kang, M. S.; Rhee, J. G.; Levitt, S. H. Effect of hyperthermia on vascular function in normal and neoplastic tissues. *Ann. NY Acad. Sci.* **1980,** 335, 35-47.

64. Wong, C.; Stylianopoulos, T.; Cui, J.; Martin, J.; Chauhan, V. P.; Jiang, W.; Popović, Z.; Jain, R. K.; Bawendi, M. G.; Fukumura, D. Multistage nanoparticle delivery system for deep penetration into tumor tissue. *Proc. Natl. Acad. Sci. USA*. **2011,** 108, 2426-2431.

CHAPTER 7

CONCLUSIONS AND FUTURE DIRECTIONS

7.1: Conclusions

The work presented in this dissertation aimed to address a major barrier in drug delivery, i.e.; localized, tumor selective and efficient delivery to cancerous cells. The inability to direct drug delivery to locally advanced prostate tumors prevents its use in the clinic and thus limits therapy to hormone and radiotherapy. While these two treatment strategies have a high degree of success, the synergistic combination of targeted drug delivery, heat and radiotherapy may further improve outcome. In this dissertation, PPTT was used as a tool to guide HPMA copolymer localization to prostate tumors. This concept was demonstrated over four chapters. In Chapter 3, the concept of using PPTT to improve the delivery of macromolecules such as albumin was validated.[1] Chapter 4 sought to determine if targeting GNRs directly to the tumor's vasculature would improve PPTT performance.[2] In Chapter 5, PPTT was used to direct the localization of heat shock targeted HPMA copolymers to the site of interest.[3] Finally, in Chapter 6 it was found that PPTT was also capable of enhancing the tumor mass distribution of these conjugates.[4]

The initial hypothesis of this work was that PPTT would be a useful tool to improve the delivery of polymer therapeutics. However, previous reports in the literature have shown that hyperthermia itself is not capable of improving the delivery of

nanocarriers in this size range.[5-6] Therefore, a necessary first step in this work was to validate the overall hypothesis using a well established model of macromolecular delivery. In Chapter 3, a mouse sarcoma tumor model (S180) with well characterized EPR was treated with PPTT immediately following administration of EBD to trace albumin delivery.[1] This animal model was used in this study because of its low cost, availability in the lab, ease of tumor production and known permeability to albumin. Intratumoral temperatures were monitored during treatment to correlate delivery with temperature. Indeed, 10 minutes of laser treatment caused significant heating of the tumors. This increased the delivery of albumin by 1.7-fold over the temperatures tested. Results of this study validated the overall hypothesis that PPTT was capable of improving the delivery of macromolecules in the size range which is typical of most polymer therapeutics.

As PPTT is used in this dissertation to regulate blood flow and vascular permeability, it was hypothesized in Chapter 4 that targeting GNRs directly to the tumor's vasculature would provide some benefit. This hypothesis was tested by conjugating the RGDfK peptide to the PEG brush and evaluating its targeting capacity both *in vitro* and *in vivo*.[2] When incubated with both prostate cancer and endothelial cells, RGDfK conjugated GNRs were found to bind and be uptaken to a very high extent relative to the untargeted GNRs. This was particularly the case for endothelial cells which have higher expression of the targeted receptors. When both GNR conjugates were administered to prostate tumor bearing mice, the untargeted GNRs were found to accumulate in prostate tumors to a much higher extent. The reason for this discrepancy between the *in vitro* and *in vivo* results is likely due to fast blood clearance of the

RGDfK-GNRs. This rapid blood clearance then reduced the opportunity of the GNRs to target blood vessels to a higher extent. Because of this, it was determined that vascular targeting GNRs, at least the ones that were tested, were not likely to provide significant benefit and therefore untargeted GNRs were chosen for subsequent studies.

In Chapter 5, PPTT was used to direct the delivery of HPMA copolymers to prostate tumors.[3] HPMA copolymers were synthesized to contain a number of functional monomers including drug, imaging agents, as well as a targeting peptide. The targeting peptide used in this study, WIFPWIQL, was chosen because of its capacity to binding to surface expressed HSPs. Therefore, directed delivery in this way allows these copolymers to specifically target cells which have previously been treated with hyperthermia. To test this overall study concept, first the heat shock targeting approach was validated. Treatment of cells with hyperthermia was found to increase the uptake of heat shock targeted HPMA copolymers. To test the system *in vivo*, prostate tumors were developed in mice and the tumors were heated with PPTT immediately following administration of either untargeted or heat shock targeted HPMA copolymers. PPTT resulted in a burst accumulation of both conjugates up to four hours. After four hours, while the untargeted conjugates diffused back out of the tumor, the heat shock targeted copolymers were retained for an extended period of time due to heat shock targeting. This study therefore provides evidence that PPTT is capable of directing the delivery of HPMA copolymers. This is particularly the case when these conjugates are targeted to heat shock proteins as greater tumor retention and cell uptake is possible.

While Chapter 5 showed that PPTT can be used to direct HPMA copolymer delivery to prostate tumors, effective delivery is not possible unless the delivery strategy

facilitates greater tumor mass penetration. This is because vascular heterogeneity produces large regions of unperfused tissue which are not typically accessible by nanocarriers. Therefore, it was hypothesized in Chapter 6 that PPTT was also capable of enhancing tumor mass penetration.[4] This hypothesis was tested by imaging tumor delivery after treatment with PPTT by MR and fluorescence imaging. HPMA copolymers were synthesized to contain either Gd or FITC and injected in prostate tumor bearing mice immediately before PPTT treatment. Subsequent imaging of copolymer accumulation in the treated and untreated tumors provided evidence that treatment with PPTT is capable of increasing both the accumulation and penetration of HPMA copolymers. A histogram of pixel intensities showed that a higher percentage of pixels in the PPTT treated tumors has higher concentrations of HPMA copolymers. This study therefore confirms that PPTT is also a useful tool to improve HPMA copolymer interstitial transport.

In conclusion, as new tools to selectively and controllably heat tumors enter into the clinical setting, such as PPTT, it may be possible to further unlock the full potential of hyperthermia in adjuvant therapy of cancer. In this dissertation, it was shown that PPTT is useful to improve the delivery of polymer-drug conjugates. In the future, PPTT may be used to treat a wide variety of other diseases that are also heat sensitive.

7.2: Future Directions

The work described in this dissertation is a new project in the lab and there are many questions, ideas and studies that remain. Also, as the ultimate goal is to develop this approach for use in the clinic, a significant amount of preclinical and clinical

development is required. Below are a few of the potential studies that may be done in the future.

The scope of the work described in this dissertation did not include testing the efficacy of this approach when the conjugates had drugs attached. Therefore, the next phase of this project will focus on testing efficacy. The choice in drug for this study may or may not be important in the context of achieving synergism with hyperthermia. As described in Section 2.2.2.6, the activity of some drugs such as cisplatin is potentiated with heat. Though the mechanism of thermal enhancement may not translate when bound to polymers. Therefore, before the initiation of a well-designed efficacy study, thermal enhancement activity of polymers with different drugs and heat shock targeting receptors should be tested to achieve the best study outcome.

In the bulk of this work, PPTT was applied by heating tumors between 42-43°C for 10 minutes to enhance delivery. While this thermal dose was chosen based on information available in the literature, it is well known that tumor blood flow and vascular permeability is highly dependent on this experimental parameter. Therefore, an obvious future study would be to evaluate the enhancement of HPMA copolymer delivery as a function of thermal dose. Varying the temperature in the tumor from 37°C to 43°C, including thermal ablation temperatures above this established limit, as well as varying the time of laser radiation could potentially identify the ideal thermal dose to maximize conjugate delivery. Additionally, this effect should be characterized as a function of conjugate size and type (i.e. PPTT with linear polymers, liposomes, micelles or inorganic nanoparticles). In this research, HPMA copolymers which were large in size (60-80 kDa) were used because this size range is slightly above the threshold for renal

clearance. Because of this, they were able to circulate for an extended period of time. However, the nondegradable nature of these conjugates is of concern. Therefore, it will be interesting to see if smaller sized conjugates (20-45 kDa) which are capable of being cleared via the kidneys will experience similar delivery enhancement.

Another very interesting concept is to apply this approach to enhance the delivery of polymers carrying therapeutic radionuclides. For several decades, companies and academic labs have been using antibodies to deliver radionuclides as an alternative to external beam radiotherapy or brachytherapy. Previously, HPMA copolymers have also been used to deliver yittrium-90 to prostate tumors.[7] Therefore, PPTT may be used to enhance the delivery of these targeted radiotherapies. There is potential that this concept may be more effective than PPTT plus chemotherapy as hyperthermia is known to better potentiate radiotherapy. Extending this concept further, it may be even more interesting to conjugate both a chemotherapeutic agent such as docetaxel and a therapeutic radionuclide such as yittrium-90 to the same copolymer backbone. Then, treatment of prostate tumors with PPTT to enhance the delivery of both chemotherapy and radiotherapy would provide a highly combined approach towards treatment; hyperthermia plus chemotherapy plus radiotherapy.

Gold nanocages, also have a tunable SPR in the NIR spectra and are hollow such that drugs can be loaded within its core.[8] These nanocages can be surface coated with pNIPAAm so that during nanoparticle heating, the polymer brush collapses for triggered drug release. This technique is interesting and may be useful in regards to the approach described in this dissertation. Simultaneous release of heat and drugs which act on the tumor's vasculature such as vascular disrupting agents could synergistically improve

polymer therapeutic delivery. For example, DMXAA is a low molecular weight drug which acts to disrupt cell-cell junctions between endothelial cells and therefore increases vascular permeability.[9] It is also known to work synergistically with hyperthermia and stimulate the production of TNF-α and nitric oxide, two potent agents which increase vasopermeability.[10] Therefore, combined treatment with heat and DMXAA using PPTT could significantly increase the delivery of other therapeutics.

Finally, efforts to begin translation of this approach may begin once enough data is acquired to confirm its usefulness in the clinic. Of particular importance in this regard is assessing the safety of both GNRs and the HPMA copolymer conjugates. Several clinical trials testing similar components are either pending or completed.[11-14] Full and satisfactory evaluation of safety will not be easy, however, as both are nondegradable. This is particularly the case for AuNPs which are not easily excreted. Because of this, many preclinical studies testing the toxic effects of these conjugates is required.

7.3: References

1. Gormley, A. J.; Greish, K.; Ray, A.; Robinson, R.; Gustafson, J. A.; Ghandehari, H. Gold nanorod mediated plasmonic photothermal therapy: A tool to enhance macromolecular delivery. *Int. J. Pharm.* **2011,** 415, 315-318.

2. Gormley, A. J.; Malugin, A.; Ray, A.; Robinson, R.; Ghandehari, H. Biological evaluation of RGDfK-gold nanorod conjugates for prostate cancer treatment. *J. Drug Target.* **2011,** 19, 915-924.

3. Gormley, A. J.; Larson, N.; Sadekar, S.; Robinson, R.; Ray, A.; Ghandehari, H. Guided delivery of polymer therapeutics using plasmonic photothermal therapy. *Nano Today* **2012,** 7, 158-167.

4. Gormley, A. J.; Larson, N.; Banisadr, A.; Robinson, R.; Frazier, N.; Ray, A.; Ghandehari, H. Plasmonic photothermal therapy increases the tumor mass penetration of HPMA copolymers. *J. Control. Release* **Submitted**.

5. Lammers, T.; Peschke, P.; Kühnlein, R.; Subr, V.; Ulbrich, K.; Debus, J.; Huber, P.; Hennink, W.; Storm, G. Effect of radiotherapy and hyperthermia on the tumor accumulation of HPMA copolymer-based drug delivery systems. *J. Control. Release* **2007,** 117, 333-341.

6. Kong, G.; Braun, R. D.; Dewhirst, M. W. Hyperthermia enables tumor-specific nanoparticle delivery: effect of particle size. *Cancer Res.* **2000,** 60, 4440-4445.

7. Mitra, A.; Nan, A.; Papadimitriou, J. C.; Ghandehari, H.; Line, B. R. Polymer-peptide conjugates for angiogenesis targeted tumor radiotherapy. *Nucl. Med. Biol.* **2006,** 33, 43-52.

8. Yavuz, M. S.; Cheng, Y.; Chen, J.; Cobley, C. M.; Zhang, Q.; Rycenga, M.; Xie, J.; Kim, C.; Song, K. H.; Schwartz, A. G.; Wang, L. V.; Xia, Y. Gold nanocages covered by smart polymers for controlled release with near-infrared light. *Nat. Mater.* **2009,** 8, 935-939.

9. Zhao, L.; Ching, L. M.; Kestell, P.; Kelland, L. R.; Baguley, B. C. Mechanisms of tumor vascular shutdown induced by 5, 6-dimethylxanthenone-4-acetic acid (DMXAA): Increased tumor vascular permeability. *Int. J. Cancer* **2005,** 116, 322-326.

10. Murata, J. O., MR Horsman, R. Potentiation of the anti-tumour effect of hyperthermia by combining with the vascular targeting agent 5, 6-dimethylxanthenone-4-acetic acid. *Int. J. Hyperthermia* **2001,** 17, 508-519.

11. Vasey, P. A.; Kaye, S. B.; Morrison, R.; Twelves, C.; Wilson, P.; Duncan, R.; Thomson, A. H.; Murray, L. S.; Hilditch, T. E.; Murray, T. Phase I clinical and pharmacokinetic study of PK1 [*N*-(2-hydroxypropyl) methacrylamide copolymer doxorubicin]: first member of a new class of chemotherapeutic agents—drug-polymer conjugates. *Clin. Cancer Res.* **1999,** 5, 83-94.

12. Seymour, L. W.; Ferry, D. R.; Kerr, D. J.; Rea, D.; Whitlock, M.; Poyner, R.; Boivin, C.; Hesslewood, S.; Twelves, C.; Blackie, R. Phase II studies of polymer-doxorubicin (PK1, FCE28068) in the treatment of breast, lung and colorectal cancer. *Int. J. Oncol.* **2009,** 34, 1629-1636.

13. Paciotti, G. F.; Myer, L.; Weinreich, D.; Goia, D.; Pavel, N.; McLaughlin, R. E.; Tamarkin, L. Colloidal gold: a novel nanoparticle vector for tumor directed drug delivery. *Drug Deliv.* **2004,** 11, 169-183.

14. Schwartz, J. A.; Shetty, A. M.; Price, R. E.; Stafford, R. J.; Wang, J. C.; Uthamanthil, R. K.; Pham, K.; McNichols, R. J.; Coleman, C. L.; Payne, J. D. Feasibility study of particle-assisted laser ablation of brain tumors in orthotopic canine model. *Cancer Res.* **2009,** 69, 1659-1667.

APPENDIX A

CHARACTERIZATION DATA OF HPMA COPOLYMERS

Mn (g / mol)	43276.62893
Mw (g / mol)	62419.87081
PDI (Mw / Mn)	1.442345958

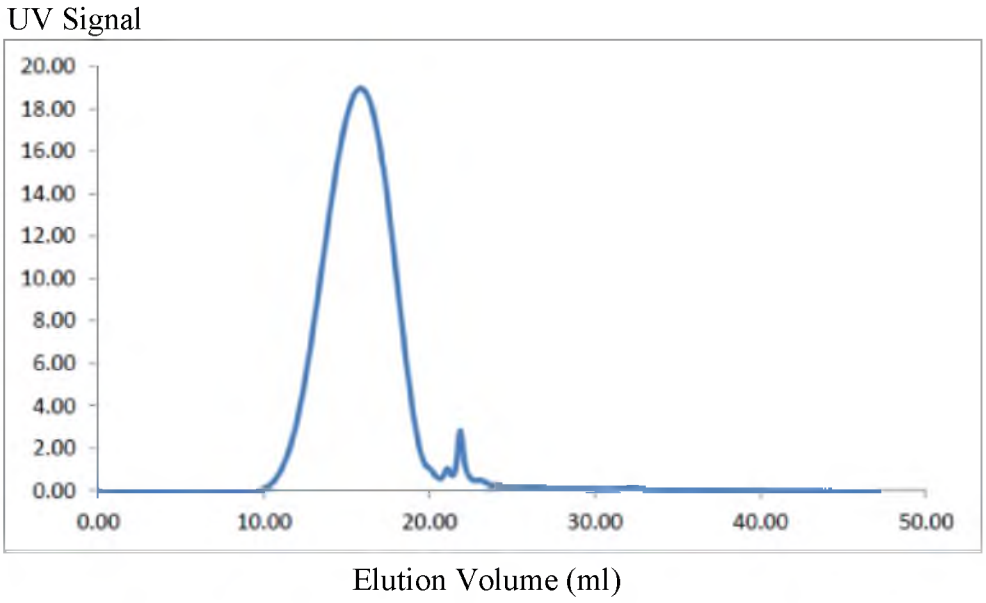

Figure A.1. SEC of HPMA-FITC precursor copolymer.

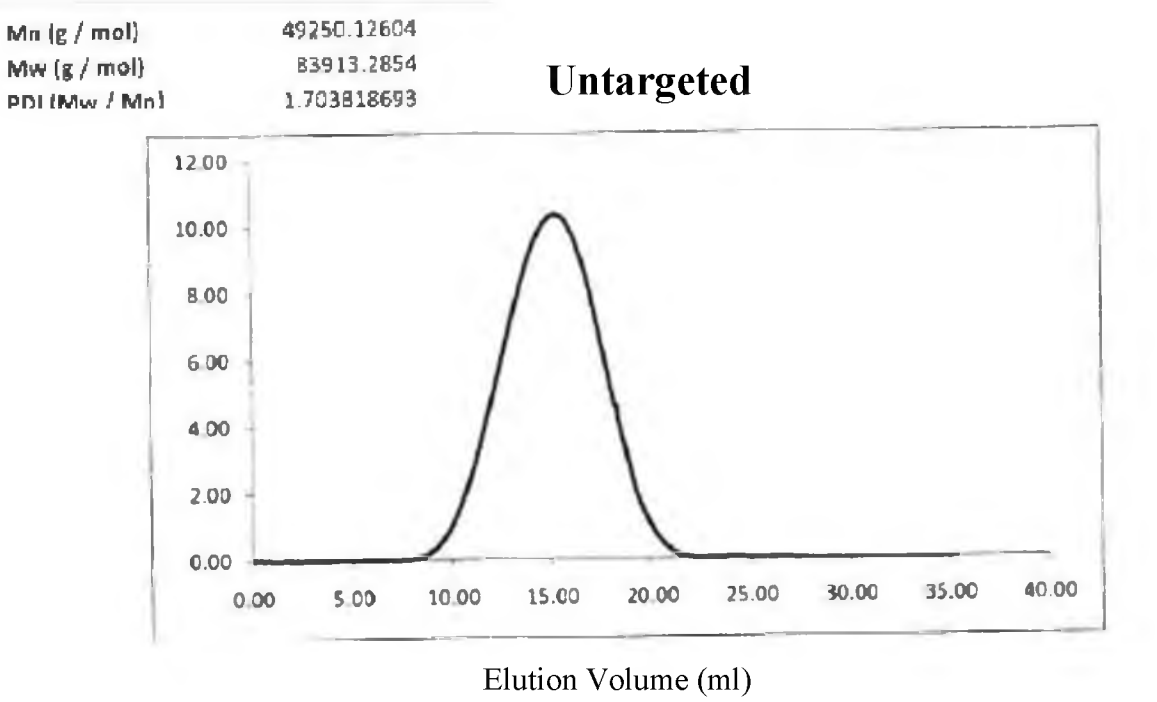

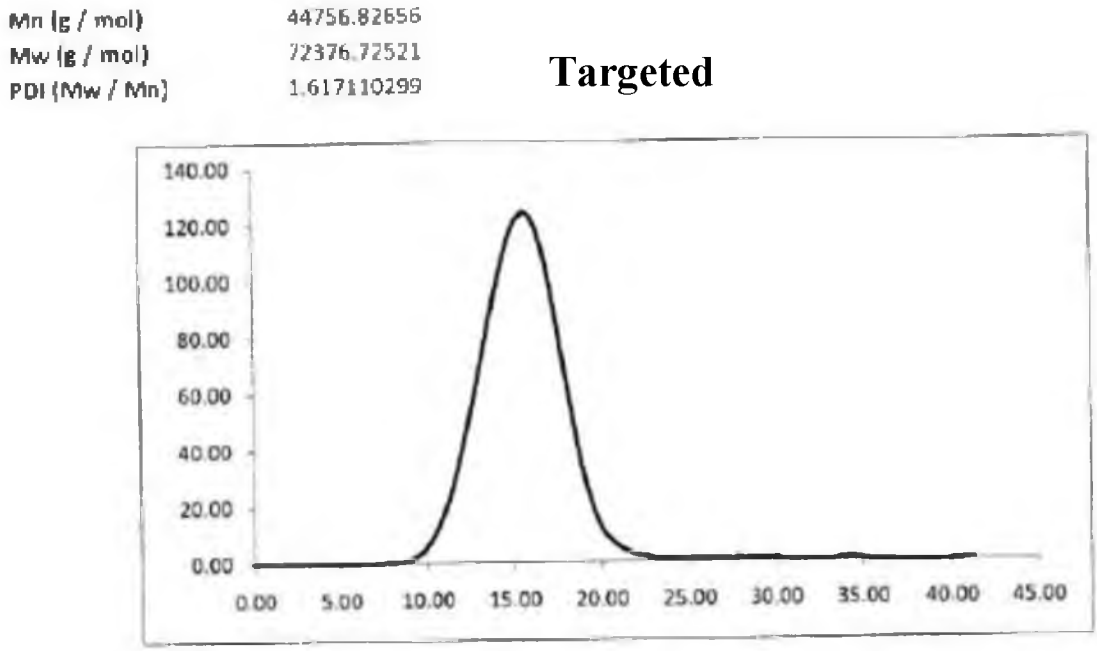

Figure A.2. SEC of HPMA-Tyr-$CONH_2$ copolymers.

L-8800 Amino Acid Analyzer Report

Sample ID: 1325-hama grp78
Analyzed: 5/13/2011 10:57:01 PM
Method: C:\EZChrom Elite\Enterprise\Projects\Default\Method\help2.met
Inj. Volume(uL): 100
Multiplier: 4

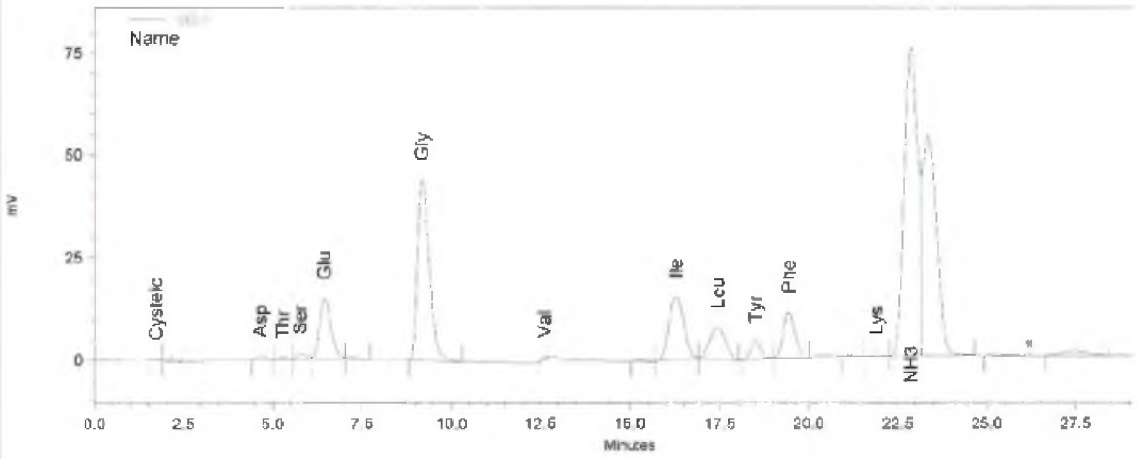

VIS 1 Results

Pk #	Retention Time	Name	Area	Total nmol per sample
1	1.723	Cysteic	17901	3.833
3	4.660	Asp	66952	0.151
4	5.280	Thr	40280	0.086
5	5.763	Ser	121751	0.244
6	6.450	Glu	1342258	2.950
8	9.180	Gly	4035578	9.368
		Ala		0.000 BDL
		Cys		0.000 BDL
9	12.613	Val	24636	0.080
		Met		0.000 BDL
11	16.273	Ile	1797306	4.427
12	17.450	Leu	971406	2.488
13	18.500	Tyr	348264	0.821
14	19.443	Phe	986770	2.152
16	21.900	Lys	45954	0.088
17	22.873	NH3	7984840	15.880
		His		0.000 BDL
		Arg		0.000 BDL

Figure A.3. Amino acid analysis report of heat shock targeted HPMA copolymers.

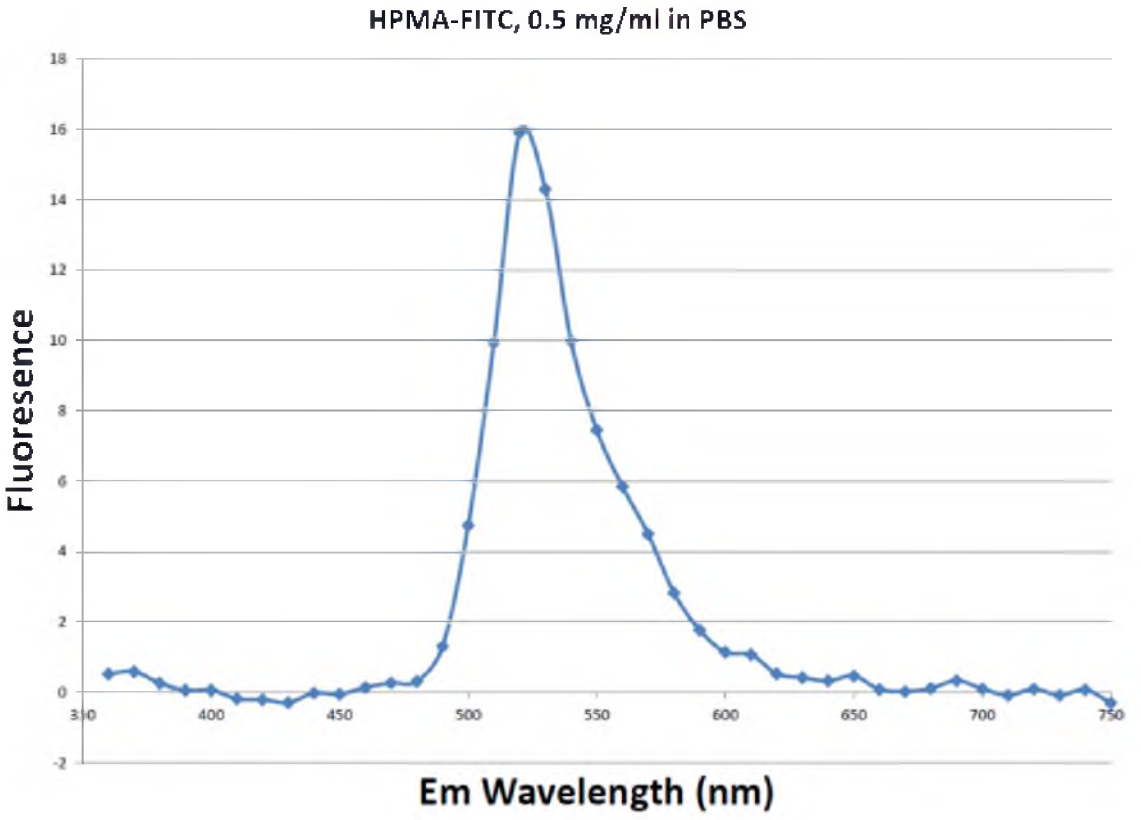

Figure A.4. Fluorescence of HPMA-FITC copolymers.

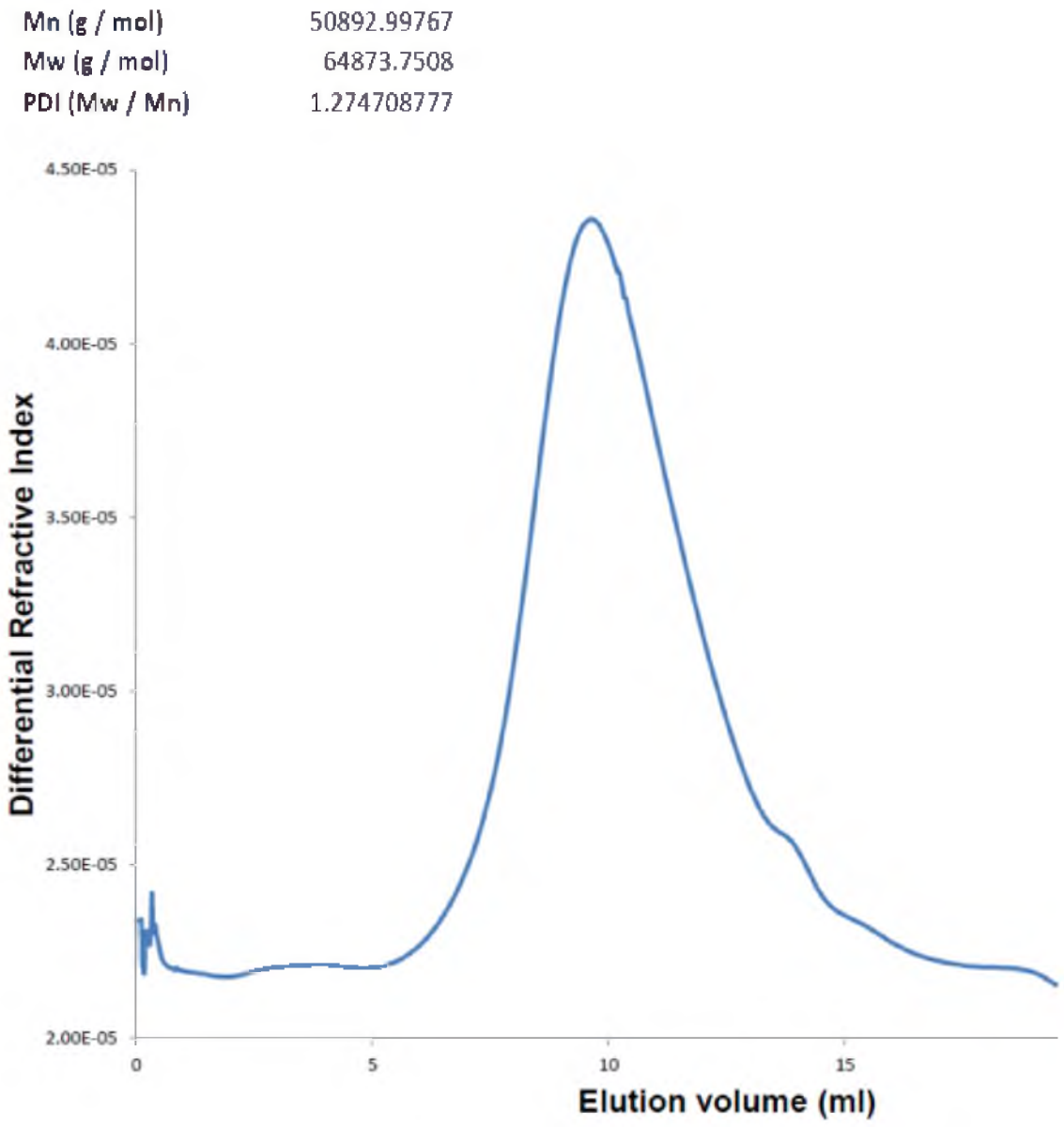

Figure A.5. SEC of HPMA-Gd copolymer final product.

smp #	Sample Description		Gd ppm		
		LoD	0.08		
1-020812	**1 ppm**		0.82	mg/L	
2-020812	**10 ppm**		8.6	1	0.82
3-020812	**50 ppm**		41.4	10	8.6
4-020812	**100 ppm**		82.3	50	41.4
5-020812	**Sample**		46.5	100	82.3

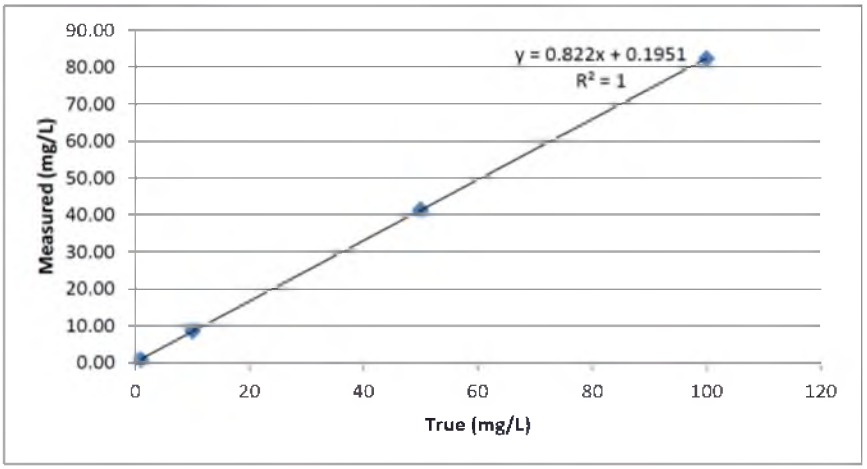

Polymer content 58.8 mg/L
0.37 mmol Gd/g polymer

Figure A.6. ICP-MS characterization of Gd content.

Gd (mM)	R1 (1/s)
2.33	16.333
1.165	8.213
0.5825	3.995
0.29125	1.913

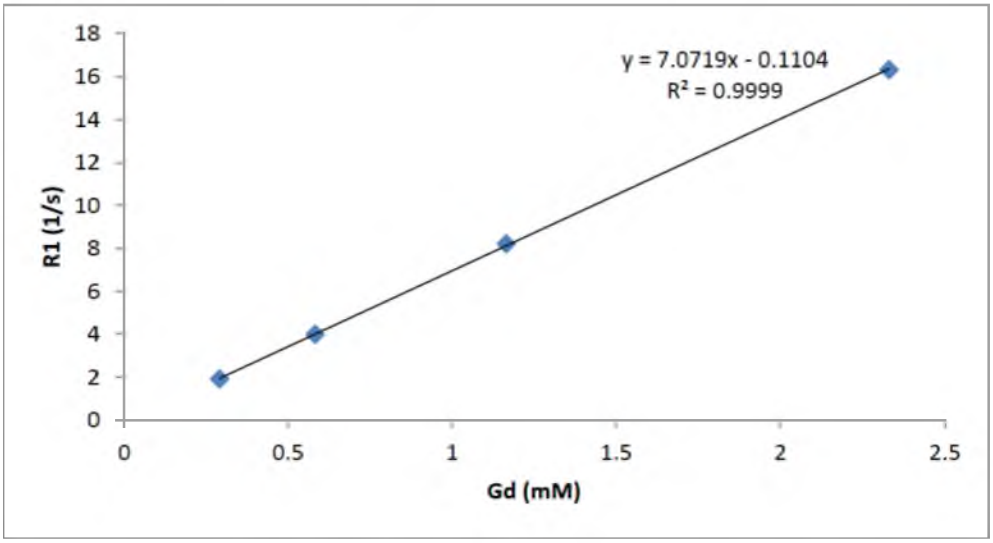

Figure A.7. MRI relaxivity characterization of HPMA-Gd copolymer.